

HYDROLOGIC CONNECTIVITY BETWEEN LANDSCAPES AND STREAMS:  
TRANSFERRING REACH AND PLOT SCALE UNDERSTANDING TO THE  
CATCHMENT SCALE

by

Kelsey Graham Jencso

A dissertation submitted in partial fulfillment  
of the requirements for the degree

of

Doctor of Philosophy

in

Ecology and Environmental Sciences

MONTANA STATE UNIVERSITY  
Bozeman, Montana

November, 2010

©COPYRIGHT

by

Kelsey Graham Jencso

2010

All Rights Reserved

APPROVAL

of a dissertation submitted by

Kelsey Graham Jencso

This dissertation has been read by each member of the dissertation committee and has been found to be satisfactory regarding content, English usage, format, citation, bibliographic style, and consistency, and is ready for submission to the Division of Graduate Education.

Dr. Brian L. McGlynn

Approved for the Department Land Resources and Environmental Sciences

Dr. Tracy M. Sterling

Approved for the Division of Graduate Education

Dr. Carl A. Fox

## STATEMENT OF PERMISSION TO USE

In presenting this dissertation in partial fulfillment of the requirements for a doctoral degree at Montana State University, I agree that the Library shall make it available to borrowers under rules of the Library. I further agree that copying of this dissertation is allowable only for scholarly purposes, consistent with “fair use” as prescribed in the U.S. Copyright Law. Requests for extensive copying or reproduction of this dissertation should be referred to ProQuest Information and Learning, 300 North Zeeb Road, Ann Arbor, Michigan 48106, to whom I have granted “the exclusive right to reproduce and distribute my dissertation in and from microform along with the non-exclusive right to reproduce and distribute my abstract in any format in whole or in part.”

Kelsey Graham Jencso

November, 2010

## ACKNOWLEDGEMENTS

Writing this dissertation has been one of the most significant challenges I have had the privilege to experience. Without the support, patience, and guidance of the following people, this study would not have been completed. It is to them that I owe my deepest gratitude. First and foremost I would like to thank my advisor Brian McGlynn whose knowledge of and commitment to the highest standards in hydrological sciences inspired and motivated me. Brian's own PhD work and foresight provided a substantial foundation upon which the objectives and discoveries in this dissertation were built upon. I feel privileged to have had such a guide for my PhD education and look forward to pursuing hydrology science understanding with him in the future. I would also like to thank my committee members Lucy Marshall, Mike Gooseff, and Ryan Emanuel and collaborators Steve Wondzell, Ken Bencala, Thomas Grabs, Rob Payn, and Jan Seibert. Their collaborative and technical support was an essential part of developing this thesis. Additionally, USGS reviewers (Jamie Shanley, Stephanie Ewing, Douglas Burns, and David Wolock) and many anonymous journal reviewers provided comments that improved the content of papers composing this dissertation. Danny Welsch and Craig Caupp were exceptional mentors during my undergraduate at Frostburg State and initiated my interest in hydrology. I am grateful to all of my labmates in the watershed hydrology laboratory for their friendship and shared times (Diego, Vince, Tim, Kristin, Becca, Galena, John, Fabian, and Seth). Diego Riveros and Vince Pacific were constant companions in the field at TCEF. Their discipline and work ethic provided a context which I strived to follow as a graduate student.

## DEDICATION

This dissertation is dedicated to my wonderful friends and family. First and foremost, I would like to express my heartfelt gratitude and love to my wife Jennifer Jencso without whom this effort would have meant nothing. Your love, support, and constant patience have taught me much about sacrifice, discipline, and compromise. I would like to say thank you to my daughter Jayne Ellen Jencso who was born near the completion of this dissertation. Your presence has been the source of my countless smiles during the last few years. My love and thanks go to my parents Dallet and Kathryn Jencso, my mother Barbara Graham, and my sisters Emily, Hayley and Kaitlin, who have always supported, encouraged, and believed in me, in all of my endeavors. I am also grateful to Joe Kelleher and Larry Swallows for their friendship and guidance while working at Shaw E&I. I would not be where I am today without their encouragement and oversight. Finally I would like to say thank you to my friends Sean O'Callaghan and Joseph Gilpin for getting me out of the office for many hiking, fishing, biking, and hunting adventures in the mountains of Montana.

## TABLE OF CONTENTS

|   |    |
|---|----|
| 1. INTRODUCTION .....   | 1  |
| Dissertation Objectives .....   | 8  |
| Site Description .....  | 8  |
| Dissertation Organization .....   | 10 |
| Chapter 2 .....   | 10 |
| Chapter 3 .....   | 11 |
| Chapter 4 .....   | 12 |
| Chapter 5 .....   | 13 |
| Chapter 6 .....   | 13 |
| Chapter 7 .....   | 14 |
| References Cited .....  | 15 |
| 2. HYDROLOGIC CONNECTIVITY BETWEEN LANDSCAPES AND<br>STREAMS: TRANSFERRING REACH- AND PLOT-SCALE<br>UNDERSTANDING TO THE CATCHMENT SCALE.....         | 21 |
| Contribution of Authors .....   | 21 |
| Manuscript Information .....  | 22 |
| Abstract .....  | 23 |
| Introduction .....  | 23 |
| Site Description .....  | 24 |
| Methods .....   | 25 |
| Landscape Analysis .....  | 25 |
| Hydrometric Monitoring .....  | 26 |
| Hillslope-Riparian Shallow Water Table Measurements .....   | 26 |
| Results .....   | 27 |
| Landscape Analysis .....  | 27 |
| Snowmelt and Precipitation Characterization .....   | 27 |
| Detailed Description of HRS Water Table Response Dynamics .....   | 28 |
| Summary of HRS Water Table Dynamics and Connections According to<br>UAA .....   | 28 |
| Scaling Source Area Connectivity to an Entire Stream Network .....  | 29 |
| Discussion .....  | 29 |
| Does the Size of Hillslope UAA Explain the Development and Persistence<br>of HRS Water Table Connectivity? .....                                      | 31 |
| Can Topographic Analysis Be Implemented to Scale Observed Transect<br>HRS Hydrologic Connections to the Stream Network and Catchment<br>Scales? ..... | 32 |
| How Do Spatial Patterns and Frequency of Landscape Hydrologic<br>Connectivity Relate to Catchment Runoff Dynamics? .....                              | 32 |

## TABLE OF CONTENTS – CONTINUED

|   |    |
|---|----|
| Implications.....   | 34 |
| Conclusion .....  | 35 |
| Appendix A: Detailed Description of HRS Water Table Response Dynamics .....   | 35 |
| A1: Tenderfoot Transect 2 North.....  | 35 |
| A2: Tenderfoot Transect 2 South.....  | 36 |
| A3: Tenderfoot Transect 4 North.....  | 36 |
| A4: Tenderfoot Transect 4 South.....  | 36 |
| A5: Tenderfoot Transect 5 North.....  | 36 |
| A6: Tenderfoot Transect 5 South.....  | 36 |
| A7: Stringer Transect 1 West.....   | 36 |
| A8: Stringer Transect 1 East .....  | 37 |
| A9: Stringer Transect 5 West.....   | 37 |
| A10: Stringer Transect 5 East.....  | 37 |
| Acknowledgements.....   | 37 |
| References Cited .....  | 37 |
| <br>  |    |
| 3. HYDROLOGIC CONNECTIVITY CONTROLS RIPARIAN<br>GROUNDWATER TURNOVER: IMPLICATIONS OF CATCHMENT<br>STRUCTURE FOR RIPARIAN BUFFERING AND SREAM WATER<br>SOURCES..... | 39 |
| <br>  |    |
| Contribution of Authors.....  | 39 |
| Manuscript Information .....  | 40 |
| <br>  |    |
| Abstract.....   | 41 |
| Introduction.....   | 41 |
| Site Description.....   | 42 |
| Methods.....  | 43 |
| Terrain Analysis.....   | 43 |
| Hydrometric Monitoring.....   | 44 |
| Chemical Monitoring.....  | 44 |
| Specific Conductance as a Tracer of Water Sources .....   | 44 |
| Modeling Riparian Groundwater Turnover .....  | 45 |
| Hydrograph Separations for Hillslope, Riparian, and Saturated Area<br>Overland Flow .....   | 45 |
| Results.....  | 46 |
| Precipitation Dynamics.....   | 46 |
| Hillslope and Riparian Hydrologic Connectivity and Specific Conductance<br>Dynamics .....   | 47 |
| Quantifying the Capacity of the Riparian Zone to “Buffer” Hillslope<br>Connections.....   | 47 |

## TABLE OF CONTENTS – CONTINUED

|  |        |
|--|--------|
| Comparing Internal Distributions of Riparian Buffering and Turnover to Source Water Separations at the Catchment Outlet.....                                 | 48     |
| Discussion.....  | 52     |
| What is the Effect of HRS Connectivity Duration on the Degree of Turnover of Water and Solutes in Riparian Zones?.....                                       | 52     |
| How Does Landscape Structure Influence Stream Network Hydrologic Dynamics and the Timing and Amount of Source Waters Detected at the Catchment Outlet? ..... | 53     |
| Landscape Connectivity Conceptual Model of Runoff Generation, Riparian Buffering, and Source Water Mixing.....   | 54     |
| Watershed Management Implications of Riparian Buffering and Landscape Hydrologic Connectivity.....   | 55     |
| Conclusions.....   | 55     |
| Appendix A.....  | 56     |
| Acknowledgements.....  | 56     |
| References Cited.....  | 56     |
| <br>4. VARIABLE FLUSHING MECHANISMS AND LANDSCAPE STRUCTURE CONTROL STREAM DOC EXPORT DURING SNOWMELT IN A SET OF NESTED CATCHMENTS .....                    | <br>59 |
| Contribution of Authors.....   | 59     |
| Manuscript Information .....   | 60     |
| Abstract.....  | 61     |
| Introduction.....  | 61     |
| Site Description.....  | 63     |
| Methods.....   | 64     |
| Terrain Analysis.....  | 64     |
| Measurement Locations .....  | 65     |
| Hydrometric Monitoring.....  | 65     |
| Water Sampling .....   | 65     |
| DOC Analysis .....   | 65     |
| Solute Analysis .....  | 66     |
| Cumulative DOC Export.....   | 66     |
| Results.....   | 66     |
| Landscape Analysis .....   | 66     |
| Snowmelt and Precipitation .....   | 66     |
| Transect Water Table Dynamics and DOC Concentrations .....   | 67     |
| ST1-East.....  | 67     |
| ST1-West .....   | 68     |
| ST5-West .....   | 68     |
| Calcium Dynamics.....  | 70     |

## TABLE OF CONTENTS – CONTINUED

|  |    |
|--|----|
| Stream Discharge and DOC Dynamics.....   | 70 |
| Tenderfoot Creek .....   | 70 |
| Stringer Creek.....  | 70 |
| Spring Park Creek.....   | 71 |
| Sun Creek.....   | 71 |
| Bubbling Creek.....  | 72 |
| Cumulative Stream DOC Export .....   | 72 |
| Discussion.....  | 73 |
| What are the dominant DOC source areas during Snowmelt .....   | 73 |
| How does the spatial extent and frequency of dominant landscape<br>settings impact DOC export at the catchment scale?.....         | 74 |
| Intersection between size of DOC source area and degree of hydrologic<br>connectivity.....   | 76 |
| Comparison to other studies.....   | 76 |
| Conclusions.....   | 77 |
| Acknowledgements.....  | 77 |
| References Cited.....  | 77 |
| <br>   |    |
| 5. HIERARCHICAL CONTROLS ON RUNOFF GENERATION:<br>TOPOGRAPHICALLY DRIVEN HYDROLOGIC CONNECTIVITY,<br>VEGETATION, AND GEOLOGY ..... | 80 |
| <br>   |    |
| Contribution of Authors.....   | 80 |
| Manuscript Information .....   | 81 |
| <br>   |    |
| Abstract.....  | 82 |
| Introduction.....  | 83 |
| Site Description.....  | 86 |
| Methods.....   | 87 |
| Physical Hydrology.....  | 87 |
| Terrain Analyses .....   | 88 |
| Stream Network Delineation.....  | 88 |
| Catchment and Hillslope Scale Terrain Indices.....   | 88 |
| Geology and Vegetative Cover.....  | 90 |
| Stream Network Connectivity.....   | 90 |
| Stream Network Connectivity-Runoff Distributions and<br>“Connectivity Yield” .....   | 91 |
| Univariate and Multiple Linear Assessments of Factors that<br>Influence Connectivity Yield.....                                    | 92 |
| Results.....   | 93 |
| Correlations Between Connectivity and Runoff Distributions<br>Across Catchments.....   | 93 |
| Predictors of Con <sub>yield</sub> Across Catchments .....   | 95 |

TABLE OF CONTENTS – CONTINUED

|  |         |
|--|---------|
| Discussion.....  | 97      |
| How Does HRS Connectivity Relate to Runoff Observed at Each<br>Catchment Outlet? .....                       | 97      |
| What Factors Contribute to Differences in the Connectivity Yield<br>Observed Across the 11 Catchments? ..... | 100     |
| DFC/GTC.....   | 101     |
| Vegetation.....  | 102     |
| Intersection of Surface Topography and Geology .....   | 104     |
| Implications.....  | 106     |
| Conclusion .....   | 108     |
| Acknowledgements.....  | 110     |
| References Cited.....  | 111     |
| <br>6. CALCULATING TERRAIN INDICES ALONG STREAMS – A NEW<br>METHOD FOR SEPARATING STREAM SIDES .....         | <br>131 |
| Contribution of Authors.....   | 131     |
| Manuscript Information .....   | 132     |
| Abstract.....  | 133     |
| Introduction.....  | 134     |
| New Algorithm .....  | 136     |
| Stream Side Determination.....   | 136     |
| Calculation of Lateral Contributing Areas.....   | 139     |
| Case Study .....   | 141     |
| Results.....   | 143     |
| Discussion.....  | 145     |
| Concluding Remarks.....  | 148     |
| Acknowledgements.....  | 149     |
| References Cited.....  | 149     |
| <br>7. DISSERTATION SUMMARY .....  | <br>164 |
| Summary.....   | 164     |
| Implications and Recommendations for Future Research .....   | 169     |
| References Cited.....  | 174     |

## LIST OF TABLES

| Table  | Page |
|--|------|
| 2.1 Tenderfoot Creek transect characteristics.....   | 28   |
| 2.2 Stringer creek transect characteristics.....   | 28   |
| 3.1 Transect attributes.....   | 45   |
| 3.2 Tenderfoot Creek Experimental Forest catchment landscape distributions, riparian turnover, and runoff.....   | 50   |
| 4.1 Stringer Creek transect characteristics of upslope accumulated area (UAA), hillslope-riparian-stream connectivity, riparian width, and slope of hillslope. Hydrologic connectivity across the hillslope-riparian-stream (HRS) continuum was calculated by dividing the number of days that a hillslope water table was present by the total snowmelt period (April 15 - July 15).....  | 66   |
| 4.2 UAA, percentage of stream network with hillslope-riparian-stream (HRS) hydrologic connectivity, ratio of riparian:upland area, and cumulative stream DOC export from April 15 - July 15, 2007 for the 3 sections of Stringer Creek and the 7 sub-catchments of Tenderfoot Creek. ....  | 67   |
| 5.1 Terrain predictor variables extracted from landscape analysis.....   | 119  |
| 5.2 Median values of retained landscape predictor variables and $Con_{yield}$ for the annual, wet, transition, and dry time periods. $Con_{yield}$ was estimated based on the linear (annual and wet), exponential (transition), and logarithmic (dry), fits to the relationship between stream network connectivity and runoff magnitude at 1 percentile increments. The slope of each of these relationships is indicated in bold along with the correlation value. Predictor variables were input into linear regression models to explain the differences in $Con_{yield}$ across catchments and time periods..... | 120  |
| 5.3 Multiple linear models listed in order of decreasing streamflow. Regression coefficients are listed with their associated p-value (bold). A missing value indicates that the predictor was not   |      |

## LIST OF TABLES – CONTINUED

| Table |   | Page |
|-------|---|------|
|       | retained in the final model. Variables that were not found to be significant during any of the flow states were omitted ..... | 121  |
| 6.1   | Overview of symbols and abbreviations.....  | 153  |
| 6.2   | List of parameters used in the SAGA GIS “Channel Network” module.....   | 154  |

## LIST OF FIGURES

| Figure | Page  |
|--------|---|
| 1.1    | Site location and instrumentation of the Tenderfoot Experimental Forest. (a) Catchment location in the Rocky Mountains, MT. (b) Catchment flumes, well transects, SNOTEL, and eddy covariance instrumentation locations. Transect extents are not drawn to scale.....19   |
| 1.2    | Landscape analysis framework. (a) The landscape analysis method outlined by McGlynn and Seibert [2003]. Potential hydrologic connectivity and riparian buffering are represented by total hillslope area and total riparian areas respectively [McGlynn and Seibert, 2003]. (b) A refined method whereby hillslope and riparian areas are separated according to respective left and right stream sides. This method provides a context for more accurate and distributed assessments of HRS hydrologic connectivity and riparian buffering. ....20 |
| 2.1    | Site location and instrumentation of the Tenderfoot Experimental Forest (TCEF). (a) Catchment location in the Rocky Mountains, MT. (b) Catchment flumes, well transects, and SNOTEL, instrumentation locations. Transect extents are not drawn to scale.....25  |
| 2.2    | Measured versus terrain analysis derived riparian widths. The dashed line is the 1:1 line. The slope of the regression was 0.93 and the y intercept was 1.4m.....26   |
| 2.3    | TCEF (a) upslope accumulated area (UAA) for each pixel and (b) an example riparian area extent derived from terrain analysis .....27  |
| 2.4    | Snow and rainwater inputs, snow water equivalent (SWE), and runoff separated into baseflow, snowmelt, rain, and recession observation periods .....29   |
| 2.5    | Transect hillslope and riparian water table and runoff dynamics. Runoff for each transect was obtained from the nearest flume location. The total time of HRS connectivity (days) is listed on the upper left corner of each hillslope time series. Maps are each transects UAA, riparian extents, and well locations. Letters on the map designate the location of hillslope and riparian well where water table dynamics were measured .....30  |

## LIST OF FIGURES - CONTINUED

| Figure |  | Page |
|--------|--|------|
| 2.6    | Binary summary of 24 transects of hillslope-riparian-stream water table connectivity dynamics for the 2007 water year. (a) Small UAA exhibits a transient connection or no connection. (b) Midrange UAA exhibits a sustained connection during large snowmelt and rain events and a transient connection during periods of low antecedent wetness. (c) Large UAA exhibits a continuous connection.....   | 31   |
| 2.7    | UAA regressed against the percentage of the water year that a hillslope-riparian-stream water table connection existed for 24 well transects. A connection was recorded when there was streamflow and water levels were recorded in both the riparian and hillslope wells. The inset plot shows the same data with a linear x axis.....  | 31   |
| 2.8    | UAA flow accumulation patterns (shading) and the regression-derived hillslope-riparian-stream water table connectivity along the left (red bars) and right (black bars) sides of the Tenderfoot Creek stream network. Predicted hydrologic connectivity ranged from 0 to 100% of the year (represented by bar heights).....  | 32   |
| 2.9    | TCEF catchment (a) UAA distribution curve based on 3108 10 m pixels along the stream network (both sides). (b) Comparison of the regression-derived connectivity duration curve (CDC) based on HRS water table connectivity for each 10 m UAA pixel along the stream network and the 2007 Lower Tenderfoot Creek flow duration curve (FDC). Periods of lowest runoff are associated with lowest network connectivity and large UAA values. Increased runoff is associated with increasing network connectivity from HRS connections at smaller UAA values..... | 33   |
| 2.10   | (a) Linear regression analysis between the estimated annual network CDC (3108 10 m pixels along both sides of the stream network) and the TCEF catchment FDC (8762 hourly measurements). (b) Linear regression for the same distributions separated into the dry, transitional, and wet catchment states. Each point represents 5% of the CDC and FDC distribution.....  | 33   |
| 3.1    | Site location and instrumentation of the TCEF catchment. (a) Catchment location in the Rocky Mountains, MT. (b) Catchment  |      |

## LIST OF FIGURES - CONTINUED

| Figure | Page   |
|--------|--|
|        | flumes, well transects, and SNOTEL instrumentation locations. Specific transects highlighted in this study are filled in black and labeled T1-T4. Transect extents are not drawn to scale.....43   |
| 3.2    | Water year 2007 cumulative snow water equivalent, snowmelt, and rain .....46   |
| 3.3    | (a-d) Time series of riparian and hillslope water table dynamics and specific conductance at transects 1-4. Times of hillslope-riparian-stream hydrologic connectivity are indicated with gray shading. Runoff (dark gray shading) and specific conductance (black line) dynamics at the Lower Tenderfoot Creek Flume are shown (e) for comparison to the transect dynamics.....47   |
| 3.4    | Exponential decline of riparian groundwater specific conductance toward the hillslope signature following the snowmelt induced hydrologic connection. The slopes of these lines indicate the rate of riparian water turnover or dilution by hillslope water. The inverse of the slope is the turnover time constant for each site (Table 1) and provides a measure of riparian buffering of hillslope throughflow. The dotted line represents the exponential decline of the LTC stream specific conductance during the same time period. ....47 |
| 3.5    | Logarithmic relationship between the riparian buffering ratio (riparian area divided by hillslope area) at each transect and the time that it takes for 50% of the initial riparian specific conductance signature to be turned over or diluted by hillslope water (Table 1; Equation (2)).....48  |
| 3.6    | Estimated hillslope-riparian-stream connectivity duration required for 95% of the initial riparian water to be replaced or diluted by hillslope throughflow (shaded bars) and the observed HRS connectivity duration for the study observation period (white rectangles). The riparian zone is estimated to be turned over when SC reaches hillslope signatures (white shading) denoted in each shaded bar. ....48   |
| 3.7    | TCEF subcatchment distributions of stream network (a) HRS connectivity, (b) riparian buffering, and the resultant (c) riparian   |

## LIST OF FIGURES - CONTINUED

| Figure  | Page  |    |
|---|---|----|
| <p>groundwater turnover times. Riparian water turnover times (riparian buffering) are a function of hydrologic connectivity and the size of the riparian area relative to the adjacent hillslope. Catchments with fast turnover times had more sustained HRS connectivity and less riparian buffering of hillslope inputs. Catchments with longer duration turnover times had shorter duration hillslope ground water table connectivity to their riparian zones and more effective riparian buffering along the stream network. ....</p> | 49  |    |
| 3.8   | <p>Subcatchment (a-c) hillslope UAA, riparian area, and riparian buffering potential (black and red bars), (d-f) the HRS stream network turnover distribution derived from the riparian buffering-turnover relationship (Equation 5), and (g-i) spatial source water separations for each subcatchment. Catchments with higher riparian buffering and turnover time distributions have a more sustained riparian groundwater contribution to their annual snowmelt hydrographs. ....</p>  | 50 |
| 3.9   | <p>Spatial source water separations for the TCEF subcatchments and the TCEF UAA accumulation patterns and stream network riparian buffering (ratio of local riparian and hillslope area). Runoff was separated into hillslope, riparian and riparian saturation overland flow components. Error bars indicate the uncertainty in the hillslope and riparian components. The frequency of different magnitude riparian buffering and turnover times along the stream network determined the spatial sources of water detected at each catchment's outlet. Catchments with a greater frequency of high riparian buffering of hillslope inputs and long turnover times had more sustained riparian contributions in their snowmelt hydrographs. ....</p> | 51 |
| 3.10  | <p>The riparian percentage of total runoff during the snowmelt period plotted against the percentage of riparian area for each TCEF catchment. ....</p>   | 52 |
| 3.11  | <p>The percentage of riparian runoff during the snowmelt period plotted against the median of the riparian turnover half life distribution for each TCEF subcatchment. The total riparian runoff</p>  |    |

## LIST OF FIGURES - CONTINUED

| Figure  | Page |
|---|------|
| observed at each catchment outlet was a function of the distribution of riparian turnover times within each catchment .....   | 52   |
| 4.1 Conceptual model of DOC export from the soil to the stream. During times of low flow, such as baseflow, groundwater travels through low DOC mineral soil, and stream DOC concentrations are low (Scenario 1). As flow begins to increase during snowmelt or precipitation events, the groundwater table rises into shallow organic-rich riparian soil, and inputs of DOC from the soil to the stream increase (Scenario 2). As the groundwater table continues to rise, a hydrologic connection develops across the upland-riparian-stream continuum (Scenario 3). An initial pulse of high DOC water from the uplands is transmitted along preferential flow paths (3a). Runoff from the uplands is then diluted by low DOC matrix water traveling through mineral soil (3b) ..... | 62   |
| 4.2 Location of the Tenderfoot Creek Experimental Forest (TCEF), with delineations of the sub-catchments, and locations of the flumes (at the outlet of each sub-catchment) and the Lower Stringer Creek SNOTEL site. Transect locations are denoted by rectangles, and the 3 utilized for this study within the Stringer Creek Watershed are shown in black .....  | 63   |
| 4.3 a) Soil water inputs from snowmelt (black bars) and precipitation (grey bars); b) ST1-E riparian toeslope well; c) ST1-E upland well; d) riparian and upland groundwater height and Ca concentrations; and e) stream DOC concentrations and discharge from April 15 to July 15, 2007. The percentage of the study period that hillslope-riparian-stream connectivity existed, and upslope accumulated area (UAA) at the toeslope measurement location are listed at the top of the figure. Stream discharge is from the Lower Stringer Creek Flume. ....  | 64   |
| 4.4 a) soil water inputs from snowmelt (black bars) and precipitation (grey bars); b) ST1-W riparian toeslope well DOC concentrations and groundwater height; c) statement of no upland water table development above the bedrock interface at 100 cm; and d) stream DOC concentrations and discharge from April 15 to July 15, 2007. The percentage of the study period that hillslope-riparian-stream   |      |

## LIST OF FIGURES - CONTINUED

| Figure | Page   |
|--------|--|
|        | connectivity existed, and upslope accumulated area (UAA) at the toeslope measurement location are listed at the top of the figure. Stream discharge is from the Lower Stringer Creek Flume. ....68   |
| 4.5    | a) soil water inputs from snowmelt (black bars) and precipitation (grey bars); b) ST5-W riparian toeslope well DOC concentrations and groundwater height; c) ST5-W upland well DOC concentrations and groundwater height; d) riparian and upland groundwater height and Ca concentrations; and e) stream DOC concentrations and discharge from April 15 to July 15, 2007. Note the difference in scale for DOC at (b) and (c). The percentage of the study period that hillslope-riparian-stream connectivity existed, and upslope accumulated area (UAA) at the toeslope measurement location are listed at the top of the figure. Stream discharge is from the Lower Stringer Creek Flume.....69 |
| 4.6    | a) soil water inputs from snowmelt (black bars) and precipitation (grey bars); b) discharge and DOC concentrations at ST1 on Stringer Creek; c) snow water equivalent and snowmelt; and d) stage height and DOC concentrations at Upper Tenderfoot Creek (Onion Park) from April 15 to July 15, 2007. Discharge could not be calculated at Onion Park as no flume was installed. ....69  |
| 4.7    | a-c) upstream to downstream Stringer Creek DOC concentrations at a) Transect 1; b) Middle Stringer Creek Flume (MSC); and c) Lower Stringer Creek Flume (LSC) from April 15 to July 15, 2007. d-f) cumulative DOC export from each sub-catchment. The percentage of riparian to upland area within each sub-catchment is also shown.....71   |
| 4.8    | Comparison of discharge, DOC concentrations, and cumulative DOC export at the catchment outlet of a) Spring Park Creek; b) Upper Tenderfoot Creek; c) Sun Creek; d) Bubbling Creek; e) Lower Tenderfoot Creek; f) Lower Stringer Creek, and g) Middle Stringer Creek from April 15 to July 15, 2007. Riparian:upland extent (R:U) and cumulative stream DOC export is given for each sub-catchment. ....72   |

LIST OF FIGURES - CONTINUED

| Figure |   | Page |
|--------|---|------|
| 4.9    | Cumulative DOC export between April 15 and July 15, 2007 at each of the sub-catchments in the Tenderfoot Creek Watershed (including the 3 sub-catchments within the Stringer Creek Watershed) as a function of a) riparian:upland ratio; and b) percent of the stream network with URS hydrologic connectivity at peak runoff.....  | 73   |
| 5.1    | Site location and instrumentation of the TCEF catchment. (a) Catchment location in the Rocky Mountains, MT. (b) Catchment flumes, well transects installed by Jencso et al. [2009], and SNOTEL instrumentation locations. Transect extents are not drawn to scale. ....   | 122  |
| 5.2    | The linear relationship (a) between the local inflows of UAA and HRS shallow groundwater connectivity duration observed by Jencso et al. [2009]. This relationship was applied to each 10 m HRS source area assemblage to estimate stream network connectivity. The inset plot (b) indicates where each of the 24 HRS well transects falls within the stream network distribution of UAA. ....  | 123  |
| 5.3    | Comparison of the TCEF catchment connectivity duration curves (CDC) and the annual flow duration curve (FDC). (a) CDCs were derived from the frequency distribution of HRS water table connectivity at each 10 m pixel along the stream network (both sides). FDCs were derived from hourly runoff values for the 2007 water year (8732 values). Periods of lowest runoff are associated with the lowest connectivity that occurs among the largest UAA values. Larger magnitude runoff is associated with increasing hydrologic connectivity across subsequently smaller stream network UAA values (increasing from large to small)..... | 124  |
| 5.4    | Distributions of (a) stream network HRS connectivity, (b) runoff and (c) annual stream network connectivity versus runoff for each catchment. Each CDC and FDC was plotted at 1 percentile increments.....  | 125  |
| 5.5    | Linear fit to the relationship between the percentage of the stream network connected (CDC) and runoff magnitude (FDC) for the 2007 water year (0-100% exceedance). The lower right panel   |      |

## LIST OF FIGURES - CONTINUED

| Figure | Page  |
|--------|---|
|        | depicts all of the linear fits to highlight annual variability in $Con_{yield}$ across catchments.....126   |
| 5.6    | Linear fit to the relationship between the percentage of the stream network connected (CDC) and runoff magnitude (FDC) during the wettest catchment states (0-10% exceedance). The lower right panel depicts all of the linear fits to highlight variability in $Con_{yield}$ during peak flow across catchments .....127   |
| 5.7    | Exponential fit to the relationship between the percentage of the stream network connected (CDC) and runoff magnitude (FDC) during the transition from wet to dry states (10-50% exceedance). The lower right panel depicts all of the exponential fits to highlight variability in $Con_{yield}$ during the wet up and dry down across catchments.....128  |
| 5.8    | Logarithmic fit to the relationship between the percentage of the stream network connected (CDC) and runoff magnitude (FDC) during the driest catchment states (50-100% exceedance). The lower right panel depicts all of the exponential fits to highlight variability in $Con_{yield}$ across catchments during low flow conditions .....129  |
| 5.9    | Linear relationships between $Con_{yield}$ for each TCEF catchment during the annual, wet, transition, and dry periods and the median values of the (a) DFC/GTC, (b) tree height, and (c) percentage of catchment sandstone overlain by UAA greater than 5,000m <sup>2</sup> . Combinations of these predictors explained variability in catchment $Con_{yield}$ across flow states within multiple linear models.....130   |
| 6.1    | Directions relative to the center grid cell X are coded from 1 to 8 clockwise from northeast (NE) to north (N). The corresponding vector notation is illustrated for a flow line vector $f$ in direction 1 (dotted arrow) and for a streamflow vector $s$ in direction 6 (plain arrow). Calculating the cross product $f \times s$ reveals a positive $z$ -component and therefore the flow line vector $f$ is located on the left relative to the stream vector $s$ .....155 |
| 6.2    | Different configurations fo flow lines $f$ (dotted arrows) and stream vectors $s$ , $i \geq 0$ (plain arrows). The left paragraph depicts a flow  |

## LIST OF FIGURES - CONTINUED

| Figure  | Page  |
|---|---|
| <p>line vector <math>f</math> pointing to a stream junction. In this case, the flow line is located on the right stream side because it is on the right side relative to all stream vectors <math>s_i</math>. A sharp stream bend is shown in the middle graph. <math>f</math> is on the left side relative to <math>s_0</math> and on the right side relative to <math>s_1</math> and therefore on the outer side of the bend. Since the cross product <math>s_1 \times s_2</math> has a positive <math>z</math>-component the inner bend must be located on the left stream side and <math>f</math> hence on the right stream side. The graph on the right illustrates a channel head. In this case the orientation of the flow line relative to <math>s_0</math> is not definable.....</p> | 156   |
| 6.3   | Flowchart illustrating the determination of a hillslope position. Symbols and abbreviations are defined in Table 1 .....157   |
| 6.4   | Illustrations of a flow direction map and maps showing values of specific lateral contributing area $a_c$ . The flow direction map shows hillslope and stream flow directions. The three lower maps feature $a_c$ entering the stream from left, $a_{c,L}$ and $a_c$ entering the stream from the right, $a_{c,R}$ as well as the total $a_c$ , which equals the sum of $a_{c,L}$ and $a_{c,R}$ . For simplicity, the $a_c$ values presented in the illustration are equal to the number of contributing grid cells.....158 |
| 6.5   | Spatial representation of contributing area $A_c$ (grey-shaded flow lines) and side-separated specific contributing area values $a_c$ (dark-grey and light-grey bars).....159   |
| 6.6   | Scatter plot of right specific lateral contributing areas ( $a_{c,R}$ ) versus their counterpart on the left stream side ( $a_{c,L}$ ) along the stream network of the 23km <sup>2</sup> TCEF catchment. The labels 1 and 2 refer to explanations in the text .....160  |
| 6.7   | Comparison of riparian-hillslope ratios ( $R/H$ ) calculated based on total and side-separated values. a) Cumulative area-weighted distributions of riparian to hillslope ratios ( $(R/H)_{sep}$ , and $(R/H)_{tot}$ . b) the ratios of the above distribution functions. The labels 1 and 2 refer to explanations in the text.....161  |
| 6.8   | Hillslope $a_c$ regressed against the percentage of the water year that a hillslope-riparian-stream water table connection existed for 24   |

## LIST OF FIGURES - CONTINUED

| Figure  | Page |
|---|------|
| well transects. a) Total $a_c$ from both sides of a transect cross section and b) $a_c$ separated into left and right sides of the stream. A connection was defined as occasions when there was stream flow and water levels were recorded in both the riparian and hillslope wells (modified from Jencso et al. [2009]) .....  | 162  |
| 6.9 Stringer Transect 5 East and West hillslope and riparian water table (black lines, elevation is relative to the local datum) and runoff (grey lines) dynamics. Specific area for each side of the transect and the total time of HRS connectivity (days) during the 2007 water year is listed below each time series. The map in the middle depicts the transects contributing area $A_c$ (dark to light shading), riparian zone extents (white dashed lines), well locations (white circles) and stream position (black line).....   | 163  |
| 7.1 Conceptual model of runoff generation and solute mobilization for the TCEF catchment. (a) The topographically driven lateral redistribution of water (UAA) determines the frequency and duration of hydrologic connectivity across the stream network. The intersection of connectivity with flowpath length/gradient, vegetation, and geology determine the magnitude of runoff observed at the catchment outlet. (b) The intersection of hydrologic connectivity frequency and duration with riparian area extents determines the degree of riparian buffering/turnover and the spatial sources of water and solutes observed at the catchment outlet ..... | 176  |
| 7.2 1999-2008 Stringer Creek discharge and cumulative melt + rain time series (top) and discharge (bottom). The 2007 water year is highlighted in black. Changes in HRS connectivity duration, as a function of precipitation variability and wetness state, could alter the degree of turnover within HRS sequences along the stream network. This may significantly alter the amount, timing, and riparian buffering of water and solutes exiting a catchment as a function of the intersection of climatic variability and catchment structure.....  | 177  |

## ABSTRACT

Transferring plot and reach scale hydrologic understanding to the catchment scale and elucidating the link between catchment structure and runoff and solute response remains a challenge. To address this challenge, I pursued the following questions as part of this dissertation: How do spatiotemporal distributions of hillslope-riparian-stream (HRS) hydrologic connectivity influence whole catchment hydrologic dynamics and what are the implications of this for stream biogeochemistry? What are the implications of catchment structure for riparian buffering and streamflow source water composition? What are the hierarchical controls on hydrologic connectivity and catchment runoff dynamics across 11 diverse headwater catchments and across flow states? I addressed these questions through detailed hydrometric monitoring and analysis (160 recording wells across 24 HRS transects and stream discharge across 11 catchments), tracer sampling and analysis (groundwater, soil water, and stream water sampling of major ions, specific conductance and dissolved organic carbon (DOC)), and newly developed digital landscape and terrain analyses. I installed this unprecedented network of instrumentation to address these questions across 11 adjacent and nested catchments within the Tenderfoot Creek Experimental Forest (TCEF), Rocky Mountains, MT. I determined that 1) hillslope topography, specifically upslope accumulated area (UAA), was the first order control on the duration of transient water table connectivity observed across HRS landscape positions; 2) the intersection of HRS connectivity with riparian area extents determined the degree of riparian groundwater turnover, riparian buffering of upslope water, and the magnitude of DOC transport to streams; 3) 11 catchments' stream network hydrologic connectivity duration curves were highly correlated to streamflow duration curves and the variable slopes of these relationships were explained by vegetation, geology, and within catchment distributions flowpath length and gradient ratios. This dissertation consists of five key chapters / manuscripts that address how landscape structure/organization within and across catchments can control the timing and magnitude of water and solutes observed at catchment outlets.

## CHAPTER 1

Introduction<sup>1</sup>

Transferring plot and reach scale hydrologic understanding to the catchment scale and elucidating the link between catchment structure and runoff response remains a challenge [Jencso *et al.*, 2009]. Important questions in catchment hydrology related to this challenge include: What are the first order controls on the hydrologic connections that can occur between landscape source areas? How do spatiotemporal distributions of source area connectivity influence whole catchment hydrologic and solute response dynamics and what are the implications of this for stream biogeochemistry? How do we transfer understanding gained from landscape scale hydrologic and tracer based measurements to the stream network and catchment scales? In this thesis we sought to address these questions through combined hydrometric, tracer, and landscape analysis based approaches. We combined these approaches across adjacent and nested catchments in the Tenderfoot Creek Experimental Forest (TCEF; Figure 1) to demonstrate and test their utility for scaling hydrologic dynamics across the plot, stream network, and catchment scales.

Many recent advances in catchment hydrology have focused on the discretization, behavior, and connections between catchment source areas according to their

---

<sup>1</sup> This introduction is a modified and collective version of introductory material presented in successive chapters.

topographic-topologic, hydrologic, and chemical attributes. Landscape discretization is the separation of a catchment into landscape elements that exhibit hydrologically or biogeochemically similar behavior [McGlynn and Seibert, 2003]. Hydrologic connectivity refers to the development of water table continuity across hillslope-riparian-stream interfaces [Jencso *et al.*, 2009]. A fundamental theme throughout this dissertation is that analysis of spatial patterns of landscape streamflow source areas, coupled with observations of their hydrologic connectivity and hydro-chemical response, provides a context for the distributed assessment of the relative contributions by each to catchment hydrology and solute response. In headwater catchments with relatively uniform soil depths and organized drainages, dominant landscape source areas can often be reduced to hillslope and riparian zones.

Hillslopes are the most extensive landscape source area. Hillslope soils are often shallow and located on moderate to steep slopes. Hillslopes typically have low antecedent wetness due to their steep slopes and well drained soils. During periods of high wetness, transient hillslope water tables can develop and hillslope soils can be highly transmissive thereby contributing significant quantities of water to near stream areas and the stream network [Peters *et al.*, 1995]. This hydrologic connectivity is a requisite for the flushing of solutes and nutrients downslope through the riparian zone to the stream [Creed *et al.*, 1996; Buttle *et al.*, 2001; Stieglitz *et al.*, 2003].

Riparian zones (near stream source areas) are located between hillslopes and the channel network, in topographic lows, often at the base of organized hillslope drainages and can remain at or near saturation with minor to modest water table fluctuations in the

upper soil profile. Characteristics of riparian zones often include anoxic conditions, high organic matter content, and low hydraulic conductivity associated with the predominance of organic, silt, and clay size particles. These characteristics can lead to the potential buffering of hillslope inputs of water [McGlynn *et al.*, 1999; McGlynn and Seibert, 2003] and nutrients [Burt *et al.*, 1998; Hill *et al.*, 2000; Carlyle and Hill, 2001; McGlynn and McDonnell, 2003] to streams.

Development of water table connectivity between hillslope and riparian zones has been associated with threshold behavior in catchment scale runoff production [Devito *et al.*, 1996; Sidle *et al.*, 2000; Buttle *et al.*, 2004], mechanisms of rapid delivery of pre-event water [McGlynn and McDonnell, 2002; McGlynn and McDonnell, 2003b], dissolved organic carbon (DOC) dynamics [McGlynn and McDonnell, 2003a], and nutrient transport at various timescales [Creed *et al.*, 1996; Vidon and Hill, 2004; Ocampo, 2006]. Therefore, identifying the spatial and temporal hydrologic connectivity of hillslope and riparian source areas is an important step for understanding how landscape level dynamics can lead to whole catchment hydrologic and solute response.

Plot and catchment scale investigations have cited water table connectivity between riparian and hillslope landscape source areas as a first order control on runoff response. It has been shown that hillslope and riparian source areas can exhibit independent water table dynamics, characteristic of each landscape area [Seibert *et al.*, 2003; Ocampo *et al.*, 2006]. These investigations demonstrated that the steady state assumption of uniform groundwater rise and fall across the landscape is often unrealistic. Water table timing differences across riparian-hillslope transitions were attributed to

different antecedent soil moisture deficits and drainage characteristics. Catchment scale investigations by McGlynn et al. [2004] related riparian water table dynamics, hillslope runoff contributions, and total runoff in five nested catchments to landscape topography and the organization of hillslope and riparian landscape area. Increasing synchronicity of runoff and solute response was attributed to increasing antecedent wetness, event size, and the resulting increased riparian-hillslope hydrologic connectivity.

Hydrologic connectivity between hillslopes and riparian zones is also an important consideration for interpreting the spatial sources of water and solutes observed in streamflow. Because of their location between hillslopes and streams, riparian zones can modulate or buffer the delivery of water and solutes when hillslope connectivity is established across the stream network [Hill, 2000]. The definitions of riparian buffering are diverse and depend on the water quality or hydrologic process of interest. One use of the term refers to biogeochemical transformations [Cirimo and McDonnell, 1997] that often occur (e.g., redox reactions and denitrification). Another common use of the term refers to the volumetric buffering of upslope runoff by resident near stream groundwater [McGlynn and McDonnell, 2003b; McGlynn and Seibert, 2003]. Here we focus mainly on the volumetric form of riparian buffering with implications for biogeochemical transformations.

Identifying spatial and temporal hydrologic connectivity among HRS zones can be an important step in understanding the evolution of stream solute and source water signatures during storm events. When a HRS connection is established, hillslope groundwater moves from the slope, down through the adjacent riparian zone. Plot scale

investigations have suggested the mixing and displacement of riparian groundwater (turnover) by hillslope runoff is a first-order control on hillslope water [McGlynn *et al.*, 1999], solute [McGlynn and McDonnell, 2003b] and nutrient [Burt *et al.*, 1999; Hill, 2000; Carlyle and Hill, 2001; McGlynn and McDonnell, 2003a; Ocampo *et al.*, 2006] signatures expressed in stream flow. Source water separations at the catchment outlet and theoretical exercises have also suggested that the rate at which turnover occurs may be proportional to the size of the riparian zone and the timing, duration, or magnitude of hillslope hydrologic connectivity to the riparian zone.

Previous studies highlight the importance of HRS connectivity and riparian zones for the explanation and prediction of catchment hydro-chemical response. However, inferences derived from these studies are primarily based on monitoring across single landscape positions or chemical monitoring at the catchment outlet. This has hindered the transfer of information between the two scales. Traditionally these studies have lacked either spatial or temporal coverage, thus providing little insight into spatio-temporal upland to stream connectivity and its controlling variables across space and time. A framework combining high-frequency, spatially distributed source area connectivity observations along with metrics of their controlling hydro geomorphic attributes is needed to link internal HRS source area response to runoff and solute dynamics as measured at the catchment outlet.

In headwater catchments there are often strong relationships between landscape topography and runoff generation [Dunne and Black, 1970; Anderson and Burt, 1978; Beven, 1978; Burt and Butcher, 1985], runoff spatial sources [Sidle *et al.*, 2000; McGlynn

and McDonnell, 2003b] and water residence times [McGlynn *et al.*, 2004; McGuire *et al.*, 2005; Tetzlaff *et al.*, 2009]. A specific topographic metric of interest in this dissertation is upslope accumulated area (UAA); the amount of land draining to a point in the landscape and a proxy for lateral water redistribution. Many of the formative hillslope hydrology studies [Hewlett and Hibbert, 1967; Dunne and Black, 1970; Harr, 1977; Anderson and Burt, 1978] observed increased subsurface water accumulation in topographically convergent hillslope areas and in areas of higher UAA.

Other variables that could additionally influence and even dominate water storage, redistribution, and therefore connectivity initiation and duration between source areas and the stream network include bedrock geology and its permeability [Huff *et al.*, 1982; Wolock *et al.*, 1997; Burns *et al.*, 1998; Shaman *et al.*, 2004b; Uchida *et al.*, 2005], soil characteristics [Buttle *et al.*, 2004; Devito *et al.*, 2005; Soulsby *et al.*, 2006], and vegetation [Ivanov *et al.*, 2010; Emanuel *et al.*, in press]. While all of these factors are likely to influence the distribution of source area hydrologic connectivity and in turn, riparian buffering, and stream flow response, few empirical studies have explored their combined and hierarchical influence across space and time. This limits our understanding of the spatial and temporal sources of runoff both within and across catchments

Landscape analysis, based on topography, typically represented by digital elevation models (DEMS), can be used to characterize catchment structure (topography and geology), catchment cover (vegetation and land use) and the topology between hillslopes and riparian zones. McGlynn and Seibert [2003] outlined an approach for

mapping source area topology based on hillslope and riparian UAA (Figure 2a).

Potential hydrologic connectivity among hillslopes and riparian zones was characterized by total lateral contributing area to the stream network. Riparian buffering along a stream reach was defined as the ratio between total riparian and hillslope areas on both sides of the stream. This approach provides a potential way to upscale hydrologic process observations. However, a limitation of this method was that hillslope and riparian area from both sides of the stream network were combined despite potentially large differences in hillslope and riparian dynamics on opposing stream sides. New landscape analysis techniques are needed to distinguish between stream sides for a more accurate representation and up-scaling of hillslope and riparian zone hydrology (Figure 2b; [Chapter 6 of this dissertation; *Grabs et al., In Press*]).

In this dissertation we address some of the venerable challenges in catchment hydrology by combining refined landscape analysis techniques with field and catchment scale investigative approaches. This method is iterative, in that the landscape analysis guided the selection of hillslope and riparian areas for experimental observation and provided the basis to scale up the results to the network and catchment scales. The central idea throughout this dissertation is that landscape analysis can be used to link plot and reach scale hydrological dynamics with topographic/geomorphic/land cover controls and provide a context to transfer plot- and reach-scale results to the catchment scale. We use this methodology to address the following objectives:

### Dissertation Objectives

1. Quantify the first order controls on HRS hydrologic connectivity and determine the relationship between the frequency of stream network HRS connectivity and catchment scale runoff dynamics.
2. Determine the relationship between HRS hydrologic connectivity, riparian groundwater turnover, and the timing and spatial sources of runoff and solutes observed at the catchment outlet.
3. Assess the role of catchment structure and HRS hydrologic connectivity for dissolved organic carbon export at the landscape and catchment scales.
4. Quantify how catchment topography, geology, and land cover/vegetation characteristics influence the relationship between stream network connectivity and runoff across adjacent but contrasting catchments.
5. Develop and test new terrain analysis techniques that can better quantify the topology between hillslope and riparian zones and their potential hydrologic and chemical contributions to streams.

### Site Description

We addressed the objectives of this dissertation at the Tenderfoot Creek Experimental Forest (TCEF) located in the Little Belt Mountains of Montana (Figure 1). The TCEF consists of 11 nested headwater catchments that drain into Smith River a tributary to the Missouri River. The climate in the Little Belt Mountains is continental. Annual precipitation in the TCEF averages 880 mm and ranges from 594 to 1,050 mm

from the lowest to highest elevations. Snowfall comprises 75% of the annual precipitation with snowmelt and peak runoff generally occurring in late May or early June. Lowest runoff occurs in late summer through the winter months. Catchment headwater zones are typified by moderately sloping (avg. slope  $\sim 8^\circ$ ) extensive (up to 1200m long) hillslopes and variable width riparian zones. Approaching the main stem of Tenderfoot Creek the streams become more incised, hillslopes become shorter ( $< 500\text{m}$ ) and steeper (average slope  $\sim 20^\circ$ ), and riparian areas narrow relative to the catchment headwaters. The geology is comprised of Flathead Sandstone and Wolsey Shale at higher elevations and transitions to Granite Gneiss at lower elevations [Reynolds, 1995].

Geologic strata are considered relatively impermeable with the greatest potential for deeper groundwater exchange at geologic contacts, fractures in the Wolsey shale [Reynolds, 1995] and along the more permeable sandstone strata. Soil depths are relatively consistent across the landscape (0.5-1.0m in hillslope positions and 1-2 m in riparian positions) with localized upland areas of deeper soils. The major soil types have been characterized as loamy skeletal, mixed Typic Cryochrepts located along hillslope positions and clayey, mixed Aquic Cryboralfs in riparian zones and parks [Holdorf, 1981]. The dominant forms of vegetation include lodgepole pine (overstory; *Pinus contorta*) and grouse whortleberry (understory; *Vaccinium scoparium*) in hillslope positions and bluejoint reedgrass (*Calamagrostis canadensis*) in riparian positions [Farnes et al., 1995; Mincemoyer and Birdsall, 2006]. Previous reports provide more detailed descriptions of TCEF climatic [Farnes et al., 1995], geologic [Reynolds, 1995a; Schmidt

*et al.*, 1996], and vegetative [*Farnes et al.*, 1995; *Mincemoyer and Birdsall*, 2006] characteristics.

### Dissertation Organization

The following chapters address the implications of landscape structure for runoff generation and solute mobilization from subalpine catchments in the northern Rocky Mountains, Montana. Chapters are organized to build iterative understanding of the role of landscape structure/topography in mediating hydrologic connectivity between source areas and the stream network, runoff and solute generation, and the how these relationships transcend across time and space.

#### Chapter 2

Topographic convergence and divergence and the accumulation of hillslope contributing area have long been hypothesized as important controls for water redistribution. However limited field based research has been conducted to explore how variability in hillslope topography can affect runoff generation at the hillslope, stream network, and catchment scales. This has resulted in plot specific conclusions with little transferability to other catchments or development of general principles. Chapter 2 examines the role of landscape topography and topology in mediating shallow groundwater connections that can occur between hillslope and riparian landscape source areas and the implications of spatial patterns of connectivity for runoff dynamics. We monitored hillslope and riparian water table connectivity dynamics across 24 HRS well transects with a range of UAA size, at hourly intervals, for an entire year. We combined

digital elevation model (DEM) based terrain analysis and hillslope-riparian area discretization with these high frequency connectivity observations to address the following questions:

1. Does the size of hillslope UAA explain the development and persistence of HRS water table connectivity?
2. Can topographic analysis be implemented to scale observed transect HRS hydrologic connections to the stream network and catchment scales?
3. How do spatial patterns and frequency of landscape hydrologic connectivity relate to catchment runoff dynamics?

### Chapter 3

Chapter 3 extends the conceptualization of the HRS hydrologic connectivity developed in chapter 2 to the spatial sources of water and solutes observed in streamflow. Hydrologic connectivity between catchment source areas such as hillslopes and riparian zones is essential for the transmission of water and solutes to streams. However, our current understanding of the role of riparian zones in mediating landscape hydrologic connectivity and the catchment scale export of water and solutes is limited. In this paper we tested the relationship between the initiation and duration of HRS hydrologic connectivity and the rate and degree of riparian groundwater turnover when a hydrologic connection was established. We combined landscape analysis of HRS connectivity and riparian buffering with high frequency, spatially distributed, observations of HRS shallow groundwater connectivity and solute dynamics. We extrapolated these observations across seven stream networks with contrasting catchment structure and compared them to

hillslope and riparian chemical source water separations to address the following questions:

1. What is the effect of HRS connectivity duration on the degree of turnover of water and solutes in riparian zones?
2. How does landscape structure influence stream network hydrologic dynamics and the timing and amount of hillslope and riparian source waters detected at the catchment outlet?

#### Chapter 4

Stream DOC dynamics during snowmelt have been the focus of much research, and numerous DOC mobilization and delivery mechanisms have been proposed. However, landscape structure controls on DOC export from riparian and hillslope landscape source areas remains poorly understood. This lack of understanding represents a significant knowledge gap since DOC export can represent a large fraction of the carbon cycle. In chapter 4 we investigated the effect of catchment structure and hydrologic connectivity on the spatial and temporal variability of stream DOC export during snowmelt. We analyzed stream and groundwater dynamics across three transects and seven of the TCEF catchments to address the following questions:

1. What are the relative contributions of DOC from riparian and hillslope source areas during snowmelt?
2. How does the spatial extent and frequency of DOC source areas impact DOC export at the catchment scale?

## Chapter 5

Hydrologic investigations have been conducted across diverse research catchments and have identified numerous controls on runoff generation, including topography, soil distributions, vegetation, and geology. However, few studies have investigated the hierarchy and intersection of these mediating variables through space and time across structurally diverse, but adjacent catchments. In chapter 5 we sought to provide some insight into the complex way in which catchment characteristics such as topography, vegetation, and geology can affect hydrological connectivity, water redistribution-storage, and resultant runoff dynamics. We combined high frequency, spatially distributed observations of HRS shallow groundwater connectivity and runoff dynamics with landscape analysis of HRS connectivity. HRS connectivity observations were extrapolated across 11 stream networks with contrasting topography, geology, and land cover-vegetation characteristics and compared to runoff dynamics at each catchment outlet to address the following questions:

1. How does the distribution of stream network HRS connectivity relate to runoff observed at each catchment outlet?
2. What factors contribute to temporal differences in the connectivity yield observed across the 11 catchments?

## Chapter 6

Chapter 6 describes a new method developed by Thomas Grabs for deriving terrain indices that represent catchment hydrological and chemical processes. Typical landscape analysis approaches in GIS software packages do not differentiate between left

and right sides of stream networks when calculating terrain indices (Figure 1). This distinction is important because water and solute dynamics can be drastically different on either side of the stream according to differences in hillslope and riparian topography and topology. A new algorithm (SIDE; Stream Index Division Equations) is presented in this paper. Its utility for describing HRS connectivity and riparian buffering was demonstrated for the TCEF. The SIDE methodology was applied within the analyses of chapters 2, 3, and 5 and was therefore fundamental to the understanding developed throughout this dissertation.

### Chapter 7

Chapter 7 provides a brief summary of the main findings of each chapter of this dissertation, addresses their implications, and offers recommendations for future catchment hydrology studies. Integration of these chapters herein provides a synthesis of some of the primary controls on catchment hydrology and solute response in headwater catchments. The research described in this dissertation highlights terrain metrics that link hydrologic process observations to landscape and catchment scale response. This approach discretizes the catchments into its component landscape elements and analyzes their topographic and topologic attributes as surrogates for their hydrologic connectedness, as measured through detailed, physically based, field observations.

References Cited

- Anderson, M. G., and T. P. Burt (1978), The role of topography in controlling throughflow generation, *Earth Surfaces Processes and Landforms*, 3, 331-334.
- Beven, K. J. (1978), The hydrological response of headwater and sideslope areas, *Hydrological Sciences Bulletin*, 23, 419-437.
- Burns, D. A., P. S. Murdoch, G. B. Lawrence, and R. L. Michel (1998), Effect of groundwater springs on NO<sub>3</sub><sup>-</sup> concentrations during summer in Catskill Mountain streams, *Water Resources Research*, 34(8), 1987-1996.
- Burt, T. P., L. S. Matchett, K. W. T. Goulding, C. P. Webster, and N. E. Haycock (1999), Denitrification in riparian buffer zones: the role of floodplain hydrology, *Hydrological Processes*, 13(10), 1451-1463.
- Burt, T. P., and D. Butcher (1985), Topographic controls on soil moisture distribution, *Journal of Soil Science*, 36, 469-476.
- Buttle, J. M., P. J. Dillon, and G. R. Eerkes (2004), Hydrologic coupling of slopes, riparian zones and streams: an example from the Canadian Shield, *Journal of Hydrology*, 287(1-4), 161-177. 10.1016/j.jhydrol.2003.09.022|ISSN 0022-1694
- Buttle, J. M., S. W. Lister, and A. R. Hill (2001), Controls on runoff components on a forested slope and implications for N transport, *Hydrological Processes*, 15, 1065-1070.
- Carlyle, G. C., and A. R. Hill (2001), Groundwater phosphate dynamics in a river riparian zone: effects of hydrologic flowpaths, lithology, and redox chemistry., *Journal of Hydrology*, 247, 151-168.
- Cirimo, C. P., and J. J. McDonnell (1997), Linking the hydrologic and biochemical controls of nitrogen transport in near-stream zones of temperate-forested catchments: A review, *Journal of Hydrology*, 199(1-2), 88-120.
- Creed, I. F., L. E. Band, N. W. Foster, I. K. Morrison, J. A. Nicolson, R. S. Semkin, and D. S. Jeffries (1996), Regulation of nitrate-N release from temperate forests: A test of the N flushing hypothesis, *Water Resources Research*, 32(11), 3337-3354.
- Devito, K., I. Creed, T. Gan, C. Mendoza, R. Petrone, U. Silins, and B. Smerdon (2005), A framework for broad-scale classification of hydrologic response units on the

Boreal Plain: is topography the last thing to consider?, *Hydrological Processes*, 19(8), 1705-1714. 10.1002/hyp.5881

- Dunne, T., and R. D. Black (1970), Partial area contributions to storm runoff in a small New England watershed., *Water Resources Research*, 6(5), 1296-1311.
- Farnes, P. E., R. C. Shearer, W. W. McCaughey, and K. J. Hansen (1995), Comparisons of Hydrology, Geology, and Physical Characteristics Between Tenderfoot Creek Experimental Forest (East Side) Montana, and Coram Experimental Forest (West Side) Montana, 19 pp, USDA Forest Service, Intermountain Research Station, Forestry Sciences Laboratory, Bozeman, MT.
- Grabs, T., K.G. Jencso , B.L. McGlynn, J. Seibert (2010), Calculating terrain indices along streams - a new method for separating stream sides. *Water Resources Research*.
- Harr, R. D. (1977), Water flux in soil and subsoil on a steep forested slope., *Journal of Hydrology*, 33, 37-58.
- Hewlett, J. D., and A. R. Hibbert (1967), Factors affecting the response of small watersheds to precipitation in humid areas., in *Forest Hydrology*., edited by W. E. Sopper and H. W. Lull, pp. 275-291, Pergamon Press, New York.
- Hill, A. R. (2000), Stream chemistry and riparian zones In *Streams and Groundwaters*, in *Streams and Ground Waters*, edited by J. Jones and P. J. Mulholland, pp. 83-110, Academic Press, London.
- Holdorf, H. D. (1981), Soil Resource Inventory, Lewis and Clark National Forest Interim In-Service Report, On file with the Lewis and Clark National Forest, Forest Supervisor's Office, Great Falls, MT.
- Huff, D. D., R. V. Oneill, W. R. Emanuel, J. W. Elwood, and J. D. Newbold (1982), Flow variability and hillslope hydrology, *Earth Surface Processes and Landforms*, 7(1), 91-94.
- Ivanov, V. Y., R. L. Bras, and E. R. Vivoni (2008b), Vegetation-hydrology dynamics in complex terrain of semiarid areas: 2. Energy-water controls of vegetation spatiotemporal dynamics and topographic niches of favorability, *Water Resources Research*, 44(3), 20. W0343010.1029/2006wr005595
- Peters, D. L., J. M. Buttle, C. H. Taylor, and B. D. LaZerte (1995), Runoff production in a forested, shallow soil, Canadian Shield basin, *Water Resources Research*, 31(5), 1291-1304.

- McGlynn, B. L., and J. J. McDonnell (2003a), Role of discrete landscape units in controlling catchment dissolved organic carbon dynamics, *Water Resources Research*, 39(4). 1090
- McGlynn, B. L., and J. J. McDonnell (2003b), Quantifying the relative contributions of riparian and hillslope zones to catchment runoff, *Water Resources Research*, 39(11), 20. 131010.1029/2003wr002091
- McGlynn, B. L., and J. Seibert (2003), Distributed assessment of contributing area and riparian buffering along stream networks, *Water Resour. Res.*, 39(4), 1082. 10.1029/2002wr001521
- McGlynn, B. L., J. J. McDonnell, J. B. Shanley, and C. Kendall (1999), Riparian zone flowpath dynamics during snowmelt in a small headwater catchment, *Journal of Hydrology*, 222(1-4), 75-92.
- McGlynn, B. L., J. J. McDonnell, J. Seibert, and C. Kendall (2004), Scale effects on headwater catchment runoff timing, flow sources, and groundwater-streamflow relations, *Water Resources Research*, 40(7). W07504
- McGuire, K. J., J. J. McDonnell, M. Weiler, C. Kendall, B. L. McGlynn, J. M. Welker, and J. Seibert (2005), The role of topography on catchment-scale water residence time, *Water Resour. Res.*, 41(5), W05002. 10.1029/2004wr003657
- Mincemoyer, S. A., and J. L. Birdsall (2006), Vascular flora of the Tenderfoot Creek Experimental, Little Belt Mountains, Montana, *MADRONO*, 53(3), 211-222.
- Ocampo, C. J., M. Sivapalan, and C. Oldham (2006), Hydrological connectivity of upland-riparian zones in agricultural catchments: Implications for runoff generation and nitrate transport, *Journal of Hydrology*, 331(3-4), 643-658. 10.1016/j.jhydrol.2006.06.010
- Reynolds, M. (1995), Geology of Tenderfoot Creek Experimental Forest, Little Belt Mountains, Meagher County, Montana, in *Hydrologic and Geologic Characteristics of Tenderfoot Creek Experimental Forest, Montana, Final Rep. RJVA-INT-92734*, edited by P. Farnes, Intermt. Res. Stn., For. Serv., U.S. Dep. of Agric., Bozeman, Mont.
- Schmidt, W. C., J. L. Friede, and Compilers (1996), Experimental forests, ranges and watersheds in the Northern Rocky Mountains: a compendium of outdoor laboratories in Utah, Idaho and Montana, U.S. Department of Agriculture, Forest Service, Ogden, UT

- Shaman, J., M. Stieglitz, and D. Burns (2004), Are big basins just the sum of small catchments?, *Hydrological Processes*, 18, 3195-3206.
- Sidele, R. C., Y. Tsuboyama, S. Noguchi, I. Hosoda, M. Fujieda, and T. Shimizu (2000), Stormflow generation in steep forested headwaters: a linked hydrogeomorphic paradigm, *Hydrological Processes*, 14(3), 369-385.
- Soulsby, C., D. Tetzlaff, P. Rodgers, S. Dunn, and S. Waldron (2006), Runoff processes, stream water residence times and controlling landscape characteristics in a mesoscale catchment: An initial evaluation, *Journal of Hydrology*, 325(1-4), 197-221. 10.1016/j.jhydrol.2005.10.024
- Stieglitz, M., J. Shaman, J. McNamara, V. Engel, J. Shanley, and G. W. Kling (2003), An approach to understanding hydrologic connectivity on the hillslope and the implications for nutrient transport, *Global Biogeochemical Cycles*, 17(4), 1105
- Tetzlaff, D., J. Seibert, K. J. McGuire, H. Laudon, D. A. Burns, S. M. Dunn, and C. Soulsby (2009), How does landscape structure influence catchment transit time across different geomorphic provinces?, *Hydrological Processes*, 23(6), 945-953. 10.1002/hyp.7240
- Uchida, T., Y. Asano, Y. Onda, and S. Miyata (2005), Are headwaters just the sum of hillslopes?, *Hydrological Processes*, 19(16), 3251-3261. 10.1002/hyp.6004
- Vidon, P. G. F., and A. R. Hill (2004), Landscape controls on the hydrology of stream riparian zones, *Journal of Hydrology*, 292(1-4), 210-228. 10.1016/j.jhydrol.2004.01.005
- Wolock, D. M., J. Fan, and G. B. Lawrence (1997), Effects of basin size on low-flow stream chemistry and subsurface contact time in the Neversink River watershed, New York., *Hydrological Processes*, 11, 1273-1286.

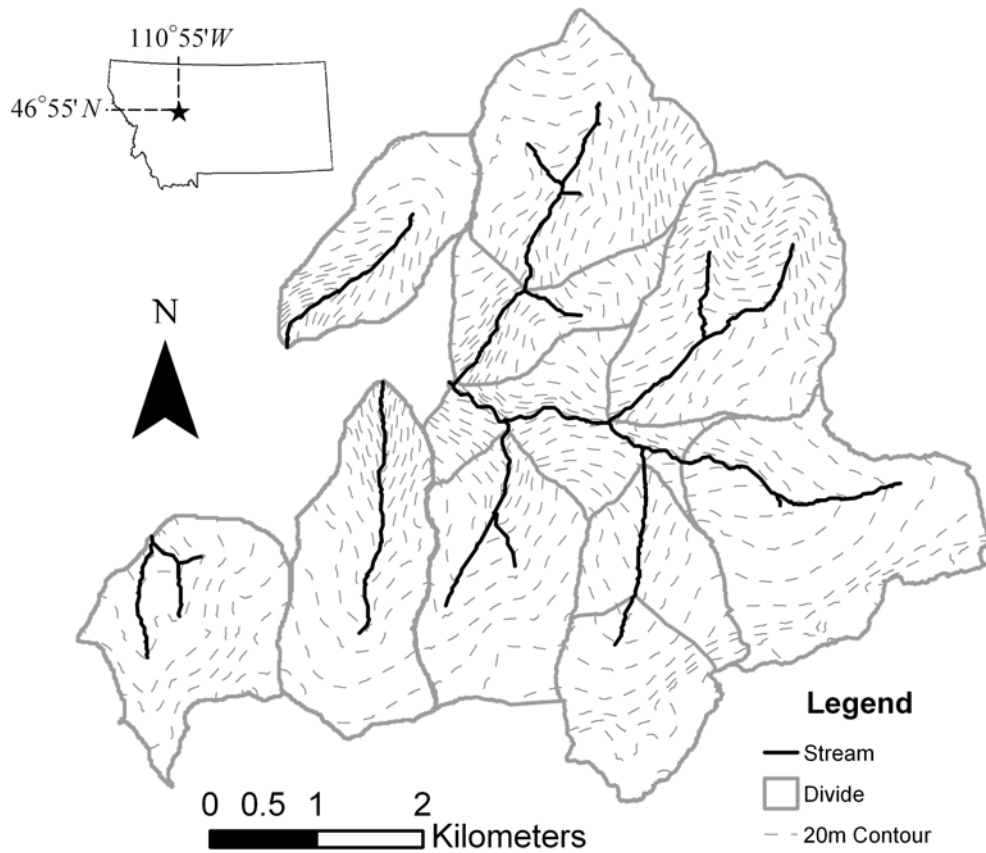
Figures

Figure 1: The Tenderfoot Creek Experimental Forest (TCEF). TCEF is located in the Rocky Mountains of Montana. Tenderfoot Creek forms the headwaters of the Smith River, a tributary of the Missouri River. Catchments within the TCEF encompass a range of topography, geology, and vegetative characteristics. This makes the TCEF an ideal site for studies of catchment structural controls on water quality and quantity.

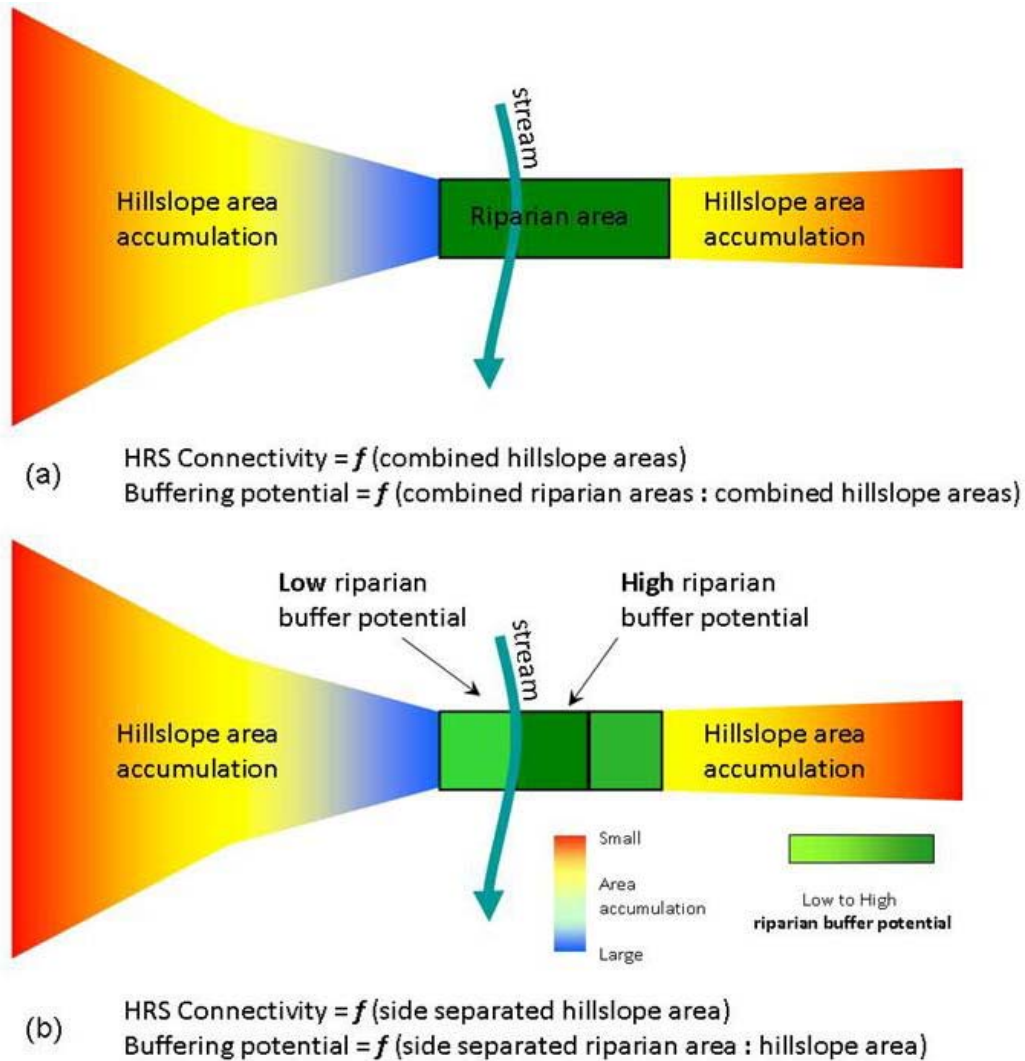


Figure 2: Landscape analysis framework. (a) The landscape analysis method outlined by McGlynn and Seibert [2003]. Potential hydrologic connectivity and riparian buffering are represented by total hillslope area and total hillslope and riparian area ratios respectively [McGlynn and Seibert, 2003]. (b) A refined method whereby hillslope and riparian area are separated according to their respective left and right stream sides. This provides a context for more accurate and distributed assessments of HRS hydrologic connectivity and riparian buffering.

Contribution of Authors

Chapter 2: Hydrologic connectivity between landscapes and streams: Transferring reach- and plot-scale understanding to the catchment scale

First author: Kelsey G. Jencso

Co-authors: Brian L. McGlynn, Michael N. Gooseff, Steven M. Wondzell, Kenneth E. Bencala, and Lucy A. Marshall

Contributions: I was responsible for all field instrumentation and data collection, figure development and the majority of data analysis and writing of this paper. Brian McGlynn contributed significant critique and ideas for development of intellectual content within the paper, and edited the original and final versions of the manuscript. Mike Gooseff, Steve Wondzell, Kenneth Bencala, and Lucy Marshall provided technical and collaborative discussions throughout the papers development and edited the final version of the manuscript.

Manuscript Information

Jencso, K. G., B. L. McGlynn, M. N. Gooseff, S. M. Wondzell, K. E. Bencala, and L.A. Marshall. 2009. Hydrologic connectivity between landscapes and streams: Transferring reach and plot scale understanding to the catchment scale, *Water Resources Research*. doi:10.1029/2008WR007225.

- Journal: Water Resources Research
- Status of manuscript (check one)
  - Prepared for submission to a peer-reviewed journal
  - Officially submitted to a peer-reviewed journal
  - Accepted by a peer-reviewed journal
  - Published in a peer-reviewed journal
- Publisher: American Geophysical Union
- Date of submission: June 13, 2008
- Date manuscript was published: April 29, 2009
- Issue in which manuscript appeared: Volume 45, WO4428

Reproduced by kind permission of the American Geophysical Union



## Hydrologic connectivity between landscapes and streams: Transferring reach- and plot-scale understanding to the catchment scale

Kelsey G. Jencso,<sup>1</sup> Brian L. McGlynn,<sup>1</sup> Michael N. Gooseff,<sup>2</sup> Steven M. Wondzell,<sup>3</sup> Kenneth E. Bencala,<sup>4</sup> and Lucy A. Marshall<sup>1</sup>

Received 13 June 2008; revised 4 November 2008; accepted 9 February 2009; published 29 April 2009.

[1] The relationship between catchment structure and runoff characteristics is poorly understood. In steep headwater catchments with shallow soils the accumulation of hillslope area (upslope accumulated area (UAA)) is a hypothesized first-order control on the distribution of soil water and groundwater. Hillslope-riparian water table connectivity represents the linkage between the dominant catchment landscape elements (hillslopes and riparian zones) and the channel network. Hydrologic connectivity between hillslope-riparian-stream (HRS) landscape elements is heterogeneous in space and often temporally transient. We sought to test the relationship between UAA and the existence and longevity of HRS shallow groundwater connectivity. We quantified water table connectivity based on 84 recording wells distributed across 24 HRS transects within the Tenderfoot Creek Experimental Forest (U.S. Forest Service), northern Rocky Mountains, Montana. Correlations were observed between the longevity of HRS water table connectivity and the size of each transect's UAA ( $r^2 = 0.91$ ). We applied this relationship to the entire stream network to quantify landscape-scale connectivity through time and ascertain its relationship to catchment-scale runoff dynamics. We found that the shape of the estimated annual landscape connectivity duration curve was highly related to the catchment flow duration curve ( $r^2 = 0.95$ ). This research suggests internal catchment landscape structure (topography and topology) as a first-order control on runoff source area and whole catchment response characteristics.

**Citation:** Jencso, K. G., B. L. McGlynn, M. N. Gooseff, S. M. Wondzell, K. E. Bencala, and L. A. Marshall (2009), Hydrologic connectivity between landscapes and streams: Transferring reach- and plot-scale understanding to the catchment scale, *Water Resour. Res.*, 45, W04428, doi:10.1029/2008WR007225.

### 1. Introduction

[2] Transferring plot and reach-scale hydrologic understanding to the catchment scale and elucidating the link between catchment structure and runoff response remains a challenge. En route to addressing this dilemma many recent advances in catchment hydrology have focused on the discretization, function, and connection of catchment landscape elements according to their topographic [Welsch *et al.*, 2001; Seibert and McGlynn, 2007], hydrologic [McGlynn *et al.*, 2004], and hydrochemical [Covino and McGlynn, 2007] attributes. In steep mountain catchments with relatively uniform soil depths and organized drainages, dominant landscape elements can often be reduced to hillslope, riparian, and stream zones. Hydrologic connections between

hillslope-riparian-stream (HRS) zones occur when water table continuity develops across their interfaces and stream-flow is present.

[3] Development of water table connectivity between riparian and hillslope zones has been associated with threshold behavior in catchment-scale runoff production [Devito *et al.*, 1996; Sidle *et al.*, 2000; Buttle *et al.*, 2004], mechanisms of rapid delivery of pre-event water [McGlynn *et al.*, 2002; McGlynn and McDonnell, 2003b], dissolved carbon dynamics [McGlynn and McDonnell, 2003a] and nutrient transport [Creed *et al.*, 1996; Vidon and Hill, 2004], at various timescales. Identifying the spatial and temporal hydrologic connectivity of runoff source areas within a catchment is an important step in understanding how landscape level hydrologic dynamics lead to whole catchment hydrologic and solute response.

[4] In forested mountain landscapes hillslopes comprise the major landscape element. Hillslope soils are often shallow and located on moderate to steep slopes. Hillslopes typically have relatively low antecedent wetness due to their steep slopes and well drained soils. During periods of high wetness hillslope soils can be highly transmissive and contribute significant quantities of water to near stream areas and the stream network [Peters *et al.*, 1995; McGlynn and McDonnell, 2003b]. This hydrologic connectivity is

<sup>1</sup>Department of Land Resources and Environmental Sciences, Montana State University, Bozeman, Montana, USA.

<sup>2</sup>Department of Civil and Environmental Engineering, Pennsylvania State University, University Park, Pennsylvania, USA.

<sup>3</sup>Olympia Forestry Sciences Laboratory, Pacific Northwest Research Station, U.S. Forest Service, Olympia, Washington, USA.

<sup>4</sup>U.S. Geological Survey, Menlo Park, California, USA.

requisite for the flushing of solutes and nutrients downslope through the riparian zone to the stream [Creed *et al.*, 1996; Buttle *et al.*, 2001; Stieglitz *et al.*, 2003].

[5] Riparian zones (near stream areas) are located between the hillslope and stream interfaces, in topographic lows, often at the base of organized hillslope drainages and can remain at or near saturation with minor to modest water table fluctuations in the upper soil profile. Characteristics of riparian zones often include anoxic conditions, high organic matter content, and low hydraulic conductivity associated with the predominance of organic, silt and clay sized particles. These characteristics lead to potential buffering of hillslope inputs of water [McGlynn *et al.*, 1999; McGlynn and Seibert, 2003] and nutrients [Burt *et al.*, 1999; Hill, 2000; Carlyle and Hill, 2001; McGlynn and McDonnell, 2003a] to streams.

[6] At the plot scale, it has been shown that hillslope and riparian elements can exhibit independent water table dynamics, characteristic of each landscape element [Seibert *et al.*, 2003; Ocampo *et al.*, 2006]. These investigations demonstrated that the steady state assumption of uniform groundwater rise and fall across the landscape is often unrealistic. Timing differences between hillslope and riparian water table dynamics were attributed to different antecedent soil moisture deficits and drainage characteristics.

[7] Research at the catchment scale has also cited water table connectivity between riparian and hillslope landscape elements as a first-order control on solute and runoff response. McGlynn *et al.* [2004] related riparian water table dynamics, hillslope runoff contributions, and total runoff in five nested catchments to landscape topography and the organization of hillslope and riparian landscape elements. Increasing synchronicity of runoff and solute response across scales was attributed to increasing antecedent wetness, event size, and the resulting increased riparian-hillslope landscape hydrologic connectivity.

[8] These previous studies highlight the importance of HRS connectivity for the explanation and prediction of hydrologic response. However, they lacked either spatial or temporal coverage, thus providing little insight into spatiotemporal upland to stream connectivity and its controlling variables. A framework combining high-frequency, spatially distributed, source area connectivity observations along with a metric of their important hydrogeomorphic attributes is needed to link internal source area response to runoff dynamics as measured at the catchment outlet.

[9] In steep mountain catchments topographic convergence and divergence and the accumulation of contributing area are considered important hydrogeomorphic controls on the conductance of subsurface water from hillslopes to riparian and stream zones [Freeze, 1972]. Many of the formative hillslope hydrology studies [Hewlett and Hibbert, 1967; Dunne and Black, 1970; Harr, 1977; Anderson and Burt, 1978; Beven, 1978] observed increased subsurface water accumulation in areas with topographically convergent hillslopes and higher upslope accumulated area (UAA). Upslope accumulated area is the area of land draining to a particular point in the landscape and has also been referred to as local contributing area. While topographically convergent areas often exhibit higher UAA, the same UAA magnitude is possible with a range of upslope morphologies or shapes (degrees of convergence and divergence).

[10] We sought to investigate the hydrogeomorphic controls on HRS hydrologic connectivity, their spatial and temporal distributions, and their implications for catchment-scale runoff generation. We combined digital elevation model (DEM) based terrain analyses with high-frequency water table measurements across 24 HRS transitions at catchment scales ranging from 0.4 to 17.2 km<sup>2</sup> to address the following questions: (1) Does the size of hillslope UAA explain the development and persistence of HRS water table connectivity? (2) Can topographic analysis be implemented to scale observed transect HRS hydrologic connections to the stream network and catchment scales? (3) How do spatial patterns and frequency of landscape hydrologic connectivity relate to catchment runoff dynamics? We present a framework for quantifying the spatial distribution of runoff source areas and exploring the spatially explicit links between source area connectivity and runoff generation.

## 2. Site Description

[11] This study was conducted in the Tenderfoot Creek Experimental Forest (TCEF) (lat. 46.55°N, long. 110.52°W), located in the Little Belt Mountains of the Lewis and Clark National Forest in Central Montana (Figure 1). The research area consists of seven gauged catchments that form the headwaters of Tenderfoot Creek (22.8 km<sup>2</sup>), which drains into the Smith River, a tributary of the Missouri River.

[12] The climate of the Little Belt Mountains is continental with occasional Pacific maritime influence along the Continental Divide. Annual precipitation averages 840 mm. Monthly precipitation generally peaks in December or January (100 to 120 mm per month) and declines to a late July through October dry period (45 to 55 mm per month). Approximately 75% of the annual precipitation falls during November through May, predominantly as snow. During the study period (1 October 2006 to 1 October 2007), 845 mm of precipitation was recorded; 688 mm as snow and 157 mm as rain. Peak runoff typically occurs in late May or early June and is generated by snowmelt or rain on snow events. Lowest flows occur from August through the winter months.

[13] Upland areas of the experimental forest are dominated by lodgepole pine. Sedges (*Carex* spp.) and rushes (*Juncaceae* spp.) dominate riparian vegetation in headwater areas with fine silt and clay textured soils and where water tables are generally near the surface. Willows (*Salix* spp.) dominate riparian areas where water tables are deeper and soils are coarsely textured.

[14] The seven TCEF gauged subcatchment areas range in size from 3 to 22.8 km<sup>2</sup>. Catchment headwater zones are typified by moderately sloping (average slope ~8°) extensive (up to 1200 m long) hillslopes and variable width riparian zones. Treeless parks are prominent at the headwaters of each catchment. Approaching the main stem of Tenderfoot Creek the streams become more incised, hillslopes become shorter (<500 m) and steeper (average slope ~20°), and riparian areas narrow relative to the catchment headwaters.

[15] Major soil groups in the TCEF are loamy Typic Cryochrepts located along hillslope positions and clayey Aquic Cryoboralfs in riparian zones and parks [Holdorf, 1981]. Riparian soils are 0.5–2.0 m deep, dark colored clay loams and gravelly loams high in organic matter.

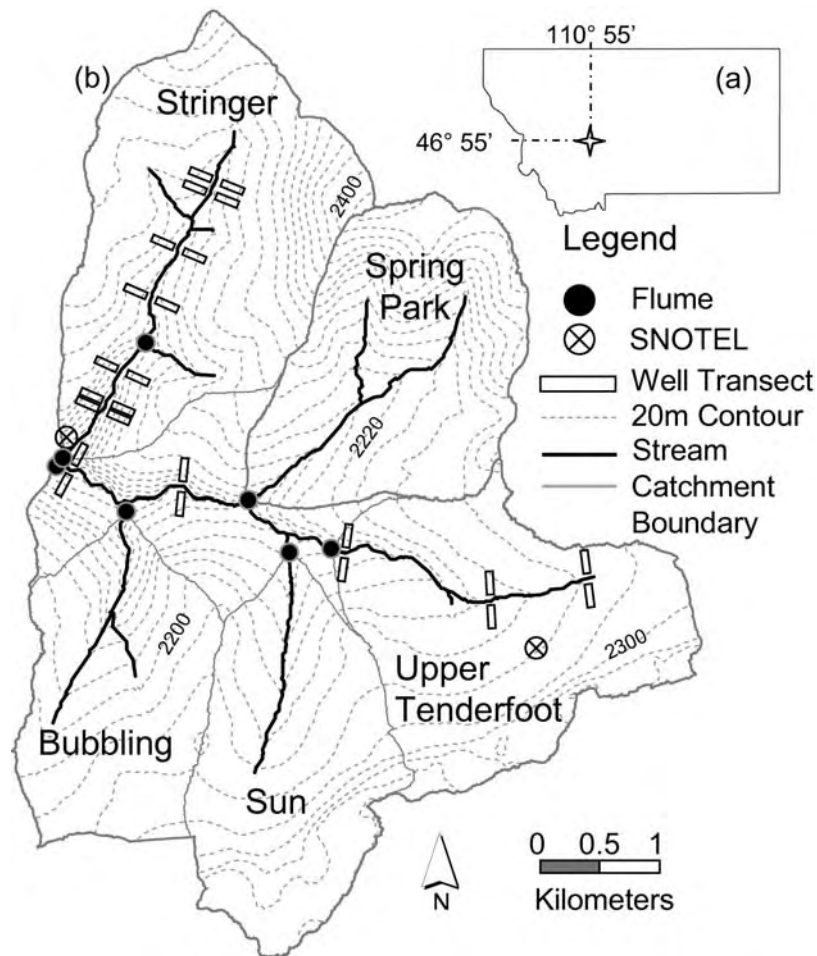


**Figure 1.** Site location and instrumentation of the Tenderfoot Creek Experimental Forest (TCEF) catchment. (a) Catchment location in the Rocky Mountains, Montana. (b) Catchment flumes, well transects, and SNOTEL instrumentation locations. Transect extents are not drawn to scale.

[16] The parent material consists of igneous intrusive sills of quartz porphyry, Wolsey shales, Flathead quartzite and granite gneiss [Farnes *et al.*, 1995]. Basement rocks of granite gneiss occur at lower elevations and are frequently seen as exposed, steep cliffs and talus slopes depending on landscape position. Flathead sandstone overlies the gneiss in mid catchment positions, followed by Wolsey shale and gentler slopes in headwater areas.

[17] Historic records dating from 1996 to the present are available for climatologic and hydrologic variables, courtesy of United States Forest Service (USFS) instrumentation. Two snow survey telemetry (SNOTEL) stations located in TCEF (Onion Park, 2259 m, and Stringer Creek, 1996 m) record real-time data on snow depth, snow water equivalent, precipitation, radiation, and wind speed. Hydrologic monitoring of the Experimental Forest includes seven flumes and one weir for eight gauged catchments where continuous streamflow is measured with stream level recorders (Figure 1).

[18] TCEF is an ideal site for the development of new techniques for linking landscape characteristics to water table and runoff response because it includes numerous catchments with a full range of upslope extents and degrees of topographic divergence and convergence. Topography is characterized by few sinks (i.e., digital elevation model

(DEM) grid cell with no neighboring cells with lower elevations than itself) and a clear distinction between hillslope and riparian landscape elements. Soil depths are relatively consistent across hillslope (0.5–1.0 m) and riparian (1–2.0 m) zones with localized upland areas of deeper soils. In addition, the abundance of existing infrastructure and historic data provide a wealth of information regarding past hydrologic response to climatic variables.

### 3. Methods

#### 3.1. Landscape Analysis

[19] We selected 24 hillslope-riparian-stream transects based on preliminary terrain analysis of a coarse 30 m USGS DEM, later refined with 1 m resolution airborne laser swath mapping (ALSM) data (courtesy of the National Center for Airborne Laser Mapping-NCALM). Upstream contributing areas at each transect (watershed areas) ranged from 0.41 to 17.2 km<sup>2</sup>, each composed of a range of hillslope and riparian UAA, as well as slope, aspect, and other terrain variables. We installed control points along Stringer and Tenderfoot Creek and at all flume locations with a Trimble survey grade GPS 5700 receiver operating in “fast static mode”. All GPS control points were accurate to

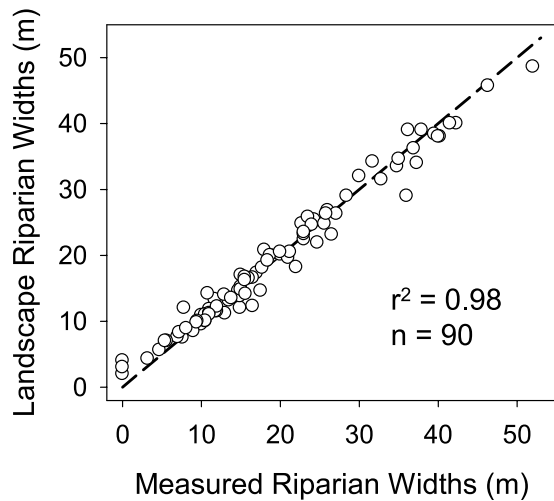


**Figure 2.** Measured versus terrain analysis derived riparian widths. The dashed line is the 1:1 line. The slope of the regression was 0.93, and the y intercept was 1.4 m.

within 1–5 cm. From these control points we performed surveys of Stringer and Tenderfoot Creek thalwegs, flume locations at each subcatchment outlet, well locations along each transect, and riparian zone extents. Survey data was corroborated with the ALSM derived DEM.

[20] The TCEF stream network, riparian areas, hillslope areas, and terrain indices were delineated using ALSM DEMs at 1, 3, 5, 10, and 30 m grid cell resolutions. ALSM elevation measurements were achieved at a horizontal sampling interval of the order  $<1$  m, with vertical accuracies of  $\pm 0.05$  to  $\pm 0.15$  m. ALSM data provided a detailed,  $1 \times 1$  m grid cell DEM.

[21] Quantification of each transect's hillslope and riparian UAA followed landscape analysis methods developed by *Seibert and McGlynn* [2007]. The first step in this landscape analysis approach was to compute the stream network from the DEM using a creek threshold area method corroborated with field reconnaissance. Depending on the time of year (spring snowmelt versus summer base flow) many of the stream heads in TCEF shift in location along the channel. The creek threshold initiation area was estimated as 40 ha based on field surveys of channel initiation points in TCEF. Channel initiation points were identified with morphological indicators (scoured streambeds, defined banks, and incisions into the ground surface) set forth by *Dietrich and Dunne* [1993].

[22] UAA for each stream cell, or the lateral area flowing into the stream network, was calculated using a triangular multiple flow-direction algorithm ( $MD_{\infty}$ ) [*Seibert and McGlynn*, 2007]. Once the accumulated area exceeded the 40 ha threshold value, it was routed downslope as “creek area” and all cells along the downslope flow path were labeled “creek cells”. The UAA measurements for each transect's hillslope were taken at the toe-slope (transition from hillslope to riparian zone) well position. Additional coverages generated from the base DEM were local inflows of UAA to each stream cell separated into contributions from each side of the stream (T. Grabs et al., manuscript in preparation, 2009), the topographic index [*Beven and Kirkby*, 1979], and catchment area at each stream cell.

[23] The TCEF riparian areas were mapped using a DEM analysis threshold method, whereby all accumulated area less than two meters in elevation above the stream cell it flows into was designated as riparian area. To compare the 2 m threshold landscape analysis derived riparian widths to actual riparian widths at TCEF, we surveyed 90 riparian cross sections in Stringer Creek, Spring Park Creek, and Tenderfoot Creek. Riparian-hillslope boundaries were determined in the field based on breaks in slope, soil characteristics (i.e., gleying, organic accumulation, color, and texture), and terrain characteristics. A regression relationship ( $r^2 = 0.97$ ) corroborated our terrain based riparian mapping (Figure 2).

### 3.2. Hydrometric Monitoring

[24] We recorded liquid precipitation at 15 min intervals with tipping bucket rain gauges (Texas Electronics 525MM-L, 0.1 mm increments). Rain gauges were installed at ST1, ST4, and a riparian eddy-covariance tower near ST2. Additional hourly precipitation measurements were obtained from gauges at National Resources Conservation Service SNOTEL stations located near the Lower Stringer flume (1996 m) and near (2259 m) the headwaters of Tenderfoot Creek. SNOTEL measurements were also used for hourly measurements of snow depth and snow water equivalent. Runoff was measured for each of seven gauged catchments using three H-flumes and four Parshall flumes. Stage at each flume was recorded at 30 min intervals with float potentiometers (USFS) and TruTrack, Inc., water level capacitance rods ( $\pm 1$  mm resolution).

### 3.3. Hillslope-Riparian Shallow Water Table Measurements

[25] We monitored 24 transect locations, located along 12 stream network positions, spanning a range of hillslope and riparian slope and UAA combinations (landscape element assemblages). Individual transects reflect the respective difference in UAA inputs and riparian widths on either side of the stream. UAA inflows and riparian extents on each side of the stream were independent of one another due to differential convergence and divergence of catchment topography and hillslope lengths (T. Grabs et al., manuscript in preparation, 2009). Fourteen transects were installed along Stringer Creek (Figure 1) and ten were installed along Tenderfoot Creek (Figure 1). Transects along Stringer Creek are referred to as ST1 through 7, followed by an E (east) or W (west) and those along Tenderfoot Creek are referred to as TFT1 through 5, followed by an N (north) or S (south). In all cases, transects are numbered sequentially, with 1 designating the most upstream transect.

[26] Transects consisted of three to six wells (84 total) located on the lower hillslope (1–5 m above the break in slope), toe-slope (the break in slope from riparian to hillslope zones), and riparian zone (1 m from stream channel), along groundwater flow paths to the stream. Additional riparian wells were installed 5–10 m upstream of the riparian and toeslope wells to ascertain the direction of groundwater flow and shifts in direction during events using 3-point triangulation of total potential gradients. Wells consisted of 1.5 inch diameter PVC conduit screened across the completion depth to 10 cm below the ground surface. Completion depths to bedrock ranged from 0.8 to 1.5 m on hillslopes to 1–2.0 m in the riparian zones. These comple-

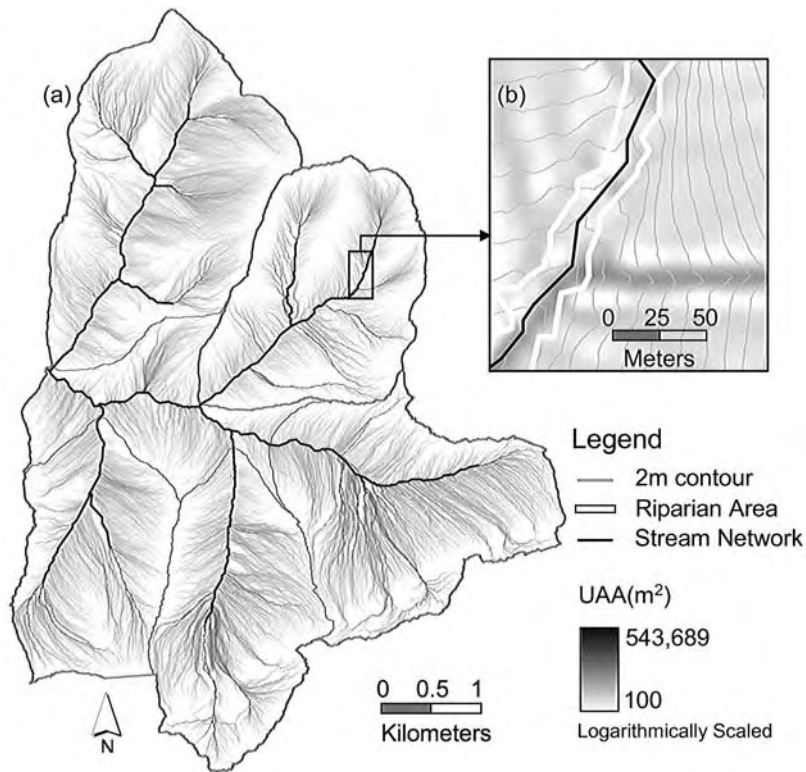


**Figure 3.** TCEF. (a) Upslope accumulated area (UAA) for each pixel and (b) an example riparian area extent derived from terrain analysis.

tion depths are corroborated by  $\sim 12$  soil pits excavated to bedrock and 100s of soil probe depth measurements across hillslope to riparian transitions. Wells were installed with a solid steel rod inserted into the PVC casing. The rod and well casing were driven until refusal at the bed rock boundary and the rod removed. A clay seal and small mound derived from local materials was applied to prevent surface water intrusion. Well water levels were recorded at 30 min intervals with TruTrack, Inc., capacitance rods. Complementary water level measurements were collected weekly using an electric water level tape to corroborate capacitance rod measures.

[27] Hydrologic connectivity between HRS zones was inferred from the presence of saturation measured in well transects spanning the hillslope, toeslope, and riparian positions. We define a hillslope-riparian-stream connection as a time interval during which streamflow occurred and both the riparian and adjacent hillslope wells recorded water levels above bedrock. We do not discern between the mechanisms responsible for water table development and HRS water table connectivity, rather if, when, and for how long water table connectivity was present.

## 4. Results

### 4.1. Landscape Analysis

[28] We resampled the original 1 m DEM to determine the DEM cell size that was most robust for relating water table dynamics and UAA. The 1 m ALSM derived DEM was sampled discretely to obtain 3, 5, 10 and 30 m cell size DEMs. When implementing the flow accumulation/UAA algorithms, the 3 m and 5 m DEMs appeared more

susceptible to micro topographic influences such as fallen trees, boulders, etc., which exert negligible control on subsurface water redistribution. Conversely, the 30 m grid size was too coarse to reflect slope breaks between riparian and hillslope transitions and observed convergence and divergence in upland areas. The 10 m DEM provided a realistic representation of the topography, reflecting convergence and divergence and providing the most robust relation to water table dynamics observed across all 24 well transects (Figure 3). Tables 1 and 2 summarize subcatchment area, hillslope UAA (measured at each transects toe-slope well location), riparian widths, and the slope and soil depths of hillslope and riparian zones for transects located in the Stringer and Tenderfoot Creek catchments, respectively.

### 4.2. Snowmelt and Precipitation Characterization

[29] We present snow accumulation and melt data from the Upper Tenderfoot Creek (relatively flat  $0^\circ$  aspect, elevation 2259 m) SNOTEL site (Figure 4). Rainfall data are presented from the Stringer Transect 1 rain gauge (elevation 2169 m). During the base flow observation period (1 October 2006 to 27 April 2007), snow fall increased the snowpack snow water equivalent (SWE) to a maximum of 358 mm. Twenty-two minor melt events, ranging from 5 to 10 mm, occurred during this base flow period. Springtime warming lead to an isothermal snowpack and most of the snowpack melted between 27 April 2007 and 19 May 2007. Average daily SWE losses were 15 mm and reached a maximum of 35 mm on 13 May 2007. A final spring snow fall and subsequent melt occurred between 24 May 2007 and 1 June 2007, yielding 97 mm of water. Four days following the end of snowmelt, the rain period was

**Table 1.** Tenderfoot Creek Transect Characteristics

| Transect | Catchment Area (km <sup>2</sup> ) | UAA (m <sup>2</sup> ) | Riparian Width (m) | Hillslope (deg slope) | Riparian (deg slope) | Hillslope Soil Depth (m) | Riparian Soil Depth (m) | HRS Connectivity (% of year) |
|----------|-----------------------------------|-----------------------|--------------------|-----------------------|----------------------|--------------------------|-------------------------|------------------------------|
| TFT1N    | 0.42                              | 8,151                 | 8                  | 5.5                   | 3.3                  | 1.0–1.10                 | 1.20–1.50               | 27                           |
| TFT1S    | 0.42                              | 11,152                | 12                 | 3.6                   | 2.8                  | 1.0–1.10                 | 0.80–1.0                | 22                           |
| TFT2N    | 1.37                              | 5,044                 | 3.8                | 4.8                   | 2.3                  | 0.90–1.20                | 0.95–1.0                | 24                           |
| TFT2S    | 1.37                              | 32,111                | 19.6               | 5.8                   | 1.8                  | 0.75–2.50                | 1.0–1.45                | 61                           |
| TFT3N    | 4.33                              | 2,367                 | 8.5                | 17.7                  | 2.2                  | 0.60–0.85                | 0.60–1.20               | 0                            |
| TFT3S    | 4.33                              | 7,070                 | 7.2                | 23                    | 9.5                  | 0.90–1.0                 | 0.70–1.20               | 15                           |
| TFT4N    | 13.16                             | 25,753                | 9.3                | 22                    | 7.7                  | 0.20–0.55                | 0.70–0.85               | 40                           |
| TFT4S    | 13.16                             | 1,186                 | 4.4                | 42                    | 2.9                  | 0.60–1.0                 | 0.50–0.75               | 0                            |
| TFT5N    | 17.21                             | 1,527                 | 9.1                | 26                    | 5.2                  | 0.60–0.75                | 0.70–0.85               | 4                            |
| TFT5S    | 17.21                             | 7,842                 | 2.9                | 37                    | 6.8                  | 0.20–0.50                | 0.55–0.75               | 7                            |

initiated with a series of low-intensity rain storms (4–7 June 2007 and 13–18 June 2007), totaling 30 and 22 mm respectively. Following this rain period the recessional period began. Precipitation inputs during the recession period were minor, except for one summer thunderstorm on 26 July 2007 yielding 34 mm of rain over a 7 h period. Total precipitation inputs (snowmelt and rain) to the TCEF catchment over the course of the 2007 water year totaled 845 mm.

#### 4.3. Detailed Description of HRS Water Table Response Dynamics

[30] Detailed results for a subset of transects characteristic of the primary HRS landscape assemblages found within TCEF, their associated water table responses, and their hydrologic connectivity frequency and duration are presented in Appendix A and illustrated in Figure 5.

#### 4.4. Summary of HRS Water Table Dynamics and Connections According to UAA

[31] The 24 transects of HRS assemblages demonstrated clear differences in groundwater connectivity as a function of their UAA size (Figure 6). While this relationship is continuous, we describe three general UAA typologies to emphasize the degree to which the range of transects exhibited a hydrologic connection. Transects with small

UAA (699–3869 m<sup>2</sup>) generally exhibited no HRS connection or a rapid and transient connection during large events (Figures 5i, 5k, 5p, 6x, and Figure 6a). When the time of their connectivity was summed for the 2007 water year these transects were connected no longer than 14% of the water year. Excluding ST2E which exhibited a 14% connection with only 3000 m<sup>2</sup> UAA, the small sized UAA transects remained connected for only up to 4% of the water year, primarily during peak snowmelt and rain event periods.

[32] Transects with UAA size ranging from 4900–32,100 m<sup>2</sup> generally exhibited a more sustained hydrologic connectivity during large snowmelt and rain events (Figures 5a, 5f, 5n, 5s, and Figure 6b). Transient connectivity was observed for these midranged areas during base flow or recession periods in response to isolated snowmelt or rain events. Annual connectivity ranged from 3 to 61% of the water year, primarily during the snowmelt and recession periods when larger UAA transects reflected persistent water tables from drainage of their extensive upslope areas.

[33] Two transects, ST2W and ST5W, were installed with UAA sizes of 44,395 and 46,112 m<sup>2</sup>, respectively. These transects exhibited continuous HRS connectivity (Figure 5u and Figure 6c). Though HRS connections were not measured for areas with UAA above 46,000 m<sup>2</sup>, there are TCEF catchment locations with larger sized UAA. Visual obser-

**Table 2.** Stringer Creek Transect Characteristics

| Transect | Catchment Area (km <sup>2</sup> ) | UAA (m <sup>2</sup> ) | Riparian Width (m) | Hillslope (deg slope) | Riparian (deg slope) | Hillslope Soil Depth (m) | Riparian Soil Depth (m) | HRS Connectivity (% of year) |
|----------|-----------------------------------|-----------------------|--------------------|-----------------------|----------------------|--------------------------|-------------------------|------------------------------|
| ST1W     | 1.26                              | 1,563                 | 12.7               | 12.5                  | 4.2                  | 0.80–0.95                | 0.60–1.0                | 0                            |
| ST1E     | 1.26                              | 10,165                | 11.8               | 15.6                  | 5.9                  | 0.60–1.30                | 0.60–1.05               | 8                            |
| ST2W     | 1.39                              | 44,395                | 21                 | 8.6                   | 6                    | 0.70–1.20                | 0.70–2.0                | 100                          |
| ST2E     | 1.39                              | 3,000                 | 8.3                | 18.15                 | 6.2                  | 0.95–1.30                | 1.0–1.50                | 14                           |
| ST3W     | 2.98                              | 3,869                 | 11.7               | 19.6                  | 2.9                  | 1.0–1.35                 | 0.50–1.0                | 2                            |
| ST3E     | 2.98                              | 3,029                 | 6.5                | 19.8                  | 2                    | 0.80–1.40                | 1.0–1.30                | 2                            |
| ST4W     | 3.59                              | 699                   | 4.7                | 22                    | 7.5                  | 0.80–1.0                 | 0.95–1.0                | 0                            |
| ST4E     | 3.59                              | 4,930                 | 9.9                | 21                    | 8                    | 0.60–1.40                | 1.0–1.15                | 19                           |
| ST5W     | 4.80                              | 46,112                | 16.5               | 20.8                  | 5.07                 | 0.90–1.0                 | 0.70–1.80               | 100                          |
| ST5E     | 4.80                              | 1,923                 | 7.7                | 26                    | 7                    | 0.90–1.40                | 1.0–1.50                | 3                            |
| ST6W     | 5.17                              | 6,176                 | 9.7                | 21                    | 6.9                  | 0.80–1.0                 | 1.10–1.35               | 7                            |
| ST6E     | 5.17                              | 3,287                 | 4.5                | 36                    | 10.3                 | 1.0–1.50                 | 0.65–1.0                | 0                            |
| ST7W     | 5.27                              | 6,201                 | 9                  | 27                    | 7.5                  | 0.90–1.10                | 0.80–1.10               | 3                            |
| ST7E     | 5.27                              | 9,854                 | 8.8                | 28                    | 7.4                  | 0.90–1.0                 | 1.10–1.40               | 10                           |

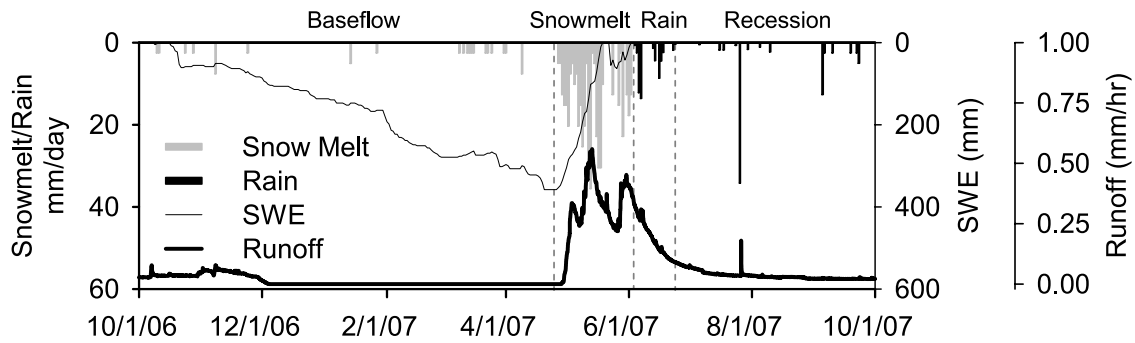


**Figure 4.** Snow and rainwater inputs, snow water equivalent (SWE), and runoff separated into base flow, snowmelt, rain, and recession observation periods.

vations along these extensive, highly convergent hillslopes and headwater areas, confirmed the presence of near surface water tables above the break in slope as well as surface saturated conditions year-round in their associated riparian zones.

[34] The timing of the connection and disconnection of HRS zones also varied according to UAA. Transects with midrange UAA lagged the transient hillslope responses of low UAA transects during early snowmelt, but were more sustained once a hillslope water table was established (Figures 6a and 6b).

#### 4.5. Scaling Source Area Connectivity to an Entire Stream Network

[35] Patterns across transects indicated a strong UAA influence on the timing and persistence of connectivity between streams and their associated riparian and hillslope zones. To further explore the UAA-connectivity duration relationship we regressed the total time each HRS transect was connected during the 2007 water year against the size of UAA at their hillslope to riparian transition. The duration of HRS water table connectivity was highly correlated ( $r^2 = 0.91$ ) to the size of each transects UAA (Figure 7; equation (1)):

$$\%TimeConnected = (0.00002 * UAA - 0.0216) * 100. \quad (1)$$

We also tested the topographic index [Beven and Kirkby, 1979] but did not find improved explanatory power ( $r^2 = 0.84$ ).

[36] We applied equation (1) to all of the UAA inflows along the entire Tenderfoot Creek stream network to assess catchment-scale connectivity distributions and elucidate their implications for catchment-scale hydrologic response. Lateral inflows of UAA for each stream cell were separated into their component left and right side UAAs using an algorithm developed by T. Grabs et al. (manuscript in preparation, 2009). HRS water table connectivity was heterogeneous from reach to reach along Tenderfoot Creek according to the location of UAA inputs (Figure 8). The majority (70%) of the stream network comprises small UAAs in the size range of 0 to 5000 m<sup>2</sup> (Figure 9a). HRS connectivity for these areas was estimated between 0 to 8% of the year. Medium ranged UAA reaches (5,000–30,000 m<sup>2</sup>) composed ~25% (Figure 9a) of the network and were estimated connected between 8 and 62% of the year. The remaining 5% of the stream network included

large headwater areas and convergent hillslope hollows with UAA in the size range of 30,000 to ~75,000 m<sup>2</sup> (Figure 9a). These UAA sizes were estimated to be connected for 62 to 100% of the year.

[37] We compared Tenderfoot Creek's connectivity duration curve (CDC) to the catchment annual flow duration curve (FDC) to assess how HRS connectivity was related to catchment level hydrologic response (Figures 9b and 10a and 10b). The FDC was derived from 8762 hourly observations of runoff at the Lower Tenderfoot flume for the 2007 water year. The CDC was derived from the combined 10 m left and right stream bank frequencies (3108 10 m cells) of HRS connectivity for the 2007 water year (equation (1)).

[38] The CDC and FDC for Tenderfoot Creek were highly correlated (Figures 9b and 10a), suggesting a relationship between the amount of the stream network connected to its uplands and streamflow magnitude. While the annual regression was strong ( $r^2 = 0.95$  Figure 10a), we also investigated the regression relationships for each of three flow states (base flow, transition, and wet) and found differential predictive power in each period (Figure 10b). Approximately 55% of the year during the driest periods (fall and winter base flow) the lowest runoff values 0.015–0.03 mm/h were associated with the lowest amount (<4%) of HRS connectivity across the stream network. During the transition from dry to wet times (~35% of the year) more HRS assemblages became connected and runoff increased to 0.10 mm/h. Divergence between the CDC and FDC was greatest during this transitional period. The FDC showed a sharp increase at 0.06 mm/h runoff while the CDC increased gradually. Peak snowmelt and large rain events (~10% of the time) resulted in the highest network connectivity (up to 67%) which was associated with peak runoff up to a maximum of 0.54 mm/h and close correspondence between the FDC and CDC.

## 5. Discussion

[39] Streams, riparian zones, and hillslopes have been intensively studied at small spatial scales (stream reaches < 1 km, plots of 10–100 m<sup>2</sup>). At the other end of the spectrum, entire catchments have been studied without explicit understanding of how their internal landscape hydrologic processes are distributed, interact, or integrate across the stream network to produce whole watershed behavior. This has resulted in detailed plot and reach-specific process understanding with little transferability

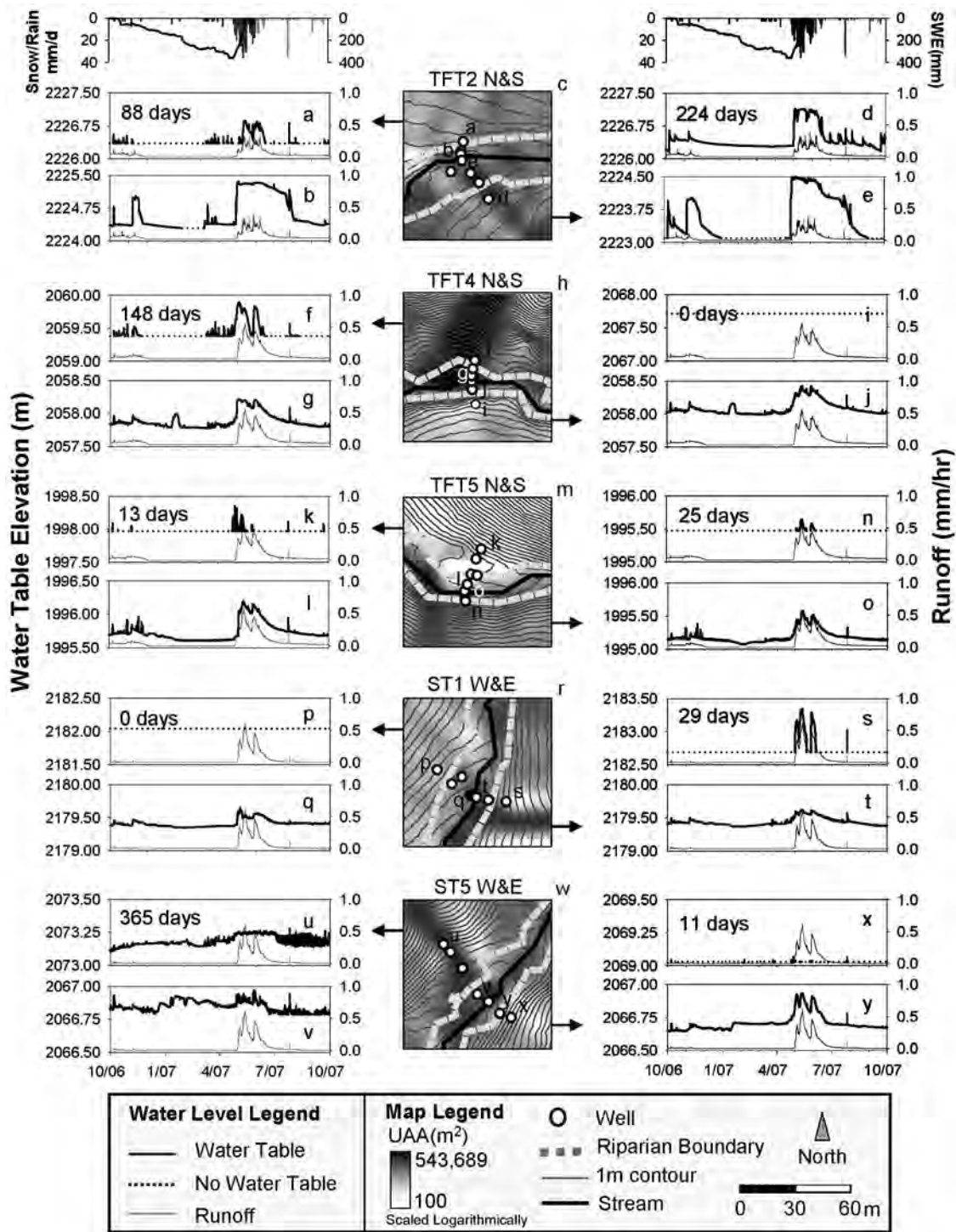


**Figure 5.** Transect hillslope and riparian water table and runoff dynamics. Runoff for each transect was obtained from the nearest flume location. The total time of HRS connectivity (days) is listed on the upper left corner of each hillslope time series. Maps are each transect's UAA, riparian extents, and well locations. Letters on the map designate the location of hillslope and riparian well where water table dynamics were measured.

within a given catchment, to other catchments, or to development of general principles. We utilized an extensive well network across 24 HRS transects and catchment sizes from 0.4 to 23 km<sup>2</sup> to develop methods to scale plot-scale measurements of the hydrologic processes that link hillslopes and riparian areas to whole catchments and transfer

our understanding to larger portions of the landscape. Our analyses included landscape level topographic analysis, process-based field investigations, and catchment-scale integration to identify the factors controlling the hydrologic connectivity between source areas generating runoff and the flow paths that link source areas to streams.

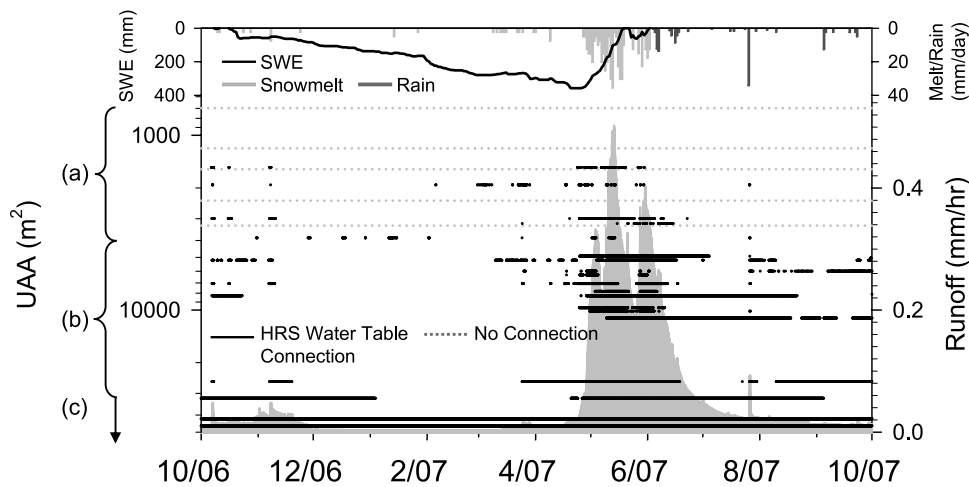


**Figure 6.** Binary summary of 24 transects of hillslope-riparian-stream water table connectivity dynamics for the 2007 water year. (a) Small UAA exhibits a transient connection or no connection. (b) Midrange UAA exhibits a sustained connection during large snowmelt and rain events and a transient connection during periods of low antecedent wetness. (c) Large UAA exhibits a continuous connection.

### 5.1. Does the Size of Hillslope UAA Explain the Development and Persistence of HRS Water Table Connectivity?

[40] Landscape assemblages exhibit different hydrologic thresholds depending on event size, antecedent moisture conditions, surface and bedrock topography [Freer *et al.*, 1997; Sidle *et al.*, 2000; McGlynn *et al.*, 2004] and distance from the stream [Seibert *et al.*, 2003]. This heterogeneity in space and time has previously hampered watershed-scale understanding. Once heterogeneity is integrated over sufficiently large spatial and temporal extents, however, emergent behavior may become apparent. Our high-frequency continuous observations of 24 transects of water level data indicated that the location, duration, and timing of hillslope water table development and its connectivity to the stream was controlled by the magnitude of UAA measured at each transects toe-slope well.

[41] The relationship between UAA and HRS hydrologic connectivity is evident in the duration of connectivity at each transect. Hillslope water levels never existed or were transient (Figure 6a) along transects with small UAAs. Figures 5k and 5x indicate that even during peak snowmelt, when soil wetness was at its annual maxima, only a brief water table response, on the order of hours to days, occurred along hillslope landscape elements with low UAA. The hillslope water table quickly subsided after this period of maximum wetness. We attribute transient connectivity in transects with small UAA to the limited accumulation of contributing area (and therefore water) along their downslope flow paths.

[42] Convergence of subsurface water into hillslope zones with medium to large UAA caused a sustained water table response at the base of hillslopes (Figures 5a, 5d, 5f, 5s, and 5u). Once HRS connectivity was established, lateral slope drainage, and periodic rejuvenation of hillslope soil moisture from events sustained the larger UAA hillslope water tables and the resulting HRS water table connection. In some cases the connection lasted from snowmelt well into the recession period. The two transects possessing the

largest hillslope UAA inflows, ST2W and ST5W, remained hydrologically connected for the entire year (Figures 5u and Figure 6c).

[43] Water table initiation, cessation, and duration varied between transects partially as a function of UAA size, however variance was observed between transects with comparable UAA (Figure 6). The duration of HRS connectivity for 8 of the 24 transects under observation fall outside of the 95% confidence limits of equation (1). These timing differences may be attributed to the geometry (curvature, slope, etc.) of the UAA which can affect the “time of concentration” of snowmelt inputs. In addition, differences

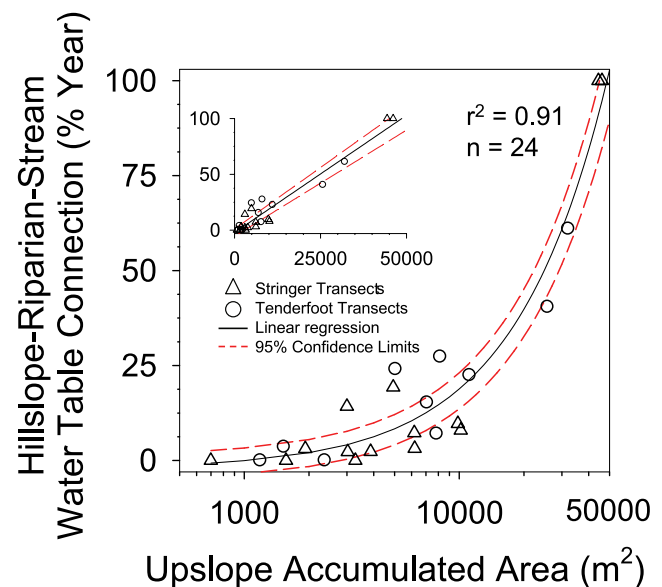


**Figure 7.** UAA regressed against the percentage of the water year that a hillslope-riparian-stream water table connection existed for 24 well transects. A connection was recorded when there was streamflow and water levels were recorded in both the riparian and hillslope wells. The inset plot shows the same data with a linear x axis.

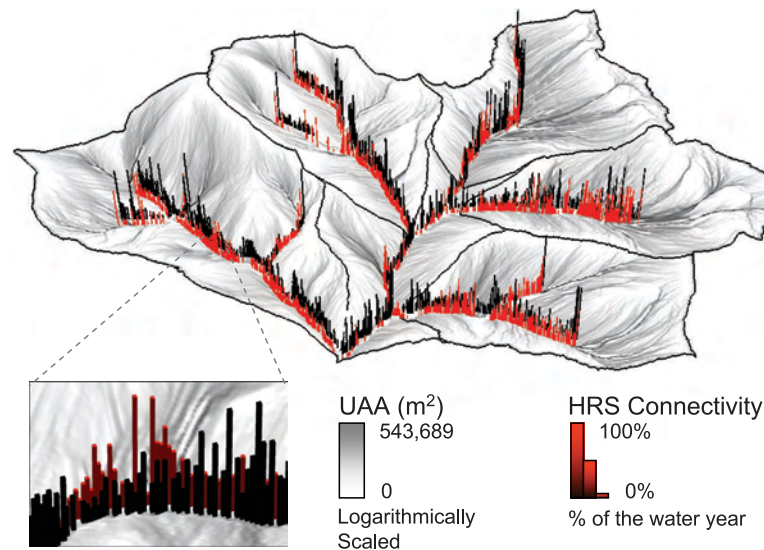


**Figure 8.** UAA flow accumulation patterns (shading) and the regression-derived hillslope-riparian-stream water table connectivity along the left (red bars) and right (black bars) sides of the Tenderfoot Creek network. Predicted hydrologic connectivity ranged from 0 to 100% of the year (represented by bar heights).

and combinations of aspect, precipitation/snowmelt variability, elevation, local soil and bedrock properties (including small differences in depth), vegetation, and antecedent wetness can all impact water table dynamics. Despite these differences, the overall response timing is coherent and suggests a strong UAA control on water table initiation, cessation, and duration across the TCEF catchment.

### 5.2. Can Topographic Analysis Be Implemented to Scale Observed Transect HRS Hydrologic Connections to the Stream Network and Catchment Scales?

[44] Analysis of our high-frequency measurements across 24 HRS assemblages indicated that the size of hillslope UAA controlled the development and persistence of HRS water table connectivity in TCEF. These results relating contrasting patterns of water table development to hillslope UAA size are consistent with past observations along individual landscape assemblages [Dunne and Black, 1970; Harr, 1977; Anderson and Burt, 1978] and hillslope trench sections [Woods and Rowe, 1996]. These prior observations were important for describing processes occurring at the plot scale, but they lacked a quantifiable framework, or relationship, for assessing the role of these source areas along the stream network and extrapolation to the catchment scale.

[45] When we regressed the duration of HRS connectivity for all 24 transects against their UAA size, the duration of landscape hydrologic connectedness was linearly related to the size of each transect's UAA (Figure 7). This relationship provided a framework for estimating the duration of connectivity of each landscape source area along the stream network. We applied equation (1) to the UAA flowing into each stream pixel across Tenderfoot Creek (separated into each side of the stream). This distributed measure of landscape connectivity provided insight into the spatially and temporally variable hydrologic connectivity that existed for each landscape assemblage along the stream network throughout the year (Figure 8).

[46] Network connectivity results for TCEF indicated that runoff source area contributions were driven by transient connectivity during the wettest time periods. A high proportion of the Tenderfoot Creek network is composed of hillslopes with small UAA sizes (Figure 9a). Few of these hillslopes were hydrologically connected to their riparian and stream zones. For example, during the entire 2007 water year, a maximum of 67% of the stream network actually exhibited HRS water table connectivity (Figure 9b). The remaining 33% of the stream network, associated with the smallest UAAs remained disconnected for the entire year. As catchment wetness increased during snowmelt, small and medium UAAs developed hillslope water tables and became hydrologically connected. Landscape assemblages with small UAA accrued limited water year connectivity (0–8%), and then only after snowmelt and large rain events, in accordance with their transient hillslope responses. Only 10% of the stream network, associated with the medium to high ranged UAA inflows (Figure 9b), exceeded a 30% water year HRS water table connection. Approximately 2% of the TCEF stream network remained hydrologically connected for the entire water year (Figure 9b). These stream segments were associated with hillslopes possessing the largest UAA.

### 5.3. How Do Spatial Patterns and Frequency of Landscape Hydrologic Connectivity Relate to Catchment Runoff Dynamics?

[47] The relationship between UAA and the duration of hillslope-riparian-stream water table connectivity was linear (Figure 7). However, the distribution of UAA sizes along the network was heterogeneous and highly nonlinear due to catchment structure and topographic convergence and divergence in the landscape (Figure 9a). Since UAA size controlled landscape level connectivity, the distribution of HRS connectivity across the stream network was also heterogeneous and nonlinear.

[48] We compared Tenderfoot Creek's frequency distribution of HRS connectivity (i.e., connectivity duration

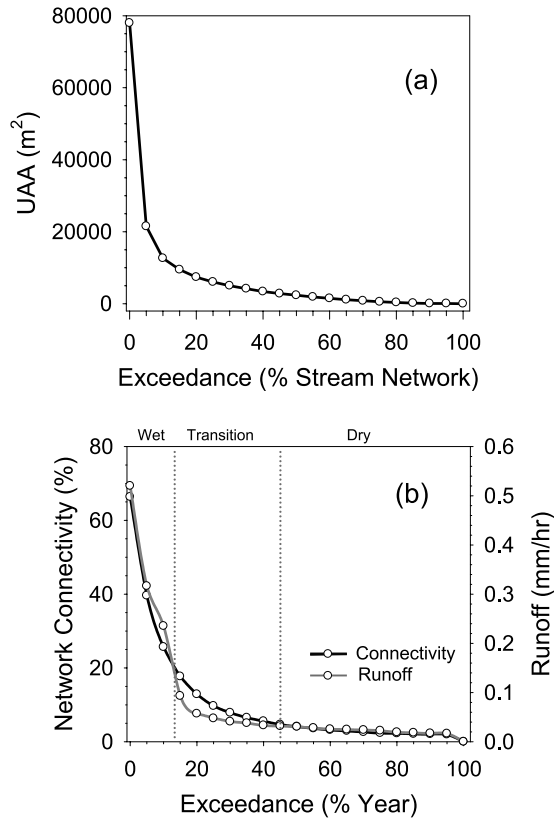


**Figure 9.** TCEF catchment. (a) UAA distribution curve based on 3108 10 m pixels along the stream network (both sides). (b) Comparison of the regression-derived connectivity duration curve (CDC) based on HRS water table connectivity for each 10 m UAA pixel along the stream network and the 2007 Lower Tenderfoot Creek flow duration curve (FDC). Periods of lowest runoff are associated with lowest network connectivity and large UAA values. Increased runoff is associated with increasing network connectivity from HRS connections at small UAA values.

curve, CDC) to its flow duration curve (FDC) to determine the relationship between network connectivity and the magnitude of catchment runoff through the year. The network CDC was strongly correlated ( $r^2 = 0.95$ ) to the FDC (Figure 10a) over the full range of catchment wetness states. This suggests that the shape of the FDC is controlled by the fraction of the stream network hydrologically connected to its uplands throughout the year.

[49] To elucidate potential differences across catchment wetness states, we subdivided the annual relationship into dry, transition, and wet periods and found different relationships between the CDC and FDC for each period ( $r^2 = 0.84$ , 0.9 and 0.99, respectively.) This suggests that while the annual relationship was strong, there was different predictive power during each period, improving with increasing wetness.

[50] Dry fall and winter periods (55% of the year) corresponded to the lowest runoff (0.03 mm/h) and the lowest amount (<4%) of the stream network connected to its uplands (Figure 9b). The relationship between the CDC and FDC distributions during drier base flow periods ( $r^2 = 0.84$ , Figure 10b) indicates that HRS connectivity is one source of base flow runoff. However, three points of the distribution fall outside of the 95% confidence intervals during this time period. Consideration of other mechanisms such as bedrock flow paths [Shaman *et al.*, 2004; Uchida *et al.*, 2005] could help explain base flow runoff generation when the catchment is in a dry state.

[51] A break in slope (inflection point) of the stream FDC at  $\sim 0.05$  mm/h corresponded to a paralleled increase in network connectivity (Figure 9b). These synchronous inflection points corresponded to early snowmelt and early summer dry-down which were the transition period between wet and dry catchment states. Greatest divergence in the FDC and CDC relationship was apparent during these transitions and may be related to the differential timing of water table connection-disconnection among areas with similar UAA sizes and riparian area saturation excess overland flow (Figures 9b and 10a). This divergence also corresponded to the region of the regression relationship (equation (1)) with the least robust model fit (Figure 7) Heterogeneity in slope, aspect, snowmelt timing, and soil

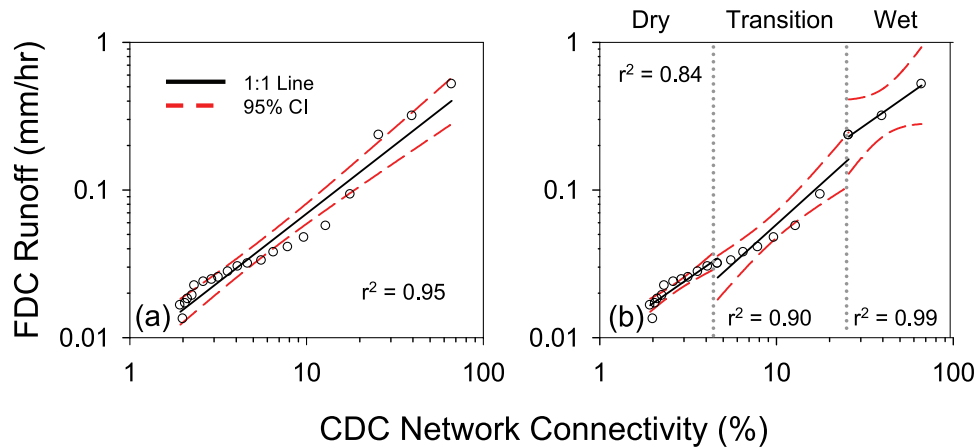


**Figure 10.** (a) Linear regression analysis between the estimated annual network CDC (3108 10 m pixels along both sides of the stream network) and the TCEF catchment FDC (8762 hourly measurements). (b) Linear regression for the same distributions separated into the dry, transitional, and wet catchment states. Each point represents 5% of the CDC and FDC distribution.

depth distributions would be most influential on the timing of HRS connectivity during transition periods and could explain some of the variability in the regression relationship. The correlation between the CDC and FDC (Figure 10b) improved (from  $r^2 = 0.84$  to  $r^2 = 0.90$ ) between the dry and transition periods. This improved correlation likely reflects increasing UAA/topographic controls on runoff production as the catchment became progressively wetter.

[52] During the wettest catchment states (snowmelt and the largest rain events), hillslopes associated with the smaller UAAs became hydrologically connected. The cumulative connections of small UAA coupled with previously connected medium and large UAAs, led to increasing network connectivity and subsequently larger magnitude runoff. During the highest flows (~10% of the year) up to 67% of the stream network was hydrologically connected to its uplands, resulting in peak runoff ranging from 0.24–0.54 mm/h (Figure 9b). The correlation between the CDC and FDC was also greatest during this time period ( $r^2 = 0.99$ ). This suggests that the use of topographic metrics such as UAA as a surrogate for the lateral redistribution of water and prediction of runoff generation may be most robust during wetter time periods.

[53] Discretization of the annual relationship between the CDC and the FDC into dry, transition, and wet catchment states suggest that the relationship is strongest during wet periods. However, despite differential relationships for each wetness state, the annual relationship was robust ( $r^2 = 0.95$ ) and suggests a single regression can explain most of the variability in the relationship between the CDC and FDC.

#### 5.4. Implications

[54] Our observations highlight the importance of understanding hydrologic connectivity and how it is distributed in space and time along the stream network. The relationship between the FDC and CDC indicated that the period of time riparian and stream zones remain connected to their hillslope elements is highly related to catchment-scale runoff response (Figure 10a). Simply stated, the fraction of the network connected to its uplands controls runoff magnitude. These observations have important implications for modeling of catchment response to precipitation inputs and interpreting local process observations in the context of catchment runoff.

[55] Typically models of catchment response are developed from a sparse number of observations at a few points. It is assumed that the processes that occur in these locations are representative of other catchment locations and reflect dominant controls on catchment runoff. Runoff mechanisms including transmissivity feedback [Kendall *et al.*, 1999], piston flow displacement [McGlynn and McDonnell, 2003a], interflow [Beven, 1989], macropore flow [McDonnell, 1990], etc., are often used to explain threshold stream responses not predicted by limited process observations. These mechanisms do occur in many catchments [McDonnell, 1990b; Buttle, 1994; Burns *et al.*, 1998, 2001] and models incorporating them are often successful for mimicking individual hydrographs. However, difficulties arise when trying to predict stream response to multiple events across varying catchment wetness states, testing internal catchment consistency with model assumptions, and extrapolating to larger catchment sizes. These difficulties are partially a result of poor understanding of the spatial

sources of runoff through time across varying catchment wetness states.

[56] We suggest an alternate process explanation for nonlinear runoff response, namely the spatiotemporal distribution of connectivity. Our observations indicate that each landscape assemblage along the stream network exhibits a distinct time period of water table connectivity strongly related to its UAA. During driest times the largest UAA HRS assemblages are the primary contributors to stream runoff. As the amount of snowmelt or precipitation inputs increase more of the stream network associated with smaller UAA HRS assemblages becomes “switched on”, and subsequently higher-magnitude runoff is generated. The magnitude of runoff is controlled by how many HRS assemblages along the stream network have reached their individual connectivity threshold, the duration of time they remain connected, and the amount of water flowing through them. These observed relationships suggest landscape structure (topography and topology) as a first-order control on runoff response characteristics.

[57] Given that at every point in time, a different fraction of the watershed is active in the runoff process (hydrologically connected via shallow groundwater to the stream channel); runoff biogeochemistry must also be interpreted in this context. We observed network connectivity ranging from ~4–67% of the stream network and suggest that biogeochemistry data interpretation and modeling should include appreciation of the dynamics of connectivity in space and time to attribute/represent appropriate causal mechanisms to runoff-biogeochemical observations. Hydrologic connectivity between catchment landscape elements is requisite for the retention or mobilization of dissolved organic carbon [Boyer *et al.*, 1997; McGlynn and McDonnell, 2003a], nutrients [Creed *et al.*, 1996; Vidon and Hill, 2004; Ocampo *et al.*, 2006] and other solutes [Wilson *et al.*, 1991; Burns *et al.*, 1998], to streams. For example, Boyer *et al.* [1997] demonstrated that the activation of shallow subsurface flow paths within the near stream saturated area was the dominant cause of DOC flushing in an alpine catchment. Implicit in this interpretation is lateral connectivity of the shallow groundwater flow paths that link the uplands and riparian areas to the stream network. The relationship between topographic metrics such as UAA and connectivity may provide a tool for identifying the location and duration of these lateral connections and testing their potential influence on stream water chemistry.

[58] The relationship between UAA and connectivity quantified in this study is likely nonstationary in time. The slope of the UAA:HRS water table connectivity relationship could increase or decrease between wet and dry years. However, the spatial pattern of connectivity is likely persistent due to the relatively static nature of landscape structure. This suggests that once a relationship is elucidated, fewer monitoring locations might be used to predict the slope of the UAA-connectivity duration relationship as a function of climatic variability. These results further suggest bidirectional prediction potential between the catchment flow duration curve and the catchment connectivity duration curve, providing a method for estimating network connectivity at a given runoff magnitude.

[59] This study is the first to identify relationships between catchment morphology and source area connectivity and

demonstrate how this integrated landscape-scale connectivity relates to the magnitude of catchment runoff. While the relationships between source area water table connectivity and whole catchment response have not previously been quantified, they are apparent in previous investigations relating the residence time of water to internal catchment structure [McGlynn *et al.*, 2003; McGuire *et al.*, 2005]. These studies found significant relationships for internal catchment topographic metrics including flow path length and gradient and median subcatchment area.

[60] Most studies seeking to link catchment topography to water redistribution have been conducted in headwater catchments sharing similar physical attributes: they tend to be located in steep mountainous landscapes; hillslope soils are shallow and underlain by relatively impervious bedrock; and valley-floor widths tend to be narrow relative to the width of the subtending catchment (i.e., Maimai, Hubbard Brook, Coweeta, HJ Andrews, etc.). The TCEF catchments compare favorably with these previous studies, suggesting that topographic control of whole catchment response may well be the norm in mountainous catchments.

[61] It remains an open question if topography or some other aspect of catchment structure will exert similarly strong control under other geomorphic and climatic conditions. For example, we could imagine that in areas with very low topographic relief, with deep soils and relatively shallow water tables, that precipitation inputs would percolate vertically through the soil profile until reaching the water table and the lateral redistribution of this water would then follow regional-scale groundwater flow paths. Under this scenario, groundwater inflows to stream would occur where ever stream channels intercept the regional water table so that runoff would not be strongly controlled by catchment topography. Conversely, even in areas of low topographic relief, during periods of high precipitation inputs (snowmelt season or large, long-duration rainstorms) some lateral redistribution of soil moisture occurs within the upper soil profile and would be affected by the topographic relations that we identify here. It is possible then, that some types of catchments might exhibit seasonal differences such that topography exerts primary control over catchment response during high flow but not during base flow [Grayson *et al.*, 1997; Western *et al.*, 1999]. Catchments underlain by highly fractured bedrock could also exhibit additional complexities and controls on water redistribution.

[62] More multiscale studies focused on landscape level hydrologic connectivity within a catchment-scale context, across a range of morphologic, climatic and topographic conditions, are needed to fully evaluate the relationships presented here. However, the relationships presented suggest that a measure of internal catchment topography and structure, easily measured from DEMs, may be used for a priori model development and prediction of hydrologic response. Measures of landscape element connectivity provide an integrated measure of hillslope process complexity and when integrated across the watershed provide a metric for prediction of runoff observed at the catchment outlet.

## 6. Conclusion

[63] How hillslope inputs along stream networks are linked to catchment-scale response has been poorly under-

stood. Often, research is conducted along a specific plot/stream reach or at a single catchment scale. The results have therefore been plot and reach specific conclusions with little transferability to other catchments or development of general principles. We developed a metric of hillslope-riparian-stream water table connectivity as an integrative measure of runoff source area contributions through time. We tested this metric across 24 hillslope-riparian-stream landscape assemblages for the 2007 water year. On the basis of analysis of our high-frequency, long-duration observations coupled within a landscape analysis framework we conclude:

[64] 1. The topographically driven lateral redistribution of water (as represented by UAA) controls upland-stream connectivity and transient connectivity drives runoff generation through time.

[65] 2. This emerging space-time behavior represents the relationship between landscape structure/topology and runoff dynamics.

[66] 3. Analysis of catchment structure provides a context for scaling source area dynamics to those observed at the catchment outlet and provides a framework for exploring the spatially explicit links between source area connectivity and runoff generation.

[67] 4. Bidirectional prediction (as evidenced by the CDC-FDC relationship) of runoff generation and source area dynamics may be possible through analysis of catchment structure and topology.

[68] We have presented a landscape analysis framework for identifying runoff source areas based on their topographic characteristics (UAA). Where hydrologic connectivity occurs and the duration of these connections across the catchment is critical to guiding model development and understanding the link between landscape structure and stream flow. Future endeavors incorporating landscape analysis may include application of the terrain-morphology connectivity relationship across a range of catchments with different morphologies and antecedent conditions. These relationships may also prove valuable for linking internal landscape structure to stream nutrient and chemical signatures.

## Appendix A: Detailed Description of HRS Water Table Response Dynamics

[69] We present detailed results for a subset of transects characteristic of the primary HRS landscape assemblages found within TCEF, their associated water table responses, and their hydrologic connectivity frequency and duration. These are: the headwaters of Upper Tenderfoot Creek (TFT2N and S), Middle Tenderfoot Creek (TFT4N and S), the outlet of Tenderfoot Creek (TFT5N and S), the headwaters of Stringer Creek (ST1E and W), and Middle Stringer Creek (ST5E and W).

### A1. Tenderfoot Transect 2 North

[70] TFT2N groundwater table dynamics exhibited responses typical of headwater catchment landscape assemblages with midrange hillslope UAA (5044 m<sup>2</sup>), minimal riparian area (3.8 m), and gentle (~4.8°) upland slopes (Figure 5c). Similar water table dynamics were

exhibited at TFT1N and TFT1S which have similar topographic and accumulated area characteristics (Table 1), 840 m upstream. Transient hillslope and riparian water table responses were observed during the base flow period in response to early snowmelt events (Figures 5a and 5b). Hillslope water levels at TFT2N were sustained for 41 days during the snowmelt period (Figure 5a). Throughout the recession period transient hillslope responses were observed for large rain events. At the onset of the snowmelt period the riparian water table rose 98 cm to the ground surface over a 3 day period (Figure 5b). The development of a riparian water table coincided with the emergence of streamflow at this headwater transect (visual observation). A sharp decrease in riparian water levels beginning on 8/9/07 also corresponded with the cessation of streamflow and a decrease of the hillslope water table at the adjacent TFT2S transect. HRS water table connectivity was observed for 24% of the year (88 days).

#### A2. Tenderfoot Transect 2 South

[71] TFT2S was located along a broad convergent hillslope (UAA = 32,111 m<sup>2</sup>) with low-angle hillslopes (~5.8°), and a 19.6 m wide riparian zone (Figure 5c). Stream and riparian water table dynamics were similar to those discussed for the TFT2N transect (Figure 5e). Hillslope water tables were observed for the entire water year (Figure 5d). During the base flow and recession periods hillslope water levels remained ~84 cm below the ground surface. Dynamic responses to individual rain events were observed during these time periods. At the onset of the snowmelt period water levels rose 85 cm to the ground surface. This rise coincided with the establishment of riparian water tables in both TFT2N and TFT2S and the initiation of streamflow (visual observation) at this transect. Following the rain period hillslope water levels declined to base flow levels. The timing of this decline was synchronous with a gradual decrease in riparian water levels and a decrease in runoff at the UTC flume 1500 m downstream. Though the hillslope well at this transect recorded water for the entire year, a HRS connection was only observed for 61% of the year (224 days).

#### A3. Tenderfoot Transect 4 North

[72] TFT4N was located along the main stem of Tenderfoot Creek near the base of a large convergent talus slope (UAA = 25,753 m<sup>2</sup>) with ~22° hillslopes and a 9.3 m wide riparian zone (Figure 5h). Soil (60 cm on hillslopes, 80 cm in riparian zones) was only present on the lower portions of the hillslope where the monitoring wells were installed. The riparian water table remained ~40 cm below the ground surface during base flow and recession periods and rose to the ground surface during snowmelt (Figure 5g). Hillslope responses to snowmelt and rain events during both the base flow and recession periods were rapid and transient (Figure 5f). At the onset of snowmelt, the hillslope water table developed (rising 50 cm from base flow conditions) 7 days before increased runoff was observed at the Lower Tenderfoot flume. Hillslope water levels were recorded from the late base flow period, through snowmelt, to the end of the

rain period. HRS connectivity was observed for 41% of the water year (147.6 days).

#### A4. Tenderfoot Transect 4 South

[73] TFT4S was selected as an end-member in the hillslope-riparian-stream continuum. Near the transects hillslope base, a ~42°, 10 m cliff effectively disconnected the small hillslope UAA (1,186) from its 4.4 m wide riparian zone below (Figure 5h). Riparian water level fluctuations mimicked those of streamflow measured at the LTC flume (Figure 5j) and the stream stage recorder located along this transect. No water was recorded in the hillslope well located near the precipice of the cliff approximately 10 m above the riparian zone (Figure 5i). Hillslope-riparian-stream water table connectivity was not observed at this transect location.

#### A5. Tenderfoot Transect 5 North

[74] TFT5N water table responses were typical of landscape positions with steep (~26°) divergent hillslopes, small UAA (1,527 m<sup>2</sup>), and moderately wide (9.1 m) talus abundant riparian zones (Figure 5m). Riparian water table dynamics were similar to the stream hydrograph as recorded at the Lower Tenderfoot Creek flume and rose to within 15 cm of the ground surface during snowmelt (Figure 5l). The hillslope water table responses to rain and snow events were rapid and transient (Figure 5k). Small, ~12 cm rises were observed during the early base flow period. At the onset of the snowmelt period, water tables were observed in the hillslope well 2 days before rises in the riparian and stream water levels. During peak snowmelt, progressive diurnal water table increases and subsequent decreases of up to 40 cm were observed. HRS connectivity was observed for 4% of the water year (13.2 days).

#### A6. Tenderfoot Transect 5 South

[75] TFT5S groundwater table dynamics exhibited responses characteristic of headwater catchment landscape positions with moderate hillslope UAA (7,842 m<sup>2</sup>), steep hillslopes (~37°), and small (2.9 m) riparian areas (Figure 5m). Riparian water table dynamics were synchronous with runoff, rising 40 cm up to the ground surface during snowmelt (Figure 5o). Hillslope water tables were observed only 10 days after substantial rises in the riparian water table during peak snowmelt and remained elevated for 26 days (Figure 5n). HRS connectivity was observed for 7% of the water year (25 days).

#### A7. Stringer Transect 1 West

[76] ST1W is situated along a planar hillslope, with diffuse inputs of UAA (Figure 5r). Water table responses were characteristic of landscape assemblages possessing low UAA (1563 m<sup>2</sup>), moderate riparian zones (12.7 m), and upland slopes (~12.5°). The riparian water table remained within 20 cm of the ground surface for the majority of the water year, with near surface saturation during snowmelt and rain events (Figure 5q). The adjacent hillslope remained disconnected for the entirety of the

study period (Figure 5p). HRS water table connectivity was not observed at this transect.

### A8. Stringer Transect 1 East

[77] Located near the base of a convergent hillslope hollow, ST1E (Figure 6r) groundwater dynamics exhibited responses typical of landscape positions with midrange UAA (10,165 m<sup>2</sup>), moderate riparian widths (11.8 m), and moderate upland slopes (~15.6°). Riparian zone water tables remained within 20 cm of the ground surface for the entire year with surface saturation during snowmelt and rain events (Figure 6t). A Hillslope water table was observed for the first time on 12 May 2006, exhibiting a rapid water table rise and sustained connection to its associated riparian zone (Figure 5s). These rapid water table rises and sustained HRS connections were observed during snowmelt (21 day connection) and the subsequent rain periods (8 day connection). A final connection was observed during the summer thunderstorm during the recession period. HRS water table connectivity was observed for 8% (29.2 days) of the water year at ST1E.

### A9. Stringer Transect 5 West

[78] ST5W is located at the base of a convergent hillslope (Figure 5w). It had the largest observed UAA (46,112 m<sup>2</sup>), a wide riparian zone (16.5 m) and ~20.5° hillslopes. The riparian zone exhibited a relatively constant water table approximately 65 cm below the ground surface but rose to within 12 cm of the ground surface during the snowmelt and rain periods (Figure 5v). Groundwater was recorded within 15 cm of the ground surface in the hillslope well, located 5 m upslope of the toeslope break, for the duration of the water year (Figure 5u). Surface saturation and return flow (visual observations) at the toeslope transition occurred during snowmelt and large rain events. HRS water table connectivity was observed for the entire year at ST5W.

### A10. Stringer Transect 5 East

[79] ST5E is located along a moderately steep (~26°), divergent hillslope (UAA = 1923 m<sup>2</sup>) with a 7.7 m wide riparian zone (Figure 5w). Riparian water levels remained between 80 and 60 cm below the ground surface throughout the year except during snowmelt when it rose to within 25 cm of the ground surface (Figure 5y). Hillslope water table responses to events were rapid and transient (Figure 5x). Water levels in the hillslope well were observed during the base flow period in response to minor snowmelt events. During peak snowmelt and the summer thunderstorm hillslope water tables of 2 to 10 cm were sustained for a maximum of two days. HRS connectivity was observed for 3% (11.2 days) of the water year.

[80] **Acknowledgments.** This work was made possible by NSF grant EAR-0337650 to McGlynn, EAR-0337781 to Gooseff, and an INRA fellowship awarded to Jencso. The authors appreciate extensive logistic collaboration with the USDA, Forest Service, Rocky Mountain Research Station, especially, Ward McCaughey, scientist-in-charge of the Tenderfoot Creek Experimental Forest. Airborne Laser Mapping was provided by the National Science Foundation supported Center for Airborne Laser Mapping (NCALM) at the University of California, Berkeley. We thank Jan Seibert and Thomas Grabs for technical and collaborative support. We are grateful

to Jennifer Jencso, Robert Payn, Vince Pacific, Diego Riveros-Iregui, Rebecca McNamara, and especially Austin Allen for invaluable assistance in the field.

## References

- Anderson, M. G., and T. P. Burt (1978), The role of topography in controlling throughflow generation, *Earth Surf. Processes Landforms*, 3, 331–334.
- Beven, K. J. (1978), The hydrological response of headwater and sideslope areas, *Hydrol. Sci. Bull.*, 23, 419–437.
- Beven, K. (1989), Interflow, in *Unsaturated Flow in Hydrologic Modeling Theory and Practice*, edited by H. J. Morel-Seyoux, pp. 191–219, Springer, New York.
- Beven, K. J., and M. J. Kirkby (1979), A physically based, variable contributing area model of basin hydrology, *Hydrol. Sci. J.*, 24, 43–69.
- Boyer, E. W., G. M. Hornberger, K. E. Bencala, and D. M. McKnight (1997), Response characteristics of DOC flushing in an alpine catchment, *Hydrol. Processes*, 11(12), 1635–1647, doi:10.1002/(SICI)1099-1085(19971015)11:12<1635::AID-HYP494>3.0.CO;2-H.
- Burns, D. A., R. P. Hooper, J. J. McDonnell, J. E. Freer, C. Kendall, and K. Beven (1998), Base cation concentrations in subsurface flow from a forested hillslope: The role of flushing frequency, *Water Resour. Res.*, 34(12), 3535–3544, doi:10.1029/98WR02450.
- Burns, D. A., J. J. McDonnell, R. P. Hooper, N. E. Peters, J. E. Freer, C. Kendall, and K. Beven (2001), Quantifying contributions to storm runoff through end-member mixing analysis and hydrologic measurements at the Panola Mountain Research Watershed (Georgia, USA), *Hydrol. Processes*, 15, 1903–1924, doi:10.1002/hyp.246.
- Burt, T. P., L. S. Matchett, K. W. T. Goulding, C. P. Webster, and N. E. Haycock (1999), Denitrification in riparian buffer zones: The role of floodplain hydrology, *Hydrol. Processes*, 13(10), 1451–1463, doi:10.1002/(SICI)1099-1085(199907)13:10<1451::AID-HYP822>3.0.CO;2-W.
- Buttle, J. M. (1994), Isotope hydrograph separations and rapid delivery of pre-event water from drainage basins, *Prog. Phys. Geogr.*, 18(1), 16–41, doi:10.1177/030913339401800102.
- Buttle, J. M., S. W. Lister, and A. R. Hill (2001), Controls on runoff components on a forested slope and implications for N transport, *Hydrol. Processes*, 15, 1065–1070, doi:10.1002/hyp.450.
- Buttle, J. M., P. J. Dillon, and G. R. Eerkes (2004), Hydrologic coupling of slopes, riparian zones and streams: An example from the Canadian Shield, *J. Hydrol.*, 287(1–4), 161–177, doi:10.1016/j.jhydrol.2003.09.022|ISSN 0022-1694.
- Carlyle, G. C., and A. R. Hill (2001), Groundwater phosphate dynamics in a river riparian zone: Effects of hydrologic flowpaths, lithology, and redox chemistry, *J. Hydrol.*, 247, 151–168, doi:10.1016/S0022-1694(01)00375-4.
- Covino, T. P., and B. L. McGlynn (2007), Stream gains and losses across a mountain-to-valley transition: Impacts on watershed hydrology and stream water chemistry, *Water Resour. Res.*, 43, W10431, doi:10.1029/2006WR005544.
- Creed, I. F., L. E. Band, N. W. Foster, I. K. Morrison, J. A. Nicolson, R. S. Semkin, and D. S. Jeffries (1996), Regulation of nitrate-N release from temperate forests: A test of the N flushing hypothesis, *Water Resour. Res.*, 32(11), 3337–3354, doi:10.1029/96WR02399.
- Devito, K. J., A. R. Hill, and N. Roulet (1996), Groundwater-surface water interactions in headwater forested wetlands of the Canadian Shield, *J. Hydrol.*, 181, 127–147, doi:10.1016/0022-1694(95)02912-5.
- Dietrich, W. E., and T. Dunne (1993), The channel head, in *Channel Network Hydrology*, edited by K. Beven and M. Kirkby, pp. 175–220, John Wiley, Chichester, UK.
- Dunne, T., and R. D. Black (1970), Partial area contributions to storm runoff in a small New England watershed, *Water Resour. Res.*, 6(5), 1296–1311, doi:10.1029/WR006i005p1296.
- Farnes, P. E., R. C. Shearer, W. W. McCaughey, and K. J. Hanson (1995), Comparisons of hydrology, geology and physical characteristics between Tenderfoot Creek Experimental Forest (East Side) Montana, and Coram Experimental Forest (West Side) Montana, *Final Rep. RJA-INT-92734*, 19 pp., For. Sci. Lab., USDA For. Serv. Intermountain Res. Stn., Bozeman, Mont.
- Freer, J., J. McDonnell, K. J. Beven, D. Brammer, R. P. Hooper, and C. Kendall (1997), Topographic controls on subsurface storm flow at the hillslope scale for two hydrologically distinct small catchments, *Hydrol. Processes*, 11, 1347–1352, doi:10.1002/(SICI)1099-1085(199707)11:9<1347::AID-HYP592>3.0.CO;2-R.

- Freeze, A. R. (1972), Role of subsurface flow in generating surface runoff: 2. Upstream source areas, *Water Resour. Res.*, 8(5), 1272–1283, doi:10.1029/WR008i005p01272.
- Grayson, R. B., A. W. Western, F. H. S. Chiew, and G. Bloschl (1997), Preferred states in spatial soil moisture patterns: Local and nonlocal controls, *Water Resour. Res.*, 33(12), 2897–2908, doi:10.1029/97WR02174.
- Harr, R. D. (1977), Water flux in soil and subsoil on a steep forested slope, *J. Hydrol.*, 33, 37–58, doi:10.1016/0022-1694(77)90097-X.
- Hewlett, J. D., and A. R. Hibbert (1967), Factors affecting the response of small watersheds to precipitation in humid areas, in *Forest Hydrology*, edited by W. E. Sopper and H. W. Lull, pp. 275–291, Pergamon, New York.
- Hill, A. R. (2000), Stream chemistry and riparian zones, in *Streams and Ground Waters*, pp. 83–110, Academic, San Diego, Calif.
- Holdorf, H. D. (1981), Soil resource inventory, Lewis and Clark National Forest: Interim in service report, Lewis and Clark Natl. For., For. Supervisor's Off, Great Falls, Mont.
- Kendall, K. A., J. B. Shanley, and J. J. McDonnell (1999), A hydrometric and geochemical approach to test the transmissivity feedback hypothesis during snowmelt, *J. Hydrol.*, 219(3–4), 188–205, doi:10.1016/S0022-1694(99)00059-1.
- McDonnell, J. J. (1990), Rationale for old water discharge through macropores in a steep, humid catchment, *Water Resour. Res.*, 26, 2821–2832.
- McGlynn, B. L., and J. J. McDonnell (2003a), Role of discrete landscape units in controlling catchment dissolved organic carbon dynamics, *Water Resour. Res.*, 39(4), 1090, doi:10.1029/2002WR001525.
- McGlynn, B. L., and J. J. McDonnell (2003b), Quantifying the relative contributions of riparian and hillslope zones to catchment runoff, *Water Resour. Res.*, 39(11), 1310, doi:10.1029/2003WR002091.
- McGlynn, B. L., and J. Seibert (2003), Distributed assessment of contributing area and riparian buffering along stream networks, *Water Resour. Res.*, 39(4), 1082, doi:10.1029/2002WR001521.
- McGlynn, B. L., J. J. McDonnell, J. B. Shanley, and C. Kendall (1999), Riparian zone flowpath dynamics during snowmelt in a small headwater catchment, *J. Hydrol. Amsterdam*, 222(1–4), 75–92, doi:10.1016/S0022-1694(99)00102-X.
- McGlynn, B. L., J. J. McDonnell, and J. J. Bammer (2002), A review of the evolving perceptual model of hillslope flow paths at the Maimai catchments, *N. Z. J. Hydrol.*, 257, 1–26.
- McGlynn, B., J. J. McDonnell, M. Stewart, and J. Seibert (2003), On the relationships between catchment scale and streamwater mean residence time, *Hydrol. Processes*, 17(1), 175–181, doi:10.1002/hyp.5085.
- McGlynn, B. L., J. J. McDonnell, J. Seibert, and C. Kendall (2004), Scale effects on headwater catchment runoff timing, flow sources, and groundwater-streamflow relations, *Water Resour. Res.*, 40, W07504, doi:10.1029/2003WR002494.
- McGuire, K. J., J. J. McDonnell, M. Weiler, C. Kendall, B. L. McGlynn, J. M. Welker, and J. Seibert (2005), The role of topography on catchment-scale water residence time, *Water Resour. Res.*, 41, W05002, doi:10.1029/2004WR003657.
- Ocampo, C. J., M. Sivapalan, and C. Oldham (2006), Hydrological connectivity of upland-riparian zones in agricultural catchments: Implications for runoff generation and nitrate transport, *J. Hydrol.*, 331(3–4), 643–658, doi:10.1016/j.jhydrol.2006.06.010.
- Peters, D. L., J. M. Buttle, C. H. Taylor, and B. D. LaZerte (1995), Runoff production in a forested, shallow soil, Canadian Shield basin, *Water Resour. Res.*, 31(5), 1291–1304, doi:10.1029/94WR03286.
- Seibert, J., and B. L. McGlynn (2007), A new triangular multiple flow direction algorithm for computing upslope areas from gridded digital elevation models, *Water Resour. Res.*, 43, W04501, doi:10.1029/2006WR005128.
- Seibert, J., K. Bishop, A. Rodhe, and J. J. McDonnell (2003), Groundwater dynamics along a hillslope: A test of the steady state hypothesis, *Water Resour. Res.*, 39(1), 1014, doi:10.1029/2002WR001404.
- Shaman, J., M. Stieglitz, and D. Burns (2004), Are big basins just the sum of small catchments?, *Hydrol. Processes*, 18(16), 3195–3206, doi:10.1002/hyp.5739.
- Sidle, R. C., Y. Tsuboyama, S. Noguchi, I. Hosoda, M. Fujieda, and T. Shimizu (2000), Stormflow generation in steep forested headwaters: A linked hydrogeomorphic paradigm, *Hydrol. Processes*, 14(3), 369–385, doi:10.1002/(SICI)1099-1085(20000228)14:3<369::AID-HYP943>3.0.CO;2-P.
- Stieglitz, M., J. Shaman, J. McNamara, V. Engel, J. Shanley, and G. W. Kling (2003), An approach to understanding hydrologic connectivity on the hillslope and the implications for nutrient transport, *Global Biogeochem. Cycles*, 17(4), 1105, doi:10.1029/2003GB002041.
- Uchida, T., Y. Asano, Y. Onda, and S. Miyata (2005), Are headwaters just the sum of hillslopes?, *Hydrol. Processes*, 19(16), 3251–3261, doi:10.1002/hyp.6004.
- Vidon, P. G. F., and A. R. Hill (2004), Landscape controls on nitrate removal in stream riparian zones, *Water Resour. Res.*, 40, W03201, doi:10.1029/2003WR002473.
- Welsch, D. L., C. N. Kroll, J. J. McDonnell, and D. A. Burns (2001), Topographic controls on the chemistry of subsurface stormflow, *Hydrol. Processes*, 15, 1925–1938, doi:10.1002/hyp.247.
- Western, A. W., R. B. Grayson, G. Blöschl, G. R. Willgoose, and T. A. McMahon (1999), Observed spatial organization of soil moisture and its relation to terrain indices, *Water Resour. Res.*, 35, 797–810, doi:10.1029/1998WR900065.
- Wilson, G. V., P. M. Jardine, R. J. Luxmoore, L. W. Zelazny, D. A. Lietzke, and D. E. Todd (1991), Hydrogeochemical processes controlling subsurface transport from an upper subcatchment of Walker Branch watershed during storm events: 1. Hydrologic transport processes, *J. Hydrol.*, 123, 297–316, doi:10.1016/0022-1694(91)90096-Z.
- Woods, R. A., and L. K. Rowe (1996), The changing spatial variability of subsurface flow across a hillside, *N. Z. J. Hydrol.*, 35, 51–86.

K. E. Bencala, U.S. Geological Survey, 345 Middlefield Road, Menlo Park, CA 94025, USA.

M. N. Gooseff, Department of Civil and Environmental Engineering, Pennsylvania State University, 212 Sackett Building, University Park, PA 16802, USA.

K. G. Jencso, L. A. Marshall, and B. L. McGlynn, Department of Land Resources and Environmental Sciences, Montana State University, Bozeman, MT 59717, USA. (kelsey.jencso@myportal.montana.edu)

S. M. Wondzell, Olympia Forestry Sciences Laboratory, Pacific Northwest Research Station, U.S. Forest Service, Olympia, WA 98512, USA.

Contribution of Authors

Chapter 3: Hillslope hydrologic connectivity controls riparian groundwater turnover: Implications of catchment structure for riparian buffering and stream water sources

First author: Kelsey G. Jencso

Co-authors: Brian L. McGlynn, Michael N. Gooseff, Kenneth E. Bencala, and Steven M. Wondzell

Contributions: I was responsible for all field instrumentation and data collection, figure development and the majority of data analysis and writing of this paper. Brian McGlynn contributed significant critique and ideas for development of intellectual content within the paper and edited successive versions of the manuscript. Mike Gooseff, Steve Wondzell, and Kenneth Bencala provided technical and collaborative discussions throughout the writing process and edited the final version of the manuscript.

Manuscript Information

Jencso, K.G., B.L. McGlynn, M.N. Gooseff, K.E. Bencala. and S.M. Wondzell. 2010. Hillslope hydrologic connectivity controls riparian groundwater turnover: Implications of catchment structure for riparian buffering and stream water sources. *Water Resources Research* VOL. 46, W10524, doi:10.1029/2009WR008818, 2010

- Journal: Water Resources Research
- Status of manuscript (check one)
  - Prepared for submission to a peer-reviewed journal
  - Officially submitted to a peer-reviewed journal
  - Accepted by a peer-reviewed journal
  - Published in a peer-reviewed journal
- Publisher: American Geophysical Union
- Date of submission: October 27, 2009
- Date manuscript was published: October 15, 2010
- Issue in which manuscript appeared: Volume 46, W10524

Reproduced by kind permission of the American Geophysical Union

# Hillslope hydrologic connectivity controls riparian groundwater turnover: Implications of catchment structure for riparian buffering and stream water sources

Kelsey G. Jencso,<sup>1</sup> Brian L. McGlynn,<sup>1</sup> Michael N. Gooseff,<sup>2</sup> Kenneth E. Bencala,<sup>3</sup> and Steven M. Wondzell<sup>4</sup>

Received 27 October 2009; revised 7 March 2010; accepted 18 May 2010; published 15 October 2010.

[1] Hydrologic connectivity between catchment upland and near stream areas is essential for the transmission of water, solutes, and nutrients to streams. However, our current understanding of the role of riparian zones in mediating landscape hydrologic connectivity and the catchment scale export of water and solutes is limited. We tested the relationship between the duration of hillslope-riparian-stream (HRS) hydrologic connectivity and the rate and degree of riparian shallow groundwater turnover along four HRS well transects within a set of nested mountain catchments (Tenderfoot Creek Experimental Forest, MT). Transect HRS water table connectivity ranged from 9 to 123 days during the annual snowmelt hydrograph. Hillslope water was always characterized by low specific conductance ( $\sim 27 \mu\text{S cm}^{-1}$ ). In transects with transient hillslope water tables, riparian groundwater specific conductance was elevated during base flow conditions ( $\sim 127 \mu\text{S cm}^{-1}$ ) but shifted toward hillslope signatures once a HRS groundwater connection was established. The degree of riparian groundwater turnover was proportional to the duration of HRS connectivity and inversely related to the riparian: hillslope area ratios (buffer ratio;  $r^2 = 0.95$ ). We applied this relationship to the stream network in seven subcatchments within the Tenderfoot Creek Experimental Forest and compared their turnover distributions to source water contributions measured at each catchment outlet. The amount of riparian groundwater exiting each of the seven catchments was linearly related ( $r^2 = 0.92$ ) to their median riparian turnover time. Our observations suggest that the size and spatial arrangement of hillslope and riparian zones along a stream network and the timing and duration of groundwater connectivity between them is a first-order control on the magnitude and timing of water and solutes observed at the catchment outlet.

**Citation:** Jencso, K. G., B. L. McGlynn, M. N. Gooseff, K. E. Bencala, and S. M. Wondzell (2010), Hillslope hydrologic connectivity controls riparian groundwater turnover: Implications of catchment structure for riparian buffering and stream water sources, *Water Resour. Res.*, 46, W10524, doi:10.1029/2009WR008818.

## 1. Introduction

[2] Hydrologic investigations have been conducted across a wide array of research catchments and have identified numerous controls on runoff generation, including topography [Anderson and Burt, 1978; Beven, 1978; McGuire et al., 2005], soil distributions [Buttle et al., 2004; Soulsby et al., 2004; Soulsby et al., 2006], and geology [Shaman et al., 2004; Uchida et al., 2005]. Landscape structure (topography and

topology) can be particularly important for spatial patterns of water and solute movement in catchments with shallow soils. However, the relationship between variability in catchment structure and the timing, magnitude, and distribution of runoff and solute sources remains unclear. This lack of clarity is partially due to poor understanding of the role of riparian zones in mediating/buffering the upslope delivery of water and solutes across stream networks. We suggest that our understanding of catchment hydrology and biogeochemistry can be advanced through assessment of the dominant controls on hydrological connectivity among hillslope-riparian source areas and quantification of riparian buffering.

[3] Hydrologic connectivity between hillslope and riparian zones is typically transient but can occur when saturation develops across their interfaces [Jencso et al., 2009]. Hillslope hydrologic connections to riparian zones may be largely controlled by topography in catchments with shallow soil and poorly permeable bedrock. Especially important is the convergence and divergence of catchment topography which controls the size of upslope accumulated area (UAA)

<sup>1</sup>Department of Land Resources and Environmental Sciences, Montana State University, Bozeman, Montana, USA.

<sup>2</sup>Civil Environmental Engineering Department, Penn State University, University Park, Pennsylvania, USA.

<sup>3</sup>U.S. Geological Survey, Menlo Park, California, USA.

<sup>4</sup>U.S. Forest Service, Pacific Northwest Research Station Olympia Forestry Sciences Lab, Olympia, Washington, USA.

[Anderson and Burt, 1977; Beven, 1978]. Because of variability in topography within catchments, hillslope UAA sizes and therefore transient groundwater inputs to riparian zones can be spatially variable throughout the stream network [Weyman, 1970].

[4] Jenciso et al. [2009] recently compared the duration of hillslope-riparian-stream (HRS) water table connectivity to hillslope UAA size. They found that the size of hillslope UAA was a first-order control on the duration of HRS shallow groundwater connectivity across 24 HRS landscape transitions ( $r^2 = 0.91$ ). Larger hillslope sizes exhibited sustained connections to their riparian and stream zones, whereas more transient connections occurred across HRS sequences with smaller hillslope sizes. They applied this relationship to the entire stream network to quantify catchment scale hydrologic connectivity through time and found that the amount of the stream network's riparian zones that were connected to the uplands varied from 4% to 67% during the year.

[5] Because of their location between hillslopes and streams, riparian zones can modulate or buffer the delivery of water and solutes when hillslope connectivity is established across the stream network [Hill, 2000]. Research in headwater catchments has emphasized the importance of the riparian zone as a relatively restricted part of the catchment which can exert a disproportionately large influence on stream hydrologic and chemical response [Mulholland, 1992; Brinson, 1993; Cirimo and McDonnell, 1997]. The definitions of riparian buffering are diverse and often depend on the water quality or hydrologic process of interest. One use of the term refers to biogeochemical transformations [Cirimo and McDonnell, 1997] that often occur in near stream zones (e.g., redox reactions and denitrification). Another common use of the term refers to the volumetric buffering of upslope runoff by resident near stream groundwater [McGlynn and McDonnell, 2003b]. In the context of this study we focus on the volume buffering and source water mixing aspects of riparian function.

[6] Identifying spatial and temporal hydrologic connectivity among HRS zones can be an important step in understanding the evolution of stream solute and source water signatures during storm events. When a HRS connection is established, hillslope groundwater moves from the slope down through the adjacent riparian zone. Plot scale investigations have suggested that the mixing and displacement of riparian groundwater (turnover) by hillslope runoff is a first-order control on hillslope water [McGlynn et al., 1999], solute [McGlynn and McDonnell, 2003b], and nutrient [Burt et al., 1999; Hill, 2000; Carlyle and Hill, 2001; McGlynn and McDonnell, 2003a; Ocampo et al., 2006; Pacific et al., 2010] signatures expressed in streamflow. Source water separations at the catchment outlet [Hooper et al., 1997; Burns et al., 2001; McGlynn and McDonnell, 2003b] and theoretical exercises [Chanaat and Hornberger, 2003; McGlynn and Seibert, 2003] have also suggested that the rate at which turnover occurs may be proportional to the size of the riparian zone and the timing, duration, or magnitude of hillslope hydrologic connectivity to the riparian zone.

[7] Information gleaned from individual plot or catchment scale tracer investigations have suggested hydrologic connectivity to the riparian zone as a factor in the timing of water and solute delivery to the stream. Despite these pre-

vious investigations a general conceptualization of how a stream's spatial sources of water change through an event remains elusive. Little field research to date has explored how HRS hydrologic connectivity frequency and duration relates to the turnover of water and solutes in the riparian zone, how riparian zones "buffer" hillslope connectivity, and how these dynamics are distributed across entire stream networks. This limits our ability to move forward and assess riparian buffering of hillslope groundwater connections in a whole catchment context.

[8] In this paper we combine landscape analysis of HRS connectivity [Jenciso et al., 2009] and riparian buffering [McGlynn and Seibert, 2003] with high-frequency, spatially distributed observations of HRS shallow groundwater connectivity (24 well transects; 146 wells) and solute dynamics (4 hillslope-riparian-stream transitions). We extrapolate these observations across seven stream networks with contrasting catchment structure and compare them with catchment-scale hillslope and riparian spatial source water separations during the annual snowmelt hydrograph to address the following questions:

[9] 1. What is the effect of HRS connectivity duration on the degree of turnover of water and solutes in riparian zones?

[10] 2. How does landscape structure influence stream network hydrologic dynamics and the timing and amount of source waters detected at the catchment outlet?

[11] We utilize a landscape analysis-based framework to link landscape-scale hydrologic and solute dynamics with their topographic/geomorphic controls and present a way to transfer these dynamics across stream networks and catchments of differing structure.

## 2. Site Description

[12] The Tenderfoot Creek Experimental Forest (TCEF) (latitude, 46°55'N, longitude, 110°52'W) is located in the Little Belt Mountains of the Lewis and Clark National Forest in Central Montana, USA (Figure 1). Tenderfoot Creek forms the headwaters of the Smith River, a tributary of the Missouri. The TCEF is an ideal site for ascertaining relationships between variability in landscape structure and catchment hydrochemical response because it is composed of seven gauged catchments with a range of topographic complexity, watershed shapes, and hillslope and riparian sizes.

[13] The seven TCEF subcatchments range in size from 3 to 22.8 km<sup>2</sup>. In general, the catchment headwaters possess moderately sloping (average slope ~8°) extensive (up to 1200 m long) hillslopes and variable width riparian zones [Jenciso et al., 2009]. Flathead Sandstone and Wolsey Shale comprise the parent material in the upper portions of each catchment [Farnes et al., 1995]. Approaching the main stem of Tenderfoot Creek the streams become more incised, hillslopes become shorter (<500 m) and steeper (average slope ~20°), and riparian areas are narrower than in the catchment headwaters [Jenciso et al., 2009]. Basement rocks of granite gneiss occur at lower elevations [Farnes et al., 1995], and they are visible as exposed cliffs and talus slopes. All three rock strata in the TCEF are relatively impermeable with potential for deeper groundwater transmission along geologic contacts and fractures within the Wolsey shale [Reynolds, 1995].

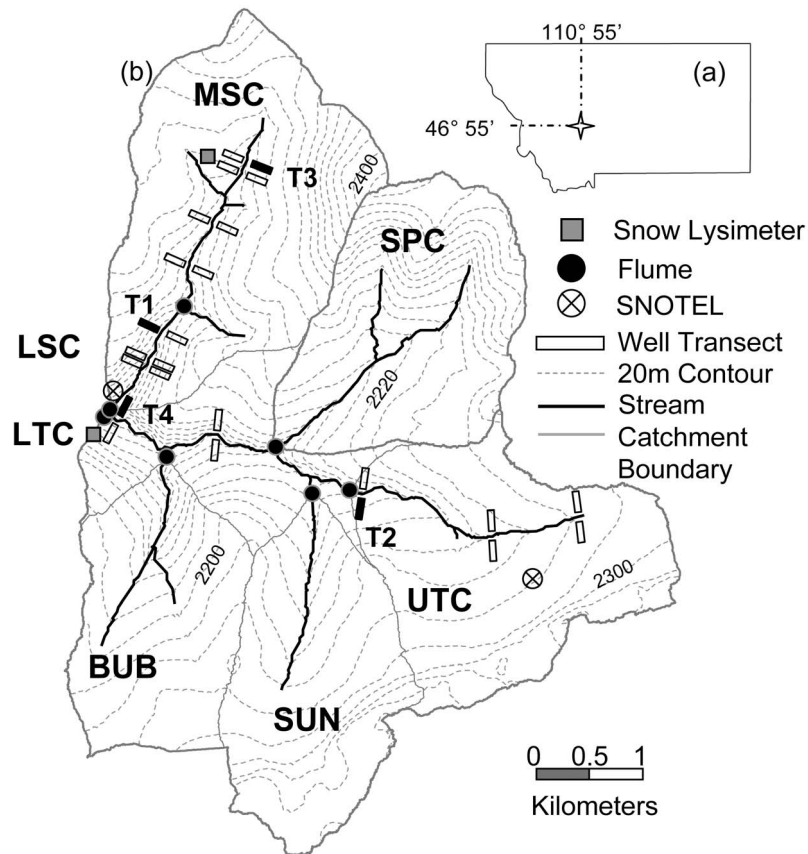


**Figure 1.** Site location and instrumentation of the TCEF catchment. (a) Catchment location in the Rocky Mountains, MT. (b) Catchment flumes, well transects, and SNOTEL instrumentation locations. Specific transects highlighted in this study are filled in black and labeled T1–T4. Transect extents are not drawn to scale.

[14] Soil depths are relatively consistent across hillslope (0.5–1.0 m) and riparian (1–2.0 m) zones with localized upland areas of deeper soils. The most extensive soil types in the TCEF are loamy skeletal, mixed Typic Cryochrepts located along hillslope positions and clayey, mixed Aquic Cryoboralfs in riparian zones and parks [Holdorf, 1981]. Riparian soils have high organic matter.

[15] The TCEF is a snowmelt dominated catchment. The 1961–1990 average annual precipitation is 840 mm [Farnes *et al.*, 1995]. Monthly precipitation generally peaks in December or January (100–120 mm per month) and declines to a late July through October dry period (45–55 mm per month). Approximately 75% of the annual precipitation falls during November through May, primarily as snow. Snowmelt and peak runoff typically occur in late May or early June. Lowest runoff occurs in the late summer through winter months.

### 3. Methods

#### 3.1. Terrain Analysis

[16] The TCEF stream network, riparian area, hillslope area, and their buffer ratios were delineated using a 1 m Airborne Laser Swath Mapping digital elevation model (DEM) resampled to a 10 m grid cell size. Elevation measurements were achieved at a horizontal sampling interval of the order <1 m, with vertical accuracies of  $\pm 0.05$  to  $\pm 0.15$  m.

We used the 10 m DEM to quantify each catchment's hillslope and riparian UAA sizes following DEM landscape analysis methods outlined by McGlynn and Seibert [2003].

[17] The area required for perennial stream flow (creek threshold initiation area) was estimated as 40 ha for Lower Tenderfoot Creek (LTC), Upper Tenderfoot Creek (UTC), Sun Creek (SUN), Spring Park Creek (SPC), Lower Stringer Creek (LSC), and Middle Stringer Creek (MSC) and 120 ha for Bubbling Creek (BUB). Creek threshold initiation areas were based on field surveys of channel initiation points in TCEF [Jencso *et al.*, 2009]. Accumulated area entering the stream network was calculated using a triangular multiple flow-direction algorithm [Seibert and McGlynn, 2007]. Once the accumulated area exceeded the creek threshold value, it was routed downslope as stream area using a single direction algorithm. To avoid instances where parallel streams were computed, we used the iterative procedure suggested by McGlynn and Seibert [2003]. Any stream pixel where we derived more than one adjacent stream pixel in a downslope direction was in the next iteration forced to drain to the downslope stream pixel with the largest accumulated area. We repeated this procedure until a stream network without parallel streams was obtained.

[18] The TCEF riparian areas were mapped based on the field relationship described in the study by Jencso *et al.* [2009]. Landscape analysis-derived riparian area was delineated as all areas less than 2 m in elevation above the stream

network pixel into which they flow. To compare the landscape analysis-derived riparian widths to actual riparian widths at TCEF, *Jencso et al.* [2009] surveyed 90 riparian cross sections in Stringer Creek, Spring Park Creek, and Tenderfoot Creek. A regression relationship ( $r^2 = 0.97$ ) corroborated their terrain-based riparian extent mapping [*Jencso et al.*, 2009].

[19] The local area entering the stream network is the incremental increase in catchment area for each stream pixel (not counting upstream contributions) and is a combination of hillslope and riparian area on either side of the stream network. We separated local hillslope UAA and riparian area into contributions from each side of the stream following methods developed by *Grabs et al.* [2010]. The UAA measurements for each transect's hillslope were calculated at the toe-slope well position. The riparian buffer ratio was computed as the ratio of local riparian area divided by the local inflows of hillslope area associated with each stream pixel (separately for each side of the stream). The "buffer ratio" represents the capacity of each riparian zone to modulate its adjacent hillslope water inputs. Riparian buffer ratio values were measured at the riparian well position.

[20] *Jencso et al.* [2009] determined the HRS connectivity for the catchments stream network based on a relationship between UAA size and HRS connectivity duration across 24 transects of HRS groundwater recording wells:

$$\% \text{Time Connected} = (0.00002 * \text{UAA} - 0.0216) * 100. \quad (1)$$

They found that the duration of a shallow groundwater table connection from hillslopes to the riparian and stream zones was linearly related ( $r^2 = 0.92$ ) to UAA size. For the purposes of this study, we refer to UAA size as a surrogate for the duration of groundwater table connectivity between HRS zones, based on the relationship observed by *Jencso et al.* [2009]. Larger UAA sizes indicate longer periods of connectivity duration while smaller UAA sizes are indicative of transient connections that only occur during the largest snowmelt events. We applied this relationship to the hillslope UAA values along each stream network in the seven TCEF subcatchments to determine the connectivity to riparian zones through time.

### 3.2. Hydrometric Monitoring

[21] *Jencso et al.* [2009] instrumented 24 sites in TCEF with transects of shallow recording groundwater wells and piezometers (146 total). At a minimum, groundwater wells were installed across each transect's hillslope (1–5 m above the break in slope), toe slope (the break in slope between riparian and hillslope positions), and riparian position (1–2 m from the stream). All wells were completed to bedrock, and they were screened from 10 cm below the ground surface to their completion depths. Groundwater levels in each well were recorded with Tru Track Inc. capacitance rods ( $\pm 1$  mm resolution) at hourly intervals for the 2007 water year. Hydrologic connectivity between HRS zones was inferred from the presence of saturation measured in well transects spanning the hillslope, toe slope, and riparian positions. Following *Jencso et al.* [2009], we define a hillslope-riparian-stream connection as a time interval during which stream flow occurred, and the riparian, toe slope, and adjacent hillslope wells recorded water levels above bedrock.

[22] Runoff was recorded in each of the seven nested catchments using a combination of Parshall and H-Flumes installed by the USFS (Figure 1). Stage in each flume was measured at hourly intervals with Tru Track Inc. water level recorders and every 15 min by USFS float potentiometers. Manual measurements of both the well groundwater levels (electric tape) and flume stage (visual stage readings) were conducted biweekly during the summer months and monthly during the winter to corroborate capacitance rod measurements.

### 3.3. Chemical Monitoring

[23] We collected snowmelt, shallow groundwater, and stream samples once a month during the winter, every 1–3 days during snowmelt according to runoff magnitude, and biweekly during the subsequent recession period of the hydrograph. In this paper we highlight the hydrochemical response of four well transects sampled from the 24 transects where physical hydrology was measured. These transects were selected to cover a range of hillslope and riparian area size and the ratio of their areas (riparian buffer ratios). High-frequency solute and SC monitoring was limited to four transects due to the time constraints associated with foot travel across the TCEF catchment during isothermal conditions in a 2 m snowpack. The four transects in this study are named in order of increasing riparian buffer ratios sequentially from one through four (T1–4). Wells were purged to ensure a composite sample along the screened interval before sample collection. Samples for solute analysis were collected in 250 mL high-density polyethylene bottles and filtered through a 0.45  $\mu\text{m}$  polytetrafluorethylene membrane filter. They were stored at 4°C before analyses of major cations with a Metrohm-Peak (Herisau, Switzerland) compact ion chromatograph at Montana State University. Sodium (Na), ammonium ( $\text{NH}_4$ ), potassium (K), calcium (Ca), and magnesium (Mg) were measured on a Metrosep C-2-250 cation column. Detection limits for major cations were 5–10  $\mu\text{g L}^{-1}$  and accuracy was within 5% of standards. Groundwater specific conductance (SC) was measured with a handheld YSI EC300 meter ( $\pm 0.1 \mu\text{S cm}^{-1}$  resolution and accuracy within  $\pm 1\%$  of reading). We also monitored groundwater chemistry and SC in each of the 24 transects installed by *Jencso et al.* [2009] at a bimonthly interval. This corroborated the range of SC dynamics observed at the four transects used in this study and helped to determine base flow SC across the range of riparian zone sizes in TCEF. Stream specific conductance and temperature in each subcatchment's flume was also measured at hourly intervals with Campbell Scientific CS547A conductivity probes ( $\pm 0.1 \mu\text{S cm}^{-1}$  resolution and accuracy within  $\pm 1\%$  of reading).

### 3.4. Specific Conductance as a Tracer of Water Sources

[24] Hillslope shallow groundwater specific conductance was  $\sim 80\%$  less than the SC observed in riparian wells during base flow periods of the hydrograph. We used specific conductance to distinguish between hillslope and riparian shallow groundwater and riparian saturation overland flow. Previous studies have used SC to distinguish the spatial sources of water within catchments [*Kobayashi*, 1986; *McDonnell et al.*, 1991; *Hasnain and Thayer*, 1994; *Caissie et al.*, 1996; *Laudon and Slaymaker*, 1997; *Kobayashi et al.*, 1999; *Ahmad and Hasnain*, 2002; *Covino and McGlynn*,

**Table 1.** Transect Attributes

| Transect | Riparian Soil Depths (m) | Riparian UAA (m <sup>2</sup> ) | Hillslope UAA (m <sup>2</sup> ) | HRS Connection (days) | Riparian Buffer Ratio | Turnover Time Constant (days) | t50% Turnover (days) | t95% Turnover (days) | Riparian Volumes Turned Over |
|----------|--------------------------|--------------------------------|---------------------------------|-----------------------|-----------------------|-------------------------------|----------------------|----------------------|------------------------------|
| T1       | 0.7–1.80                 | 783                            | 46112                           | 123                   | 0.017                 | 4                             | 3                    | 13                   | 27                           |
| T2       | 0.7–1.20                 | 163                            | 7070                            | 46                    | 0.023                 | 8                             | 6                    | 25                   | 6                            |
| T3       | 0.6–1.10                 | 1148                           | 10165                           | 29                    | 0.113                 | 29                            | 20                   | 86                   | 1.0                          |
| T4       | 0.7–0.85                 | 700                            | 1527                            | 9                     | 0.458                 | 39                            | 27                   | 115                  | 0.2                          |

2007; Stewart *et al.*, 2007], but validation of SC with its constituent solutes is recommended [Laudon and Slaymaker, 1997; Covino and McGlynn, 2007]. We compared SC measurements with a composite ( $n = 126$ ) of major cation concentrations in hillslope, riparian, stream, and snowmelt grab samples determined through IC analysis. A strong linear relationship existed between SC and Ca ( $r^2 = 0.92$ ) and SC and Mg ( $r^2 = 0.89$ ) for each spatial source supporting the use of SC as a surrogate tracer for calcium and magnesium concentrations in solution. Hydrochemical tracers, such as Ca<sup>+</sup>, Mg<sup>2</sup> are commonly used in comparable studies and when related to Specific conductance, recording SC probes provide high-resolution measurements for source water separations. We restrict the use of SC and solutes as tracers to the snowmelt portion of the hydrograph (1 May 2007 to 1 July 2007) to minimize the potential impacts of weathering and nonconservative behavior.

### 3.5. Modeling Riparian Groundwater Turnover

[25] We applied a simple continuously stirred tank reactor (CSTR) [Ramaswami *et al.*, 2005]) mixing model to each riparian SC time series to quantify the turnover rate of riparian groundwater in response to hillslope water table development and HRS connectivity. This basic exponential model has been previously used to estimate [Boyer *et al.*, 1997] and model [Scanlon *et al.*, 2001] flushing time constants of dissolved organic carbon and silica from riparian areas and whole catchments.

[26] We fit an exponential decay regression relationship to the riparian well water SC time series at each transect. The time period analyzed for each riparian SC time series was the highest observed SC before snowmelt initiation and HRS connectivity until the time of lowest SC observations. Similar to Boyer *et al.* [1997], we selected sequential data points over this period to determine the linear fit to the relationship between  $\ln(\text{SC})$  and time. The slopes of these regressions are the turnover rate constants ( $\lambda$ ) or how fast the solutes that comprise SC in the riparian reservoir are turned over or mixed with more dilute hillslope inputs. The inverse of this slope represents the “turnover constant” of each site ( $\tau$ ), the time in days it took for the SC in the riparian zone to decrease to 37% of its initial value (Table 1) and for one volume to be flushed [Ramaswami *et al.*, 2005]:

$$\tau = \frac{1}{\lambda}. \quad (2)$$

We believe a more intuitive way of describing exponential decay is the time required for the decaying mixture to decline to 50% of its initial concentration. This is commonly

called the half-life and in the context of this paper is referred to as the turnover half-life ( $t_{50}$ ):

$$t_{50} = \frac{\ln 0.5}{\lambda} = -\tau \ln(0.5) \quad (3)$$

Similarly, we calculated the time it would take to fully turn over all of the original riparian SC in each transect ( $t_{95}$ ). While an exponential model can never fully reach a baseline concentration, we chose 95% as an acceptable limit at which the riparian zone water SC is deemed similar to water coming from the adjacent hillslope. Thus, 5% of the original riparian SC was considered the baseline at which all initial riparian water was considered turned over from a riparian zone:

$$t_{95} = -\tau \ln(0.05). \quad (4)$$

We also estimated how many riparian volumes moved through the riparian zone at each transect during its corresponding time of HRS connectivity. Riparian volume turnover was calculated by dividing the HRS water table connection duration by the calculated turnover constant:

$$\text{Riparian volumes} = \frac{\text{HRS water table connection duration}}{\tau}. \quad (5)$$

Here we incorporate the duration of the HRS connection; the magnitude of hillslope throughflow associated with each HRS connection is incorporated within the exponential relationship developed from the decay rate of the riparian SC time series.

### 3.6. Hydrograph Separations for Hillslope, Riparian, and Saturated Area Overland Flow

[27] Hydrograph separations are commonly used tools for separating the spatial and temporal sources of water exiting a catchment. They can provide an integrated measure of source area contributions and their overall effect on hydrologic dynamics observed at the catchment outlet. We implemented 3 component hydrograph separations to determine the spatial contributions to stream runoff from hillslope, riparian, and saturated overland flow sources during the annual snowmelt hydrograph (1 May 2007 to 1 July 07). “Real-time” separations were developed for each subcatchment in TCEF using continuous measurements of riparian-saturated overland flow [Dewalle *et al.*, 1988] and specific conductance.

[28] Saturation overland flow is limited to the near stream riparian areas in TCEF due to upland soils with high infiltration rates. We determined the runoff contributions from riparian overland flow using continuous measurements of

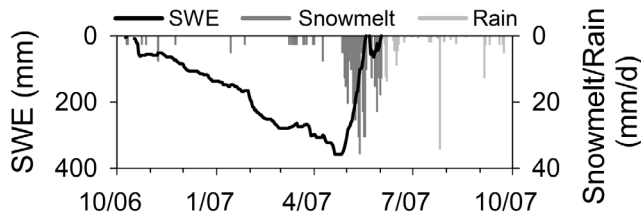


**Figure 2.** Water year 2007 cumulative snow water equivalent, snowmelt, and rain.

snowmelt rates and riparian area extents delineated with terrain analysis, similar to methods outlined by *Dewalle et al.* [1988]. Riparian snowmelt inputs were computed using a 6 hour exponential smoothing of spatially averaged snowmelt rates obtained from snowmelt lysimeters installed at ST2 and LTC (5 min intervals; Figure 1) and the Onion Park and LSF SNOTEL locations (3 h intervals; Figure 1). Riparian area derived from terrain analysis for each catchment was considered the maximum extent of riparian saturated overland flow. Riparian area saturated overland flow contributions ( $Q_{RS}$ ) were then calculated as the product of riparian area and average snowmelt rates:

$$Q_{RS} = \text{Catchment riparian area} \times \text{Riparian snowmelt.} \quad (6)$$

Observed stream flow ( $Q_{ST}$ ) and SC ( $SC_{ST}$ ) at each subcatchment outlet were adjusted for contributions by saturated riparian overland flow:

$$Q_{STA} = Q_{ST} - Q_{RS} \quad (7)$$

$$SC_{STA} = \frac{(SC_{ST} \times Q_{ST}) - (Q_{RS} \times SC_{RS})}{Q_{ST} - Q_{RS}}, \quad (8)$$

where  $Q$  and  $SC$  are runoff and specific conductance and the subscripts STA, ST, and RS represent adjusted stream flow, observed stream flow, and riparian overland flow, respectively. Average riparian overland flow SC was held constant at  $15 \mu\text{S cm}^{-1}$  based on average SC measurements of overland flow during snowmelt ( $n = 70$ ;  $\sigma \pm 3 \mu\text{S cm}^{-1}$ ).

[29] Hillslope and riparian contributions ( $Q_H$  and  $Q_R$ , respectively) were determined using a traditional two-component hydrograph separation and adjusted stream runoff and SC values:

$$Q_H = \left[ \frac{SC_{STA} - SC_R}{SC_H - SC_R} \right] Q_{STA} \quad (9)$$

$$Q_R = \left[ \frac{SC_{STA} - SC_H}{SC_R - SC_H} \right] Q_{STA}, \quad (10)$$

where  $Q$  and  $SC$  are runoff and specific conductance and the subscripts H, R, and STA represent hillslope groundwater, riparian groundwater, and stream flow adjusted for riparian overland flow contributions. Riparian and hillslope groundwater measurements collected from all 24 transects were used to determine their respective end-member SC signatures. We selected three sample time periods (1 October 2006, 18 February 2007, and 26 April 2007) during base

flow to determine average riparian groundwater SC. Riparian SC measurements collected during base flow ( $n = 72$ ) ranged from  $92$  to  $194 \mu\text{S cm}^{-1}$ . The mean of these was  $126 \mu\text{S cm}^{-1}$ , and the standard deviation was  $\pm 36 \mu\text{S cm}^{-1}$ . Hillslope groundwater SC ( $n = 88$ ) over the course of the study period was relatively constant ranging from  $22$  to  $39 \mu\text{S cm}^{-1}$ . The average SC was  $27 \mu\text{S cm}^{-1}$ , and the standard deviation was  $\pm 6 \mu\text{S cm}^{-1}$ . Each spatial source's average SC was used as its end-member SC. Stream flow ( $Q_{ST}$ ) at the outlet of the TCEF subcatchments was then a mixture of hillslope, riparian, and riparian saturation overland flow ( $Q_{RS}$ ) components:

$$Q_{ST} = Q_R + Q_H + Q_{RS} \quad (11)$$

and source water contributions were separated continuously during the study period.

[30] We applied uncertainty analyses to the hillslope and riparian separations following the methods of *Genereux* [1998] using

$$W_{fH} = \left\{ \left[ \frac{SC_R - SC_{ST}}{(SC_R - SC_H)^2} W_{scH} \right]^2 + \left[ \frac{SC_{ST} - SC_H}{(SC_R - SC_H)^2} W_{scR} \right]^2 + \left[ \frac{-1}{(SC_R - SC_H)} W_{scST} \right]^2 \right\}^{1/2} \quad (12)$$

$$W_{fR} = \left\{ \left[ \frac{SC_H - SC_{ST}}{(SC_H - SC_R)^2} W_{scR} \right]^2 + \left[ \frac{SC_{ST} - SC_H}{(SC_H - SC_R)^2} W_{scH} \right]^2 + \left[ \frac{-1}{(SC_H - SC_R)} W_{scST} \right]^2 \right\}^{1/2}, \quad (13)$$

where  $W_{fH}$  is the relative uncertainty in the hillslope groundwater component,  $W_{fR}$  is the relative uncertainty in the riparian groundwater component,  $W_{scST}$  is the analytical error in the stream SC measurements,  $W_{scH}$  and  $W_{scR}$  is the spatial variability of SC in hillslope and riparian groundwater samples (standard deviations of SC for each component), and  $SC_H$ ,  $SC_R$ , and  $SC_{ST}$  are hillslope, riparian, and stream SC.

## 4. Results

### 4.1. Precipitation Dynamics

[31] We present snow accumulation and melt data from the Upper Tenderfoot Creek (relatively flat  $0^\circ$  aspect, elevation 2259 m) SNOTEL site and rain data from the Stringer Creek tipping bucket rain gauge as a reference for HRS groundwater and runoff response timing in response to precipitation dynamics (Figure 2). The maximum snow pack snow water equivalent before melt was 358 mm. Springtime warming lead to an isothermal snowpack, and most of the snowpack melted between 27 April 2007 to 19 May 2007. Average daily snow water equivalent losses were 15 mm and reached a maximum of 35 mm on 13 May 2007. A final spring snowfall and subsequent melt occurred between 24 May 2007 and 1 June 2007, yielding 97 mm of water.

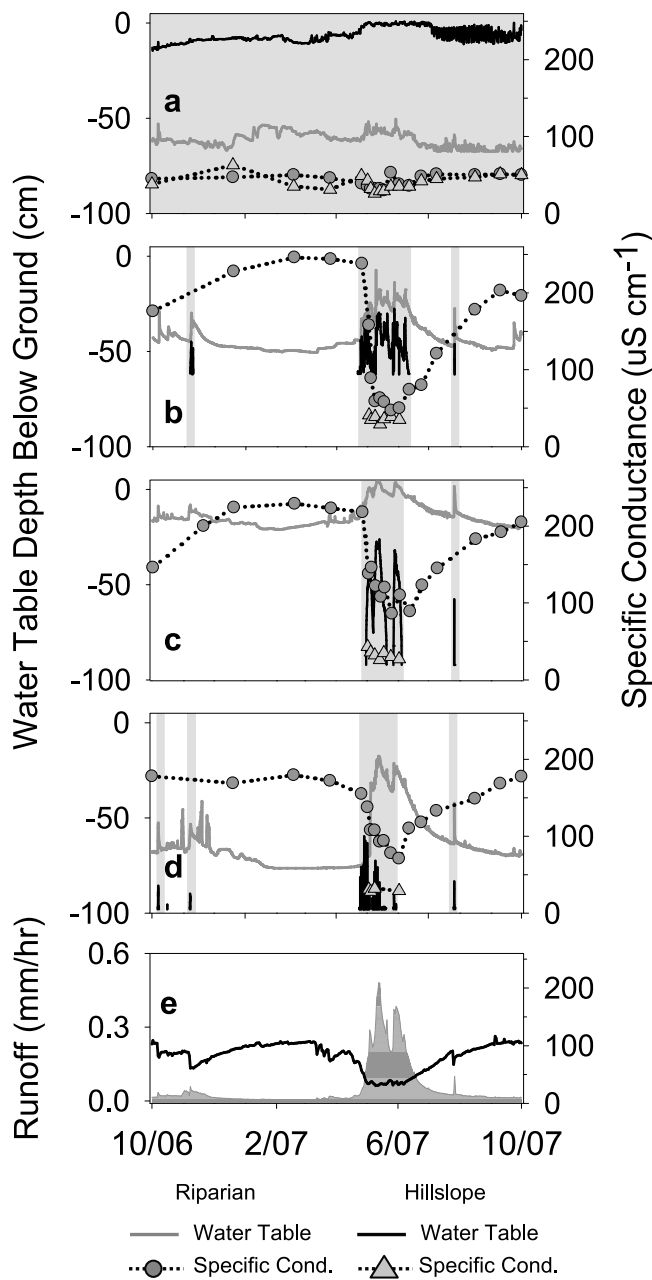


**Figure 3.** (a–d) Time series of riparian and hillslope water table dynamics and specific conductance at transects 1–4. Times of hillslope-riparian-stream hydrologic connectivity are indicated with gray shading. Runoff (dark gray shading) and specific conductance (black line) dynamics at the Lower Tenderfoot Creek flume are shown (e) for comparison to the transect dynamics.

Four days following the end of snowmelt, two low-intensity rain storms (totaling 30 and 22 mm, respectively) occurred.

#### 4.2. Hillslope and Riparian Hydrologic Connectivity and Specific Conductance Dynamics

[32] We present a detailed description of each transect’s landscape attributes and resulting HRS connectivity and SC dynamics in Appendix A. Figure 3 depicts each transect’s HRS water table connectivity, specific conductance dynamics,

and runoff and SC observed at the LTC catchment outlet. Hillslope to riparian water table connectivity ranged from 9 to 123 days across the four transects during the study observation period (1 April 2007 to 1 August 2007; Table 1). Hillslope groundwater was characterized by low specific conductance ( $\sim 27 \mu\text{S cm}^{-1}$ ,  $\pm 6.5 \mu\text{S cm}^{-1}$ ,  $n = 88$ ). At transects with transient hillslope water tables, riparian groundwater SC was higher during base flow conditions ( $\sim 127 \pm 36 \mu\text{S cm}^{-1}$ ,  $n = 72$ ) but shifted by varying degrees toward hillslope signatures following HRS connectivity during snowmelt (Figure 3).

#### 4.3. Quantifying the Capacity of the Riparian Zone to “Buffer” Hillslope Connections

[33] When hillslope water tables were present, their SC was consistent and dilute relative to riparian groundwater (Figure 3). Riparian groundwater before spring melt provided a background SC and its change through snowmelt provided an indication of hillslope/riparian mixing, rates of riparian water turnover, and riparian buffering. We applied a CSTR mixing model to each riparian SC time series to quantify the rate of decreasing riparian SC in response to hillslope water table development and HRS connectivity.

[34] During snowmelt, HRS water table connectivity developed across each transect that indirectly led to a significant decrease in riparian SC as more dilute hillslope water entered and mixed with resident riparian water. Each transect exhibited a different turnover rate of riparian water (Figure 4) and goodness of fit to the relationship between  $\ln(\text{SC})$  and time ( $r^2$  ranging from 0.62 to 0.96). T4, the transect

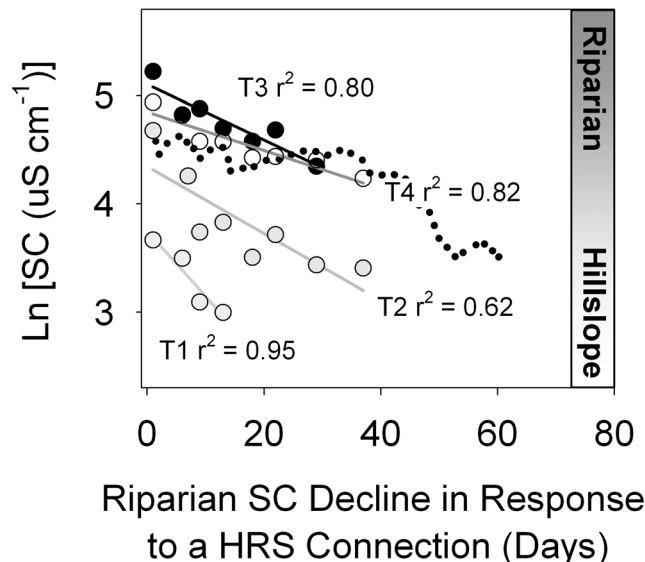


**Figure 4.** Exponential decline of riparian groundwater specific conductance toward the hillslope signature following the snowmelt induced HRS hydrologic connection. The slopes of these lines indicate the rate of riparian water turnover or dilution by hillslope water. The inverse of the slope is the turnover time constant for each site (Table 1) and provides a measure of riparian buffering of hillslope throughflow. The dotted line represents the exponential decline of LTC stream specific conductance during the same time period.

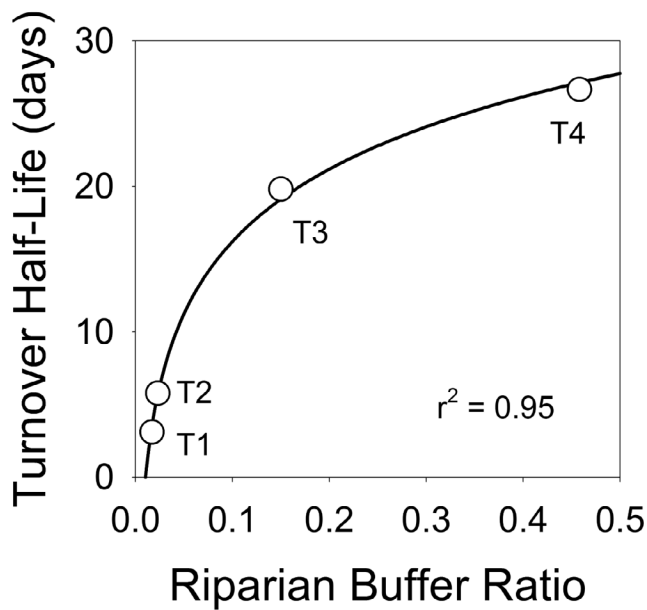


**Figure 5.** Logarithmic relationship between the riparian buffering ratio (riparian area divided by hillslope area) at each transect and the time that it takes for 50% of the initial riparian concentration to be turned over or diluted by hillslope water (Table 1; equation (2)).

with the lowest frequency of HRS connectivity and a large riparian zone turned over at the slowest rate. In contrast, T1 had a continuous connection throughout snowmelt and the fastest riparian turnover rate. The two intermediary transects (T2 and T3) exhibited sustained HRS connectivity. T2's riparian SC decreased more rapidly from the time of its initial HRS connection relative to T3. T3 had a much larger riparian zone (1148 m<sup>2</sup>) compared to T2 (163 m<sup>2</sup>), and its riparian zone was connected to the hillslope for a shorter duration (Table 1).

[35] We plotted the time it took for each riparian zone's SC to decrease to half of its initial value ( $t_{50}$ , equation (3)) against its riparian buffer ratio (riparian area/hillslope area) to determine the potential of each riparian zone to modulate its corresponding hillslope water table connection. We found a logarithmic relationship between the buffer ratio and the  $t_{50}$  time ( $r^2 = 0.95$ ) at each transect (Figure 5; equation (14)):

$$t_{50} = 6.13 \ln(\text{Riparian buffer ratio}) + 29. \quad (14)$$

T1 had the lowest buffer ratio, and it took only 3 days for the riparian SC to be reduced by half by hillslope inputs. During its continuous HRS connectivity throughout the study period (123 days), approximately 27 riparian volumes were turned over (equation (5); Table 1). T2 had a small riparian area relative to its hillslope connection duration and the second shortest turnover half-life (6 days). Six riparian volumes were exchanged in T2 during its 46 day HRS connectivity time period. The turnover half-life for T3 was 20 days, and ~1 riparian volume of mixed hillslope and riparian water was removed during its 29 day HRS connectivity time period. T4 had the longest observed turnover half-life (27 days) associated with its large riparian buffer-

ing ratio. Only 26% of the original riparian volume was turned over during its 9 day HRS connectivity duration.

[36] One or more (up to 27) riparian volumes passed through the transects (T1 and T2) with low riparian buffering ratios and sustained HRS connections resulting in a predominantly hillslope water SC signature in these riparian zones. The two transects (T3 and T4) with larger buffer ratios never approached hillslope SC during their HRS connectivity duration. We calculated the time it would take to deplete the original riparian SC at each transect (equation (4)) to evaluate the effect of changing HRS connectivity duration on the degree of turnover that can occur at each transect.

[37] Figure 6 illustrates the time required; incorporating each transect's time constant, for the initial riparian water to be mixed or replaced by dilute hillslope inflows. T4 would require 115 days to completely turn over its riparian water, but it was only connected for a total of 9 days during snowmelt. T3 would require 86 days to turn over but was only connected 29 days. T2 would require 25 days, which was less than its observed 46 day HRS connection duration. This was consistent with the observed riparian SC time series (Figure 3b) that indicated that riparian SC decreased to the hillslope groundwater SC over the course of spring runoff. Similarly, T1's riparian zone only required 13 days to fully turn over, and its SC dynamics followed those of the hillslope throughout its continuous connectivity duration.

#### 4.4. Comparing Internal Distributions of Riparian Buffering and Turnover to Source Water Separations at the Catchment Outlet

[38] Plot scale hydrochemical time series indicated that the size of a riparian zone relative to duration of groundwater connectivity to its uplands (as represented by UAA size [Jencso et al., 2009]) may be a predictor of the turnover rate of riparian water (equation (14); Figure 5). Riparian and

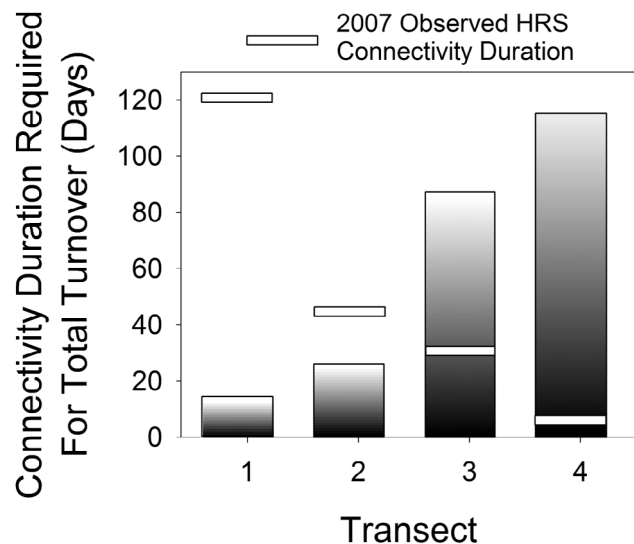


**Figure 6.** Estimated hillslope-riparian-stream connectivity duration required for 95% of the initial riparian water to be replaced or diluted by hillslope throughflow (shaded bars) and the observed HRS connectivity duration for the study observation period (white rectangles). The riparian zone is estimated to be turned over when SC reaches hillslope signatures (white shading) denoted in each shaded bar.

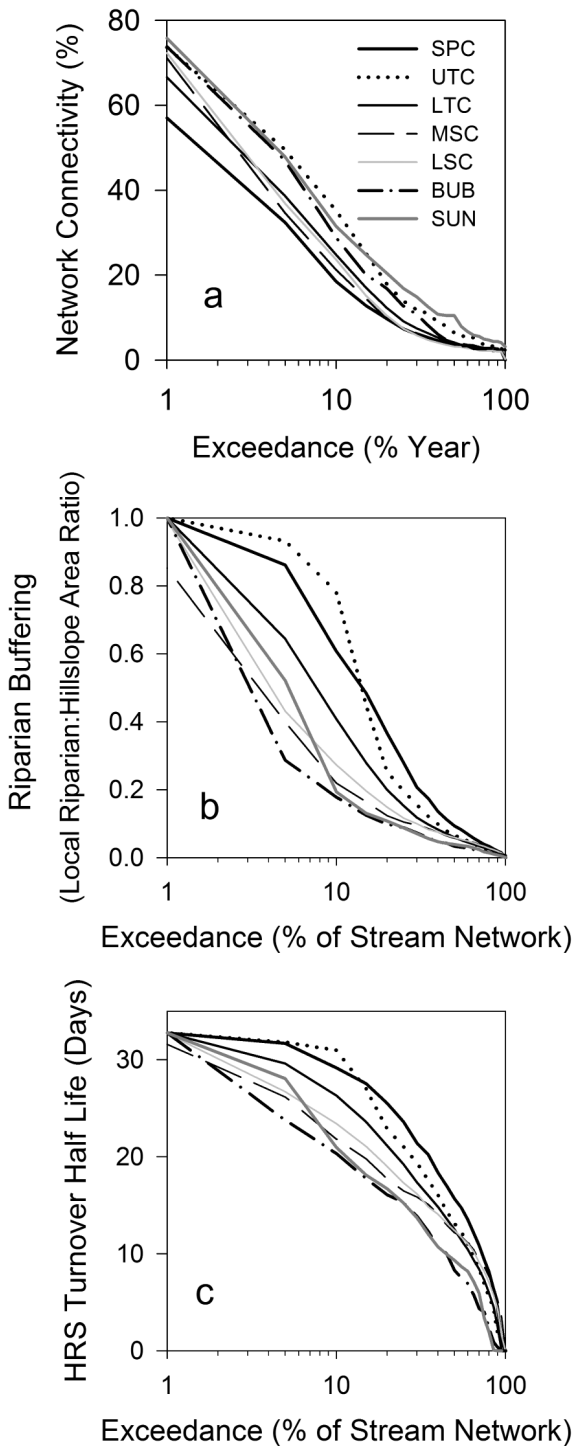


**Figure 7.** TCEF subcatchment distributions of stream network (a) HRS connectivity, (b) riparian buffering, and the resultant (c) riparian groundwater turnover times. Riparian water turnover times (riparian buffering) are a function of hydrologic connectivity and the size of the riparian area relative to the adjacent hillslope. Catchments with fast turnover times had more sustained HRS connectivity and less riparian buffering of hillslope inputs. Catchments with longer duration turnover times had shorter duration hillslope groundwater table connectivity to their riparian zones and more effective riparian buffering along the stream network.

hillslope area typically are not distributed homogeneously along stream networks. Different distributions and combinations of each can be found in neighboring catchments according to their landscape structure [McGlynn and Seibert, 2003]. We examined how HRS connectivity durations (function of UAA), riparian buffering, and riparian groundwater turnover were distributed within each subcatchment in TCEF (Figure 7).

[39] Figure 7a illustrates connectivity duration curves (CDCs) [Jencso *et al.*, 2009] for each stream network. Each CDC was derived from the combined 10 m left and right stream bank frequencies of HRS connectivity for the 2007 water year (equation (1)). Catchments with less topographic complexity and a higher proportion of larger UAA sizes exhibited elevated annual HRS connectivity and a higher magnitude peak connectivity. Decreased annual connectivity and lower magnitude peak connectivity was characteristic of catchments with more convergence and divergence in the landscape and a higher frequency of small UAA sizes.

[40] How riparian areas were arranged next to their adjacent hillslopes determined the distribution of stream network riparian buffering (Figure 7b) and the resultant turnover times (equation (14); Figure 7c). Catchments with a higher frequency of larger UAA relative to riparian extents had less stream network riparian buffering and a higher frequency of fast riparian groundwater turnover times (and vice versa).

[41] We compared the distribution of riparian buffering and turnover with the timing and total amounts of riparian groundwater in each subcatchment's annual snowmelt hydrograph (Table 2). To elucidate potential differences of source water contributions across catchments, we determined the percentage of riparian, hillslope, and riparian overland flow contributions to the snowmelt hydrograph before snowmelt (1 April), and during the rising (1 May), peak (14 May), and recession (1 July) of the hydrograph. Figure 8 depicts riparian buffering maps, estimated turnover along the stream network, and snowmelt hydrograph separations for SPC, LSC, and SUN catchments. These catchments span the range of turnover distributions and resultant riparian groundwater contributions found across all seven nested catchments within TCEF (Figure 9).

[42] SPC was characteristic of catchments with a high degree of riparian buffering (Figures 7b and 8a) and long duration riparian turnover times (Figures 7c and 8d). A significant amount of riparian area and buffering potential is accumulated along the two headwater tributaries of SPC and its mainstem (Figure 8a). This resulted in a high proportion of long duration turnover times along the stream network (Figure 8d) and a median catchment riparian turnover half-life of 15.3 days (Table 2 and Figure 7c). SPC also had the largest riparian groundwater contribution in its annual snowmelt hydrograph (Table 2 and Figure 9, SPC). Total riparian runoff was 97.4 mm for the entire study period. Riparian groundwater contributions were persistent before snowmelt (61%) and during the rising (26%), peak (30%), and falling limb (53%) of the annual snowmelt hydrograph (Figure 8g).

[43] LSC was more characteristic of other TCEF catchments (UTC, LTC, and MSC) with more moderate values of riparian buffering (Figure 8b) and turnover half-life values along their stream length (Figure 7c UTC, LTC, MSC, and LSC, and Figure 8e). Within these catchments, the majority

**Table 2.** Tenderfoot Creek Experimental Forest Catchment Landscape Distributions and Riparian Turnover and Runoff

| Catchment | % Riparian Area | Median Hillslope UAA (m <sup>2</sup> ) | Median Riparian UAA (m <sup>2</sup> ) | Median Buffer Ratio | Median <i>t</i> <sub>50</sub> time (days) | Total Riparian Runoff (mm) | Riparian Runoff (%) |
|-----------|-----------------|--|---------------------------------------|---------------------|---|----------------------------|---------------------|
| SPC       | 6.10            | 1695                                   | 148                                   | 0.1330              | 15.3                                      | 97.4                       | 36                  |
| UTC       | 4.99            | 3510                                   | 167                                   | 0.0640              | 12.98                                     | 34.8                       | 17                  |
| LSC       | 3.0             | 2357                                   | 148                                   | 0.0591              | 12.5                                      | 45.0                       | 14                  |
| LTC       | 3.90            | 2403                                   | 145                                   | 0.0597              | 12.6                                      | 39.7                       | 12                  |
| MSC       | 3.10            | 2983                                   | 181                                   | 0.0578              | 12.45                                     | 37.9                       | 11.3                |
| SUN       | 1.70            | 4488                                   | 156                                   | 0.0419              | 9.8                                       | 4.8                        | 1.9                 |
| BUB       | 0.89            | 3345                                   | 124                                   | 0.0348              | 9.3                                       | 3.2                        | 1.3                 |

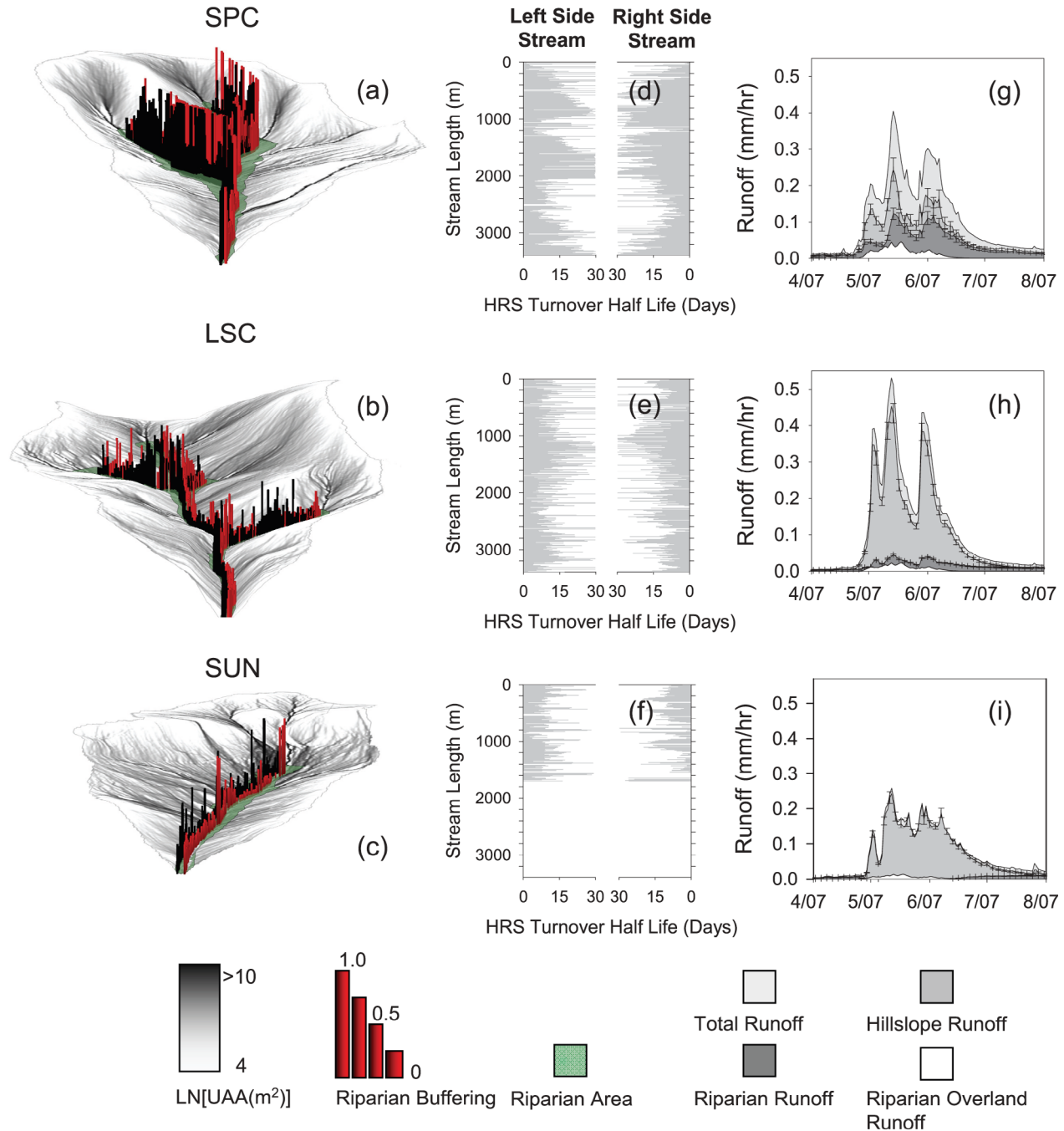


**Figure 8.** Subcatchment (a–c) hillslope UAA, riparian area, and riparian buffering potential (black and red bars), (d–f) the HRS stream network turnover distribution derived from the riparian buffering-turnover relationship (equation (5)), and (g–i) spatial source water separations for each subcatchment. Catchments with higher riparian buffering and turnover time distributions have a more sustained riparian groundwater contribution to their annual snowmelt hydrographs.

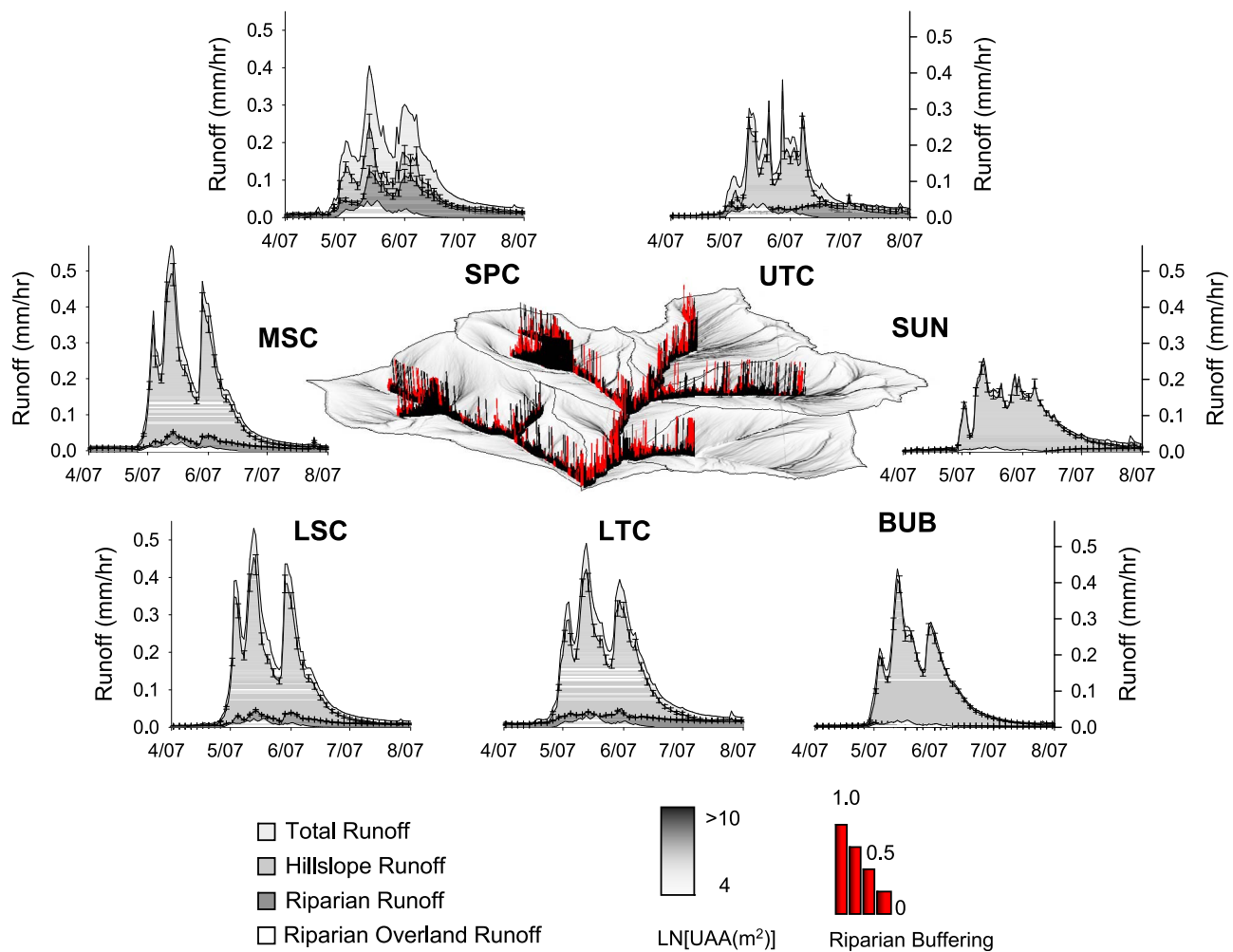


**Figure 9.** Spatial source water separations for the TCEF subcatchments and the TCEF UAA accumulation patterns and stream network riparian buffering (ratio of local riparian and hillslope area). Runoff was separated into hillslope, riparian, and riparian saturation overland flow components. Error bars indicate the uncertainty in the hillslope and riparian components. The frequency of different magnitude riparian buffering and turnover times along the stream network determined the spatial sources of water detected at each catchment's outlet. Catchments with a greater frequency of high riparian buffering of hillslope inputs and long turnover times had more sustained riparian contributions in their snowmelt hydrographs.

of large riparian buffering values are positioned along the catchment headwaters and at interspersed locations along each stream network's main stem (Figure 8b). The extent of riparian area relative to hillslope area inputs at the majority of stream network positions is smaller and hillslope inputs were often more focused through small riparian zones. This resulted in less riparian buffering along the stream network (median buffer ratio 0.64–0.59; Table 2) relative to SPC and median catchment riparian turnover half-lives ranging from 12.5 to 13.0 days. Riparian and hillslope groundwater contributions were also more typical of TCEF catchments with moderate  $t_{50}$  distributions (UTC, LTC, MSC, and LSC; Figure 8h; Figure 9). As an example, LSC's percent riparian runoff contributions decreased during the transition from base flow (58%) to the rising limb (17%). The magnitude of riparian runoff increased throughout the peak of the snowmelt hydrograph and was synchronous with runoff dynamics, albeit it was a small percentage of total runoff (12%) relative to hillslope contributions. During the recession, riparian runoff increased to 32%. Total riparian runoff for

LSC during the snowmelt period was 45 mm, within the range (34.8–45.0 mm) observed for other TCEF catchments with moderate  $t_{50}$  times.

[44] SUN and BUB creek were characteristic of catchments with the highest frequency of small riparian buffering values (Figures 7c and 8c) and  $t_{50}$  times (Figure 7c SUN and BUB, and Figure 8f) along the stream network. Both are first-order stream networks with less dissected hillslope topography and higher median hillslope inflows (Table 2) that are more evenly distributed along the stream network (Figure 8c). They also have the smallest percentages of total riparian area (1.70 and 0.89) along their stream networks and minimal buffering of hillslope UAA (Figure 8c). The combination of small riparian area relative to large hillslope UAA sizes resulted in a high frequency of fast riparian turnover times (Figure 8f) and median catchment turnover half-lives of 9.8 and 9.3 days (Figure 7c SUN and BUB). Riparian groundwater contributions were also typical of TCEF catchments with fast riparian turnover times (Table 2 and Figure 9 SUN and BUB). For example, SUN's base

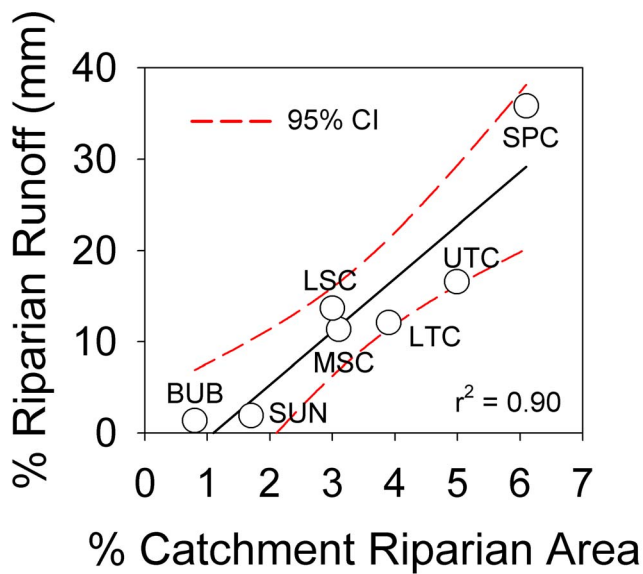


**Figure 10.** The riparian percentage of total runoff during the snowmelt period plotted against the percentage of riparian area for each TCEF catchment.

flow riparian contributions initially comprised 67% of runoff. Riparian contributions initially increased during the rising limb but decreased to only 1% during peak runoff (Figure 8i; Figure 9 SUN and BUB). During the recession, riparian contributions progressively increased to 17% of total runoff. Total riparian runoff for SUN was small (4.8 mm) relative to the majority of the other TCEF catchments. BUB was the other TCEF catchment with a similar median turnover time (9.3 days), and it exhibited similar riparian runoff dynamics (Figure 9 BUB and Table 2) and total contributions (3.8 mm).

[45] We compared the percentage of each catchment's total riparian area to its total riparian runoff contributions during the snowmelt hydrograph (Figure 10). A strong linear relationship ( $r^2 = 0.90$ ) suggested that increasing total catchment riparian area can result in increased riparian groundwater contributions. While this relationship was strong, it provides little insight into the relationship between the internal interactions and connections that can occur between hillslope and riparian settings within a catchment.

[46] We also plotted the median value of each catchment's  $t_{50}$  time (equation (2); Figure 7) against its riparian groundwater contribution (Figure 9) to better elucidate how the distribution of water table connectivity (as represented by hillslope UAA size [Jencso et al., 2009]) among local hillslope and riparian area assemblages can affect whole watershed response (Figure 11). The amount of riparian runoff exiting each catchment increased linearly with increasing catchment median  $t_{50}$  time duration (Figure 11;  $r^2 = 0.91$ ).

## 5. Discussion

### 5.1. What is the Effect of HRS Connectivity Duration on the Degree of Turnover of Water and Solutes in Riparian Zones?

[47] Transient hillslope groundwater tables are important to the timing and magnitude of runoff and delivery of

solutes to stream networks. Equally important is the potential for the riparian zone to buffer hillslope groundwater inputs and thereby stream water composition. We investigated shallow groundwater hydrologic and specific conductance (as a surrogate of solute concentrations) dynamics across four hillslope-riparian-stream (HRS) transects with different riparian and hillslope sizes to ascertain controls on riparian buffering of hillslope runoff and the resulting expression of hillslope solute signatures in stream water. Our results indicate that the intersection of HRS connectivity (as controlled by hillslope UAA size [Jencso et al., 2009]) with riparian area extents is a first-order control on the degree of riparian water turnover during snowmelt.

[48] Stream positions with riparian zones adjacent to larger hillslope UAA were poorly buffered. These positions had longer duration hillslope-riparian-stream hydrologic connectivity (T1 and T2) and riparian groundwater SC that maintained or approached hillslope SC signatures over the course of spring runoff (Figure 4, T1 and T2). This indicated that riparian water in the riparian zone before snowmelt was fully mixed and displaced by hillslope groundwater with connectivity initiation and maintenance. For example, T1, the HRS sequence with the largest hillslope UAA size and continuous HRS hydrologic connectivity, had the fastest turnover time (3 days) across the four transects under observation. The riparian zone of T1 was relatively large compared to other transects with longer turnover times. However, riparian groundwater SC was always similar to hillslope groundwater SC (Figure 3a). This suggests that the continuous delivery of hillslope water to the riparian zone minimized its buffering potential. Along HRS sequences with large hillslope UAA relative to riparian area extents,

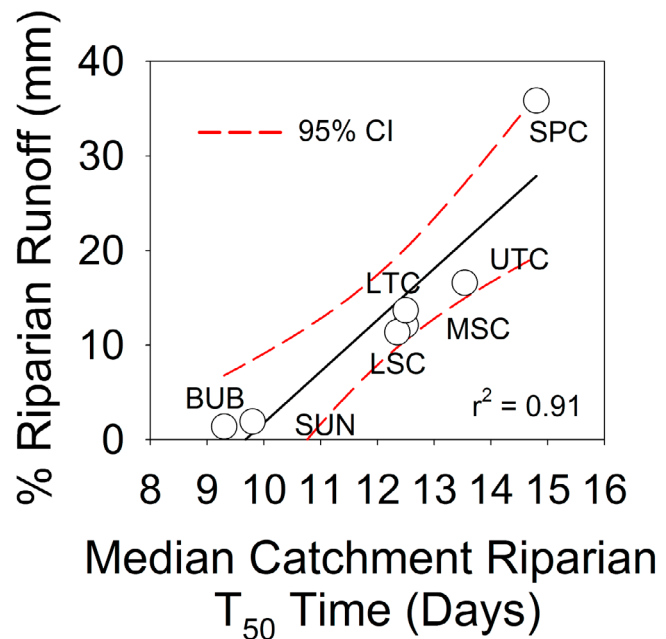


**Figure 11.** The percentage of riparian runoff during the snowmelt period plotted against the median of the riparian turnover half life distribution for each TCEF subcatchment. The total riparian runoff observed at each catchment outlet was a function of the distribution of riparian turnover times within each catchment.

the riparian zone exerts minimal control on stream water composition.

[49] Stream positions with larger riparian zones adjacent to smaller hillslope inputs were better buffered. These positions (T3 and T4) exhibited shorter duration HRS hydrologic connectivity [Jencso *et al.*, 2009], and riparian groundwater SC never reached hillslope groundwater signatures. The rate of riparian SC decline was also less than along transects with smaller riparian: hillslope zone buffer ratios (Figure 4). This is exemplified in transect T3 where the HRS hydrologic connection was sustained for 29 days during the snowmelt period and the riparian zone was the largest under observation. Only one riparian volume was turned over along T3 during its connectivity duration. Transect 4 exhibited transient hillslope connectivity (9 days) relative to its medium-sized riparian zone. This resulted in the greatest observed riparian buffering and turnover of only 26% of the original riparian water in response to HRS connectivity. These dynamics suggest that the decline of riparian groundwater SC toward hillslope signatures was limited by the HRS hydrologic connectivity duration and the relatively large amount of water stored in the riparian zone before connectivity initiation.

[50] This study has considered the topographically driven connections that can initiate riparian groundwater turnover and mixing during wetter catchment states. While topographic controls were strong across all four transects, each exhibited a different goodness of fit relationship between the dilution in riparian SC and time (Figure 4;  $r^2$  ranging from 0.62 to 0.96). These differences could be associated with additional controls on riparian groundwater turnover including vertical infiltration of snowmelt directly into the riparian zone and/or incomplete mixing of riparian and hillslope groundwater. Emergence of groundwater from deeper bedrock flow paths [Vidon and Smith, 2007], stream water ingress to the riparian zone [Burt *et al.*, 2002; Duval and Hill, 2006], and down valley shifts in equipotential gradients [Larkin and Sharp, 1992; Vidon and Hill, 2004b] could also introduce complexities in stream reaches with different morphologies and during drier time periods.

[51] In this investigation, HRS connectivity initiation and duration was the primary driver of riparian water and solute turnover during the snowmelt period. We suggest that the ratio between riparian and hillslope area can be interpreted as a buffer capacity index (Figure 5) within a landscape analysis framework [McGlynn and Seibert, 2003] and, when combined with estimates of connectivity duration [Jencso *et al.*, 2009], can provide a surrogate measure of the groundwater turnover/mixing that occurs along individual HRS landscape sequences in a stream network.

[52] Physical hydrologic mechanisms (e.g., hydrologic connectivity and riparian water turnover dynamics) are important context, and we suggest necessary considerations before one interprets and attempts to quantify biogeochemical cycling and water quality buffering potential in riparian zones [Peterjohn and Correll, 1984]. For example, a common finding across field studies of riparian zones in diverse landscape settings is the importance of water movement rates on the potential for nitrate removal from shallow groundwater via denitrification [Burt and Arkell, 1987; Lowrance, 1992; Hill, 1996; Creed and Band, 1998; Welsch *et al.*, 2001; Vidon and Hill, 2004b]. Water quality functions often attributed to riparian areas can be strongly affected by

the rate of water movement [Schlesinger, 1991] and together with biogeochemical transformations and simple volume buffering can mediate streamwater nutrient loading.

[53] Variability in the duration of connectivity between hillslopes and riparian zones is also important to consider when assessing riparian buffering efficacy through time. Landscape-scale results suggested turnover dynamics will be variable from year to year in response to changes in precipitation magnitude, duration, and frequency. For example, in this study, T4 would have required 115 days (31% of the water year) of HRS connectivity to fully turn over the adjacent riparian zone (Table 1 and Figure 6). However, the hillslope UAA for this transect was 1527 m<sup>2</sup>, and typical HRS groundwater connectivity dynamics reported for hillslopes in this UAA size range by Jencso *et al.* [2009] were limited to ~29 days (8% of the water year). A substantial increase in annual precipitation would be required to sustain HRS connectivity duration at T4 to 115 days and fully turn over riparian zone water. This suggests that some riparian positions along the stream network could shift from well to poorly buffered in wetter years. Alternatively, a decrease in annual precipitation would decrease the HRS connectivity duration across the entire range of UAA sizes and result in less mixing and displacement of riparian groundwater and subsequently more effective riparian buffering of hillslope runoff. Both of these scenarios suggest significant interplay between climate variability, stream source water contributions, and riparian buffering efficiency across time.

## 5.2. How Does Landscape Structure Influence Stream Network Hydrologic Dynamics and the Timing and Amount of Source Waters Detected at the Catchment Outlet?

[54] The relationship between landscape structure and runoff generation, timing, and mixing dynamics has been difficult to interpret. Investigations utilizing source water separations at the catchment outlet have suggested that contributions of hillslope and riparian zone water to streamflow are proportional to hillslope and riparian size arrangements and the degree of hydrologic connectivity that occurs between them [McGlynn and McDonnell, 2003b]. However, little research to date has investigated landscape-scale hillslope and riparian shallow groundwater connectivity and mixing dynamics and how they are distributed across entire stream networks.

[55] Our results demonstrated that landscape structure strongly influenced the maximum HRS shallow groundwater connectivity (ranging from 56% to 80% of the stream network) and its temporal change within each catchment. Topographic convergence and divergence in the landscape is one measure of catchment complexity and is reflected in the frequency distribution of hillslope upslope accumulated area sizes along the stream network. Catchments (e.g., SPC) with more dissected landscapes had more diffuse hillslope area inputs and lower median catchment UAA values. This resulted in a higher proportion of short duration HRS connectivity along the stream network and less HRS connectivity during peak snowmelt (~56% network connectivity in SPC; Figure 7a). Less dissected catchments (e.g., SUN) had higher median UAA values, elevated annual connectivity, and higher maximum HRS network connectivity (~80% network connectivity in SUN; Figure 7a).

[56] The intersection of hillslope area accumulation with its adjacent riparian area indicated riparian buffering potential (equation (14)). We measured an order of magnitude difference in the median riparian buffering values across the seven subcatchments even though they had similar median riparian extents (Table 2). This was a result of the spatial organization of hillslope area accumulation relative to riparian area extents along the stream network. Catchment topography and topology resulted in some catchments with more diffuse inputs of hillslope area adjacent to large riparian areas and higher median riparian buffering values (Figures 7b and 8a). Lower median riparian buffering occurred in the catchments with less convergence/divergence that focused larger hillslope inputs into smaller riparian zones (Figures 7b and 8c).

[57] Each catchment's riparian buffering (Figure 7b) and riparian turnover (Figure 7c) frequency distributions suggested that large differences in the riparian and hillslope groundwater components would be detected in catchment runoff. Catchments with higher riparian buffering would have less riparian groundwater turnover and less expression of hillslope groundwater in their snowmelt hydrographs. Lower median riparian buffering and faster riparian turnover would lead to greater hillslope contributions to streamflow as riparian zones flush in response to more sustained hillslope connectivity. Independently determined source water hydrograph separations supported these hypotheses derived from landscape analyses (Figure 11). Total riparian runoff from each of the seven catchments ranged from 3 to 97 mm during the seasonal snowmelt period. This is nearly an order of magnitude difference in riparian groundwater contributions between the seven headwater catchments; all of which are within 5 km of one another within the greater 22.8 km<sup>2</sup> Tenderfoot Creek catchment.

[58] Catchment structure also appeared to control the timing of riparian and hillslope groundwater expressed in runoff. When HRS connectivity is initiated, water moves from hillslopes through riparian zones to the stream resulting in increased stream flow. However, the hillslope water first mixes with and displaces groundwater stored in the riparian zones before the event (Figure 4). In general, a larger riparian zone results in longer turnover times of the preconnectivity riparian chemical signature (Figure 5) and a more sustained riparian groundwater contribution to stream flow. Hydrograph separation results from each catchment indicated an increase in riparian contributions with snowmelt (Figure 11), initiated by HRS connectivity (Figure 3) [Jencso *et al.*, 2009] and mixing and displacement of riparian water by hillslope water (Figure 4). However, the persistence of a riparian signature in each hydrograph varied according to the timing of turnover across each stream network (e.g., Figures 8d, 8e, and 8f). This suggests that the frequency of different HRS connectivity durations across the watershed controls runoff magnitude [Jencso *et al.*, 2009], but it is the intersection of connectivity and the turnover dynamics of the adjacent riparian reservoirs that controls the source water signature of the stream (as the mixture of hillslope and riparian source waters) through time.

[59] Our observations suggest that each catchment's structure largely controlled the hydrologic and solute dynamics measured in stream flow. Variability in landscape structure can influence the timing, magnitude, and location of water delivery from uplands to near-stream areas during a storm

event. The interaction/intersection of hillslope water and water stored in the riparian zones determines the timing and proportion of source waters measured at the catchment outlets. These observations suggest a degree of predictability when estimating where in the landscape runoff is generated and its source water composition through time in catchments of differing size and structure.

### 5.3. Landscape Connectivity Conceptual Model of Runoff Generation, Riparian Buffering, and Source Water Mixing

[60] Many field studies have characterized the heterogeneity of hydrologic response at the plot, landscape, and catchment scales. This has resulted in the development of detailed and complex characterizations of catchment dynamics but little transferability of general principles across catchment divides. We suggest hydrologic connectivity as a "mechanism to whittle down unnecessary details and transfer dominant process understanding from the hillslope to the catchment scales [Sivapalan, 2003]." The following paragraphs present a simple conceptual model of catchment response to snowmelt and precipitation events based on the relationships between landscape structure, metrics of HRS hydrologic connectivity, and riparian buffering.

[61] Jencso *et al.* [2009] found that the magnitude of runoff generation in one watershed at the TCEF was driven by variability in hillslope UAA size distributions and the frequency of their lateral connections along the stream network. During base flow periods, the majority of the stream network's riparian zones were hydrologically disconnected from their uplands except those adjacent to the largest hillslopes. As snowmelt proceeded HRS connectivity was initiated across progressively smaller hillslope UAA sizes and runoff increased with each subsequent connection. Here we suggest that the sequencing of connectivity initiation (according to topography and topology) across the stream network determines runoff magnitude through time, but that it is the intersection of connectivity frequency and duration with riparian area extents that controls riparian buffering and source water components measured at the catchment outlet.

[62] A spectrum of riparian groundwater turnover times is possible in a given watershed according to the arrangement of hillslope and riparian sizes. HRS sequences with large hillslope UAA (more persistent connections) relative to riparian area will turn over quickly and contribute predominantly hillslope water during the course of an event. At the other end of the spectrum, HRS sequences with small hillslope UAA (transient connections) and larger riparian zones will be well buffered against hillslope throughflow and contribute a more persistent quantity of riparian groundwater to the stream. Therefore, a catchment's buffering efficacy and outlet source water dynamics are a result of an integration of the frequency and timing of HRS hydrologic connectivity and associated riparian buffering (turnover) across the stream network. If the riparian buffering potential exceeds its connectivity duration across the network, then a riparian groundwater contribution will dominate the stream hydrograph. However, greater hillslope connectivity and lower riparian buffering will result in increased turnover of riparian groundwater and a greater hillslope source water signature measured at the catchment outlet. Each watershed

progresses from the well to poorly buffered case through time and with increasing antecedent wetness and event size and duration.

[63] The value of a conceptual hydrologic model can be measured by its ability to be effectively transferred to alternate catchments. Contributions of runoff and solutes to the TCEF stream network are highly variable in time and space and largely driven by the topographic redistribution of water from the uplands, through riparian zones, and into the stream network. Many studies have observed strong relationships between landscape topography and runoff generation [Dunne and Black, 1970; Anderson and Burt, 1978; Beven, 1978; Burt and Butcher, 1985], runoff spatial sources [Sidle *et al.*, 2000; McGlynn and McDonnell, 2003b], and water residence times [McGlynn *et al.*, 2004; McGuire *et al.*, 2005; Tetzlaff *et al.*, 2009]. This suggests that metrics of topography, topology, and resulting connectivity could be an organizing principle for predicting storm response in headwater catchments. In other environments, bedrock geology [Huff *et al.*, 1982; Wolock *et al.*, 1997; Burns *et al.*, 1998; Shaman *et al.*, 2004; Uchida *et al.*, 2005], soil characteristics [Buttle *et al.*, 2004; Devito *et al.*, 2005; Soulsby *et al.*, 2006; Tetzlaff *et al.*, 2009], or other catchment features could additionally influence and even dominate connectivity between source areas and the stream network.

[64] Variability in patterns of topography, soils, geology, and climate all influence runoff generation. However, their combined effect and relative importance for streamflow dynamics has been difficult to decipher. To attribute appropriate causal mechanisms to catchment outlet response, we emphasize the importance of internal/distributed hydrologic monitoring across time. Changing soil moisture states and the transition from vertical to lateral connectivity in the shallow subsurface [Grayson *et al.*, 1997] or the partitioning of water to/from deeper bedrock storage [Sidle *et al.*, 2000; Shaman *et al.*, 2004; Uchida *et al.*, 2005] can significantly alter water sources observed in streamflow. For example, a recent distributed assessment of the stream network water balance at Tenderfoot Creek indicated that runoff generation transitioned from topographically driven lateral redistribution of water and hydrologic connectivity [Jenciso *et al.*, 2009] at wetter catchment states to detectable geologic controls (~10% stream network connectivity) at low base flow [Payn *et al.*, 2009]. This suggests a potential transition in streamflow generation mechanisms as a function of catchment wetness state.

[65] Consideration of hydrologic connections and source areas within the landscape is critical to deconvolution of catchment outlet dynamics into their spatial sources and controlling mobilization processes. We suggest that the conceptualization presented here provides a simple and potentially robust description of runoff response across catchments of different size and structure and may prove useful for prediction in ungauged basins.

#### 5.4. Watershed Management Implications of Riparian Buffering of Landscape Hydrologic Connectivity

[66] Riparian zone management to protect and promote water quality is a valuable strategy across natural and disturbed landscapes. However, few tools exist to aid prioritization of riparian management by assessing the relative importance of riparian zones across the landscape and their

potential to influence upland runoff and associated water quality constituents [Allan *et al.*, 2008]. In this paper we have presented a hydrological context and volumetric buffering quantification that considers not only riparian zone size and fraction of the total catchment but also an estimate of each riparian zone's buffering potential relative to the upland delivery of runoff. We focused on the physical hydrology and tracer behavior across riparian zones. However, this context is also critical for understanding potential for biogeochemical transformations because it demonstrates the primary landscape controls on riparian water turnover rates and magnitude and provides tools to quantify these processes. For example, water delivery from hillslopes can influence the supply of oxygenated water to carbon-rich riparian zones thereby influencing redox state and the potential for microbial denitrification [Hill, 2000; Vidon and Hill, 2004a]. Better assessment of riparian zone potential to mitigate upland water quality degradation, new methods to aide prioritization of riparian management and protection across space, and tools to assess catchment-scale riparian buffering potential or conversely catchment sensitivity to upland loading have strong relevance to watershed management and applied hydrology-biogeochemistry applications. We suggest that research presented here provides some initial insight not only into how we might better characterize and quantify riparian zone buffering potential at the reach and catchment scales but also highlight the need for tools to bring these concepts to the riparian and watershed management communities.

## 6. Conclusion

[67] Hydrological science continues to search for insights into catchment response based on landscape structure. The research described in this paper highlights terrain metrics that link hydrologic process observations to landscape and catchment scale response. This approach discretizes the catchment into its component landscape elements and analyzes their topographic and topologic attributes as surrogates for their hydrologic connectedness, as measured through detailed field observations. On the basis of our high-frequency monitoring of groundwater connectivity and solute dynamics from the plot to catchment scales we conclude

[68] • The degree of riparian water turnover (riparian buffering) is a function of hydrologic connectivity and the size of the riparian area relative to the adjacent hillslope.

[69] • The frequency of stream network hydrologic connectivity and associated degree of riparian buffering (turnover) control the timing and magnitude of catchment runoff and solute export.

[70] • Catchment structure/organization strongly affects riparian buffering and runoff source water composition.

[71] • Climate variability (wet or dry years) may introduce a "quantifiable" shift in stream network connectivity and the mobilization of water and solutes from riparian and hillslope source areas.

[72] Discretization of catchments into their component landscape elements and monitoring the hydrochemical response in these landscape elements and by comparing catchments of varying structure provided insight into the spatial sources of runoff that are hidden by hydrograph separations measured at the catchment outlet alone. This approach allowed us to estimate where runoff and solute mobilization occurred within the landscape and how the

integration of these dynamics along the stream network relate to the magnitude of runoff and solute export across catchments of differing scale and structure.

## Appendix A

[73] We present specific conductance and water table results for each transect in order of increasing riparian buffer ratios (riparian area/hillslope area) and decreasing hillslope UAA size and connectivity duration (Figure 3).

[74] Transect 1 (T1) was located at the base of a  $\sim 20.5^\circ$  convergent hillslope. It had the largest observed UAA ( $46,112 \text{ m}^2$ ) of any of the 24 transects, a medium-sized riparian area ( $783 \text{ m}^2$ ), and the lowest buffer ratio (0.017). The riparian zone exhibited a relatively constant water table approximately 65 cm below the ground surface (Figure 3a). Groundwater was recorded within 15 cm of the ground surface in the hillslope well, located 5 m upslope of the toe slope break, for the entire water year. Hillslope and riparian groundwater SC remained relatively constant throughout the year with a slight dilution during peak snowmelt (Figure 3a). Riparian groundwater SC dynamics at this transect always corresponded with those measured at the hillslope well.

[75] Transect 2 (T2) was located along a  $7070 \text{ m}^2$ ,  $\sim 23^\circ$  planar hillslope with a small  $282 \text{ m}^2$  riparian area. The riparian buffer ratio at this site was 0.039. The riparian water table remained within 30 cm of the ground surface during the year and approached the surface when a hillslope water table occurred during snowmelt (Figure 3b). The transient hillslope water table first developed on 26 April 2007 and remained connected to the riparian zone through snowmelt until 11 June 2007 (46 day HRS connection). Initial riparian groundwater SC was  $108 \mu\text{S cm}^{-1}$  and decreased to  $29 \mu\text{S cm}^{-1}$  after a HRS water table connection was established (Figure 3b).

[76] Transect 3 (T3) was located near the base of a convergent hillslope hollow ( $\sim 15.6^\circ$ ) with midrange UAA ( $10,165 \text{ m}^2$ ) and a large riparian area ( $1148 \text{ m}^2$ ). The riparian buffer ratio at this transect was 0.113. Riparian zone water tables remained within 20 cm of the ground surface for the entire year and surface saturation occurred during snowmelt and rain events (Figure 3c). A hillslope water table was first observed on 12 May 2006, exhibiting a rapid rise and sustained connection to its associated riparian zone (Figure 3c). Sustained HRS connectivity was observed during snowmelt (21 day connection) and the subsequent rain periods (8 day connection), totaling 29 days. Riparian groundwater before a hillslope water table initiation was  $185 \mu\text{S cm}^{-1}$  but decreased to  $77 \mu\text{S cm}^{-1}$  after a HRS connection was established (Figure 3c). Riparian groundwater SC never reached hillslope SC at this transect.

[77] Transect 4 (T4) was located along a  $\sim 26^\circ$  divergent hillslope with small UAA ( $1527 \text{ m}^2$ ) and a large riparian area ( $700 \text{ m}^2$ ). The riparian buffer ratio at this site was 0.458. The riparian water table remained between 60 and 50 cm below the ground surface during base flow but increased to within 15 cm of the ground surface during snowmelt (Figure 3d). The hillslope water table response to rain and snow events was highly transient (Figure 3d) and early in the snowmelt period diurnal HRS water table connections/disconnections occurred in association with daily snowmelt peaks. HRS connectivity was observed for a total

of 9 days at this transect. Riparian SC was  $139 \mu\text{S cm}^{-1}$  before snowmelt and decreased to  $70 \mu\text{S cm}^{-1}$  after a hillslope groundwater table developed (Figure 3d). The riparian groundwater SC never reached hillslope values at this transect.

[78] **Acknowledgments.** This work was made possible by NSF grant EAR-0337650 to McGlynn, EAR-0337781 to Gooseff, and an INRA fellowship awarded to Jencso. The authors appreciate extensive logistic collaboration with the U. S. Department of Agriculture, Forest Service, Rocky Mountain Research Station, especially, Ward McCaughey, Scientist-in-Charge of the Tenderfoot Creek Experimental Forest. We thank Jan Siebert, Thomas Grabs, and Robert Payn for technical and collaborative support and Galena Ackerman and John Mallard for performing laboratory analyses. We are grateful to Jennifer Jencso, Vince Pacific, Diego Riveros-Iregui, and especially Austin Allen for invaluable assistance in the field.

## References

- Ahmad, S., and S. I. Hasnain (2002), Hydrograph separation by measurement of electrical conductivity and discharge for meltwaters in the Ganga Headwater basin, Garhwal Himalaya, *J. Geol. Soc. India*, 59(4), 323–329.
- Allan, C. J., P. Vidon, and R. Lowrance (2008), Frontiers in riparian zone research in the 21st century, *Hydrol. Process.*, 22, 3221–3222, doi:10.1002/hyp.7086.
- Anderson, M. G., and T. P. Burt (1977), Automatic monitoring of soil moisture conditions in a hillslope spur and hollow, *J. Hydrol.*, 33, 27–36.
- Anderson, M. G., and T. P. Burt (1978), The role of topography in controlling throughflow generation, *Earth Surf. Processes Landforms*, 3, 331–334.
- Beven, K. J. (1978), The hydrological response of headwater and sideslope areas, *Hydrol. Sci. Bull.*, 23, 419–437.
- Boyer, E. W., G. M. Hornberger, K. E. Bencala, and D. M. McKnight (1997), Response characteristics of DOC flushing in an alpine catchment, *Hydrol. Processes*, 11, 1635–1647.
- Brinson, M. M. (1993), Changes in the functioning of wetlands along environmental gradients, *Wetlands*, 13, 65–74.
- Burns, D. A., P. S. Murdoch, G. B. Lawrence, and R. L. Michel (1998), Effect of groundwater springs on  $\text{NO}_3^-$  concentrations during summer in Catskill Mountain streams, *Water Resour. Res.*, 34, 1987–1996, doi:10.1029/98WR01282.
- Burns, D. A., J. J. McDonnell, R. P. Hooper, N. E. Peters, J. E. Freer, C. Kendall, and K. Beven (2001), Quantifying contributions to storm runoff through end-member mixing analysis and hydrologic measurements at the Panola Mountain Research Watershed (Georgia, USA), *Hydrol. Process.*, 15, 1903–1924.
- Burt, T. P., and B. P. Arkell (1987), Temporal and spatial patterns of nitrate losses from an agricultural catchment, *Soil Use Manage.*, 3, 138–143.
- Burt, T. P., and D. Butcher (1985), Topographic controls on soil moisture distribution, *J. Soil Sci.*, 36, 469–476.
- Burt, T. P., L. S. Matchett, K. W. T. Goulding, C. P. Webster, and N. E. Haycock (1999), Denitrification in riparian buffer zones: The role of floodplain hydrology, *Hydrol. Process.*, 13, 1451–1463.
- Burt, T. P., et al. (2002), Water table fluctuations in the riparian zone: comparative results from a pan-European experiment, *J. Hydrol.*, 265(1–4), 129–148.
- Buttle, J. M., P. J. Dillon, and G. R. Eerkes (2004), Hydrologic coupling of slopes, riparian zones and streams: An example from the Canadian Shield, *J. Hydrol.*, 287, 161–177, doi:10.1016/j.jhydrol.2003.09.022.
- Caissie, D., T. L. Pollock, and R. A. Cunjak (1996), Variation in stream water chemistry and hydrograph separation in a small drainage basin, *J. Hydrol.*, 178, 137–157.
- Carlyle, G. C., and A. R. Hill (2001), Groundwater phosphate dynamics in a river riparian zone: effects of hydrologic flow paths, lithology, and redox chemistry, *J. Hydrology*, 247, 151–168.
- Chanat, J., and G. M. Hornberger (2003), Modeling catchment-scale mixing in the near-stream zone: Implications for chemical and isotopic hydrograph separation, *Geophys. Res. Lett.*, 30(2), 1091, doi:10.1029/2002GL016265.
- Cirno, C. P., and J. J. McDonnell (1997), Linking the hydrologic and biochemical controls of nitrogen transport in near-stream zones of temperate-forested catchments: A review, *J. Hydrol.*, 199, 88–120.

- Covino, T. P., and B. L. McGlynn (2007), Stream gains and losses across a mountain-to-valley transition: Impacts on watershed hydrology and stream water chemistry, *Water Resour. Res.*, *43*, W10431, doi:10.1029/2006WR005544.
- Creed, I. F., and L. E. Band (1998), Export of nitrogen from catchments within a temperate forest: Evidence for a unifying mechanism regulated by variable source area dynamics, *Water Resour. Res.*, *34*, 3105–3120, doi:10.1029/98WR01924.
- Devito, K., I. Creed, T. Gan, C. Mendoza, R. Petrone, U. Silins, and B. Smerdon (2005), A framework for broad-scale classification of hydrologic response units on the Boreal Plain: Is topography the last thing to consider?, *Hydrol. Process.*, *19*, 1705–1714, doi:10.1002/hyp.5881.
- Dewalle, D. R., B. R. Swistock, and W. E. Sharpe (1988), 3-component tracer model for stormflow on a small Appalachian forested catchment, *J. Hydrol.*, *104*, 301–310.
- Dunne, T., and R. D. Black (1970), Partial area contributions to storm runoff in a small New England watershed, *Water Resour. Res.*, *6*, 1296–1311, doi:10.1029/WR0061005p01296.
- Duval, T. P., and A. R. Hill (2006), Influence of stream bank seepage during low-flow conditions on riparian zone hydrology, *Water Resour. Res.*, *42*, W10425, doi:10.1029/2006WR004861.
- Farnes, P. E., R. C. Shearer, W. W. McCaughey, and K. J. Hansen (1995), Comparisons of Hydrology, Geology, and Physical Characteristics Between Tenderfoot Creek Experimental Forest (East Side) Montana, and Coram Experimental Forest (West Side) Montana, Final Report RJVA-INT-92734, USDA Forest Service, Intermountain Research Station, Forestry Sciences Laboratory, Bozeman, Mont., 19 pp.
- Geneux, D. (1998), Quantifying uncertainty in tracer-based hydrograph separations, *Water Resour. Res.*, *34*, 915–919, doi:10.1029/98WR00010.
- Grabs, T., K. J. Jencso, B. L. McGlynn, and J. Seibert (2010), Calculating terrain indices along streams—A new method for separating stream sides, *Water Resour. Res.*, doi:10.1029/2010WR009296, in press.
- Grayson, R. B., A. W. Western, F. H. S. Chiew, and G. Blöschl (1997), Preferred states in spatial soil moisture patterns: Local and nonlocal controls, *Water Resour. Res.*, *33*, 2897–2908, doi:10.1029/97WR02174.
- Hasnain, S. I., and R. J. Thayer (1994), Hydrograph separation of bulk meltwaters of Dokriani-Bamak Glacier Basin, based on electrical-conductivity, *Curr. Sci.*, *67*, 189–193.
- Hill, A. R. (1996), Nitrate removal in stream riparian zones, *J. Environ. Qual.*, *25*, 743–755.
- Hill, A. R. (2000), Stream chemistry and riparian zones, in *Streams and Ground Waters*, edited by J. Jones and P. J. Mulholland, pp. 83–110, Academic Press, London.
- Holdorf, H. D. (1981), Soil Resource Inventory of the Lewis and Clark National Forest, Interim. In-Service Report, on file with the Lewis and Clark National Forest, Forest Supervisor's Office, Great Falls, Mont.
- Hooper, R., B. Aulenbach, D. Burns, J. J. McDonnell, J. Freer, C. Kendall, and K. Beven (1997), Riparian control of streamwater chemistry: Implications for hydrochemical basin models, *LAHS Redbook*, *248*, 451–458.
- Huff, D. D., R. V. Oneill, W. R. Emanuel, J. W. Elwood, and J. D. Newbold (1982), Flow variability and hillslope hydrology, *Earth Surf. Proc. Land.*, *7*, 91–94.
- Jencso, K. G., B. L. McGlynn, M. N. Gooseff, S. M. Wondzell, K. E. Bencala, and L. A. Marshall (2009), Hydrologic connectivity between landscapes and streams: Transferring reach- and plot-scale understanding to the catchment scale, *Water Resour. Res.*, *45*, W04428, doi:10.1029/2008WR007225.
- Kobayashi, D. (1986), Separation of a snowmelt hydrograph by specific conductance, *J. Hydrol.*, *84*, 157–165.
- Kobayashi, D., Y. Ishii, and Y. Kodama (1999), Stream temperature, specific conductance and runoff process in mountain watersheds, *Hydrol. Process.*, *13*, 865–876.
- Larkin, R., and J. Sharp (1992), On the relationship between river-basin geomorphology, aquifer hydraulics, and ground-water flow direction in alluvial aquifers, *Geol. Soc. Am. Bull.*, *104*, 1608–1620.
- Laudon, H., and O. Slaymaker (1997), Hydrograph separation using stable isotopes, silica and electrical conductivity: An alpine example, *J. Hydrol.*, *201*, 82–101.
- Lowrance, R. (1992), Groundwater nitrate and denitrification in a coastal plain riparian forest, *J. Environ. Qual.*, *21*, 401–405.
- McDonnell, J. J., M. K. Stewart, and I. F. Owens (1991), Effect of catchment-scale subsurface mixing on stream isotopic response, *Water Resour. Res.*, *27*, 3065–3073, doi:10.1029/91WR02025.
- McGlynn, B. L., J. J. McDonnell, J. B. Shanley, and C. Kendall (1999), Riparian zone flow path dynamics during snowmelt in a small headwater catchment, *J. Hydrol.*, *222*, 75–92.
- McGlynn, B. L., and J. J. McDonnell (2003a), Role of discrete landscape units in controlling catchment dissolved organic carbon dynamics, *Water Resour. Res.*, *39*(4), 1090, doi:10.1029/2002WR001525.
- McGlynn, B. L., and J. J. McDonnell (2003b), Quantifying the relative contributions of riparian and hillslope zones to catchment runoff, *Water Resour. Res.*, *39*(11), 1310, doi:10.1029/2003WR002091.
- McGlynn, B. L., and J. Seibert (2003), Distributed assessment of contributing area and riparian buffering along stream networks, *Water Resour. Res.*, *39*(4), 1082, doi:10.1029/2002WR001521.
- McGlynn, B. L., J. J. McDonnell, J. Seibert, and C. Kendall (2004), Scale effects on headwater catchment runoff timing, flow sources, and groundwater-streamflow relations, *Water Resour. Res.*, *40*, W07504, doi:10.1029/2003WR002494.
- McGuire, K. J., J. J. McDonnell, M. Weiler, C. Kendall, B. L. McGlynn, J. M. Welker, and J. Seibert (2005), The role of topography on catchment-scale water residence time, *Water Resour. Res.*, *41*, W05002, doi:10.1029/2004WR003657.
- Mulholland, P. J. (1992), Regulation of nutrient concentrations in a temperate forest streams: Roles of upland, riparian, and instream processes, *Limnol. Oceanogr.*, *37*, 1512–1526.
- Ocampo, C. J., M. Sivapalan, and C. Oldham (2006), Hydrological connectivity of upland-riparian zones in agricultural catchments: Implications for runoff generation and nitrate transport, *J. Hydrol.*, *331*, 643–658, doi:10.1016/j.jhydrol.2006.06.010.
- Pacific, V. J., K. G. Jencso, and B. L. McGlynn (2010), Variable flushing mechanisms and landscape structure control stream DOC export during snowmelt in a set of nested catchments, *Biogeochemistry*, *99*, 193–211, doi:10.1007/s10533-009-9401-1.
- Payn, R. A., M. N. Gooseff, B. L. McGlynn, K. E. Bencala, and S. M. Wondzell (2009), Channel water balance and exchange with subsurface flow along a mountain headwater stream in Montana, United States, *Water Resour. Res.*, *45*, W11427, doi:10.1029/2008WR007644.
- Peterjohn, W. T., and D. L. Correll (1984), Nutrient dynamics in an agricultural watershed—Observations on the role of a riparian forest, *Ecology*, *65*, 1466–1475.
- Ramaswami, A., J. B. Milford, and M. J. Small (2005), *Integrated Environmental Modeling: Pollutant Transport, Fate, and Risk in the Environment*, 1st ed., 688 pp., Wiley.
- Reynolds, M. (1995), Geology of Tenderfoot Creek Experimental Forest, Little Belt Mountains, Meagher County, Montana, in *Hydrologic and Geologic Characteristics of Tenderfoot Creek Experimental Forest, Montana, Final Rep. RJVA-INT-92734*, edited by P. Farnes, pp. 21–32, Intermt. Res. Stn., For. Serv., U.S. Dep. of Agric., Bozeman, Mont.
- Scanlon, T. M., J. P. Raffensperger, and G. M. Hornberger (2001), Modeling transport of dissolved silica in a forested headwater catchment: Implications for defining the hydrochemical response of observed flow pathways, *Water Resour. Res.*, *37*, 1071–1082, doi:10.1029/2000WR900278.
- Schlesinger, W. H. (1991), Biogeochemistry in freshwater wetlands and lakes, in *Biogeochemistry: An analysis of global change*, edited by W. H. Schlesinger, pp. 224–260, Academic Press, London.
- Seibert, J., and B. L. McGlynn (2007), A new triangular multiple flow direction algorithm for computing upslope areas from gridded digital elevation models, *Water Resour. Res.*, *43*, W04501, doi:10.1029/2006WR005128.
- Shaman, J., M. Stieglitz, and D. Burns (2004), Are big basins just the sum of small catchments?, *Hydrol. Processes*, *18*, 3195–3206, doi:10.1002/hyp.5739.
- Sidle, R. C., Y. Tsuboyama, S. Noguchi, I. Hosoda, M. Fujieda, and T. Shimizu (2000), Stormflow generation in steep forested headwaters: A linked hydrogeomorphic paradigm, *Hydrol. Processes*, *14*, 369–385.
- Sivapalan, M. (2003), Process complexity at hillslope scale, process simplicity at the watershed scale: is there a connection?, *Hydrol. Process.*, *17*(5), 1037–1041, doi:10.1002/hyp.5109.
- Soulsby, C., P. J. Rodgers, J. Petry, D. M. Hannah, I. A. Malcolm, and S. M. Dunn (2004), Using tracers to upscale flow path understanding in mesoscale mountainous catchments: Two examples from Scotland, *J. Hydrol.*, *291*, 174–196, doi:10.1016/j.jhydrol.2003.12.042.
- Soulsby, C., D. Tetzlaff, P. Rodgers, S. Dunn, and S. Waldron (2006), Runoff processes, stream water residence times and controlling landscape characteristics in a mesoscale catchment: An initial evaluation, *J. Hydrol.*, *325*, 197–221, doi:10.1016/j.jhydrol.2005.10.024.
- Stewart, M., J. Cimino, and M. Ross (2007), Calibration of base flow separation methods with streamflow conductivity, *Ground Water*, *45*, 17–27, doi:10.1111/j.1745-6584.2006.00263.x.

- Tetzlaff, D., J. Seibert, K. J. McGuire, H. Laudon, D. A. Burn, S. M. Dunn, and C. Soulsby (2009), How does landscape structure influence catchment transit time across different geomorphic provinces?, *Hydrol. Processes*, *23*, 945–953, doi:10.1002/hyp.7240.
- Uchida, T., Y. Asano, Y. Onda, and S. Miyata (2005), Are headwaters just the sum of hillslopes?, *Hydrol. Processes*, *19*, 3251–3261, doi:10.1002/hyp.6004.
- Vidon, P., and A. R. Hill (2004a), Denitrification and patterns of electron donors and acceptors in eight riparian zones with contrasting hydrogeology, *Biogeochemistry*, *71*, 259–283.
- Vidon, P., and A. Smith (2007), Upland controls on the hydrological functioning of riparian zones in glacial till valleys of the midwest, *J. Am. Water Resour. Assoc.*, *43*, 1524–1539.
- Vidon, P. G. F., and A. R. Hill (2004b), Landscape controls on nitrate removal in stream riparian zones, *Water Resour. Res.*, *40*, W03201, doi:10.1029/2003WR002473.
- Welsch, D. L., C. N. Kroll, J. J. McDonnell, and D. A. Burns (2001), Topographic controls on the chemistry of subsurface stormflow, *Hydrol. Processes*, *15*, 1925–1938.
- Weyman, D. R. (1970), Throughflow on hillslopes and its relation to the stream hydrograph, *Bull. Int. Assoc. Scientific Hydrol.*, *15*, 25–33.
- Wolock, D. M., J. Fan, and G. B. Lawrence (1997), Effects of basin size on low-flow stream chemistry and subsurface contact time in the Neversink River Watershed, New York, *Hydrol. Process.*, *11*, 1273–1286.
- 
- K. E. Bencala, U.S. Geological Survey, 345 Middlefield Road, Menlo Park, CA 94025, USA.
- M. N. Gooseff, Civil Environmental Engineering Department, Penn State University, 212 Sackett Bldg., University Park, PA 16802, USA.
- K. G. Jencso and B. L. McGlynn, Department of Land Resources and Environmental Sciences, Montana State University, Bozeman, MT 59717, USA. (kelseyjencso@gmail.com)
- S. M. Wondzell, U.S. Forest Service, Pacific Northwest Research Station Olympia Forestry Sciences Lab, Olympia, WA 98512, USA.

Contribution of Authors

Chapter 4: Variable flushing mechanisms and landscape structure control stream DOC export during snowmelt in a set of nested catchments.

First author: Vincent J. Pacific

Co-authors: Kelsey G. Jencso and Brian L. McGlynn

Contributions: Vince Pacific wrote the majority of this paper. Both Vince Pacific and I were responsible for field instrumentation and hydrometric and chemical data collection, figure development, and the majority of data analysis. I contributed to the writing, performed the terrain analyses, and edited successive versions of the manuscript. Brian McGlynn contributed significant critique and ideas towards development of intellectual content within the paper, data analysis, and edited successive versions of the manuscript.

Manuscript Information

Pacific, V., K. Jencso, and B.L. McGlynn. 2010. Variable flushing mechanisms and landscape structure control stream DOC export during snowmelt in a set of nested catchments. *Biogeochemistry*. doi: 10.1007/s10533-009-9401-1

- Journal: Biogeochemistry
- Status of manuscript (check one)
  - Prepared for submission to a peer-reviewed journal
  - Officially submitted to a peer-reviewed journal
  - Accepted by a peer-reviewed journal
  - Published in a peer-reviewed journal
- Publisher: Springer Science and Business Media
- Date of submission: April 21, 2009
- Date manuscript was published: January 7, 2010
- Issue in which manuscript appeared: 99

Reproduced by kind permission of Springer Science and Business Media

# Variable flushing mechanisms and landscape structure control stream DOC export during snowmelt in a set of nested catchments

Vincent J. Pacific · Kelsey G. Jencso ·  
Brian L. McGlynn

Received: 21 April 2009 / Accepted: 14 December 2009 / Published online: 7 January 2010  
© Springer Science+Business Media B.V. 2010

**Abstract** Stream DOC dynamics during snowmelt have been the focus of much research, and numerous DOC mobilization and delivery mechanisms from riparian and upland areas have been proposed. However, landscape structure controls on DOC export from riparian and upland landscape elements remains poorly understood. We investigated stream and groundwater DOC dynamics across three transects and seven adjacent but diverse catchments with a range of landscape characteristics during snowmelt (April 15–July 15) in the northern Rocky Mountains, Montana. We observed a range of DOC export dynamics across riparian and upland landscape settings and varying degrees of hydrologic connectivity between the stream, riparian, and upland zones. DOC export from riparian zones required a hydrologic connection across the riparian–stream interface, and occurred at landscape positions with a wide range of upslope accumulated area (UAA) and wetness status. In contrast, mobilization of DOC from the uplands appeared restricted to areas with a hydrologic connection across the entire upland–riparian–stream continuum, which generally occurred only at areas with high UAA, and/or at times of high wetness. Further, the relative extent of DOC-rich riparian and

wetland zones strongly influenced catchment DOC export. Cumulative stream DOC export was highest from catchments with a large proportion of riparian to upland area, and ranged from 6.3 to 12.4 kg ha<sup>-1</sup> across the study period. This research suggests that the spatial/temporal intersection of hydrologic connectivity and DOC source areas drives stream DOC export.

**Keywords** Catchment · DOC · Flushing · Landscape structure · Snowmelt · Stream

## Introduction

Stream DOC export from catchments is a significant component of the carbon cycle (Laudon et al. 2004a; Neill et al. 2006; Johnson et al. 2006; Waterloo et al. 2006; Jonsson et al. 2007) and can strongly impact contaminant transport (Imai et al. 2003; Wei et al. 2008). In alpine and subalpine catchments, the majority of annual DOC flux often occurs during snowmelt (Hornberger et al. 1994; Boyer et al. 1997, 2000; Laudon et al. 2004a). The process by which DOC is transported to the stream is commonly referred to as hydrologic nutrient flushing, whereby organic material undergoes a period of accumulation in the soil, and is then released to the stream during snowmelt or precipitation events (Burns 2005). This

---

V. J. Pacific · K. G. Jencso (✉) · B. L. McGlynn  
Department of Land Resources and Environmental  
Sciences, Montana State University, 334 Leon Johnson  
Hall, Bozeman, MT 59717, USA  
e-mail: kelseyjencso@gmail.com

flushing can lead to a characteristic peak in DOC concentrations on the rising limb of the stream hydrograph (Hornberger et al. 1994; Boyer et al. 1997; Inamdar et al. 2004; Hood et al. 2006; Agren et al. 2008; van Vevrseveld et al. 2008). However, the controls on and the variability of DOC flushing at the upland, riparian, and catchment scales are poorly understood (Wieler and McDonnell 2006; van Vevrseveld et al. 2008).

DOC flushing is often used to describe different, but related processes. At baseflow, stream DOC concentrations are generally low due to groundwater inflows through deep, low DOC mineral soil (Fig. 1, Scenario 1) (Hornberger et al. 1994). However, rise of the groundwater table into shallow DOC-rich riparian soil layers at the beginning of snowmelt or precipitation events can lead to a large increase in DOC export from riparian soil to the stream (Fig. 1, Scenario 2) (Bishop et al. 1994; Hornberger et al. 1994; Boyer et al. 1997, 2000; Bishop et al. 2004; Laudon et al. 2004b). This process can be augmented by transmissivity feedback, in which the rising water table enters soils with increasing hydraulic conductivity, leading to increased lateral flow contributions to runoff (Bishop et al. 2004; Laudon et al. 2004b; Wieler and McDonnell 2006). Here, we define this rise of the water table into shallow soils a one-dimensional (1D) process. Often, there is a limited supply of DOC in riparian zones, and persistent 1D flushing can result in decreased DOC concentrations through snowmelt or precipitation events (Hornberger et al. 1994; Boyer et al. 1997).

In addition to 1D flushing, McGlynn and McDonnell (2003) proposed a two-dimensional (2D) nutrient flushing mechanism, which is supported by Bishop et al. (2004) and Hood et al. (2006). In this scenario, catchment DOC export occurs as a function of the connectivity between near-stream and upland areas (Fig. 1, Scenario 3). The initial increase in stream DOC concentrations occurs during the rise of the water table into shallow organic-rich riparian soils. A second source of high DOC on the rising limb of the stream hydrograph occurs as uplands become hydrologically connected to the riparian zones, allowing for quick transmission of upland water that is rich in DOC (Bishop et al. 2004) along preferential flow paths (Fig. 1, Scenario 3a) (McGlynn and McDonnell 2003). This high DOC initial upland runoff is then diluted with lower DOC matrix water (Fig. 1,

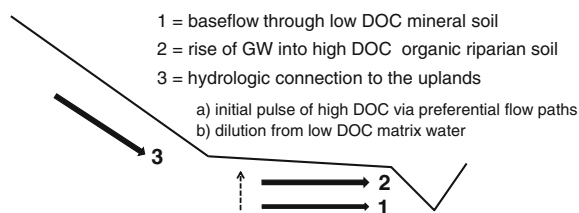


**Fig. 1** Conceptual model of DOC export from the soil to the stream. During times of low flow, such as baseflow, groundwater travels through low DOC mineral soil, and stream DOC concentrations are low (Scenario 1). As flow begins to increase during snowmelt or precipitation events, the groundwater table rises into shallow organic-rich riparian soil, and inputs of DOC from the soil to the stream increase (Scenario 2). As the groundwater table continues to rise, a hydrologic connection develops across the upland–riparian–stream continuum (Scenario 3). An initial pulse of high DOC water from the uplands is transmitted along preferential flow paths (3a). Runoff from the uplands is then diluted by low DOC matrix water traveling through mineral soil (3b)

Scenario 3b), leading to lower stream DOC concentrations on the falling limb of the stream hydrograph (McGlynn and McDonnell 2003). We suggest that in high elevation, snowmelt-dominated catchments, the relative importance of riparian and upland sources of DOC can vary strongly through space and time and is largely dependent upon riparian extent and the degree of hydrologic connectivity between the stream and the riparian and upland zones.

Landscape structure can strongly influence the degree of hydrologic connectivity across the upland–riparian–stream (URS) continuum (Jencso et al. 2009), and therefore DOC export. Following Jencso et al. (2009), we define hydrologic connectivity as the time period when a groundwater connection exists between landscape elements (e.g. stream, riparian, and upland zones). Through a combination of extensive groundwater monitoring (146 recording groundwater wells) and landscape level topographic analysis, Jencso et al. (2009) found that the duration and timing of URS hydrologic connectivity was a function of upslope accumulated area (UAA). They found a strong positive relationship between URS hydrologic connectivity and UAA ( $r^2 = 0.91$ ), with the highest and most persistent URS hydrologic connectivity at landscape positions with large UAA. Here, we seek to investigate the effect of landscape position and hydrologic connectivity on the spatial and temporal variability of stream DOC export during snowmelt in a subalpine catchment in the northern

Rocky Mountains. We analyzed stream and groundwater DOC dynamics during snowmelt (April 15–July 15) across three transects and seven diverse but adjacent catchments to address the following questions:

1. What are the dominant DOC source areas during snowmelt?
2. How does the spatial extent and frequency of DOC source areas impact DOC export at the catchment scale?

### Site description

The study site was the upper Tenderfoot Creek Catchment (2,280 ha), located within the U.S. Forest Service (USFS) Tenderfoot Creek Experimental Forest (TCEF) (lat. 46°55' N., long. 110°52' W.) in the Little Belt Mountains of central Montana (Fig. 2). Tenderfoot Creek drains into the Smith River, a tributary of the Missouri River. Elevation ranges from 1,840 to 2,421 m, with a mean of 2,205 m. Mean annual precipitation is 880 mm, with ~70% falling as snow from November through May (Farnes et al. 1995). Monthly precipitation peaks in December or January (100–120 mm per month), and declines to 45–55 mm per month from July through October. Tenderfoot Creek runoff averages 250 mm per year, with peak flows typically in late May or early June. Mean annual temperature is 0°C, and mean daily temperatures range from –8.4°C in December to 12.8°C in July (Farnes et al. 1995).

The geology is characterized by granite gneiss, shale, quartz porphyry, and quartzite (Farnes et al. 1995). In the uplands, the major soil group is loamy skeletal, mixed Typic Cryochrepts, while the riparian zones are composed of mixed Aquic Cryoboralfs (Holdorf 1981). Soil depths range from 0.5 to 1 m in the uplands, and 1 to 2.0 m in the riparian zones (Jencso et al. 2009).

Riparian vegetation is dominated by sedges (*Carex* spp.) and rushes (*Juncaceae* spp.) in the headwaters, where riparian soil is high in organic matter and fine silt and clay textured, and water tables are at or near the soil surface (Jencso et al. 2009). In riparian areas with deeper water tables and coarsely textured soils, Willows (*Salix* spp.) are often present. In the uplands, Lodgepole pine (*Pinus contorta*) is the dominant

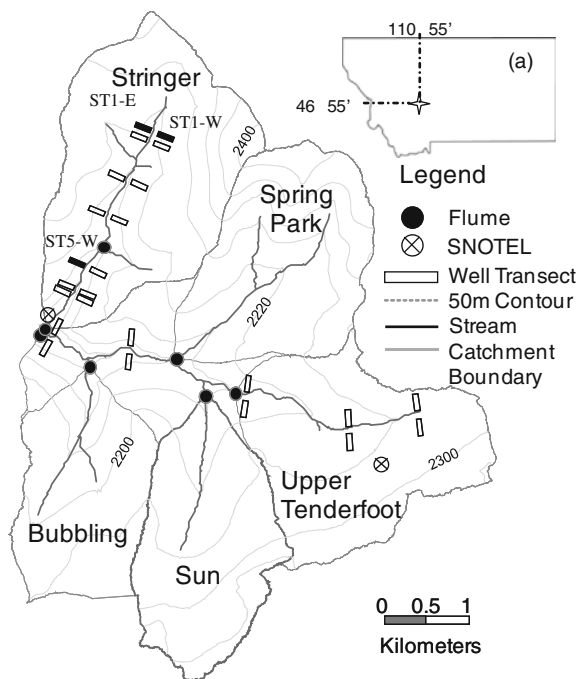


**Fig. 2** Location of the Tenderfoot Creek Experimental Forest (TCEF), with delineations of the sub-catchments, and locations of the flumes (at the outlet of each sub-catchment) and the Lower Stringer Creek SNOTEL site. Transect locations are denoted by rectangles, and the three utilized for this study within the Stringer Creek Watershed are shown in black

overstory vegetation (Farnes et al. 1995), and Grouse whortleberry (*Vaccinium scoparium*) primarily composes the understory vegetation (Mincemoyer and Birdsall 2006).

There are seven adjacent and partially nested, gauged sub-catchments in the TCEF (Table 2). In general, the catchments have gentler slopes near the headwaters, with steeper slopes near the catchment outlets. Middle Stringer Creek (MSC) and Lower Stringer Creek (LSC) have an intermediate extent of riparian and wetland area, Sun Creek (SC) has large seeps and wetland areas at the headwaters, Bubbling Creek (BC) has less extensive riparian and wetland areas, Spring Park Creek (SPC) has an extensive riparian and wetland area in the middle of the catchment, and Upper Tenderfoot Creek (UTC) has a large network of wetlands at the headwaters. Lower Tenderfoot Creek (LTC) is the largest catchment that encompasses these sub-catchments. The Stringer Creek Catchment (Middle and Lower) was utilized for more intensive data collection and divided into

three sub-catchments for data analysis. These sub-catchments were the headwaters to Transect 1 (HW–ST1), Transect 1 to MSC (T1–MSC), and MSC to LSC (MSC–LSC).

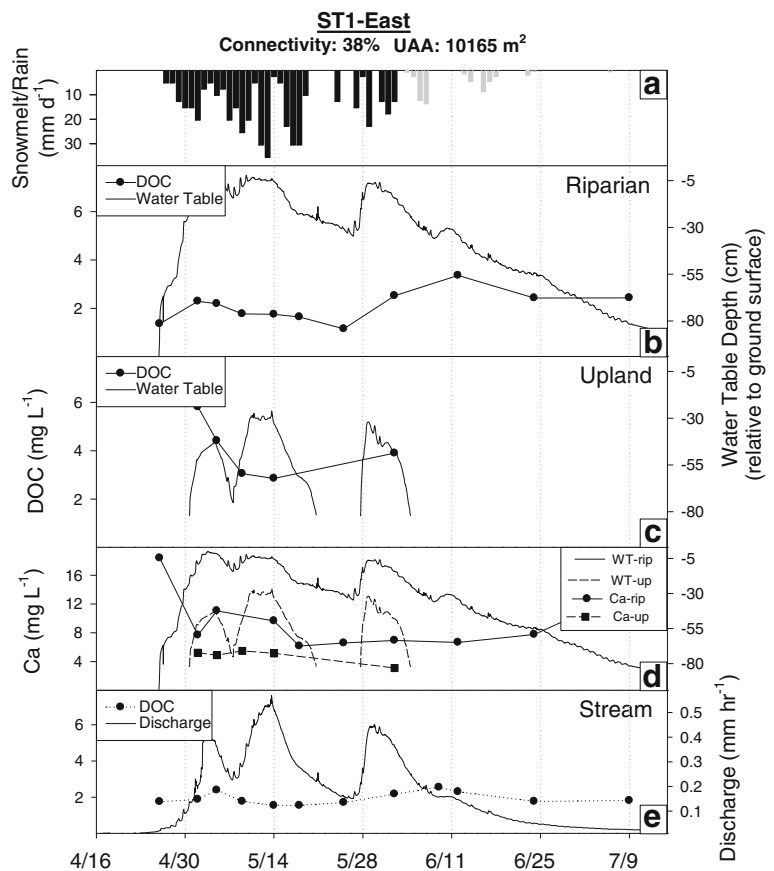
## Methods

### Terrain analysis

An ALSM (airborne laser swath mapping, commonly known as LIDAR, courtesy of the National Center for Airborne Laser Mapping—NCALM) derived 10 m digital elevation model (DEM) was used to calculate UAA (amount of land area draining to a particular location, calculated for the toeslope well position at the transition from upland to riparian zone) and slope (average slope along the fall line from the highest upland location to the toeslope along each transect). UAA was calculated using a triangular multiple flow-direction algorithm following the methods of Seibert

and McGlynn (2007) and Jencso et al. (2009). Riparian zone width was mapped with a GPS survey (Trimble GPS 5700 receiver—accurate to within 1–5 cm) and corroborated with ALSM-derived 3 m DEM analysis (Jencso et al. 2009). The riparian–upland boundary was determined in the field, based upon break in slope and change in soil characteristics (depth, gleying, organic matter accumulation, texture) (McGlynn and Seibert 2003; Seibert and McGlynn 2007; Pacific et al. 2008; Jencso et al. 2009). See Jencso et al. (2009) for a more detailed description of terrain analyses in the TCEF. We calculated the percentage of time that URS hydrologic connectivity existed by dividing the total number of days that a groundwater table was present along the URS continuum by the total snowmelt period (91 days) (Jencso et al. 2009). For this study, we define the snowmelt period as April 15–July 15, 2007, which encompassed pre-snowmelt, snowmelt, and the recession to baseflow ( $\sim 0.01 \text{ mm h}^{-1}$ ) (Fig. 3).

**Fig. 3** **a** Soil water inputs from snowmelt (black bars) and precipitation (grey bars), **b** ST1-E riparian well, **c** ST1-E upland well, **d** riparian and upland groundwater height and Ca concentrations, and **e** stream DOC concentrations and discharge from April 15 to July 15, 2007. The percentage of the study period that upland–riparian–stream connectivity existed, and upslope accumulated area (UAA) at the riparian measurement location are listed at the top of the figure. Stream discharge is from the Lower Stringer Creek Flume



## Measurement locations

This research was conducted concurrently with other research objectives and included locations and instrumentation both universal and specific to this study (Pacific et al. 2008, 2009; Riveros-Iregui et al. 2008, *in review*; Riveros-Iregui and McGlynn 2009; Jencso et al. 2009). Measurements were collected at the outlets of each of the sub-catchments within the TCEF (MSC, LSC, SPC, BC, SC, UTC, and LTC), as well as at Onion Park (headwaters of Tenderfoot Creek). In addition, 14 transects were installed by Jencso et al. (2009) in the Stringer Creek Catchment, and eight in the Tenderfoot Creek Catchment (Fig. 2). Three transects within the Stringer Creek Catchment were utilized for intensive monitoring in this study because they represented the range of landscape settings and hydrologic dynamics observed at TCEF. The Stringer Creek transects were located in seven pairs, with each pair consisting of one transect on both the east (E) and west (W) side of Stringer Creek, which flows from the north to the south. The transects are numbered sequentially from upstream to downstream, followed by an E or W, designating the east or west side of Stringer Creek. On each transect, one measurement location was installed in both the riparian and upland zones. For this study, measurements were collected on ST1-E and ST1-W (most upstream transects, at the headwaters of the Stringer Creek), and ST5-W (just below the middle of the catchment). Detailed topographic maps of these transects are presented in Fig. 5r and s in Jencso et al. (2009).

## Hydrometric monitoring

Groundwater levels were recorded at the riparian and upland well on each of the focus transects along Stringer Creek. The riparian well was located near the toe-slope (the transition point between the riparian and upland zone), and the upland well was located on the lower hillslope (1–5 m above the break in slope). The wells consisted of 3.8 cm (1.5 inch) inside-diameter PVC, screened across the completion depth (to bedrock) to 10 cm below the ground surface. Completion depths ranged from 0.5 to 1 m in the uplands and 1 to 1.5 m in the riparian zones. Groundwater levels were recorded every 60 min with water level capacitance rods (TruTrack, Inc.,  $\pm 1$  mm

resolution). Capacitance rod measurements were corroborated with manual weekly measurements using an electric water level tape.

Stream discharge was measured at flumes at the outlet of each of the seven catchments. Stage at each flume was recorded at 15 min intervals with float potentiometers (installed and maintained by the USFS) and water level capacitance rods recording at hourly intervals (TruTrack, Inc.,  $\pm 1$  mm resolution). Stage was also measured at the outlet of Onion Park, at the headwaters of Tenderfoot Creek. However, discharge could not be calculated as no flume was installed. Hourly measurements of snow water equivalent (SWE) were obtained from two Natural Resource Conservation Service snow survey telemetry (SNOTEL) stations located in TCEF, one at Onion Park (2,259 m, within 2 km and at approximately the same elevation as the headwaters of Stringer Creek), and one at LSC (1,996 m).

## Water sampling

Water samples for DOC analysis were collected in 250 ml HDPE bottles. Samples were collected approximately every 2–4 days from the flumes during high flows (beginning of May through the beginning of June) as well as from the outlet of Onion Park, which flows into the headwaters of Tenderfoot Creek. Weekly samples were collected for the weeks before and after this time period. Water samples were collected from wells (when water was present) along each transect every 3–7 days, and wells were purged until dry the day before sampling occurred. The water samples were passed through a 0.45  $\mu$ m filter into 30 ml amber high density polyethylene (HDPE) bottles within 1–12 h of collection (dependent upon location and time of sampling). Each sample was acidified to pH 1–2 with 6 N HCl, kept in a cooler during transport to Montana State University (MSU), and then frozen at  $-20^{\circ}\text{C}$  until analysis.

## DOC analysis

Total DOC was analyzed with a high-temperature combustion technique at the MSU Watershed Hydrology Analytical Facility using a Shimadzu TOC-V C-analyzer (Shimadzu Corp., Kyoto, Japan). The instrument was calibrated at the beginning of every

run with 3–5 standards ranging from 0.10 to 10.0 mg C l<sup>-1</sup> (prepared from reagent grade potassium hydrogen phthalate). Method detection limits were 0.1 mg l<sup>-1</sup>, and analytical precision was within 0.05 mg l<sup>-1</sup>.

#### Solute analysis

We collected water samples for calcium (Ca) analysis to help trace the movement of upland water into riparian zones (Covino and McGlynn 2007) and provide corroborating evidence for interpretation of riparian and upland DOC dynamics. In the TCEF, pre-snowmelt upland groundwater Ca concentrations were ~5 mg l<sup>-1</sup> and consistent across snowmelt, while riparian Ca concentrations were 10–20 mg l<sup>-1</sup>. Therefore, riparian Ca dilution by lower Ca upland water could be used to infer source water mixing (Jencso et al., [in review](#)). Water samples were collected in 250-ml HDPE bottles, filtered through a 0.45-mm PTFE membrane filter, then stored at 4°C. Calcium (Ca) concentrations were determined with a Metrohm-Peak compact ion chromatograph (Herisau, Switzerland) at Montana State University. Detection limits were 5–10 µg l<sup>-1</sup> and accuracy was within 5% of standards.

#### Cumulative DOC export

We calculated cumulative stream DOC export for the seven sub-catchments of the Tenderfoot Creek Catchment, and the three sub-catchments within the Stringer Creek Catchment. Daily stream DOC concentrations were estimated with linear interpolation between actual field measurements, and cumulative export was calculated for the 91-day study period (April 15–July 15, 2007). Cumulative stream DOC export for each sub-catchment within the Stringer Creek Catchment was estimated with the stream DOC concentration and discharge at that sub-catchment outlet after subtracting the contribution from the upstream catchments. To aid in comparison with other studies, we also estimated annual stream DOC export for the Stringer Creek Catchment. For the time outside of our study period of April 15–July 15, 2007, we used a baseflow DOC concentration of 1.6 mg l<sup>-1</sup>, as measured before and after the snowmelt period.

## Results

### Landscape analysis

Across the three transects within the Stringer Creek Catchment, there were large differences in toeslope UAA, URS hydrologic connectivity, riparian width, and slope (Table 1). ST5-W had the largest UAA, widest riparian zone, and steepest hillslope. Riparian zone width and steepness of the hillslope were similar on ST1-E and ST1-W, but UAA was higher on ST1-E. Within the three sub-catchments in the Stringer Creek Catchment, there were differences in the proportion of riparian to upland area. The riparian zone comprised 3.8% of the catchment area between ST1 and MSC, and ~1.3% in the two other sub-catchments (Table 2). The percentage of the stream channel that exhibited URS hydrologic connectivity across the entire study period (April 15–July 15) was similar across each sub-catchment in the Stringer Creek Catchment, ranging from 69 to 76% (Table 2). For the sub-catchments within the Tenderfoot Creek Catchment, there was also a wide range in the proportion of riparian to upland area (Table 2). In general, SC, BC, and LSC had a small proportion of riparian to upland area (1.7–3.0%), MSC and LTC had an intermediate proportion (3.1–3.9%), and UTC and SP a high proportion of riparian to upland area (5.0–6.1%).

### Snowmelt and precipitation

We present SWE and precipitation data from the Onion Park SNOTEL site (Fig. 3a, also shown in

**Table 1** Stringer Creek transect characteristics of upslope accumulated area (UAA), hillslope–riparian–stream connectivity, riparian width, and slope of hillslope

| Transect | UAA (m <sup>2</sup> ) | HRS connectivity (% of snowmelt) | Riparian width (m) | Hillslope (°slope) |
|----------|-----------------------|----------------------------------|--------------------|--------------------|
| ST1-E    | 10165                 | 38                               | 11.8               | 15.6               |
| ST1-W    | 1563                  | 0                                | 12.7               | 12.5               |
| ST5-W    | 46112                 | 100                              | 16.5               | 20.8               |

Hydrologic connectivity across the hillslope–riparian–stream (HRS) continuum was calculated by dividing the number of days that a hillslope water table was present by the total snowmelt period (April 15–July 15)

**Table 2** UAA, percentage of stream network with upland–riparian–stream (URS) hydrologic connectivity, ratio of riparian:upland area, and cumulative stream DOC export from April

15 to July 15, 2007 for the three sections of Stringer Creek and the seven sub-catchments of Tenderfoot Creek

| Stream section/sub-catchment | UAA (km <sup>2</sup> ) | HRS connectivity (% of catchment) | Riparian:upland (%) | Cumulative DOC export (kg ha <sup>-1</sup> ) |
|------------------------------|------------------------|-----------------------------------|---------------------|--|
| HW–ST1                       | 131                    | 76                                | 1.4                 | 6.8  |
| ST1–MSC                      | 262                    | 69                                | 3.8                 | 8.6  |
| MSC–LSC                      | 160                    | 73                                | 1.3                 | 6.3  |
| UTC                          | 446                    | 74                                | 5.0                 | 12.4   |
| LTC                          | 2260                   | 66                                | 3.9                 | 11.4   |
| MSC                          | 393                    | 71                                | 3.1                 | 8.1  |
| LSC                          | 550                    | 72                                | 3.0                 | 8.4  |
| BC                           | 309                    | 74                                | 2.5                 | 9.7  |
| SC                           | 352                    | 76                                | 1.7                 | 9.5  |
| SPC                          | 400                    | 57                                | 6.1                 | 11.9   |

Figs. 4, 5, 6) to represent general snowmelt timing. SWE peaked at 358 mm on April 20, 2007. The majority of the snowpack melted between April 27 and May 19, with average daily SWE losses of 15 mm and a maximum of 35 mm on May 13, 2007 (Jencso et al. 2009). A late spring snowfall event and subsequent melting between May 24 and June 1 yielded an additional 97 mm of water. Four days after the end of snowmelt, two rain events occurred (June 4–7, and June 13–18), totaling 30 and 22 mm, respectively.

#### Transect water table dynamics and DOC concentrations

We refer to our conceptual model of DOC export from the soil to the stream (Fig. 1) to present results of transect groundwater table fluctuations and DOC concentration dynamics in the context of soil DOC export processes. In Scenario 1, groundwater travels through low DOC mineral soil in the riparian zone during baseflow, and DOC inputs from the soil to the stream are low. As the groundwater table rises into shallow, DOC rich riparian soil during snowmelt or precipitation events, DOC inputs from the soil to the stream increase (Scenario 2). In Scenario 3, a hydrologic connection across the upland–riparian–stream continuum occurs. Once connectivity is initiated, a pulse of high DOC water is transmitted from the uplands to the stream along preferential flow paths (Scenario 3a). Low DOC upland matrix water

traveling through mineral soil can then lead to dilution of DOC concentrations (Scenario 3b).

#### ST1-East

This transect had transient URS hydrologic connectivity, totaling 38% of the study period. DOC export from the soil to the stream likely occurred via all three scenarios in our conceptual model (Fig. 1), leading to both riparian and upland sources of DOC to the stream. At the riparian well, the groundwater table was initially low (Fig. 3b) and remained in mineral soil, leading to a low groundwater DOC concentration (1.4 mg l<sup>-1</sup>) (Scenario 1). Riparian DOC concentrations increased at the end of April as the groundwater table quickly developed and entered shallow, DOC rich organic soil (Scenario 2). At the beginning of May, the groundwater table developed in the upland well (Fig. 3c), leading to a hydrologic connection across the upland–riparian–stream continuum (Scenario 3). At this time a DOC concentration of 5.8 mg l<sup>-1</sup> was measured in the upland well. A quick pulse of DOC rich water from the uplands to the riparian zone along preferential flowpaths likely contributed to increased riparian DOC concentrations at the beginning of May (Scenario 3a). Upland DOC concentrations then quickly declined (to a minimum of 2.8 mg l<sup>-1</sup> on May 14), leading to dilution of DOC concentrations in the riparian zone (Scenario 3b). The upland and riparian zone became hydrologically disconnected on May 20, and DOC dynamics in the

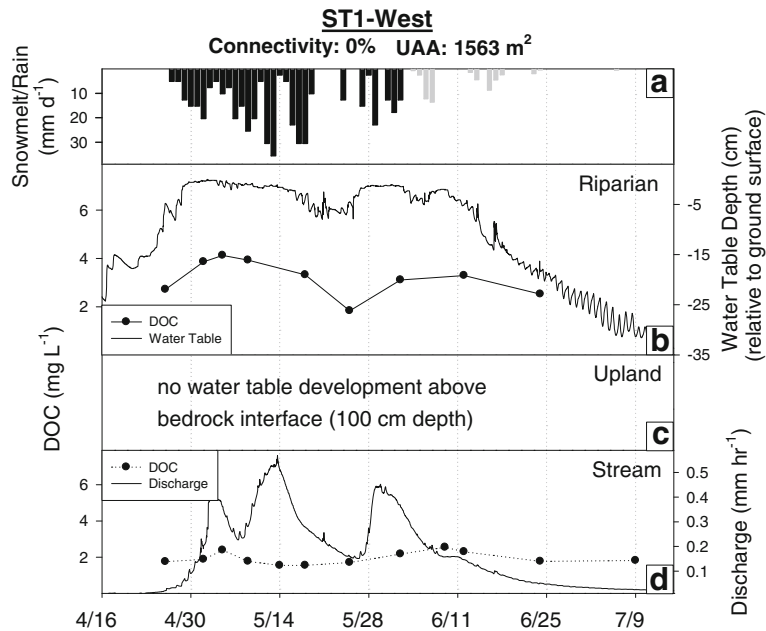


**Fig. 4** **a** Soil water inputs from snowmelt (black bars) and precipitation (grey bars), **b** ST1-W riparian well DOC concentrations and groundwater height, **c** statement of no upland water table development above the bedrock interface at 100 cm, and **d** stream DOC concentrations and discharge from

April 15 to July 15, 2007. The percentage of the study period that upland–riparian–stream connectivity existed, and upslope accumulated area (UAA) at the riparian measurement location are listed at the top of the figure. Stream discharge is from the Lower Stringer Creek Flume

riparian zone were no longer influenced by upland water (i.e. Scenario 3 ended). On May 26, the transient upland groundwater table was again initiated (return to Scenario 3), and riparian DOC concentrations increased (Fig. 3b). This increase in riparian DOC concentrations was concurrent with the rise in the riparian groundwater table, indicating the presence of Scenario 2. The upland groundwater table disconnected from the riparian zone after 8 days, then was not evident for the remainder of the study, and soil DOC export from the uplands ceased (end of Scenario 3). Riparian DOC concentrations decreased throughout June concurrent with the decline of the groundwater table into mineral soil (return to Scenario 1).

#### ST1-West

This transect never developed a hydrologic connection across the URS continuum (0% URS hydrologic connectivity) and it is likely that only Scenarios 1 and 2 from our conceptual model of DOC export from the soil to the stream occurred (Fig. 1). At the riparian well, the groundwater table was 15 cm below the

ground surface at the beginning of snowmelt (Fig. 4b). DOC export occurred from relatively deep riparian soil (which likely had lower DOC concentrations than shallower soil) (Scenario 1), and a DOC concentration of 2.4 mg l<sup>-1</sup> was observed. The groundwater table then rose into shallow, DOC rich riparian soil (reaching to within 1 cm of the ground surface by April 28), and DOC concentrations quickly increased to 4.2 mg l<sup>-1</sup> (Scenario 2). The riparian water table declined between the middle and end of May and DOC concentrations decreased. The rise of the groundwater table at the end of May led to an increase in DOC concentrations, further indicating the presence of Scenario 2. The groundwater table then gradually declined to 30 cm below the ground surface by the middle of July (Fig. 4b), concurrent with a slight decrease in DOC concentrations. In general, DOC concentrations mimicked fluctuations in the riparian groundwater table.

#### ST5-West

This transect had 100% URS hydrologic connectivity for the duration of the study (persistent groundwater

**Fig. 5** **a** Soil water inputs from snowmelt (*black bars*) and precipitation (*grey bars*), **b** ST5-W riparian well DOC concentrations and groundwater height, **c** ST5-W upland well DOC concentrations and groundwater height, **d** riparian and upland groundwater height and Ca concentrations, and **e** stream DOC concentrations and discharge from April 15 to July 15, 2007. Note the difference in scale for DOC at **b** and **c**. The percentage of the study period that upland–riparian–stream connectivity existed, and upslope accumulated area (UAA) at the riparian measurement location are listed at the *top of the figure*. Stream discharge is from the Lower Stringer Creek Flume

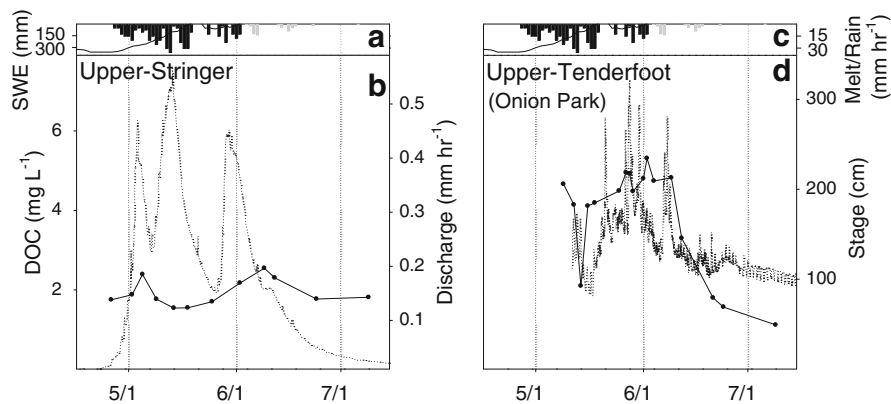
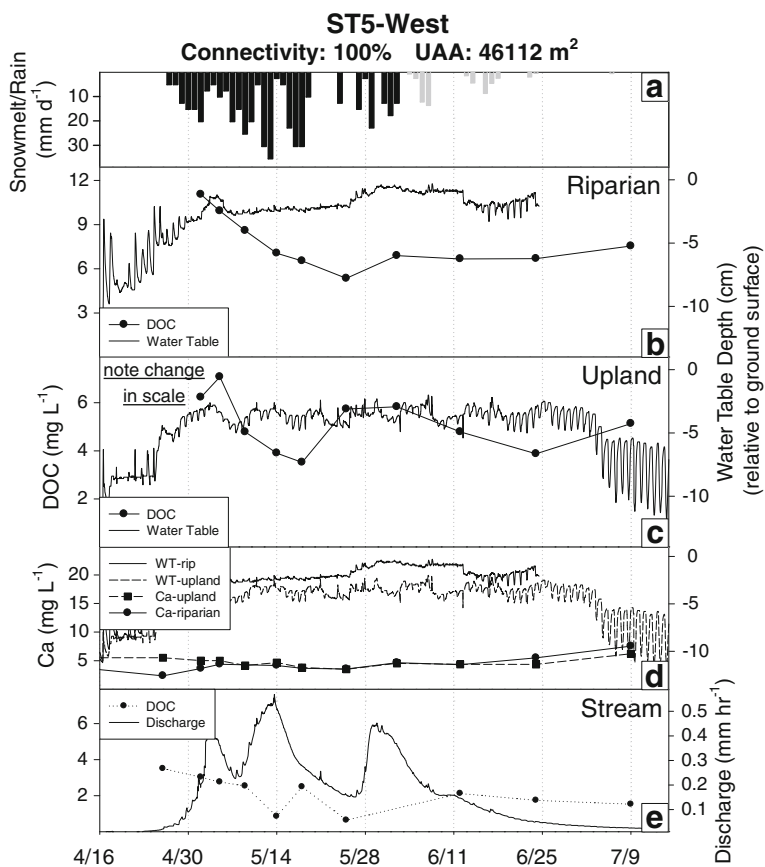


**Fig. 6** **a** Soil water inputs from snowmelt (*black bars*) and precipitation (*grey bars*), **b** discharge and DOC concentrations at ST1 on Stringer Creek, **c** snow water equivalent and snowmelt, and **d** stage height and DOC concentrations at

Upper Tenderfoot Creek (Onion Park) from April 15 to July 15, 2007. Discharge could not be calculated at Onion Park as no flume was installed

table in the upland well—Fig. 5c), and it is likely that DOC export dynamics from the soil to the stream remained in Scenario 3 of our conceptual model (Fig. 1) for the duration of the snowmelt period. At

the riparian well, the groundwater table was 10 cm below the ground surface at the beginning of snowmelt, then rose into more organic DOC rich soil by the end of April (Fig. 5b), at which point DOC

concentrations were high ( $11 \text{ mg l}^{-1}$ ). High riparian DOC concentrations at the end of April were also likely influenced by a large pulse of high DOC upland water that occurred with the rise of the upland water table (Scenario 3a). DOC concentrations then decreased concurrently in both the riparian and upland wells (Scenario 3b), further indicating the presence of a hydrologic connection across the upland–riparian–stream continuum and dilution of riparian DOC concentrations by low DOC water from the uplands. For the remainder of the study, the groundwater table remained relatively constant in both the riparian and hillslope wells (note that water table measurements ended on June 23 due to equipment malfunction), and small fluctuations of DOC concentrations were observed.

### Calcium dynamics

We used Ca as a tracer to help differentiate between upland and riparian sources of DOC, and present measurements from ST1-E and ST5-W. At ST1-E, upland Ca concentrations were  $\sim 5 \text{ mg l}^{-1}$  during the first initiation of the upland groundwater table at the beginning of May (Fig. 3d), and remained relatively constant throughout the study period (when groundwater was present). In contrast, Ca concentrations were high in the riparian zone at the beginning of snowmelt ( $18.4 \text{ mg l}^{-1}$ , Fig. 3d). However, riparian Ca concentrations quickly declined to similar values observed in the uplands, indicating upland groundwater inputs to the riparian zone. On ST5-W, Ca concentrations were  $\sim 3\text{--}5 \text{ mg l}^{-1}$  in both the riparian and upland wells for the duration of the study, indicating a constant hydrologic connection between the riparian and upland zones.

### Stream discharge and DOC dynamics

#### *Tenderfoot Creek*

DOC concentrations were also variable along Tenderfoot Creek. At Onion Park, which drains a large network of wetlands near the headwaters of Tenderfoot Creek, DOC concentrations were relatively high (Fig. 6d). Note that stage and not discharge is shown at the outlet of Onion Park, as a flume was not installed here, and therefore no rating curve was available. While high DOC concentrations were

observed during the early rise in flow ( $\sim 4 \text{ mg l}^{-1}$ ), peak concentrations were not measured until the beginning of June, following the peak in flow. DOC concentrations then decreased coincident with the decline in flow, and reached a minimum value of  $1.1 \text{ mg l}^{-1}$  on July 9 (Fig. 6d).

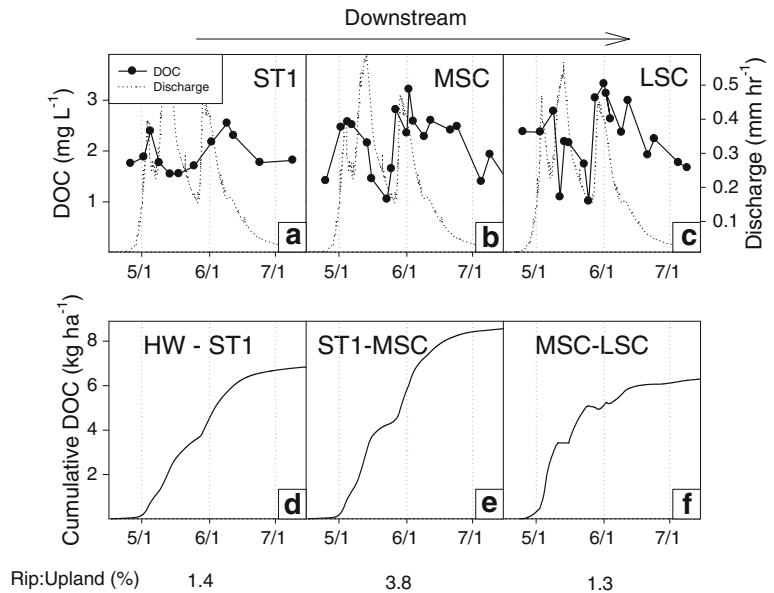
At UTC, DOC concentrations were also high (Fig. 8). The stream DOC concentration was  $\sim 3 \text{ mg l}^{-1}$  at the beginning of snowmelt, then increased by over 100% on the rising limb of the stream hydrograph. DOC concentrations fluctuated between 4 and  $7 \text{ mg l}^{-1}$  until the beginning of June, when concentrations quickly declined coincident with the recession to baseflow, and reached a minimum of  $2.1 \text{ mg l}^{-1}$  on July 9 (Fig. 8). At LTC, a similar trend was observed, however DOC concentrations were approximately half that measured at UTF and generally fluctuated between 2 and  $4 \text{ mg l}^{-1}$  (but decreased to  $0.8 \text{ mg l}^{-1}$  on May 23 following the large decline in discharge). The largest DOC concentration was measured on the falling limb of the last peak in discharge near the beginning of June.

#### *Stringer Creek*

DOC concentrations were highly variable along Stringer Creek (Fig. 7). At ST1, near the headwaters, DOC concentrations were relatively stable at  $\sim 1.8 \text{ mg l}^{-1}$ , but increased near the beginning of May, associated with the first snowmelt-driven peak in stream discharge (Fig. 7a). DOC concentrations then declined during the first streamflow recession, and continued to decline during the second rise in stream discharge near the middle of May. Stream DOC concentrations at ST1 increased during the third and final rise in discharge, and continued to rise during the recession to baseflow, with a peak concentration of  $2.6 \text{ mg l}^{-1}$  on June 9.

At MSC, located between ST1 and ST5, stream DOC concentrations were more variable (Fig. 7b). A baseflow concentration of  $1.4 \text{ mg l}^{-1}$  was measured at the end of April. DOC concentrations nearly doubled by May 2, associated with the first snowmelt-driven peak in discharge. Concentrations remained high until May 15, when they began to decline coincident with the decrease in runoff, and reached a minimum value of  $1.0 \text{ mg l}^{-1}$  on May 23. DOC concentrations then sharply increased concurrent with the third snowmelt stream discharge peak.

**Fig. 7** a–c Upstream to downstream Stringer Creek DOC concentrations at **a** Transect 1, **b** Middle Stringer Creek Flume (MSC), and **c** Lower Stringer Creek Flume (LSC) from April 15 to July 15, 2007. **d–f** Cumulative DOC export from each sub-catchment. The percentage of riparian:upland extent within each sub-catchment is also shown



Concentrations remained at  $\sim 2.5 \text{ mg l}^{-1}$  throughout June, and then returned to the baseflow concentration of  $1.4 \text{ mg l}^{-1}$  by the beginning of July (Fig. 7b).

At ST5, a peak streamflow DOC concentration of  $3.5 \text{ mg l}^{-1}$  was measured during the first sampling event on April 26 (Fig. 7c). DOC concentrations then quickly declined coincident with the peak in stream discharge. A sharp rise to  $2.5 \text{ mg l}^{-1}$  occurred on May 18 as discharge decreased. Stream DOC concentrations then declined to a minimum value of  $0.6 \text{ mg l}^{-1}$  on May 25, concurrent with the decrease in discharge at the end of May. DOC concentrations then increased following the rise in stream discharge after the late-spring snow event, and then decreased by the middle of July during the recession to baseflow. Note that stream DOC concentrations are not available for the June 2 and June 9 sampling events (Fig. 7c).

Stream DOC concentrations at LSC (catchment outlet) were  $2.4 \text{ mg l}^{-1}$  on the first sampling date at the end of April, rose slightly, and then declined to  $1 \text{ mg l}^{-1}$  by May 12, just before the peak in stream discharge (Fig. 7d). A brief rise occurred on May 14 (at peak discharge), then concentrations returned to  $1 \text{ mg l}^{-1}$  by the end of May as discharge decreased. DOC concentrations at LSC then quickly increased coincident with the rise in discharge at the end of May, and reached a peak of  $3.3 \text{ mg l}^{-1}$  at the

beginning of June. Stream DOC concentrations fluctuated between 2 and  $3 \text{ mg l}^{-1}$  throughout June, then declined during the recession to baseflow (Fig. 7d).

#### Spring Park Creek

DOC concentrations were relatively low and similar to those measured at MSC and LSC (Fig. 8). Concentrations generally fluctuated between 2 and  $3 \text{ mg l}^{-1}$  throughout snowmelt, but declined to  $\sim 1 \text{ mg l}^{-1}$  on both the rising and falling limb of the peak in stream discharge at the middle of May.

#### Sun Creek

Relative to other catchments, stream DOC concentrations were high (Fig. 8). At the beginning of snowmelt, a DOC concentration of  $4 \text{ mg l}^{-1}$  was measured, followed by a quick rise to a peak concentration of  $7 \text{ mg l}^{-1}$  on the rising limb of the initial peak in stream discharge. DOC concentrations declined to  $2.8 \text{ mg l}^{-1}$  following the decline in peak discharge at the middle of May. DOC concentrations then remained at  $\sim 5 \text{ mg l}^{-1}$  until the beginning of June, when they decreased during the recession to baseflow, reaching a minimum of  $2.5 \text{ mg l}^{-1}$  by the end of the study period (Fig. 8).

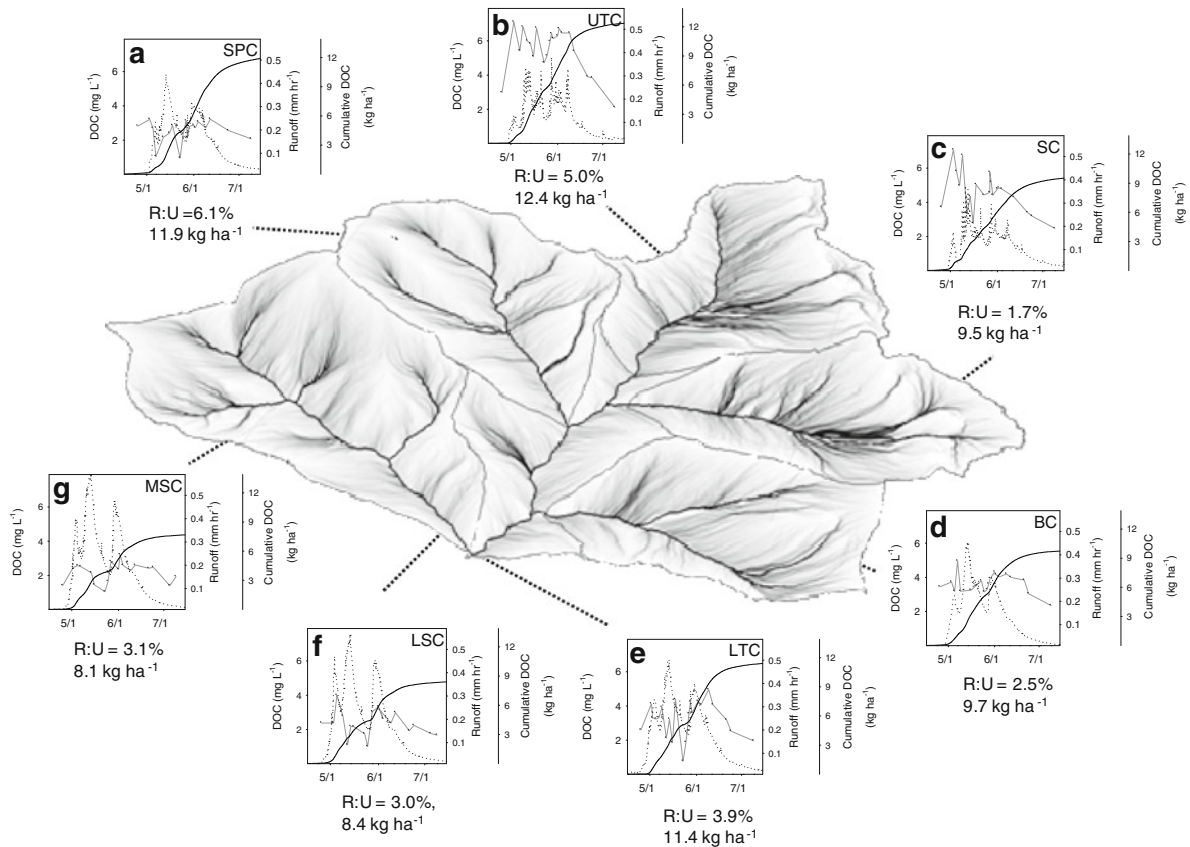


**Fig. 8** Comparison of discharge, DOC concentrations, and cumulative DOC export at the catchment outlet of **a** Spring Park Creek, **b** Upper Tenderfoot Creek, **c** Sun Creek, **d** Bubbling Creek, **e** Lower Tenderfoot Creek, **f** Lower Stringer

Creek, and **g** Middle Stringer Creek from April 15 to July 15, 2007. Riparian:upland extent (R:U) and cumulative stream DOC export is given for each sub-catchment

### Bubbling Creek

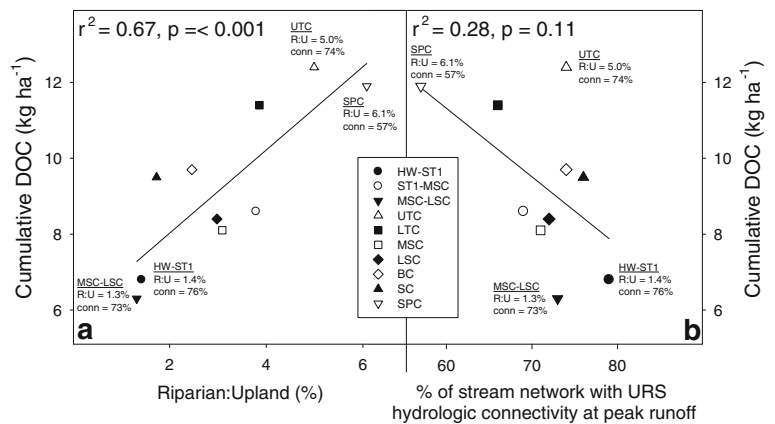
DOC concentrations were stable and remained between 3 and 4 mg l<sup>-1</sup> for the majority of the study period (Fig. 8). A peak concentration of 5 mg l<sup>-1</sup> was measured at the beginning of May coincident with the rise in discharge at the beginning of snowmelt, and a minimum concentration of 2.3 mg l<sup>-1</sup> was measured at the end of the study period as the stream receded to baseflow (~1 mm h<sup>-1</sup>) (Fig. 8).

### Cumulative stream DOC export

During the study period of April 15 to July 15, 2007, cumulative stream DOC was high for the ST1–MSC

sub-catchment (8.6 kg ha<sup>-1</sup>), while between 6.3 and 6.8 kg ha<sup>-1</sup> at the other sub-catchments (Table 2; Fig. 7). For the larger sub-catchments of the Tenderfoot Creek Catchment, cumulative stream DOC export over the study period ranged from 8.1 to 12.4 kg ha<sup>-1</sup> (Table 2). For the entire Stringer Creek Catchment, cumulative stream DOC for the entire 2007 water year was 9.6 kg ha<sup>-1</sup>. There was a strong positive relationship ( $r^2 = 0.67$ ,  $p < 0.001$ ) between cumulative stream DOC export and the proportion of riparian to upland area across all sub-catchments (Fig. 9a). There was a negative (though insignificant) relationship between cumulative stream DOC export and the percent of the stream network with hydrologic connectivity at peak runoff ( $r^2 = 0.28$ ,  $p = 0.11$ ) (Fig. 9b).

**Fig. 9** Cumulative DOC export between April 15 and July 15, 2007 at each of the sub-catchments in the Tenderfoot Creek Watershed (including the three sub-catchments within the Stringer Creek Watershed) as a function of **a** riparian:upland ratio, and **b** percent of the stream network with URS hydrologic connectivity at peak runoff



## Discussion

What are the dominant DOC source areas during snowmelt?

Hydrologic flushing is commonly referred to as the mobilization process that leads to a large release of DOC to the stream channel during snowmelt or precipitation events (Burns 2005). Both riparian and upland sources of DOC have been documented. For example, stream DOC concentrations can quickly increase at the beginning of snowmelt or precipitation events when a rising water table intersects shallow nutrient rich riparian zone soil (Fig. 1, Scenario 2) (Hornberger et al. 1994; Boyer et al. 1997, 2000; Laudon et al. 2004b). For export of DOC from organic rich riparian soil, a hydrologic connection is necessary between the riparian zone and the stream. A second source of DOC can become activated as a hydrologic connection develops across the entire upland–riparian–stream (URS) continuum (Fig. 1, Scenario 3) (McGlynn and McDonnell 2003; Bishop et al. 2004; Hood et al. 2006).

Our comparisons of DOC dynamics across three transects within the Stringer Creek Catchment illustrate the control of landscape structure on DOC export to the stream. ST1-W has a small toeslope UAA (1,563 m<sup>2</sup>) (Table 1), and the water table never developed in the uplands (Fig. 4). This lack of URS hydrologic connectivity suggested that riparian soils would be the only source of DOC to the stream (McGlynn and McDonnell 2003). Our measurements of groundwater and DOC dynamics along ST1-W support this premise. DOC concentrations in the riparian well followed fluctuations in the groundwater

table (Fig. 4b). At the beginning of snowmelt, concentrations increased as the water table rose to just below the ground surface and intersected shallow, DOC rich soils, then decreased during the initial decline in the water table. The relationship between increasing DOC concentrations and a rising water table in the riparian zone indicated riparian DOC export to the stream (Hornberger et al. 1994; Boyer et al. 1997, 2000; Inamdar and Mitchell 2006). DOC concentrations again increased coincident with the rise in the water table after a snowstorm and subsequent melt at the end of May, further supporting the occurrence of DOC export from the riparian zone. Export of DOC from upland soils was not apparent on ST1-W, since a hydrologic connection never developed across the URS continuum (i.e. no water table development in the upland well, Fig. 4c). Our measurements of water table and DOC dynamics at ST1-W indicate that in areas of small UAA and no URS hydrologic connectivity, riparian soils are likely the only source of DOC to the stream.

In contrast, we observed both riparian and upland DOC export on ST1-E, which had intermediate toeslope UAA (10,165 m<sup>2</sup>), and transient URS hydrologic connectivity (for 38% of the snowmelt period) (Table 1). Riparian groundwater DOC concentrations increased at the beginning of snowmelt (Fig. 3b) as the water table rose into organic-rich shallow soils, indicating mobilization of DOC from the riparian zone (Hornberger et al. 1994; Boyer et al. 1997, 2000). However, water table development in the upslope well (Fig. 3d) resulted in hydrologic connectivity across the URS continuum (Jencso et al. 2009). URS hydrologic connectivity is supported by the convergence of riparian Ca concentrations to

those measured in the uplands following the initiation of the upland groundwater table (indicating groundwater inputs from the uplands to the riparian zone) (Fig. 3d). DOC concentrations at the beginning of snowmelt were high in the upland well, and it is likely that this DOC-rich upland water was quickly transmitted along preferential flow paths (Freer et al. 2002; McGlynn and McDonnell 2003). This pulse of high-DOC upland water likely contributed to the increase in riparian groundwater DOC concentrations (Fig. 3b) (McGlynn and McDonnell 2003). After this initial rise in riparian DOC concentrations, continued URS hydrologic connectivity led to decreased concentrations due to dilution by low DOC matrix water from the uplands (McGlynn and McDonnell 2003). Riparian zone DOC concentrations then increased on May 20 following cessation of the upland water table and upland DOC contributions. The upland water table developed again on May 26 after a late-spring snowstorm (Fig. 3d). However, the water table in the uplands persisted for only a short period of time and did not lead to dilution of riparian zone DOC concentrations. Our measurements of water table and DOC dynamics along ST1-E indicate the presence of dynamic interactions between riparian and upland DOC export during snowmelt in an area of intermediate toeslope UAA and transient URS hydrologic connectivity.

Similar to ST1-E, both riparian and upland contributions of DOC from the soil to the stream were observed on ST5-W, which had a very large toeslope UAA (46,112 m<sup>2</sup>). A hydrologic connection across the URS continuum was present for the entire study period, which is supported by nearly identical riparian and upland groundwater Ca concentrations (Fig. 5d). A riparian groundwater DOC concentration of 11 mg l<sup>-1</sup> was measured near the beginning of snowmelt as the water table rose into shallow organic soil. However, it is likely that transmission of groundwater from the uplands also impacted DOC dynamics in the riparian zone due to constant URS hydrologic connectivity (McGlynn and McDonnell 2003). For example, DOC concentrations were high in the uplands following rise of the groundwater table at the beginning of snowmelt. DOC rich groundwater from the uplands was likely transmitted along preferential flowpaths to the riparian zone, thereby contributing to elevated riparian DOC concentrations. Following this initial rise in the groundwater table,

DOC concentrations quickly declined at the riparian well even though the water table remained relatively constant (Fig. 5b). This decline was likely due to dilution from low DOC matrix water from the uplands, indicated by a similar decline in upland DOC concentrations. These results suggest that dynamic interactions between riparian and upland DOC export can occur in areas with persistent URS hydrologic connectivity.

Comparison of well and groundwater DOC dynamics on three transects with large differences in landscape setting and URS hydrologic connectivity demonstrated the range of riparian and upland DOC export from the soil to the stream that can occur through space and time in complex mountain catchments. In areas with small UAA and 0% URS hydrologic connectivity, only riparian DOC export was apparent. In contrast, both riparian and upland DOC export was evident in areas with higher UAA and transient to persistent URS hydrologic connectivity. We suggest that in complex snowmelt-dominated catchments, measurements of water table and DOC dynamics are necessary from a range of landscape settings in order to ascertain DOC source areas and mobilization and delivery mechanisms to the stream at the catchment scale.

How does the spatial extent and frequency of dominant landscape settings impact DOC export at the catchment scale?

The results of this study indicate that stream DOC export is dependent upon the spatial extent and organization of dominant landscape settings. Wetlands (Hope et al. 1994; Creed et al. 2003, 2008; Agren et al. 2007, 2008) and shallow riparian zone soil horizons (Bishop et al. 1994; Hood et al. 2006; Nakagawa et al. 2008) generally have high DOC content. Therefore, we would expect catchment areas with large riparian and wetland extent to be large DOC source areas. This premise was true in the TCEF, as illustrated in the comparison of DOC concentrations between the headwaters of Stringer Creek and Tenderfoot Creek (at Onion Park, Fig. 6). The headwaters of Stringer Creek have a relatively small riparian and wetland extent, and stream DOC concentrations were low (~1.5–2.5 mg l<sup>-1</sup>). In contrast, the headwaters of Tenderfoot Creek have an extensive riparian and wetland network (with

intermittent hydrologic connectivity to the stream) and therefore greater contributions from organic-rich soils. DOC concentrations at the headwaters of Tenderfoot Creek were generally  $>4 \text{ mg l}^{-1}$  and therefore over 100% higher than at the headwaters of Stringer Creek. Further, there were large decreases in DOC concentrations in the headwaters of Tenderfoot Creek when flow declined at the middle of April and then again at the middle of June (Fig. 6). These decreases were likely the result of transient hydrologic connectivity between riparian and wetland DOC source areas. In contrast, the limited extent of riparian and wetland area had little effect on stream DOC concentrations at the headwaters of Stringer Creek during the transition from periods of high to low hydrologic connectivity. Our comparisons of both the timing and magnitude of stream DOC dynamics between the headwaters of Stringer Creek (little riparian and wetland area) and Tenderfoot Creek (large riparian and wetland area) indicate the strong influence that the spatial extent of organic-rich riparian and wetland areas can have on stream DOC export.

The influence of the extent of high DOC source areas on stream DOC export is also apparent when comparing the three sub-catchments of the Stringer Creek Catchment. Our results illustrate that even within a relatively small area ( $\sim 550 \text{ ha}$ ), changes in the relative proportion of riparian to upland area can lead to strong differences in stream DOC export. At ST1, near the headwaters of Stringer Creek, stream DOC concentrations were low and relatively stable (Fig. 7a), resulting in low cumulative stream DOC export during snowmelt ( $6.8 \text{ kg ha}^{-1}$ ). These dynamics likely reflect the relatively small percent of riparian to upslope area (1.4%) within the Upper Stringer Creek Catchment (Table 2). Stream DOC concentrations increased downstream between ST1 and MSC (Fig. 7b), which was likely in response to the large increase in the percentage of riparian to upland area in this sub-catchment (3.8%, Table 2) (which was nearly three times higher than observed between the headwaters and ST1). This increase in the extent of organic riparian and wetland areas near the stream led to a large increase in cumulative stream DOC export from ST1 to MSC ( $8.6 \text{ kg ha}^{-1}$ ), and demonstrates the influence of large DOC source areas on stream DOC export. Cumulative stream DOC export was low between MSC and LSC

( $6.3 \text{ kg ha}^{-1}$ ), which had a riparian to upland extent of only 1.3%. This combination of low stream DOC export with a low proportion of riparian to upland area further supports the premise that the relative amount of riparian and wetland area is a strong control on DOC export.

Comparison of cumulative stream DOC to the proportion of riparian to upland area from each of the larger sub-catchments in the Tenderfoot Creek Catchment (Table 2; Fig. 8) also demonstrates the control of the relative size of high DOC source areas on stream DOC export at the catchment scale. The greatest DOC export generally occurred from catchments with high riparian to upland ratios. For example, cumulative stream DOC export was greatest from UTC and SPC ( $12.4$  and  $11.9 \text{ kg ha}^{-1}$ , respectively). These catchments had the highest percentage of riparian to upland extent (5 and 6.1%). In contrast, cumulative stream DOC export was generally less than  $10 \text{ kg ha}^{-1}$  from catchments with smaller riparian to upland extents (ranging from 1.7 to 3.9%). The results of our study are supported by Hinton et al. (1998) and Inamdar and Mitchell (2006), who found that catchments with large wetland and riparian areas consistently had higher DOC concentrations than catchments with little to no riparian and wetland extent.

The results of our study also demonstrate how variability in internal catchment hydrologic dynamics can affect outlet DOC observations (Fig. 8). The Tenderfoot Creek Catchment is composed of seven sub-catchments, which varied in landscape structure (Jencso et al. 2009) and timing and magnitude of both stream discharge and DOC concentrations (Fig. 8). Stream discharge was low in both SC (Fig. 8b) and UTC (Fig. 8f), and almost never rose above  $0.3 \text{ mm h}^{-1}$ . At these catchments, stream DOC concentrations were very high (maximum concentrations of over  $7 \text{ mg l}^{-1}$  were observed). In contrast, peak discharge was approximately twice as high in Stringer Creek (at both MSC and LSC), and stream DOC concentrations never exceeded  $4 \text{ mg l}^{-1}$  throughout the study period. Further, while DOC concentrations increased on the rising limb of the stream hydrograph at all catchments, there was variability in the timing of peak DOC concentrations across the catchments (Fig. 8). There were also differences in DOC trends throughout the snowmelt period across the different catchments. In general,

stream DOC concentrations were relatively stable in BC, MSC, and LSC, while concentrations were much flashier in SC and UTC (Fig. 8). At the outlet of Tenderfoot Creek (LTC), stream discharge and DOC dynamics were intermediate between the dynamics observed at the individual sub-catchments of Tenderfoot Creek, and reflect the integration of variability in landscape structure across the catchment (McGlynn and McDonnell 2003; Jencso et al. 2009). Our results indicate that DOC measurements at the outlet of a catchment are often an integration of internal dynamics and therefore may not be suitable for interpretation of DOC dynamics at different landscape positions within a catchment.

#### Intersection between size of DOC source area and degree of hydrologic connectivity

The results of this study demonstrate that both the degree of hydrologic connectivity between landscape elements and the size of DOC source areas are important controls on stream DOC export. Regression analysis of cumulative stream DOC export as a function of riparian to upland extent (Fig. 9a,  $r^2 = 0.76$ ) and the percentage of the stream network with URS hydrologic connectivity at peak runoff (Fig. 9b,  $r^2 = 0.28$ ) from the Tenderfoot Creek sub-catchments suggests that the relative extent of high DOC source areas was a stronger control on DOC export (higher  $r^2$ ) than URS connectivity alone. For example, HW–ST1 and MSC–LSC (sub-catchments within the Stringer Creek Catchment) had a high degree of hydrologic connectivity across the upland–riparian–stream continuum (76 and 73%, Table 2; Fig. 9a), which suggested that cumulative stream DOC export would be high from these areas. However, DOC export was low, likely in response to the small proportion of riparian to upland area (i.e. relatively small DOC source area) (1.4 and 1.3%, Table 2; Fig. 9). In contrast, SPC had the lowest URS hydrologic connectivity of all sub-catchments (57%, Table 2; Fig. 9), suggesting that stream DOC export would be low. However, cumulative stream DOC export from SPC was high, likely in response to the high proportion of riparian to upland extent (6.1%, Table 2; Fig. 9a). These results demonstrate the importance of the relative size of a high DOC source area for soil DOC export to the stream.

The degree of hydrologic connectivity across the upland–riparian–stream continuum was not as strong of a predictor of stream DOC export. Of the sub-catchments of Tenderfoot Creek, the highest cumulative stream DOC export (12.4 kg ha<sup>-1</sup>, Table 2; Fig. 9) occurred from UTC, which had both a high proportion of riparian to upland area and high URS hydrologic connectivity. We suggest that while both the size of the DOC source area and the degree of hydrologic connectivity are individually significant controls of DOC export from the soil to the stream, it is the intersection of the two that drives stream DOC export in complex terrain. Therefore, landscapes with both large DOC source areas and a high degree of URS hydrologic connectivity may be “hotspots” for stream DOC export in complex mountain catchments. We emphasize that the spatial organization and intersection of these variables is most important. For example, a catchment may have a large extent of high DOC source areas, but if these areas are rarely or never hydrologically connected to the stream, then stream DOC export may be lower than expected. Conversely, a catchment with a small extent of high DOC source areas may have high stream DOC export if these DOC source areas are well connected to the stream. We suggest that in order to accurately quantify the controls on stream DOC export at the catchment scale and predict DOC export dynamics, future research needs to examine both the size of DOC source areas and the degree of URS hydrologic connectivity, as well as their spatial organization.

#### Comparison to other studies

To aid in comparison with other studies, we estimated annual cumulative stream DOC export from the Stringer Creek Catchment. In a review of carbon export from nearly 100 catchments across the world, Hope et al. (1994) found a range of 10 to 100 kg ha<sup>-1</sup> year<sup>-1</sup> across a wide range of catchment sizes. Our estimate of cumulative DOC export from the Stringer Creek Catchment (9.6 kg ha<sup>-1</sup> year<sup>-1</sup>) is consistent with those from catchments of similar size (~5 km<sup>2</sup>) and ecosystem type. However, Laudon et al. (2007) found that annual DOC export ranged from 35 to 76 kg ha<sup>-1</sup> year<sup>-1</sup> across seven catchments in northern Sweden, and Kortelainen et al. (1997) found a similar range across catchments in Finland. The site locations used for these studies were boreal

catchments, which have very large stores of DOC (as indicated by stream DOC concentrations of up to an order of magnitude higher than observed in Stringer Creek), and likely explains the higher DOC export relative to our study site. Our results indicate that while stream DOC export from subalpine catchments may not be as high as from boreal catchments, they can still contribute a large flux of DOC, which can have large implications for ecosystem carbon balances (Laudon et al. 2004a; Neill et al. 2006; Johnson et al. 2006; Waterloo et al. 2006; Jonsson et al. 2007). We show that even within a relatively small area such as the Tenderfoot Creek Catchment, there was large variability in cumulative stream DOC export, which was partially controlled by differences in catchment structure. We suggest that variability in stream DOC export is likely to occur across catchments even within the same physiographic and bioclimatic regions because of differing landscape structures, which must be accounted for in estimates of ecosystem carbon balances.

## Conclusions

Based upon catchment scale topographic analysis and measurements of stream and groundwater DOC dynamics during snowmelt (April 15–July 15) across three transects and seven catchments with a range of landscape settings and hydrologic connectivity between upland, riparian, and stream zones, we conclude that:

1. The relative importance of DOC source areas (riparian versus upland) on stream DOC export was dependent upon landscape position and the degree of hydrologic connectivity between the stream, riparian, and upland zones. Riparian DOC export was restricted to areas with a hydrologic connection across the riparian–stream (RS) interface, while a hydrologic connection across the entire upland–riparian–stream (URS) continuum was requisite for upland soil DOC export.
2. The relative importance of riparian versus upland DOC source areas on stream DOC export changed throughout space and time during snowmelt. In areas of small UAA and at times of low wetness status (such as baseflow), riparian zones were the dominant sources of DOC to the stream. In contrast, DOC contributions from upland soils were restricted to areas of larger UAA and times of increased wetness status (such as peak snowmelt). The relative importance of upland DOC source areas on stream DOC export increased after the initiation of snowmelt, with the greatest influence likely at peak snowmelt when the spatial extent of URS connectivity was highest throughout the catchment.
3. The intersection of hydrologic connectivity and high DOC source areas drove stream DOC export. The greatest DOC export occurred at areas with both high URS hydrologic connectivity and large DOC source areas.

This research provides insight into the spatial and temporal controls of DOC export from the soil to the stream during snowmelt. We suggest that landscape analysis coupled with multi-catchment analysis and integrated plot level measurements may provide a way forward in determining the relative importance of riparian versus upland sources of DOC on stream DOC export, and which areas of the landscape and which catchments likely provide the largest DOC contributions.

**Acknowledgements** This work was funded by National Science Foundation (NSF) grant EAR-0337650 to B.L. McGlynn, and fellowships awarded to V.J. Pacific (from the Inland Northwest Research Alliance—INRA, and the Big Sky Institute NSF GK-12 Program) and K.G. Jencso (INRA). Extensive logistic collaboration was provided by the Tenderfoot Creek Experimental Forest and the USDA, Forest Service, Rocky Mountain Research Station, especially Ward McCaughey. Airborne Laser Mapping was provided by the NSF-supported Center for Airborne Laser Mapping (NCALM). We are grateful to Diego Riveros-Iregui and Austin Allen for field assistance, and Galena Ackerman and John Mallard for performing laboratory analyses.

## References

- Agren A, Buffam I, Jansson M, Laudon H (2007) Importance of seasonality and small streams for the landscape regulation of dissolved organic carbon export. *J Geophys Res* 112:G03003. doi:10.1029/2006JG000381
- Agren A, Buffam I, Berggren M, Bishop K, Jansson M, Laudon H (2008) Dissolved organic carbon dynamics in boreal streams in a forest-wetland gradient during the transition between winter and summer. *J Geophys Res* 113:G03031. doi:10.1029/2007JG000674

- Bishop K, Pettersson C, Allard B, Lee Y-H (1994) Identification of the riparian sources of aquatic dissolved organic carbon. *Environ Int* 20:11–19
- Bishop K, Seibert J, Koher S, Laudon H (2004) Resolving the double paradox of rapidly mobilized old water with highly variable response to runoff chemistry. *Hydrol Process* 18:185–189
- Boyer EW, Hornberger GM, Bencala KE, McKnight DM (1997) Response characteristics of DOC flushing in an alpine catchment. *Hydrol Process* 11:1635–1647
- Boyer EW, Hornberger GM, Bencala KE, McKnight DM (2000) Effects of asynchronous snowmelt on flushing of dissolved organic carbon: a mixing model approach. *Hydrol Process* 14:3291–3308
- Burns D (2005) What do hydrologists mean when they use the term flushing? *Hydrol Process* 19:1325–1327
- Covino BL, McGlynn TP (2007) Stream gains and losses across a mountain-to-valley transition: impacts on watershed hydrology and stream water chemistry. *Water Resour Res* 43:W10431. doi:10.1029/2006WR005544
- Creed IF, Sanford SE, Beall FD, Molot LA, Dillon PJ (2003) Cryptic wetlands: integrating hidden wetlands in regression models of the export of dissolved organic carbon from forested landscapes. *Hydrol Process* 17:3629–3648
- Creed IF, Beall FD, Clair TA, Dillon PJ, Hesslein RH (2008) Predicting export of dissolved organic carbon from forested catchments in glaciated landscapes with shallow soils. *Global Biogeochem Cycles* 22:GB4024. doi:10.1029/2008GB003294
- Farnes PE, Shearer RC, McCaughey WW, Hanson KJ (1995) Comparisons of hydrology, geology and physical characteristics between Tenderfoot Creek Experimental Forest (East Side) Montana, and Coram Experimental Forest (West Side) Montana. Final Report RJVA-INT-92734. USDA Forest Service. Intermountain Research Station, Forestry Sciences Laboratory, Bozeman, Montana, 19 p
- Freer J, McDonnell JJ, Beven KJ, Peters NE, Burns DA, Hooper RP, Aulenbach B, Kendall C (2002) The role of bedrock topography on subsurface stormflow. *Water Resour Res* 38. doi:10.1029/2001WR000872
- Hinton MJ, Schiff SL, English MC (1998) Sources and flowpaths of dissolved organic carbon during storms in two forested catchments of the Precambrian Shield. *Biogeochemistry* 41:175–197
- Holdorf HD (1981) Soil resource inventory, Lewis and Clark National Forest, interim in-service report. On file with the Lewis and Clark National Forest. Forest Supervisor's Office, Great Falls
- Hood E, Gooseff MN, Johnson SL (2006) Changes in the character of stream water dissolved organic carbon during flushing in three small catchments, Oregon. *J Geophys Res* 111:G01007. doi:10.1029/2005JG000082
- Hope D, Billet MF, Cressner MS (1994) A review of the export of carbon in rivers: fluxes and processes. *Environ Pollut* 84:301–324
- Hornberger GM, Bencala KE, McKnight DM (1994) Hydrologic controls on dissolved organic carbon during snowmelt in the Snake River near Montezuma, Colorado. *Biogeochemistry* 25:147–165
- Imai A, Matsushige K, Nagai T (2003) Trihalomethane formation potential of dissolved organic matter in a shallow eutrophic lake. *Water Res* 37:4284–4294
- Inamdar SP, Mitchell MJ (2006) Hydrologic and topographic controls on storm-event exports of dissolved organic carbon (DOC) and nitrate across catchment scales. *Water Resour Res* 42:W03421. doi:10.1029/2005WR004212
- Inamdar SP, Christopher S, Mitchell MJ (2004) Flushing of DOC and nitrate from a forested catchment: role of hydrologic flow paths and water sources. *Hydrol Process* 18:2651–2661
- Jencso KG, McGlynn BL, Gooseff MN, Wondzell SM, Bencala KE, Marshall LA (2009) Hydrologic connectivity between landscapes and streams: transferring reach and plot scale understanding to the catchment scale. *Water Resour Res* 45:W04428. doi:10.1029/2008WR007225
- Jencso KJ, McGlynn BL, Gooseff KE, Bencala KE, Wondzell SM (in review) Hillslope hydrologic connectivity controls riparian groundwater turnover: implications of catchment structure for riparian buffering and stream water sources. *Water Resour Res*
- Johnson MS, Lehmann J, Selva EC, Abdo M, Riha S, Guimarães Couto E (2006) Organic carbon fluxes within and streamwater exports from headwater catchments in the southern Amazon. *Hydrol Process* 20:2599–2614
- Jonsson A, Algesten G, Bergstrom AK, Bishop K, Sobek S, Tranvik LJ, Jansson M (2007) Integrating aquatic carbon fluxes in a boreal catchment carbon budget. *J Hydrol* 334:141–150
- Kortelainen P, Saukkonen S, Mattson T (1997) Leaching of nitrogen from forested catchments in Finland. *Global Biogeochem Cycles* 11:627–638
- Laudon H, Kohler S, Buffam I (2004a) Seasonal TOC export from seven boreal catchments in northern Sweden. *Aquat Sci* 66:223–230
- Laudon H, Seibert J, Kohler S, Bishop K (2004b) Hydrological flowpaths during snowmelt: congruence between hydro-metric measurements and oxygen 18 in meltwater, soil water, and runoff. *Water Resour Res* 40:W03102. doi:10.1029/2003WR002455
- Laudon H, Sjöblom V, Buffam I, Seibert J, Morth M (2007) The role of catchment scale and landscape characteristics for runoff generation of boreal streams. *J Hydrol* 344:198–209
- McGlynn BL, McDonnell JJ (2003) Role of discrete landscape units in controlling catchment dissolved organic carbon dynamics. *Water Resour Res* 39. doi:10.1029/2002WR001525
- McGlynn BL, Seibert J (2003) Distributed assessment of contributing area and riparian buffering along stream networks. *Water Resour Res* 39. doi:10.1029/2002WR001521
- Mincemoyer SA, Birdsall JL (2006) Vascular flora of the Tenderfoot Creek Experimental Forest, Little Belt Mountains, Montana. *Madrono* 53:211–222
- Nakagawa Y, Shibata H, Satoh F, Sasa K (2008) Riparian control on NO<sup>3-</sup>, DOC, and dissolved Fe concentrations in mountainous streams, northern Japan. *Limnology* 9:195–206. doi:10.1007/s10201-008-0251-7
- Neill C, Elsenbeer H, Krusche AV, Lehmann J, Markewitz D, de O, Figueiredo R (2006) Hydrological and biogeochemical processes in a changing Amazon: results from

- small catchment studies and the large-scale biosphere-atmosphere experiment. *Hydrol Process* 20:2467–2476
- Pacific VJ, McGlynn BL, Riveros-Iregui DA, Welsch D, Epstein H (2008) Variability in soil CO<sub>2</sub> production and surface CO<sub>2</sub> efflux across riparian-hillslope transitions. *Biogeochemistry*. doi:[10.1007/s10533-008-9258-8](https://doi.org/10.1007/s10533-008-9258-8)
- Pacific VJ, McGlynn BL, Riveros-Iregui DA, Epstein HE, Welsch DL (2009) Differential soil respiration responses to changing hydrologic regimes. *Water Resour Res*. doi:[10.1029/2009WR007721](https://doi.org/10.1029/2009WR007721)
- Riveros-Iregui DA, McGlynn BL (2009) Landscape structure controls soil CO<sub>2</sub> efflux variability in complex terrain: scaling from point observations to catchment scale fluxes. *J Geophys Res Biogeosci*. doi:[10.1029/2008JG000885](https://doi.org/10.1029/2008JG000885)
- Riveros-Iregui DA, McGlynn BL, Epstein HE, Welsch DL (2008) Interpretation and evaluation of combined measurement techniques for soil CO<sub>2</sub> efflux: surface chambers and soil CO<sub>2</sub> concentration probes. *J Geophys Res Biogeosci*. doi:[10.1029/2008JG000811](https://doi.org/10.1029/2008JG000811)
- Riveros-Iregui DA, McGlynn BL, Epstein HE, Welsch D, Marshall L (in review) A landscape-scale assessment of a process soil CO<sub>2</sub> production and transport model. *J Geophys Res Biogeosci*
- Seibert J, McGlynn BL (2007) A new triangular multiple flow direction algorithm for computing upslope areas from gridded digital elevation models. *Water Resour Res* 43(4):W04501
- van Vevrseveld WJ, McDonnell JJ, Lajtha K (2008) A mechanistic assessment of nutrient flushing at the catchment scale. *J Hydrol* 358:268–287
- Waterloo MJ, Oliveira SM, Drucker DP, Nobre AD, Cuartas LA, Hodnett MG, Langedijk I, Jans WWP, Tomasella J, de Araújo AC, Pimentel TP, Múnera Estrada JC (2006) Export of organic carbon in run-off from an Amazonian rainforest blackwater catchment. *Hydrol Process* 20: 2581–2597
- Wei Q, Feng C, Wang D, Shi B, Zhang L, Wei Q, Tang H (2008) Seasonal variations of chemical and physical characteristics of dissolved organic matter and trihalomethane precursors in a reservoir: a case study. *J Hazard Mater* 150:257–264
- Wieler M, McDonnell J (2006) Testing nutrient flushing hypotheses at the hillslope scale: a virtual experiment approach. *J Hydrol* 319:339–356

Contribution of Authors

Chapter 5: Hierarchical controls on runoff generation: Topographically driven hydrologic connectivity, geology, and vegetation

First author: Kelsey G. Jencso

Co-authors: Brian L. McGlynn, Lucy A. Marshall

Contributions: I was responsible for all field instrumentation and data collection, figure development and the majority of data analysis and writing of this paper. Brian McGlynn contributed significant critique and ideas for development of intellectual content within the paper, and edited successive versions of the manuscript. Lucy Marshall provided technical and collaborative discussions throughout the writing process and edited the final version of the manuscript.

Manuscript Information

Jencso, K. G., B. L. McGlynn, and L.A. Marshall. 2009. Hierarchical controls on runoff generation: Topographically driven hydrologic connectivity, geology, and vegetation. Manuscript for submittal to *Water Resources Research*.

- Journal: Water Resources Research
- Status of manuscript (check one)
  - Prepared for submission to a peer-reviewed journal
  - Officially submitted to a peer-reviewed journal
  - Accepted by a peer-reviewed journal
  - Published in a peer-reviewed journal
- Publisher: American Geophysical Union
- Anticipated submission date: January 2010

## HIERARCHICAL CONTROLS ON RUNOFF GENERATION: TOPOGRAPHICALLY DRIVEN HYDROLOGIC CONNECTIVITY, VEGETATION, AND GEOLOGY

### Abstract

An understanding of the relative influences of catchment structure (topography and topology), underlying geology, and vegetation on stream network hydrologic connectivity and runoff response is key to interpreting catchment hydrology. Hillslope-riparian-stream (HRS) water table connectivity serves as the hydrologic linkage between a catchment's uplands and the channel network and facilitates the transmission of water and solutes to streams. While there has been tremendous interest in the concept of hydrological connectivity to characterize catchments, there have been relatively few studies that have quantified hydrologic connectivity at the stream network and catchment scales. Here, we examine how catchment topography, vegetation, and geology influenced patterns of stream network HRS connectivity and resultant runoff dynamics across 11 nested headwater catchments in the Tenderfoot Creek Experimental Forest (TCEF), MT. This study builds on the empirical findings of Jencso et al. (2009) who found a strong linear relationship ( $r^2 = 0.92$ ) between the upslope accumulated area (UAA) and the annual duration of shallow ground water table connectivity observed across 24 HRS transects (146 groundwater recording wells) at one TCEF catchment. We applied this relationship to the entire stream network across 11 nested catchments to quantify the frequency distribution of stream network connectivity through time and quantify its relationship to catchment-scale runoff dynamics. Each catchment's hydrologic connectivity duration curve (CDC) was highly related to its flow duration curve (FDC); albeit the slope of the relationship varied across catchments. The slope of this relationship represents the streamflow yield per unit connectivity ( $Con_{yield}$ ). We analyzed the slope of each catchment's CDC-FDC relationship or  $Con_{yield}$  (annual, peak, transition and baseflow periods) in multiple linear regression models with common terrain, land cover-vegetation, and geology explanatory variables. Significant predictors ( $p < 0.05$ ) across 11 catchments included the ratio of flow path distances and flow path gradients to the creek (DFC/GTC), geology, and a vegetation index. The order and strength of these predictors changed seasonally and highlight the hierarchical controls on headwater catchment runoff generation. Our results highlight direct and quantifiable linkages between catchment structure, vegetation, geology and hydrologic dynamics.

## Introduction

The relationship between catchment structure, stream network hydrologic connectivity, and runoff response remains only partially understood. Difficulties in discerning this relationship can be attributed to tremendous heterogeneity in key catchment variables such as topography, geology, and vegetation. Differences in the relative influence and interactions between these variables can affect runoff processes that occur across a range of space and time scales [Wagner *et al.*, 2007].

There is growing interest in the concept of hydrologic connectivity to describe and quantify catchment runoff response through time. Many definitions and conceptualizations regarding hydrologic connectivity have recently been proposed [Bracken and Croke, 2007; Ali and Roy, 2009; Hopp and McDonnell, 2009; Jencso *et al.*, 2009]. Here, we use the term to describe the initiation of a shallow ground water table across hillslopes and riparian zones [Vidon and Hill, 2004; Ocampo *et al.*, 2006; Jencso *et al.*, 2009]. While the development of water table connectivity across the hillslope-riparian-stream (HRS) continuum is considered a requisite for the flux of water [McGlynn and McDonnell, 2003b; Jencso *et al.*, 2009] and solutes [Carlyle and Hill, 2001; McGlynn and McDonnell, 2003a; Ocampo *et al.*, 2006; Pacific *et al.*, 2010; Jencso *et al.*, 2010] to streams, little work to date has focused on the distribution and drivers of connectivity through space and time across stream networks and diverse catchments.

In mountain catchments there are often strong relationships between landscape topography and runoff generation [Dunne and Black, 1970; Anderson and Burt, 1978;

*Beven, 1978; Burt and Butcher, 1985*], runoff spatial sources [*Sidle et al., 2000; McGlynn and McDonnell, 2003b*] and water residence times [*McGlynn et al., 2004; McGuire et al., 2005; Tetzlaff et al., 2009*]. A specific topographic metric of interest is upslope accumulated area (UAA); the amount of land draining to a point in the landscape. Many of the formative hillslope hydrology studies [*Hewlett and Hibbert, 1967; Dunne and Black, 1970; Harr, 1977; Anderson and Burt, 1978*] observed increased subsurface water accumulation in topographically convergent hillslope areas and in areas of higher upslope accumulated area (UAA). This historical and more recent research [*Jencso et al., 2009*] suggests that UAA may be a useful metric for predicting source area connectivity.

Other variables that could influence and even dominate water storage, redistribution, and therefore HRS connectivity initiation and duration include bedrock geology and permeability [*Huff et al., 1982; Wolock et al., 1997; Burns et al., 1998; Shaman et al., 2004b; Uchida et al., 2005*], soil characteristics [*Buttle et al., 2004; Devito et al., 2005; Tetzlaff et al., 2009*], and vegetation [*Ivanov et al., 2010; Emanuel et al., in press*]. While all of these factors are likely to influence the redistribution of water and source area hydrologic connectivity and in turn stream flow response, few empirical studies have explored their combined and hierarchical influence across space and time. This limits our understanding of the spatial and temporal controls on runoff generation both within and across catchments.

In this study we build on the work of Jencso et al. [2009] who found a strong relationship between hillslope upslope accumulated area (UAA) entering the stream network and the duration of hydrologic connectivity across the hillslope-riparian-stream

(HRS) continuum for 24 transects of shallow groundwater recording wells. This relationship was applied to the local inflows of UAA entering the stream network to estimate the duration of HRS connectivity across the stream network in one headwater catchment of the Tenderfoot Creek Experimental Forest (TCEF). The connectivity duration curve (CDC) quantified the fraction of the stream network hydrologically connected to its uplands across the year and was highly correlated to the stream flow duration curve (FDC) for one catchment. The relationship between the connectivity duration curve and the flow duration curve represents the streamflow yield per unit connectivity (Connectivity yield;  $Con_{yield}$ ).

In this study, we examine how this topographically-based relationship (CDC:FDC) transfers to adjacent catchments. We combine high frequency, spatially distributed observations of HRS shallow groundwater connectivity (24 well transects; 146 wells) and runoff dynamics (11 gauged catchments) with quantitative landscape analysis of HRS connectivity, catchment topography, surficial geology, and vegetation structure. We utilize observed flow duration curves and computed connectivity duration curves in 11 headwater catchments with differing topography, geology, and land cover / vegetation characteristics to address the following questions:

1. How does the distribution of stream network HRS connectivity relate to observed runoff dynamics at each catchment outlet?
2. What factors contribute to the spatial and temporal differences in the connectivity–yield relationship observed across the 11 catchments?

### Site Description

We addressed these questions at the Tenderfoot Creek Experimental Forest (TCEF) located in the Little Belt Mountains of Montana (Figure 1). The TCEF consists of 11 nested headwater catchments that drain into Smith River a tributary to the Missouri River. The climate in the Little Belt Mountains is continental. Annual precipitation in the TCEF averages 880 mm and ranges from 594 to 1,050 mm from the lowest to highest elevations. Snowfall comprises 75% of the annual precipitation with snowmelt and peak runoff generally occurring in late May or early June. Lowest runoff occurs in late summer through the winter months. Catchment headwater zones are typified by moderately sloping (avg. slope  $\sim 8^\circ$ ) extensive (up to 1200m long) hillslopes and variable width riparian zones. Approaching the main stem of Tenderfoot Creek the streams become more incised, hillslopes become shorter ( $< 500\text{m}$ ) and steeper (average slope  $\sim 20^\circ$ ), and riparian areas narrow relative to the catchment headwaters. The geology is comprised of Flathead Sandstone and Wolsey Shale at higher elevations and transitions to Granite Gneiss at lower elevations [Reynolds, 1995]. Geologic strata are considered relatively impermeable with the greatest potential for deeper groundwater exchange at geologic contacts, fractures in the Wolsey shale [Reynolds, 1995] and along the more permeable sandstone strata. Soil depths are relatively consistent across the landscape (0.5-1.0m in hillslope positions and 1-2 m in riparian positions) with localized upland areas of deeper soils. The major soil types have been characterized as loamy skeletal, mixed Typic Cryochrepts located along hillslope positions and clayey, mixed Aquic Cryboralfs in riparian zones and parks [Holdorf, 1981]. The dominant forms of

vegetation include lodgepole pine (overstory; *Pinus contorta*) and grouse whortleberry (understory; *Vaccinium scoparium*) in hillslope positions and bluejoint reedgrass (*Calamagrostis canadensis*) in riparian positions [Farnes et al., 1995; Mincemoyer and Birdsall, 2006]. Previous reports provide more detailed descriptions of TCEF climatic [Farnes et al., 1995], geologic [Reynolds, 1995a; Schmidt et al., 1996], and vegetative [Farnes et al., 1995; Mincemoyer and Birdsall, 2006] characteristics.

## Methods

### Physical Hydrology

Jencso et al. [2009] collected high frequency HRS ground water table connectivity observations along 24 HRS transects spanning the range of hillslope UAA sizes (699-46,000 m<sup>2</sup>) within the TCEF. At a minimum, groundwater wells were installed across each transect's hillslope (2-5 m above the break in slope), toeslope (the break in slope between riparian and hillslope positions) and riparian position (1-2 m from the stream). All wells were screened from 10 cm below the ground surface to their completion depths at the bedrock interface. Groundwater levels in each well were recorded with Tru Track Inc. capacitance rods ( $\pm 1$  mm resolution) at hourly intervals for the 2007 water year. Hydrologic connectivity between HRS zones was inferred from the presence of saturation measured in well transects spanning the hillslope, toeslope, and riparian positions. Runoff was recorded in each of the 11 nested catchments using either Parshall or H-Flumes installed by the USFS (Figure 1). Stage in each flume was measured at hourly intervals with Tru Track Inc. water level recorders and every 15

minutes by USFS float potentiometers. Manual measurements of both groundwater well levels (electric tape) and flume stage (visual stage readings) were conducted bi-weekly during the summer months and monthly during the winter to corroborate capacitance rod measurements.

### Terrain Analyses

Stream Network Delineation Terrain analyses were performed using a 10m Digital Elevation Model (DEM) re-sampled from 1m airborne laser swath mapping data (ALSM often referred to as LiDAR; courtesy of NCALM). The area required for perennial stream flow (creek threshold initiation area) was estimated as 40 ha for Lower Tenderfoot Creek (LTC), Upper Tenderfoot Creek (UTC), Sun Creek (SUN), Upper Sun Creek (USC), Spring Park Creek (SPC), Lower Stringer Creek (LSC), Middle Stringer Creek (MSC), Passionate Creek (PC), Lonesome Creek (LC), Pack Creek (PC), and 120 ha for Bubbling Creek (BC). The creek threshold initiation area was based on field surveys of channel initiation points in TCEF [Jencso *et al.*, 2009]. The  $MD_{\infty}$  algorithm (Seibert and McGlynn, 2007) was used to derive the flow accumulation grid and related stream network that was verified by field reconnaissance. Once the stream network was delineated all of the upslope DEM pixels were linked to the stream pixel to which they drained using  $MD_{\infty}$  [Seibert and McGlynn, 2007; Grabs *et al.*, In Press]. The  $MD_{\infty}$  algorithm assumes that the direction of subsurface flow follows surface topography.

Catchment and Hillslope Scale Terrain Indices Terrain indices (TIs) were calculated as distributed values across each catchment and discretely for each hillslope

contributing area entering the stream network. These indices are quantitative metrics representing the potential influence of catchment topography on hydrologic response. Distributed catchment TIs included: slope, aspect (ASP), the gradient along the flow path from each pixel to the creek (GTC), the distance from each pixel to the creek (DTC), the ratio of the flow path length and gradient from each pixel to the creek (DTC/GTC; as a surrogate for the travel time) along each flow path, the elevation of each pixel above the creek (EAC), and the percentage of catchment riparian and hillslope area (%RIP and %HILL respectively). Riparian areas were delineated as any landscape position less than two meters above the stream network following flowpaths to the creek (Grabs et al., In Press). This method was based on the relationship observed by Jencso et al. [2009]. Table 1 describes each of the distributed terrain indices and how they were calculated. We determined median values of each distributed TI for all 11 of the TCEF catchments.

Stream network terrain analyses included quantification of lateral inflows of UAA and the ratio of hillslope and riparian accumulated area (Riparian Buffering Index; RBI) entering each stream pixel (a surrogate for the volumetric buffering of hillslope inputs [McGlynn and Seibert, 2003; Jencso et al., 2010]) separately for the left and right sides of the stream. Mean values of each TI across the lateral contributing area of the left and right sides of the stream network were also calculated. These analyses incorporated the methodology developed by Grabs et al. [2010] which determines the orientation of the stream banks relative to the stream and combines this with standard flow accumulation algorithms to quantify the value of the accumulated TI. Left and right side separations were implemented within the open source software SAGA GIS [Böhner et al., 2008].

Geology and Vegetative Cover In addition to metrics that describe shallow subsurface water redistribution we calculated indices for catchment geology and vegetative cover. Catchment geology was quantified as the areal percentage of each underlying strata. These included Porphyritic Ryodacite, Wolsey Shale, Flathead Sandstone and Granite-Gneiss. Additionally we determined the percentage of the geologic stratum that coincided with UAA greater than 5,000 m<sup>2</sup> (%SS<sub>UAA>5,000m<sup>2</sup></sub>). This UAA threshold was selected as indicative of portions of the landscape that would be expected to have a more sustained shallow groundwater table ([Jencso *et al.*, 2009]; see below for more detail).

Vegetation heights were calculated as the difference between first and last returns (i.e. the difference between the top of the canopy and the ground surface) of the 1m ALSM LiDAR data. Similar LiDAR derived vegetation height indices have been shown to accurately represent ground based measurements of vegetation height [Dubayah and Drake, 2000; Lefsky *et al.*, 2002]. Vegetation heights greater than 1m were classified as conifers. From the conifer coverage we estimated the median tree height (VEG<sub>H</sub>) within each sub catchment and percentage of the catchment covered by trees (% Forest Cover; height greater than 1m). A secondary index, median height \* density (VEG<sub>B</sub>), was also calculated as a relative measure of biomass across the landscape.

Stream Network Connectivity HRS connectivity for each sub catchment's stream network was estimated based on the relationship quantified by Jencso *et al.* [2009] between lateral inflows of UAA to each stream pixel and observed HRS connectivity

duration (Figure 2). The cumulative duration of HRS connectivity was regressed against the size of each transect's hillslope UAA (Equation 2;  $r^2 = 0.92$ ) to develop a relationship for each 10m source area assemblage along the network for each side of the stream.

$$\%TimeConnected = (0.00002 * UAA - 0.0216) * 100 \quad (2)$$

For the purposes of this study we refer to UAA size as a surrogate for the duration of groundwater table connectivity between HRS zones as demonstrated with the above regression equation. Larger UAA sizes indicate longer periods of connectivity duration and smaller UAA sizes generally represent transient HRS water table connections that occur only during the largest snowmelt events (Figure 2). We applied this relationship to the local inflows of UAA for each stream pixel along each stream network (on the left and right stream sides) across the 11 TCEF catchments to estimate the frequency of HRS connectivity through time.

#### Stream Network Connectivity-Runoff Distributions and "Connectivity Yield"

The exceedance probability of each catchment's stream network connectivity fraction (connectivity duration curve; CDC) was compared to its annual flow duration curve (FDC) to assess the relationship between spatio-temporal patterns of connectivity and the magnitude of stream discharge through time. The FDCs were derived from 8762 hourly observations of runoff at each sub catchment flume for the 2007 water year. Catchment CDCs were derived from the combined 10m left and right stream bank connectivity frequencies (3108 - 344 10m cells; depending on the catchment) of for the

2007 water year. Both the CDC and FDC distributions were binned in 1 percentile increments (100 bins).

Annual correlation coefficients and the rate of change between estimated stream network connectivity and runoff were determined by plotting the catchment CDCs against their respective FDCs. This relationship can be considered the “Connectivity Yield” ( $Con_{yield}$ ) for each catchment or the rate of change of runoff with respect to increasing stream network HRS connectivity. To ascertain  $Con_{yield}$  across flow states the annual CDC-FDC relationship was separated into wet (highest runoff 0-10% of the year), transition (hydrograph rise and recession; 10-50% of the year), and dry periods (baseflow 50 to 100% of the year) using linear, exponential and logarithmic fits respectively. The slope of each of these relationships ( $Con_{yield}$ ) was used to assess runoff response to connectivity dynamics across each of the 11 catchments.

#### Univariate and Multiple Linear Assessments of Factors that Influence Connectivity Yield

Relationships between topography, source area connectivity, and runoff generation were assessed using univariate regression and stepwise multiple regression analyses. Multiple linear regression is a classic approach to fit a multivariate linear function between a response variable and a set of more than one predictors. A multivariate linear function (Equation 2) between response variable  $Y$  and predictors  $X_1, X_2, \dots, X_n$  is comprised of an intercept and coefficients  $\beta_1, \beta_2, \dots, \beta_n$  corresponding to each of the predictors. The intercept and the coefficients are estimated through a regression procedure:

$$Y = \beta_0 + \beta_1 X_1 + \beta_2 X_2 + \dots + \beta_n X_n \quad (2)$$

Median values of each TI and geologic-vegetative indices were regressed against  $Con_{yield}$  at annual, peak, transitional, and baseflow periods to assess variables that could partially explain differences in the slope of the relationship between HRS hydrologic connectivity and runoff magnitude across catchments. Model goodness of fit for each successive iteration and variable replacement was assessed *via* Akaike's information criterion (AIC). TI predictors were dropped or added according to a respective increase or decrease in the AIC. The TIs selected for each regression equation were those which were significant ( $p \leq 0.05$ ) in explaining the differences in the slope of the relationship between the CDC and FDC across catchments.

## Results

### Correlations Between Connectivity and Runoff Distributions Across Catchments

Figure 3 depicts the frequency distribution of HRS connectivity (equation 1) across each catchment's stream network and a comparison of stream network connectivity (CDC) to the flow duration curve (FDC) for the 2007 water year. Connectivity varied across catchments as a result of stream network UAA distributions. Catchments with a high frequency of longer duration connectivity values included PACK, SUN, UTC, and USC. Peak stream network connectivity in these catchments ranged from 77 to 71 percent during snowmelt and decreased to between 10 and 2 percent during the driest periods (Figure 4a). A higher frequency of transient or shorter duration connectivity was observed in catchments with more topographic convergence

and divergence in the landscape and smaller median UAA sizes. These included LSC, LTC, PASS, BUB, SPC, and LONE. In these catchments, peak connectivity was between 70 and 56 percent and decreased to between 1.8 and 0.05 percent during dry periods (Figure 4a).

Runoff dynamics were highly variable across catchments. This is exemplified by the differences in the shape and inflection of the FDCs across time (Figure 4b). Catchments with the lowest magnitude runoff during peak flow (0-10% exceedance) included USC, UTC, SUN, LONE, and BUB. Here, maximum runoff values were between 0.3 and 0.41 mm/hr. Higher magnitude runoff between 0.45 and 0.63 mm/hr was characteristic of SPC, LTC, MSC, PACK, PASS, and LSC (in increasing order). During drier time periods the general order of this relationship shifted. USC, UTC, SUN, and PACK exhibited generally higher runoff (between 0.016 and 0.008 mm/hr) relative to LONE, SPC, PASS, MSC, LSC, LTC, and BUB (between 0.007 and 0.001 mm/hr).

Correlation coefficients between the CDC and FDC distributions indicated significant relationships ( $p < 0.05$ ) between the fraction of the stream network connected and runoff magnitude across catchments and time periods (Figures 4c, 5, 6, 7, 8; table 2).

Comparison of each CDC to its respective FDC showed good general agreement in SPC, MSC, LSC, PASS, and LTC with slight divergence during the transition (inflection) periods between low and high flow states (Figure 3). The shapes of the CDC and FDC were similar in UTC, SUN, USUN, and BUB but exhibited increased connectivity relative to runoff magnitude across all flow states (Figure 3). Lone and Pack exhibited

elevated connectivity with respect to runoff during low flow periods and similar connectivity and runoff dynamics during peak flow (Figure 3).

$Con_{yield}$  (slope of the relationship between fractional network connectivity and runoff) varied across catchments for each flow state (Figures 5, 6, 7, and 8 inset panels). Table 2 includes catchment  $Con_{yield}$  values for the annual, wet, transition, and dry time periods. Individual catchment relationships were relatively consistent across the annual, peak and transition time periods. Catchments with lower  $Con_{yield}$  (SUN, USC, UTC, LONE, and LTC) exhibited consistently lower slopes across these time periods and those with higher  $Con_{yield}$  (PACK, MSC, BUB, LSC, PASS, and SPC) exhibited consistently greater slopes (Table 2). The order of  $Con_{yield}$  for the dry period was not similar to that observed during the wet and transition periods; PASS, LONE, BUB, LSC, SPC, and PACK exhibited lower  $Con_{yield}$  relative to SUN, LTC, MSC, USUN, and UTC (Table 2).

#### Predictors of $Con_{yield}$ Across Catchments

To assess landscape variables that could affect  $Con_{yield}$  across catchments and time periods we used median values of each TI distribution (Table 1) versus  $Con_{yield}$  in multiple linear models for annual, peak, transitional, and baseflow periods (Table 2). In the following paragraphs we describe the significant univariate predictors and their combined explanatory power within stepwise multiple regression models.

Significant univariate predictors and their relationships to  $Con_{yield}$  are shown in figure 9. Metrics derived from surface topography that explained a significant proportion of the variability in  $Con_{yield}$  included the DFC, GTC, and DFC/GTC. The ratio of the DTC and GTC explained the most variability and resulted in the most parsimonious

model fit. Increasing DFC/GTC ratios were correlated to decreasing  $Con_{yield}$  across the annual, peak, and transition time periods (Figure 9a;  $r^2 = 0.87, 0.82,$  and  $0.92$  respectively with  $p < 0.05$ ). A significant relationship between the DFC/GTC and  $Con_{yield}$  did not exist during the baseflow period ( $r^2 = 0.45, p > 0.05$ ). Increasing median  $VEG_H$  values were correlated to decreasing in  $Con_{yield}$  coefficients across the annual, peak, and transition time periods (Figure 9b;  $r^2 = 0.87, 0.72,$  and  $0.75$  respectively with  $p < 0.05$ ). During the dry time period the strength of this relationship decreased ( $r^2 = 0.62$ ) and the slope of the relationship became positive with increasing  $VEG_H$  correlated to increasing  $Con_{yield}$ . The  $\%SS_{UAA > 5,000m^2}$  was a significant univariate predictor of variability in catchment  $Con_{yield}$  across all flow states (Figure 9c). During the annual, wet, and transition periods the relationship was negative and weaker ( $r^2 = 0.54$  and  $0.61$  respectively with  $p < 0.05$ ) and increasing  $SS_{UAA > 5,000}$  resulted in lower  $Con_{yield}$  across catchments. This relationship shifted direction and became stronger ( $r^2 = 0.80, p < 0.05$ ) during the dry period, where increasing  $\%SS_{UAA > 5,000}$  resulted in larger  $Con_{yield}$ .

Table 3 lists combinations of significant predictors of  $Con_{yield}$  in multiple regression models during the annual, wet, transition, and dry time periods. Full water year (annual) differences in  $Con_{yield}$  across all 11 catchments were explained by the combination of DFC/GTC and  $VEG_H$ . Eighty five percent of the variance during the annual period was explained by DFC/GTC alone. This increased to 91 percent with the addition of  $VEG_H$ . DFC/GTC alone explained most of the variability in  $Con_{yield}$  during the wet ( $r^2 = 0.79$ ) and transition period ( $r^2 = 0.91$ ).  $\%SS_{UAA > 5,000m^2}$  was the only significant predictor ( $r^2 = 0.81$ ) of  $Con_{yield}$  during the dry period.

## Discussion

### How Does HRS Connectivity Relate to Runoff Observed at Each Catchment Outlet?

Many investigations have emphasized the importance of transient hydrologic connections that can occur between landscape source areas such as hillslope and riparian zones for runoff generation [Mosley, 1979; Woods and Rowe; 1996; McGlynn et al., 2004; Jensco 2010]. However, little research to date has investigated how landscape scale hillslope and riparian shallow groundwater connectivity is distributed across entire stream networks let alone across 11 adjacent yet heterogeneous catchments, examining the variables that can influence water redistribution in space and time. This has limited our understanding of the spatial and temporal sources of runoff both within and across catchments. Here, our results indicated that landscape structure, specifically the topography of hillslopes entering the stream network, imparts a strong signature to the spatial pattern and timing of HRS shallow groundwater connectivity. The sequencing of stream network connectivity through time and across space was a first order control on runoff observed at each catchment's outlet. We documented this across 11 catchments and further partitioned the annual relationship between connectivity and runoff into three hydrologic regimes and examine the factors that affect the strength and slope of these relationships.

Topographic convergence and divergence and the accumulation of contributing area have long been hypothesized as important hydro-geomorphic controls on the redistribution of water from catchment uplands to the channel network. Many of the

formative hillslope hydrology studies [Hewlett and Hibbert, 1967; Dunne and Black, 1970; Freeze, 1972; Harr, 1977; Anderson and Burt, 1978; McGlynn et al., 2002], observed increased subsurface water accumulation in topographically convergent hillslope areas and in areas of higher upslope accumulated area (UAA). This relationship was explicitly tested by Jencso et al [2009] who found a strong linear relationship between annual HRS connectivity duration and stream reach upslope accumulated area size (ranging from ~600-46,000 m<sup>2</sup>) for 24 HRS well transects. When this relationship was applied to one stream network in one catchment, the extent of stream network connectivity varied according to catchment wetness conditions and storage characteristics across the different UAA sizes. Similar conclusions to those of Jencso et al. [2009] were subsequently reported by by Detty and McGuire [2010] in their study conducted in the Hubbard Brook Experimental Forest.

Here, the amount of each catchment's stream network hydrologically connected to its uplands varied through time according to catchment wetness conditions (Figure 3). However, there was significant intra catchment variability in the spatial extent of stream network connectedness over annual and seasonal time periods. Across the 11 TCEF catchments stream network connectivity ranged from 56 - 80 percent during the wettest snowmelt conditions and decreased to 1-10 percent during summer and winter baseflow periods (Figure 4). These differences can be attributed to how hillslope area was accumulated along the stream network within each of the catchments. Catchments (e.g. SPC) with more dissected topography (greater hillslope convergence and divergence) overall had a higher frequency of smaller hillslope area inputs and lower median local

inflows of UAA to the stream network. This resulted in a higher proportion of short duration HRS connectivity along the stream network and less HRS connectivity during peak snowmelt (~56% network connectivity in SPC; Figure 3). Less dissected catchments (e.g. PACK) had higher median UAA values, elevated annual connectivity, and higher maximum HRS network connectivity (~80% network connectivity).

Each stream network CDC was strongly correlated to its respective FDC for all 11 catchments across the annual, peak, transition, and baseflow time periods (Table 2). While it is not surprising that they are positively correlated, the degree of correlation suggests process linkages that are intuitive yet not previously observed nor quantified. The shape of the FDC appears to be largely controlled by the fraction of the stream network hydrologically connected to the uplands throughout the year. During the driest fall and winter baseflow periods (50% of the year) the lowest runoff ranging from 0.016 to 0.002 mm/hr corresponded to between 1 and 10% of each catchments stream network connected to its uplands. Breaks in slope (inflection points) of the stream FDCs at between 0.21 and 0.05mm/hr corresponded to a parallel increase in network connectivity (figures 3 and 4). These synchronous inflection points temporally map to the first snowmelt and early summer dry-down which comprise the transition period between wet and dry catchment states. During the wettest catchment states (snowmelt and the largest rain events), hillslopes associated with the smaller UAAs became connected to the stream network. The cumulative connections of small UAA in addition to previously connected medium and large UAAs, led to greater stream network connectivity and subsequently larger magnitude runoff. During the largest events (~10% of the year) between 66 to 77%

of each catchments stream network was hydrologically connected to its uplands. This resulted in peak runoff ranging from 0.31 - 0.63 mm/hr across catchments. These CDC:FDC relationships suggest that the magnitude and timing of runoff response across catchments was largely a function of hydrologic connectivity frequency and duration.

Those catchments with generally higher and more sustained connectivity also exhibited the greatest divergence between the CDC and FDC across time. Catchments where these relationships diverged could be indicative of other variables impacting the relationship between topography and runoff. For example, the catchments with relatively high connectivity relative to runoff, could be affected by greater evapotranspiration (e.g. aspect or vegetation differences) or differences in geology, or slope. This suggests potential hierarchical influences for source area connectivity and runoff magnitude through time. How these interactions might combine to influence runoff generation is discussed in the following section.

#### What Factors Contribute to Differences in the Connectivity Yield Observed Across the 11 Catchments?

Empirical studies have suggested the influence of topography [*Anderson and Burt, 1978*], geology [*Genereux et al., 1993b; Montgomery et al., 1997; Onda et al., 2001; Uchida et al., 2003; Shaman et al., 2004a*] and vegetation [*Hewlett and Hibbert, 1967; Hibbert, 1967; Emanuel et al., in press*] on the redistribution of water within catchments. Differences in the magnitude and interactions between these variables can affect runoff processes that occur across a wide range of space and time scales. Here, we examined differences between the extent of stream network HRS hydrologic connectivity

and the amount of runoff observed at each catchments outlet. The CDC-FDC regression model fits were significant across all catchments yet each exhibited a different slope or rate of change of runoff with respect to stream network connectedness ( $Con_{yield}$ ; Figure 5). This suggested other factors might influence  $Con_{yield}$  and the shape of the CDC and FDC across flow states. Results from our linear models suggested that in addition to the first-order UAA variable, flowpath lengths and gradients and their ratios (DFC/GTC), vegetation structure, and geologic strata permeability might explain differences in  $Con_{ield}$  across the 11 catchments. In the following sections we describe each of these predictor variables and how we interpret their influence on HRS connectivity induced runoff generation through space and time.

DFC/GTC The frequency distribution of flowpath lengths divided by the gradient along each flowpath (DFC/GTC ratios) can be considered a catchment scale approximation of the hydraulic force driving water redistribution (i.e. Darcy's law) [McGlynn and Seibert, 2003; Seibert and McGlynn, 2003; McGuire et al., 2005; Gardner and McGlynn, 2009]. Our results suggest that while the stream network distributions of UAA largely determine the extent of stream network connectedness (Table 2), the combination of flow path lengths and gradients is important for describing the rate of water redistribution through the shallow subsurface to the stream.

The relationships between the median DFC/GTC ratios and connectivity yield ( $Con_{yield}$ ) differed across catchments. The catchments with the lowest DFC/GTC ratios exhibited highest  $Con_{yield}$  (Figure 9). This means that that in steeper and / or more highly dissected catchments with shorter flowpaths that more streamflow was generated per unit

stream network connectivity than in other catchments. In less complex catchments with longer flowpaths and / or gentler slopes, decreasing DFC/GTC ratios were correlated to decreased  $Con_{yield}$  (Figure 9). This suggests that the inclusion of metrics such as DFC/GTC that describe the velocity and relative time of concentration of water from the uplands to the stream may be more important for *a priori* estimates of the stream flow magnitude associated with a given stream network connectivity fraction.

In the multiple linear analysis, DFC/GTC was a significant predictor on the annual time scale in combination with  $VEG_H$ , and was singly significant during the wet and transition periods. These results are relatively intuitive since the initiation of lateral flow, and therefore topographic controls, depend largely on saturated soil conditions attributed to wetter catchment periods [*Western and Grayson, 2002*]. The strength of the univariate relationship between DFC/GTC and  $Con_{yield}$  decreased from the wet and transition time periods ( $r^2 = 0.82$  and  $0.92$  respectively) to the baseflow time period ( $r^2 = 0.45$ ). This shift was likely due to the depletion of upslope soil moisture storage due to lateral water redistribution and a switching from saturated to unsaturated soil conditions. This resulted in a transition from topographically mediated controls on  $Con_{yield}$  over annual and wet time periods to increasing influence of factors such as vegetation and geology during drier times.

Vegetation Forest cover can affect snow accumulation [*Woods et al., 2006*], the energy balance and snowmelt timing [*Pomeroy et al., 1998; Baldocchi et al., 2000*], landscape transpiration patterns [*Kelliher et al., 1993*], and can therefore be an important sink for water in the shallow subsurface [*Albertson and Kiely, 2001*]. Forested

catchments in strongly seasonal climates exhibit large variations in their rates of transpiration. In semi-arid climates such as TCEF up to 65% of annual precipitation can be transpired back to the atmosphere. Therefore, differences in transpiration across the landscape or across catchments could impact the water available for streamflow and thus the slope of the relationship between a catchment's CDC and FDC ( $Con_{yield}$ ).

Univariate relationships indicated that median catchment  $VEG_H$  was a significant predictor of  $Con_{yield}$  across catchments over annual, wet, and transition periods. Larger tree heights were well correlated to a reduction in stream flow for a given amount of stream network connectivity (Figure 9). At the annual, transition, and baseflow time periods this would be associated with greater leaf area index (LAI) and potentially greater rates and duration of transpiration. Additionally, higher leaf area and taller trees can increase mechanical turbulence (through variability in surface roughness) and canopy conductance, both leading to higher rates of evapotranspiration. During the wetter, snowmelt periods, reductions in  $Con_{yield}$  could be attributed to forest cover and leaf area effects on snow accumulation [Woods *et al.*, 2006], redistribution [Hiemstra *et al.*, 2002], and melt due to canopy effects on the local energy balance [Varhola *et al.*, 2010]. It is also likely that a legacy of soil moisture deficit from the previous growing season could persist in forested areas with mature, taller trees thereby affecting  $Con_{yield}$  in subsequent seasons. This may have resulted in a larger storage deficit to be overcome for initiation of lateral water redistribution and connectivity initiation during snowmelt. All of these factors could reduce the magnitude of water delivery to the stream network from hydrologically connected hillslope positions.

Multiple linear models indicated that  $VEG_H$  was only a significant predictor of  $Con_{yield}$  at the annual time scale in combination with DFC/GTC. While vegetation is likely to be strongly influential during the transitional period (growing season) in semi-arid climates such as TCEF, our analysis was not able to detect vegetative effects on lateral water redistribution during sub-annual time periods. However, given adequate time integration, these catchment scale relationships do suggest vegetative control on the partitioning and redistribution of water through the shallow subsurface that influences  $Con_{yield}$  across catchments. Further landscape scale investigations are needed to evaluate the interplay between patterns of vegetation water use efficiency, hydrologic connectivity, and runoff generation across finer space and time scales.

Intersection of Surface Topography and Geology Comparison of  $Con_{yield}$  and catchment geology suggested that surficial bedrock geology influences shallow subsurface water table dynamics. Many studies have investigated variability in runoff response among catchments with different underlying bedrock [*Freeze, 1972; Godsey et al., 2004; Onda et al., 2006*], and bedrock controls on runoff generation have been observed at the hillslope [*Hewlett and Hibbert, 1967; Tromp-van Meerveld et al., 2007; Iwagami et al., 2010*] and catchment scales [*Genereux et al., 1993a*]. Despite acknowledgement of the potential for bedrock interactions, few studies have characterized the hydrologic exchange between soil zone water tables and the underlying shallow subsurface bedrock and deeper bedrock aquifers. We suggest that these interactions can influence hydrologic connectivity across catchments of complex structure, especially during low flow conditions.

Univariate relationships between  $Con_{yield}$  and the  $\%SS_{UAA>5,000m^2}$  highlights the potential intersection of shallow groundwater connectivity with deeper bedrock flow systems. Catchments with a higher proportion of large UAA sizes (greater than  $5,000m^2$ ) intersecting the sandstone layer exhibited significantly lower runoff per unit of stream network connectivity (negative relationship) during annual, peak, and transitional periods (Figure 9). However, during the lowest flow periods the slope of this relationship shifted direction, becoming positive and stronger ( $r^2 = 0.80$ ,  $p < 0.05$ , Table 2).  $\%SS_{UAA>5,000m^2}$  was the only significant predictor of  $Con_{yield}$  during the driest catchment conditions in our multiple linear analyses, suggesting a shifting affect of geology on  $Con_{yield}$  and its dominance during low flows (Table 2). During wetter periods in persistently connected hillslope positions (large  $UAA > 5,000 m^2$ ), water in the shallow subsurface moves laterally to the stream network and also vertically recharges more permeable sandstone surficial geology. This would lead to decreased  $Con_{yield}$  during wet periods due to sandstone aquifer recharge. However, during low baseflow the sandstone could then become a source of streamflow, slowly releasing water that recharged during wetter times, and leading to a higher runoff magnitude and  $Con_{yield}$  during low flow conditions. The degree to which this recharge–discharge or sink–source status occurs across catchments is likely a function of the intersection of surficial geologic strata permeability/storage characteristics with hydrologically connected hillslope positions.

Water recharging the sandstone strata from overlying soil zones along hydrologically connected hillslopes might be less likely to follow surface topography due to bedrock dip, stratigraphy, and possible fractures. Therefore, water from shallow water

table hillslope sources could enter the stream network at locations not predicted by surface topography alone. Payn et al. [In Review] suggested that there could be a shift from topographic to bedrock controls on the spatial patterns of stream baseflow across three TCEF subcatchments from wet to dry watershed conditions. The influence of bedrock during baseflow was evident in data from intensive stream flow measurements every 200 m across LTC, LSC, and SPC stream networks. Increases in specific discharge (area normalized runoff) were generally and consistently lower in stream reaches underlain by sandstone. However, low upstream yields were compensated by high downstream yields near reaches of the sandstone to granite-gneiss contact. These observations collectively support the premise that water from hydrologically connected hillslope positions recharge the sandstone bedrock layer during wet times and re-emerge and contribute to streamflow lower in the catchment during drier time periods. This leads to a shift of the slope of the  $Con_{yield}$  - sandstone relationship across wet to dry time periods (Figure 9, Table 2).

### Implications

Between 91 and 80 percent of the variance in  $Con_{yeild}$  was explained by predictor variables in the multiple linear models across annual and seasonal time periods. These catchment scale relationships provide insight and potential hypothesis testing frameworks to further examine the influence of topography, vegetation, and geology for mediating hydrological connectivity, water redistribution/storage, and resultant runoff dynamics across space and time. These factors may also explain variance in the landscape HRS connectivity relationship (figure 2) and could be highly influential on the upslope water

balance and thresholds of connectivity initiation and cessation observed across different UAA positions. Future work that aims to physically quantify the influence of these and other factors on distributed HRS connectivity dynamics within catchments is crucial to de-convoluting their relative influence for runoff dynamics observed at the catchment outlet.

Up to 19 percent of the variance in  $Con_{yield}$  could not be explained by multiple regression models for the annual and seasonal time periods. This suggests secondary controls on water redistribution and runoff generation across the 11 TCEF catchments. Two potentially important hydrologic variables not represented in these analyses include distributions of soil depth/textural properties and spatial variability of precipitation and snowmelt. Soil depths to bedrock in the TCEF are approximately 1m and have been found to be relatively homogenous across the landscape (~300 depth measurements and soil pits). However, even slight differences in soil depth or soil characteristics such as texture/ $ksat$  and macroporosity associated with different soil types could influence water holding capacity, the switching between vertical and lateral water redistribution, and therefore connectivity initiation. This non-linearity would also be enhanced by the timing and magnitude of precipitation across the landscape. Current climate forcing in conjunction with antecedent storage conditions attributed to past forcing would strongly influence the partitioning of event water to the shallow subsurface [*Tromp-van Meerveld and McDonnell, 2006*] or to deeper groundwater flow pathways [*Iwagami et al., 2010*]. These alternate considerations in concurrence with those described previously may lead

to differences in patterns of connectivity across the landscape and result in unexplained differences in catchment  $Con_{yield}$  through time.

### Conclusion

Multiple catchment and distributed landscape scale observations in TCEF support the concept of hierarchical controls on streamflow with their relative influence varying across different time periods. Strong relationships between runoff and topographically derived hydrologic connectivity estimates indicate that streamflow from the 11 TCEF catchments is dominantly topographically driven. Variability the slope of the relationship between topographically scaled hydrological connectivity observations and stream discharge led to analysis of additional explanatory variables which varied in their explanatory power across annual and seasonal time scales. Variables included the distributions of flowpath lengths and gradients, geology, and vegetation indices. Our results and analyses provide insight into the complex combinations of catchment characteristics such as topography, vegetation, and geology that can affect hydrological connectivity, water redistribution/storage, and resultant runoff dynamics.

High frequency, spatially distributed observations of HRS shallow groundwater connectivity (24 well transects; 146 wells) were combined with landscape analysis to estimate HRS connectivity across 11 catchments. The 11 catchments had strongly contrasting topography, geology, and landcover-vegetation characteristics. We compared the slope of the relationship between stream network hydrologic connectivity and

discharge across the 11 catchments on annual and seasonal time scales to quantify controls on its variability. Based on this analysis we conclude:

1. Stream network hydrologic connectivity is the first-order control on runoff magnitude observed at catchment outlets.
2. Stream network connectivity yield ( $Con_{yield}$ ) was a function of the interaction between topographically mediated hydrologic connectivity and metrics that act to reduce or enhance water redistribution across connected landscape positions.
  - a. Increasing flow path length to gradient ratios was correlated with decreased  $Con_{yield}$ .
  - b. Taller vegetation was correlated with decreased  $Con_{yield}$  across catchments.
  - c. Increasing proportions of permeable geology underlying wetter landscape positions was correlated with decreased  $Con_{yield}$  in wetter time periods and enhanced  $Con_{yield}$  in drier time periods.
3. The relative influence of topographic, vegetative, and geologic predictors changed through time according to catchment wetness states. Topography was most influential for water redistribution and connectivity dynamics during snowmelt and the annual dry down. Vegetation and Geology become more influential during drier baseflow periods.

Our analyses highlight the importance of the intersection between shallow topographically controlled flow systems and vegetative and geologic features. We

present quantification of hierarchical controls on runoff generation across time and space in catchments of differing topographic, geologic, and vegetative structure. Our results suggest that spatio-temporal distributions of hillslope-riparian-stream hydrologic connectivity across 11 diverse but adjacent catchments can provide insight into runoff source area dynamics, runoff implications of catchment morphology and topology, and a direct and quantifiable link between catchment structure, vegetation, geology and hydrologic dynamics.

#### Acknowledgements

This work was made possible by NSF grant EAR0337650 to McGlynn and an INRA fellowship awarded to Jencso. The authors appreciate extensive logistic collaboration with the U.S. Department of Agriculture, Forest Service, Rocky Mountain Research Station, especially, Ward McCaughey, Scientist in charge of the Tenderfoot Creek Experimental Forest. We thank Thomas Grabs, Robert Payn, John Mallard and Jan Siebert for technical and collaborative support. We are grateful to Jennifer Jencso, Vince Pacific, Diego Riveros-Iregui and especially Austin Allen for invaluable assistance in the field.

References

- Albertson, J. D., and G. Kiely (2001), On the structure of soil moisture time series in the context of land surface models, *Journal of Hydrology*, 243(1-2), 101.
- Ali, G. V., and A. G. Roy (2009), Revisiting hydrologic sampling strategies for an accurate assessment of hydrologic connectivity in humid temperate systems, *Geography Compass*, 3(1), 350–374.
- Anderson, M. G., and T. P. Burt (1978), The role of topography in controlling throughflow generation, *Earth Surfaces Processes and Landforms*, 3, 331-334.
- Baldocchi, D., F. M. Kelliher, T. A. Black, and P. Jarvis (2000), Climate and vegetation controls on boreal zone energy exchange, *Global Change Biology*, 6, 69-83.
- Barnett, T. P., J. C. Adam, and D. P. Lettenmaier (2005), Potential impacts of a warming climate on water availability in snow-dominated regions, *Nature*, 438(7066), 303-309.
- Beven, K. J. (1978), The hydrological response of headwater and sideslope areas, *Hydrological Sciences Bulletin*, 23, 419-437.
- Böhner, J., T. Blaschke, and L. Montanarella (Eds.) (2008), *SAGA: System for an automated geographical analysis*, Institute of Geography, University of Hamburg, Hamburg.
- Bracken, L. J., and J. Croke (2007), The concept of hydrological connectivity and its contribution to understanding runoff-dominated geomorphic systems, *Hydrological Processes*, 21(13), 1749-1763. 10.1002/hyp.6313
- Burns, D. A., P. S. Murdoch, G. B. Lawrence, and R. L. Michel (1998), Effect of groundwater springs on NO<sub>3</sub><sup>-</sup> concentrations during summer in Catskill Mountain streams, *Water Resources Research*, 34(8), 1987-1996.
- Burt, T. P., and D. Butcher (1985), Topographic controls on soil moisture distribution, *Journal of Soil Science*, 36, 469-476.
- Buttle, J. M., P. J. Dillon, and G. R. Eerkes (2004), Hydrologic coupling of slopes, riparian zones and streams: an example from the Canadian Shield, *Journal of Hydrology*, 287(1-4), 161-177. 10.1016/j.jhydrol.2003.09.022|ISSN 0022-1694

- Carlyle, G. C., and A. R. Hill (2001), Groundwater phosphate dynamics in a river riparian zone: effects of hydrologic flowpaths, lithology, and redox chemistry., *Journal of Hydrology*, 247, 151-168.
- Detty, J. M., and K. J. McGuire (2010), Topographic controls on shallow groundwater dynamics: implications of hydrologic connectivity between hillslopes and riparian zones in a till mantled catchment, *Hydrological Processes*, 24(16), 2222-2236. 10.1002/hyp.7656
- Devito, K., I. Creed, T. Gan, C. Mendoza, R. Petrone, U. Silins, and B. Smerdon (2005), A framework for broad-scale classification of hydrologic response units on the Boreal Plain: is topography the last thing to consider?, *Hydrological Processes*, 19(8), 1705-1714. 10.1002/hyp.5881
- Dubayah, R. O., and J. B. Drake (2000), Lidar Remote Sensing for Forestry, *Journal of Forestry*, 98(44).
- Dunne, T., and R. D. Black (1970), Partial area contributions to storm runoff in a small New England watershed., *Water Resources Research*, 6(5), 1296-1311.
- Emanuel, R. E., H. E. Epstein, B. L. McGlynn, D. L. Welsch, D. J. Muth, and P. D'Odorico (in press), Spatial and temporal controls on watershed ecohydrology in the northern Rocky Mountains., *Water Resour. Res.* 10.1029/2009WR008367
- Farnes, P. E., R. C. Shearer, W. W. McCaughey, and K. J. Hansen (1995), Comparisons of Hydrology, Geology, and Physical Characteristics Between Tenderfoot Creek Experimental Forest (East Side) Montana, and Coram Experimental Forest (West Side) Montana, 19 pp, USDA Forest Service, Intermountain Research Station, Forestry Sciences Laboratory, Bozeman, MT.
- Freeze, A. R. (1972), Role of subsurface flow in generating surface runoff. 2.Upstream source areas, *Water Resources Research*, 8(5), 1272-1283.
- Gardner, K. K., and B. L. McGlynn (2009), Seasonality in spatial variability and influence of land use/land cover and watershed characteristics on stream water nitrate concentrations in a developing watershed in the Rocky Mountain West, *Water Resour. Res.*, 45(8), W08411. 10.1029/2008wr007029
- Genereux, D. P., H. F. Hemond, and P. J. Mulholl (1993), Spatial and temporal variability in streamflow generation on the West Fork of Walker Branch Watershed, *Journal of Hydrology*, 142, 137-166.
- Godsey, S., H. Elsenbeer, and R. F. Stallard (2004), Overland flow generation in two lithologically distinct rainforest catchments, *Journal of Hydrology*, 295, 276-290.

- Grabs, T. J., K. G. Jencso, B. L. McGlynn, and J. Seibert (in press), Calculating terrain indices along streams - a new method for separating stream sides, *Water Resour. Res.* 10.1029/2010WR009296
- Harr, R. D. (1977), Water flux in soil and subsoil on a steep forested slope., *Journal of Hydrology*, 33, 37-58.
- Hewlett, J. D., and A. R. Hibbert (1967), Factors affecting the response of small watersheds to precipitation in humid areas., in *Forest Hydrology.*, edited by W. E. Sopper and H. W. Lull, pp. 275-291, Pergamon Press, New York.
- Hibbert, A. R. (1967), Forest treatment effects in water yield, paper presented at Forest Hydrology, Pergamon Press, The Pennsylvania State University, University Park, PA, Aug. 29 to Sept. 10, 1965.
- Holdorf, H. D. (1981), Soil Resource Inventory, Lewis and Clark National Forest Interim In-Service Report, On file with the Lewis and Clark National Forest, Forest Supervisor's Office, Great Falls, MT.
- Hopp, L., and J. J. McDonnell (2009), Connectivity at the hillslope scale: Identifying interactions between storm size, bedrock permeability, slope angle and soil depth, *Journal of Hydrology*, 376(3-4), 378-391. 10.1016/j.jhydrol.2009.07.047
- Huff, D. D., R. V. Oneill, W. R. Emanuel, J. W. Elwood, and J. D. Newbold (1982), Flow variability and hillslope hydrology, *Earth Surface Processes and Landforms*, 7(1), 91-94.
- Istanbulluoglu, E., and R. L. Bras (2005), Vegetation-modulated landscape evolution: Effects of vegetation on landscape processes, drainage density, and topography, *J. Geophys. Res.-Earth Surf.*, 110(F2), 19. F0201210.1029/2004jf000249
- Ivanov, V. Y., R. L. Bras, and E. R. Vivoni (2008a), Vegetation-hydrology dynamics in complex terrain of semiarid areas: 1. A mechanistic approach to modeling dynamic feedbacks, *Water Resources Research*, 44(3), 34. W0342910.1029/2006wr005588
- Ivanov, V. Y., R. L. Bras, and E. R. Vivoni (2008b), Vegetation-hydrology dynamics in complex terrain of semiarid areas: 2. Energy-water controls of vegetation spatiotemporal dynamics and topographic niches of favorability, *Water Resources Research*, 44(3), 20. W0343010.1029/2006wr005595

- Ivanov, V. Y., S. Fatichi, G. D. Jenerette, J. F. Espeleta, P. A. Troch, and T. E. Huxman (2010), Hysteresis of soil moisture spatial heterogeneity and the homogenizing effect of vegetation, *Water Resour. Res.*, 46(9), W09521. 10.1029/2009wr008611
- Iwagami, S., M. Tsujimura, O. Yuichi, J. Shimada, and T. Tanaka (2010), Role of bedrock groundwater in the rainfall-runoff process in a small headwater catchment underlain by volcanic rock, *Hydrological Processes*, 24, 2771-2783. 10.1002/hyp.7690
- Hiemstra, C.A, G.E. Liston, and W.A. Reiners (2002), Snow Redistribution by Wind and Interactions with Vegetation at Upper Treeline in the Medicine Bow Mountains, Wyoming, U.S.A.. *Arctic, Antarctic, and Alpine Research*, 34, No. 3 , pp. 262-273
- Jencso, K. G., B. L. McGlynn, M. N. Gooseff, S. M. Wondzell, K. E. Bencala, and L. A. Marshall (2009), Hydrologic connectivity between landscapes and streams: Transferring reach-and plot-scale understanding to the catchment scale, *Water Resources Research*, 45, 16. W0442810.1029/2008wr007225
- Jencso, K. G., B. L. McGlynn, M. N. Gooseff, K. E. Bencala, and S. M. Wondzell (2010), Hillslope hydrologic connectivity controls riparian groundwater turnover: Implications of catchment structure for riparian buffering and stream water sources, *Water Resour. Res.* 10.1029/2009WR008818
- Kelliher, F. M., R. Leuning, and E.-D. Schulze (1993), Evaporation and canopy characteristics of coniferous forests and grasslands, *Oecologia*, 95(2), 153-163.
- Lefsky, M. A., W. B. Cohen, G. G. Parker, and D. J. Harding (2002), Lidar remote sensing for ecosystem studies, *Bioscience*, 52(1), 19-30.
- McGlynn, B. L., and J. J. McDonnell (2003a), Role of discrete landscape units in controlling catchment dissolved organic carbon dynamics, *Water Resources Research*, 39(4), 18. 109010.1029/2002wr001525
- McGlynn, B. L., and J. J. McDonnell (2003b), Quantifying the relative contributions of riparian and hillslope zones to catchment runoff, *Water Resources Research*, 39(11), 20. 131010.1029/2003wr002091
- McGlynn, B.L., McDonnell, J.J., and D. Brammer (2002), A review of the evolving perceptual model of hillslope flowpaths at the Maimai Catchments, NZ. *Journal of Hydrology*, 257(1-26).

- McGlynn, B. L., and J. Seibert (2003), Distributed assessment of contributing area and riparian buffering along stream networks, *Water Resour. Res.*, 39(4), 1082. 10.1029/2002wr001521
- McGlynn, B.L. and J. Seibert (2003), DEM-Based analysis of landscape organization: 1) riparian to hillslope area ratios, Eos Trans. EGS - AGU - EUG Joint Assembly. Meet. Suppl., Abstract #7198
- McGlynn, B. L., J. J. McDonnell, J. Seibert, and C. Kendall (2004), Scale effects on headwater catchment runoff timing, flow sources, and groundwater-streamflow relations, *Water Resources Research*, 40(7). W07504
- McGuire, K. J., J. J. McDonnell, M. Weiler, C. Kendall, B. L. McGlynn, J. M. Welker, and J. Seibert (2005), The role of topography on catchment-scale water residence time, *Water Resour. Res.*, 41(5), W05002. 10.1029/2004wr003657
- Mincemoyer, S. A., and J. L. Birdsall (2006), Vascular flora of the Tenderfoot Creek Experimental, Little Belt Mountains, Montana, *MADRONO*, 53(3), 211-222.
- Montgomery, D. R., W. E. Dietrich, R. Torres, S. P. Anderson, J. T. Heffner, and K. Loague (1997), Hydrologic response of a steep, unchanneled valley to natural and applied rainfall, *Water Resources Research*, 33(1), 91-109.
- Mosley, M.P., (1979), Streamflow generation in a forested watershed, New Zealand. *Water Resources Research* 15, 795-806.
- N.W., A. (1996), *Global Warming, River Flows and Water Resources*, Wiley, Chichester.
- Ocampo, C. J., M. Sivapalan, and C. Oldham (2006), Hydrological connectivity of upland-riparian zones in agricultural catchments: Implications for runoff generation and nitrate transport, *Journal of Hydrology*, 331(3-4), 643-658. 10.1016/j.jhydrol.2006.06.010
- Onda, Y., Y. Komatsu, M. Tsujimura, and J.-i. Fujihara (2001), The role of subsurface runoff through bedrock on storm flow generation, *Hydrological Processes*, 15, 1693-1706.
- Onda, Y., M. Tsujimura, J.-i. Fujihara, and I. Jun (2006), Runoff generation mechanisms in high-relief mountainous watersheds with different underlying geology, *Journal of hydrology*, 331, 659-673. 10.1016/j.jhydrol.2006.06.009
- Pacific, V. J., K. G. Jencso, and B. L. McGlynn (2010), Variable flushing mechanisms and landscape structure control stream DOC export during snowmelt in a set of

nested catchments, *Biogeochemistry*, 99(1-3), 193-211. 10.1007/s10533-009-9401-1

Payn, R.A., M. N. Gooseff, B. L. McGlynn, K. E. Bencala, and S. M. Wondzell (In Review), Change from surface to subsurface control of spatial patterns in stream baseflow during a seasonal recession, *Water Resources Research*.

Reynolds, M. (1995), Geology of Tenderfoot Creek Experimental Forest, Little Belt Mountains, Meagher County, Montana, in *Hydrologic and Geologic Characteristics of Tenderfoot Creek Experimental Forest, Montana, Final Rep. RJVA-INT-92734*, edited by P. Farnes, Intermt. Res. Stn., For. Serv., U.S. Dep. of Agric., Bozeman, Mont.

Rodríguez-Iturbe, I., and J. B. Valdés (1979), The geomorphologic structure of hydrologic response, *Water Resour. Res.*, 15(6), 1409-1420.  
10.1029/WR015i006p01409

Schmidt, W. C., J. L. Friede, and Compilers (1996), Experimental forests, ranges and watersheds in the Northern Rocky Mountains: a compendium of outdoor laboratories in Utah, Idaho and Montana, U.S. Department of Agriculture, Forest Service, Ogden, UT

Seibert, J. and B.L. McGlynn (2003), DEM-Based analysis of landscape organization: 2) Application to catchment comparison, Eos Trans. EGS - AGU - EUG Joint Assembly. Meet. Suppl., Abstract #9041

Seibert, J., and B. L. McGlynn (2007), A new triangular multiple flow direction algorithm for computing upslope areas from gridded digital elevation models, *Water Resources Research*, 43(4). W04501

Shaman, J., M. Stieglitz, and D. Burns (2004), Are big basins just the sum of small catchments?, *Hydrological Processes*, 18, 3195-3206.

Sidele, R. C., Y. Tsuboyama, S. Noguchi, I. Hosoda, M. Fujieda, and T. Shimizu (2000), Stormflow generation in steep forested headwaters: a linked hydrogeomorphic paradigm, *Hydrological Processes*, 14(3), 369-385.

Soulsby, C., P. J. Rodgers, J. Petry, D. M. Hannah, I. A. Malcolm, and S. M. Dunn (2004), Using tracers to upscale flow path understanding in mesoscale mountainous catchments: two examples from Scotland, *Journal of Hydrology*, 291(3-4), 174-196. 10.1016/j.jhydrol.2003.12.042

Soulsby, C., D. Tetzlaff, P. Rodgers, S. Dunn, and S. Waldron (2006), Runoff processes, stream water residence times and controlling landscape characteristics in a

mesoscale catchment: An initial evaluation, *Journal of Hydrology*, 325(1-4), 197-221. 10.1016/j.jhydrol.2005.10.024

- Tetzlaff, D., J. Seibert, K. J. McGuire, H. Laudon, D. A. Burn, S. M. Dunn, and C. Soulsby (2009), How does landscape structure influence catchment transit time across different geomorphic provinces?, *Hydrological Processes*, 23(6), 945-953. 10.1002/hyp.7240
- Tromp-van Meerveld, H. J., and J. J. McDonnell (2006), Threshold relations in subsurface stormflow 1. A 147 storm analysis of the Panola hillslope, *Water Resources Research* 42, W02410. 10.1029/2004WR003778
- Tromp-van Meerveld, H. J., N. E. Peters, and J. J. McDonnell (2007), Effect of bedrock permeability on subsurface stormflow and the water balance of a trenched hillslope at the Panola Mountain Research Watershed, Georgia, USA, *Hydrological Processes* 21, 750-769.
- Uchida, T., Y. Asano, N. Ohte, and T. Mizuyama (2003), Seepage area and rate of bedrock groundwater discharge at a granitic unchanneled hillslope, *Water Resources Research*, 39(1). 10.1029/2002WR001298
- Uchida, T., Y. Asano, Y. Onda, and S. Miyata (2005), Are headwaters just the sum of hillslopes?, *Hydrological Processes*, 19(16), 3251-3261. 10.1002/hyp.6004
- Varhola, A., N. Coops, M. Weiler, and R. D. Moore (2010), Forest canopy effects on snow accumulation and ablation: An integrative review of empirical results, *Journal of Hydrology*, 392, 219-233. 10.1016/j.jhydrol.2010.08.009
- Vidon, P. G. F., and A. R. Hill (2004), Landscape controls on the hydrology of stream riparian zones, *Journal of Hydrology*, 292(1-4), 210-228. 10.1016/j.jhydrol.2004.01.005
- Wagener, T., M. Sivapalan, T. P., and R. Woods (2007), Catchment classification and hydrologic similarity, *Geography Compass*, 1, 901-931. 10.1111/j.1749-8198.2007.00039.x
- Wolock, D. M., J. Fan, and G. B. Lawrence (1997), Effects of basin size on low-flow stream chemistry and subsurface contact time in the Neversink River watershed, New York., *Hydrological Processes*, 11, 1273-1286.
- Woods, S. W., R. Ahl, J. Sappington, and W. W. McCaughey (2006), 235, 202-211. 10.1016/j.foreco.2006.08.013

Woods, R., and L. Rowe (1996), The changing spatial variability of subsurface flow across a hillside, *Journal of Hydrology*, 35, 51-86

Tables

Table 1: Terrain predictor variables extracted from landscape analysis.

| <b>Terrain Predictor</b>                        | <b>Description</b>  |
|---|---|
| Local Inflows of UAA                            | Upslope Accumulated Area on the left and right stream sides. Used as a proxy for shallow water redistribution and HRS hydrologic connectivity.  |
| RBI   | Riparian buffering (ratio of hillslope and riparian area) on the left and right stream sides. A proxy for volumetric and chemical buffering of hillslope inputs.  |
| Slope   | Slope of each DEM pixel   |
| Aspect  | Azimuth of each DEM pixel.  |
| DFC   | Flow path distance from the stream.   |
| GTC   | Gradient along a flow path to the stream.   |
| DFC/GTC   | Ratio of flow path length and gradient.   |
| EAC   | Elevation of a DEM cell above the stream cell it flows into.  |
| % Riparian Area                                 | Percentage of riparian area in each catchment. Riparian area was delineated as all area less than 2 m above the stream network. This was estimated to be the limit of saturated overland flow generation.   |
| % Hillslope Area                                | Percentage of hillslope area in each catchment. Hillslope area was computed as the difference between total catchment area and riparian area.   |
| % Geology                                       | Areal coverage for each geologic stratum in TCEF (Granite Gniess (GG), Flathead Sandstone (SS), Wolsey Shale (WS), and Biotite Hornblende Quartz Monzonite (BHQM)).   |
| % Geology <sub>UAA &gt; 5000m<sup>2</sup></sub> | The percentage of each geologic stratum that is overlain by UAA values greater than 5,000 m <sup>2</sup> . This threshold was selected to locate UAA values that would have longer duration shallow groundwater table connectivity; based on the relationship observed by Jencso et al. [2009]. |
| VEG <sub>H</sub>                                | Catchment tree height (above a 1m threshold). Tree heights were calculated as the difference between the first and second returns of LIDAR data.  |
| % Forest Cover                                  | Percentage of catchment covered by trees taller than 1m. Vegetation height was calculated as the difference between the first and second returns of LIDAR data.   |
| VEG <sub>B</sub>                                | Vegetation height multiplied by vegetation density. A metric of the relative forested biomass within each catchment.  |

Table 2: Median values of retained landscape predictor variables and  $Con_{yield}$  for the annual, wet, transition and dry time periods.  $Con_{yield}$  was estimated based on the linear (annual and wet), exponential (transition), and logarithmic (dry) fits to the relationship between stream network connectivity and runoff magnitude at 1 percentile increments. The slope for each of these relationships is indicated in bold along with the correlation value. Predictor variables were input into linear regression models to explain the differences in  $Con_{yield}$  across catchments and time periods. Median local inflows of UAA (side separated) are listed as a relative measure of catchment topographic convergence and divergence for comparison to stream network connectivity distributions (Figures 3 and 4).

| Catchment | UAA  | DFC/<br>GTC | VEG <sub>H</sub> | %SS <sub>UAA</sub> ><br>5,000 m | Annual<br>$Con_{yield}$ | Wet<br>$Con_{yield}$         | Transition<br>$Con_{yield}$ | Dry<br>$Con_{yield}$  |
|-----------|------|-------------|------------------|---------------------------------|-------------------------|------------------------------|-----------------------------|-----------------------|
| SPC       | 1695 | 3098        | 4.85             | 13                              | <b>0.0087</b><br>0.98   | <b>0.0092</b><br>0.98        | <b>0.184</b><br>0.99        | <b>0.0045</b><br>0.89 |
| LSC       | 2357 | 3139        | 4.80             | 16                              | <b>0.0085</b><br>0.97   | <b>0.0093</b><br>0.98        | <b>0.155</b><br>0.98        | <b>0.0042</b><br>0.47 |
| LTC       | 2403 | 4443        | 5.04             | 19                              | <b>0.0074</b><br>0.98   | <b>0.0068</b><br>0.98        | <b>0.133</b><br>0.99        | <b>0.0128</b><br>0.93 |
| MSC       | 2357 | 3865        | 4.97             | 19                              | <b>0.0078</b><br>0.98   | <b>0.0080</b><br>0.98        | <b>0.139</b><br>0.93        | <b>0.0133</b><br>0.98 |
| UTC       | 3510 | 10727       | 5.52             | 27                              | <b>0.0039</b><br>0.95   | <b>0.0055</b><br>0.87        | <b>0.071</b><br>0.99        | <b>0.0192</b><br>0.91 |
| SUN       | 3326 | 7892        | 5.20             | 20                              | <b>0.0044</b><br>0.94   | <b>0.0055</b><br>0.88        | <b>0.103</b><br>0.98        | <b>0.0115</b><br>0.88 |
| BUB       | 2425 | 5000        | 5.20             | 17                              | <b>0.0053</b><br>0.93   | <b>0.0071</b><br>0.92        | <b>0.140</b><br>0.97        | <b>0.0036</b><br>0.93 |
| USC       | 6500 | 10454       | 5.36             | 22                              | <b>0.0037</b><br>0.86   | <b>0.0050</b><br>0.93        | <b>0.060</b><br>0.97        | <b>0.0144</b><br>0.78 |
| LONE      | 1350 | 7114        | 4.91             | 14                              | <b>0.0062</b><br>0.95   | <b>0.0069</b><br>0.97        | <b>0.116</b><br>0.69        | <b>0.0022</b><br>0.34 |
| PACK      | 2769 | 4358        | 4.89             | 16                              | <b>0.0075</b><br>0.97   | <b>0.0071</b><br><b>0.95</b> | <b>0.136</b><br>0.99        | <b>0.0055</b><br>0.89 |
| PASS      | 1968 | 2516        | 4.62             | 14                              | <b>0.0096</b><br>0.95   | <b>0.0089</b><br>0.99        | <b>0.180</b><br>0.90        | <b>0.0008</b><br>0.88 |

Table 3: Multiple linear models listed in order of decreasing streamflow. Regression coefficients are listed with their associated p-value (bold). A missing value indicates that the predictor was not retained in the final model. Variables that were not found to be significant during any of the flow states were omitted.

| Flow Period        | Adjusted Multiple $r^2$ | Intercept                       | DFC/GTC                     | Tree Height           | %Sandstone <sub>UAA</sub> >5,000m <sup>2</sup> |
|--------------------|-------------------------|---------------------------------|-----------------------------|-----------------------|--|
| Annual Linear fit  | 0.91                    | 0.028<br><b>&lt;0.01</b>        | -3.5E-07<br><b>0.03</b>     | -0.004<br><b>0.04</b> | ----   |
| Wet linear fit     | 0.80                    | 0.010<br><b>&lt;0.01</b>        | -4.7E-07<br><b>&lt;0.01</b> | ----                  | ----   |
| Transition Exp fit | 0.91                    | 0.20<br><b>&lt;0.01</b>         | -1.3E-05<br><b>&lt;0.01</b> | ----                  | ----   |
| Dry Log fit        | 0.81                    | <b>0.016</b><br><b>&lt;0.01</b> | ----                        | ----                  | 0.001<br><b>&lt;0.01</b>                       |

Figures

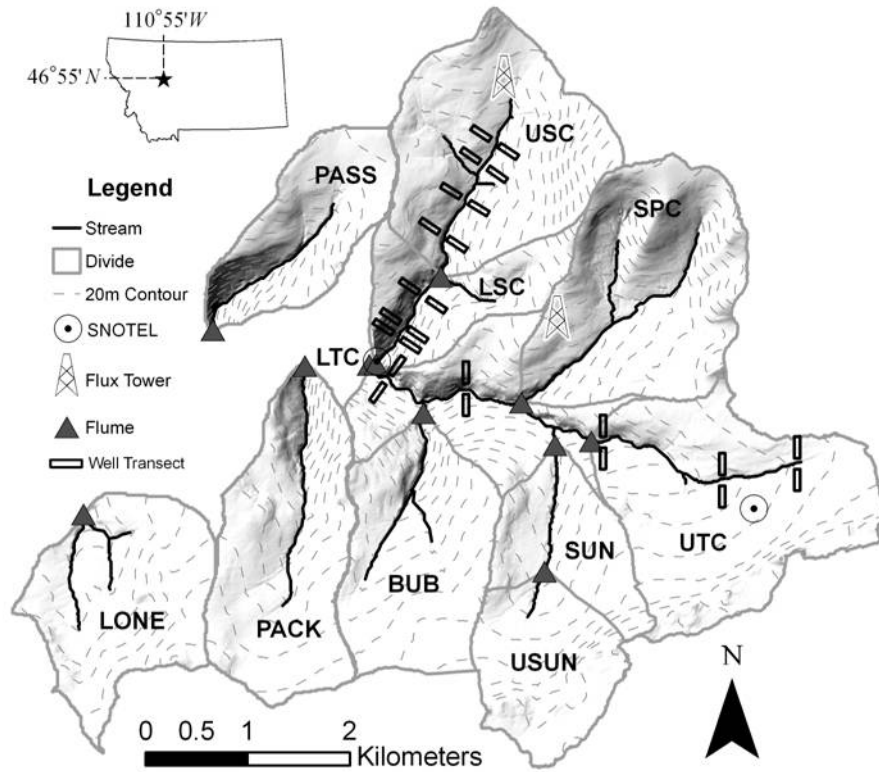


Figure 1: Site location and instrumentation of the TCEF catchment. (a) Catchment location in the Rocky Mountains, MT. (b) Catchment flumes, well transects installed by Jencso et al. (2009) and SNOTEL instrumentation locations. Transect extents are not drawn to scale.

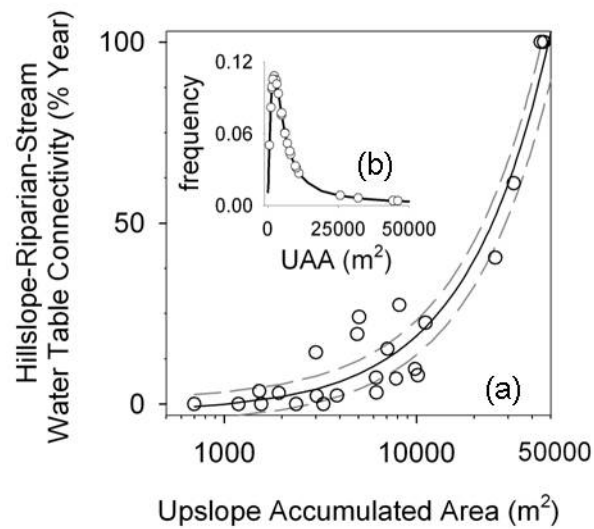


Figure 2: The linear relationship (a) between the local inflows of UAA and HRS shallow groundwater connectivity duration observed by Jencso et al. (2009). This relationship was applied to each 10m HRS source area assemblage to estimate stream network connectivity. The inset plot (b) indicates where each of the 24 HRS well transects falls within the stream network distribution of UAA.

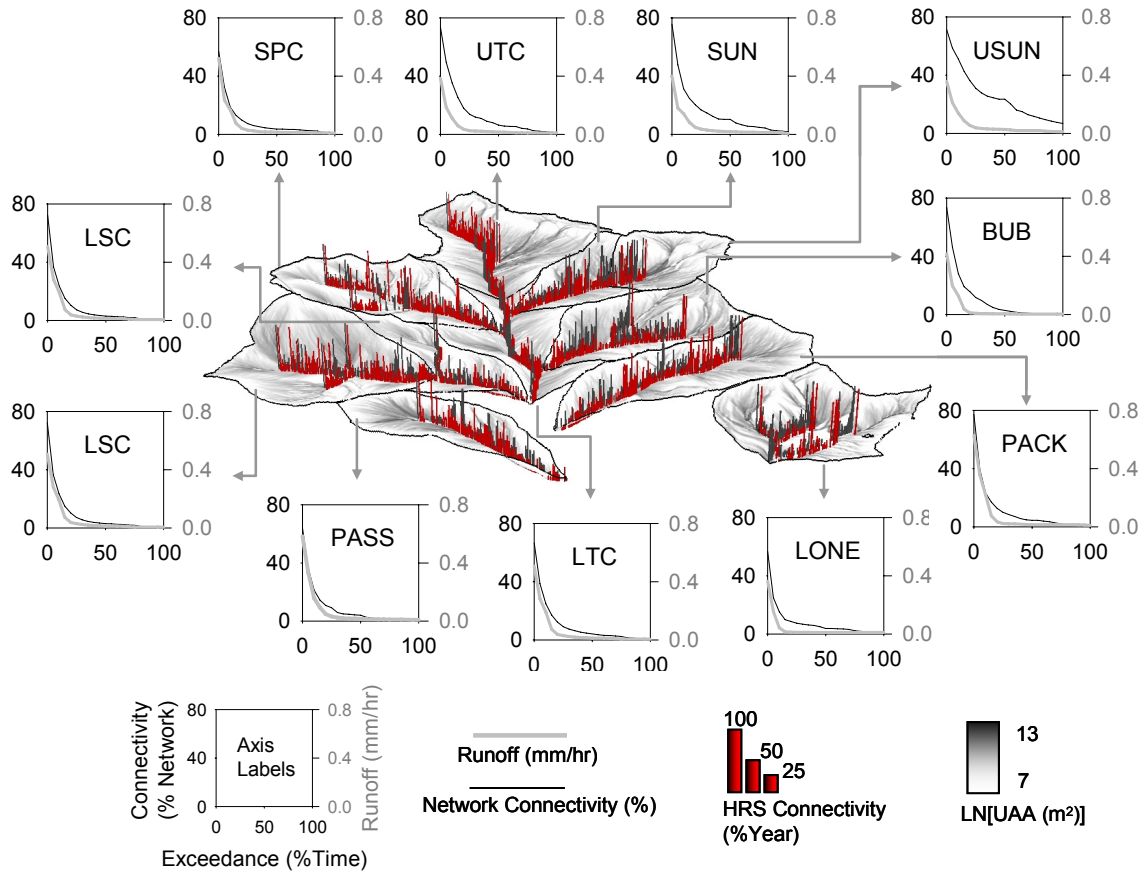


Figure 3: Comparison of the TCEF catchments connectivity duration curves (CDC) and the annual flow duration curve. (a) CDCs were derived from the frequency distribution of HRS water table connectivity at each 10 meter pixel (both sides) along the stream network. FDCs were derived from hourly runoff values for the 2007 water year (8732 values). Periods of lowest runoff are associated with the lowest connectivity that occurs among the largest UAA values. Larger magnitude runoff is associated with increasing hydrologic connectivity across subsequently smaller stream network UAA values (increasing from large to small).

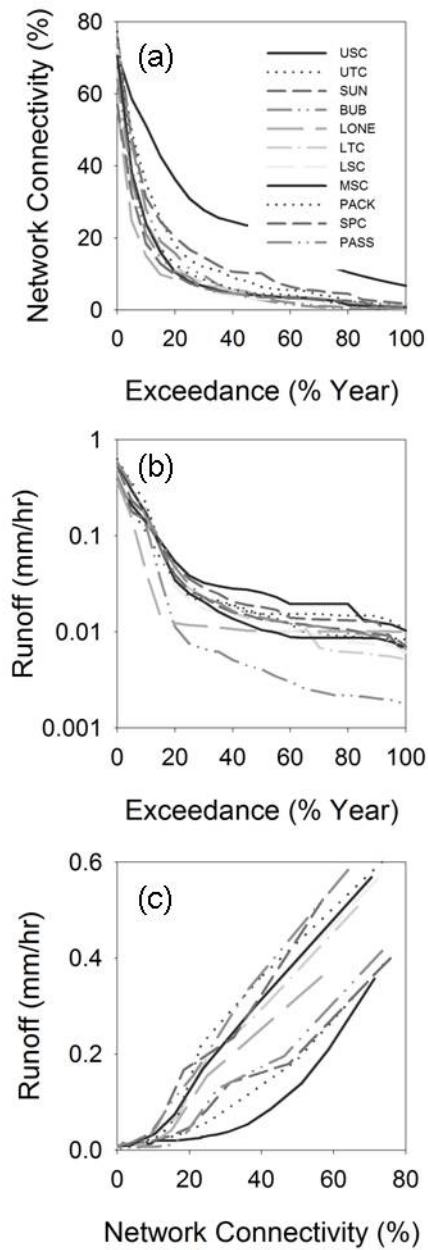


Figure 4: Distributions of (a) stream network HRS connectivity, (b) runoff and (c) annual stream network connectivity versus runoff magnitude for each catchment. Each CDC and FDC was plotted at 1 percentile increments.

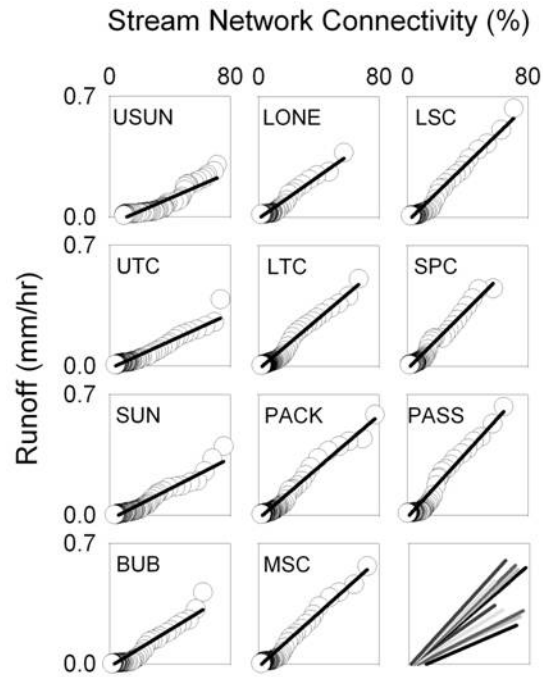


Figure 5: Linear fit to the relationship between the percentage of the stream network connected (CDC) and runoff magnitude (FDC) for the 2007 water year (0-100% exceedance). The lower right panel depicts all of the linear fits to highlight annual variability in  $Con_{yield}$  across the TCEF catchments.

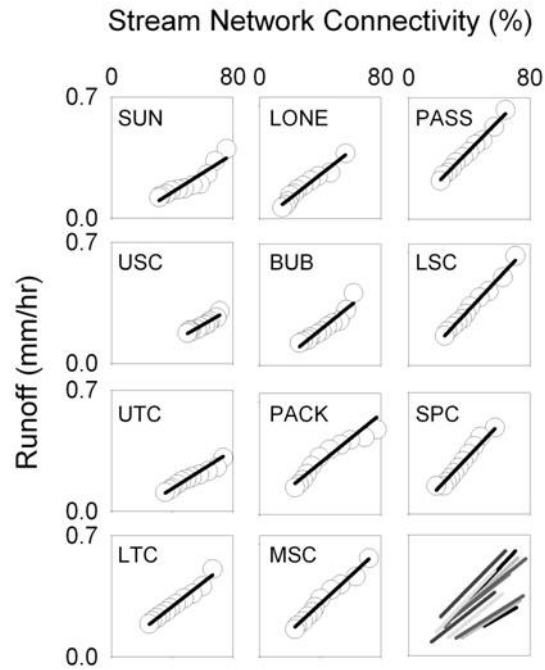


Figure 6: Linear fit to the relationship between the percentage of the stream network connected (CDC) and runoff magnitude (FDC) during the wettest catchment states (0-10% exceedance). The lower right panel depicts all of the linear fits to highlight variability in  $Con_{yield}$  during peak flow across the TCEF catchments.

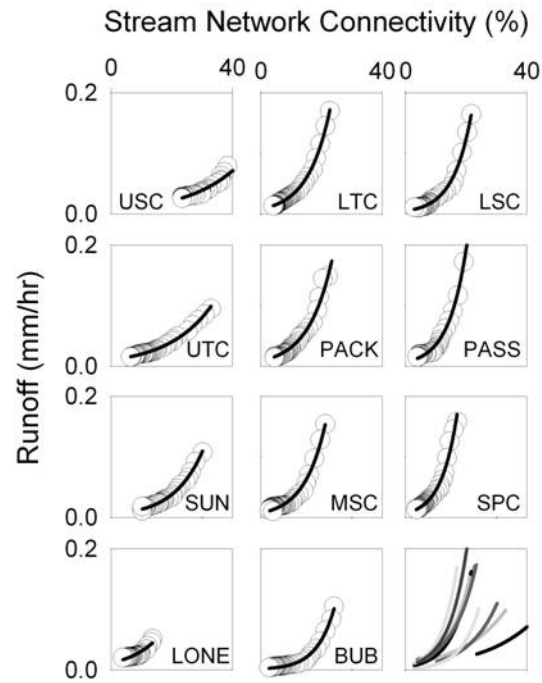


Figure 7: Exponential fit to the relationship between the percentage of the stream network connected (CDC) and runoff magnitude (FDC) during the transition from wet to dry states (10-50% exceedance). The lower right panel depicts all of the exponential fits to highlight variability in  $Con_{yield}$  during wet up and dry down across the TCEF catchments.

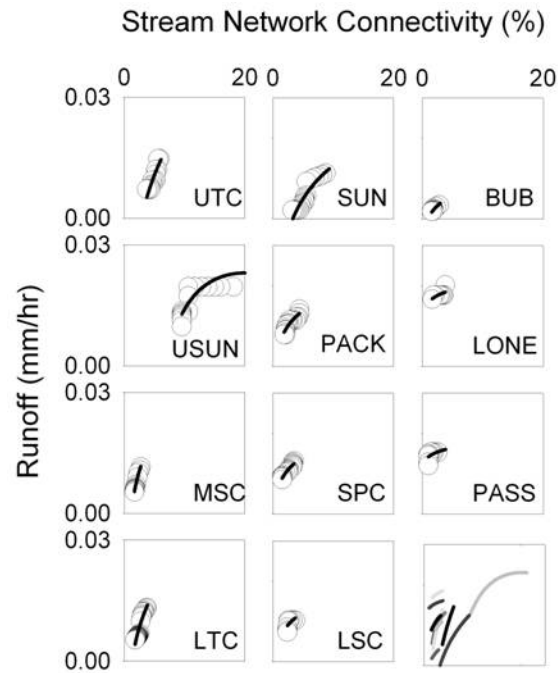


Figure 8: Logarithmic fit to the relationship between the percentage of the stream network connected (CDC) and runoff magnitude (FDC) during the driest catchment states (50-100% exceedance). The lower right panel depicts all of the log fits to highlight variability in  $Con_{yield}$  across the TCEF catchments during low flow conditions.

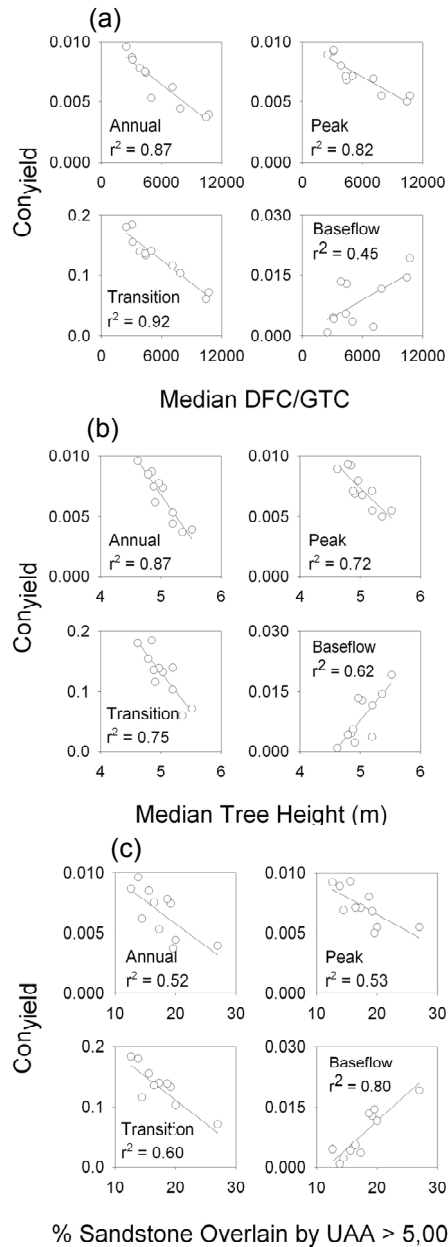


Figure 9: Linear relationships between  $Con_{yield}$  for each TCEF catchment during the annual, wet, transition, and dry periods and median values of the (a) DFC/GTC, (b) tree height, and (c) percentage of catchment sandstone overlain by UAA greater than 5,000m<sup>2</sup>. Combinations of these predictors explained variability in catchment  $Con_{yield}$  across flow states within multiple linear

Contribution of Authors

Chapter 6: Calculating terrain indices along streams – a new method for separating stream sides

First author: Thomas J. Grabs

Co-authors: Kelsey G. Jencso, Brian L. McGlynn, and Jan Seibert

Contributions: Thomas Grabs was the lead for writing, figure development, and was responsible for development and coding of the SIDE methodology within the SAGA GIS. I contributed to the writing and figure development, provided hydrometric and landscape analysis data for the method demonstration, and edited successive versions of the manuscript. Brian McGlynn and Jan Seibert contributed significant critique and ideas for development of intellectual content within the paper and edited successive versions of the manuscript. Jan Seibert also assisted Thomas Grabs with the SIDE method development and coding within the SAGA GIS.

Manuscript Information

Grabs, T., K.G. Jencso , B.L. McGlynn, J. Seibert. 2010. Calculating terrain indices along streams - a new method for separating stream sides. *Water Resources Research*.

- Journal: Water Resources Research
- Status of manuscript (check one)
  - Prepared for submission to a peer-reviewed journal
  - Officially submitted to a peer-reviewed journal
  - Accepted by a peer-reviewed journal
  - Published in a peer-reviewed journal
- Publisher: American Geophysical Union
- Date of submission: April 21, 2009
- Date manuscript was accepted: August 13, 2010

Reproduced by kind permission of the American Geophysical Union

## **Calculating terrain indices along streams - a new method for separating stream sides**

Grabs, T. J.<sup>1</sup>, Jencso, K.G.<sup>2</sup>, McGlynn, B.L.<sup>2</sup>, Seibert J.<sup>1,3</sup>

<sup>1</sup> Department of Physical Geography and Quaternary Geology, Stockholm University, Stockholm, Sweden

<sup>2</sup> Department of Land Resources and Environmental Sciences, Montana State University, Bozeman, Montana, USA

<sup>3</sup> Department of Geography, University of Zurich, Zurich, Switzerland

### **Abstract**

There is increasing interest in assessing riparian zones and their hydrological and biogeochemical buffering capacity with indices derived from hydrologic landscape analysis of digital elevation data. Upslope contributing area is a common surrogate for lateral water flows and can be used to assess the variability of local water inflows to riparian zones and streams. However, current GIS algorithms do not provide a method for easily separating riparian zone and adjacent upland lateral contributions on each side of the stream. Here we propose a new algorithm to compute side-separated contributions along stream networks. We describe the new algorithm and illustrate the importance of distinguishing between lateral inflows on each side of streams with hillslope – riparian zone – stream hydrologic connectivity results from high frequency water table data collected in the 22 km<sup>2</sup> Tenderfoot Creek catchment, Montana.

## 1. Introduction

Accurate representation of distributed hydrological processes at the watershed scale demands improved predictive tools that can maximize information derived from spatial data sets such as digital elevation models (DEMs). Hydrological terrain analysis based on topography, typically represented by DEMs, can be used to characterize stream networks and riparian zones. Over the past 30 years various flow algorithms have been developed for estimating the redistribution of water across the landscape based on topography [O'Callaghan and Mark, 1984; Freeman, 1991; Quinn *et al.*, 1991; Costa-Cabral and Burges, 1994; Tarboton, 1997; Gruber and Peckham, 2009]. These algorithms compute upslope contributing area (a surrogate for shallow groundwater flow) for a specific location in a catchment and also allow quantifying local lateral contributions entering streams [McGlynn and Seibert, 2003]. A shortcoming of these algorithms, however, is that they cannot preserve the information about the side from which local contributions enter a stream. Lateral contributions calculated in this way, thus, represent the total lateral contributions from both sides of a stream. This is problematic because groundwater dynamics and groundwater chemistry can differ considerably between left and right sides of a channel [Burns *et al.*, 1998].

Distinguishing between lateral contributions from opposing sides is also important for assessment of riparian zone function and its influence on catchment scale water chemistry. Riparian zones (RZs) are elongated strips of land directly adjacent to both sides of a stream network. Located at the land-water interface, RZs can be biogeochemical and ecological hotspots [Gregory *et al.*, 1991; McClain *et al.*, 2003] with

often distinct soils [Hill, 1996] and vegetation [Jansson *et al.*, 2007]. Their location coupled with their characteristic hydro-chemical signature [Bishop *et al.*, 1990; Hill, 1990; Cirimo and McDonnell, 1997] can give RZs significant potential to “buffer” hillslope groundwater inflows both hydrologically [McGlynn and McDonnell, 2003; Jencso *et al.*, 2010] and biogeochemically [Cirimo and McDonnell, 1997; Hooper *et al.*, 1998].

McGlynn and Seibert [2003] outlined an approach for mapping hydrologic connectivity and riparian buffering based upon terrain indices derived from a DEM in the Maimai catchment, New Zealand. In their approach, potential hydrologic connectivity among hillslopes and riparian zones is characterized by lateral contributing area. Riparian buffering potential along a stream reach is defined as the ratio between riparian and hillslope areas. A limitation of this study is that upslope and riparian areas from both sides were lumped together despite potentially large differences in riparian function and upslope controls on either side along the stream network [Vidon and Hill, 2005; Vidon and Smith, 2007].

Here we outline a novel method (SIDE; Stream Index Division Equations) that determines the orientation of flow lines (FLs) relative to the streamflow direction to distinguish between stream left and right sides. As an illustrative example we combine this method with a standard flow accumulation algorithm [Seibert and McGlynn, 2007] to compute side-separated lateral contributing area per unit stream length ( $a_c$ ) and riparian buffering ratios  $R/H$ , i.e. the local ratio of riparian area to total hillslope area [McGlynn and Seibert, 2003], for the Tenderfoot Creek Experimental Forest, Montana, USA. The utility of the new algorithm is also assessed by comparing  $a_c$  values with hillslope –

riparian – stream water table connectivity dynamics on either side of the stream network at 24 transects of groundwater recording wells [Jencso *et al.*, 2009].

## 2. New algorithm

### 2.1 *Stream side determination*

All flow routing algorithms estimate (often implicitly) flow fields for computing the downslope accumulation of area or other landscape attributes. The new SIDE method determines the orientation of flow fields relative to a stream network. This is achieved by a stepwise comparison of flow lines (FLs), i.e. the vectors of the flow field directed to streams, with streamflow directions. Performing these steps requires a DEM and a streamflow direction map (SDM) which consists of a network of connected stream vectors. Regularly gridded data is used in this study although the same methodology is applicable to other data structures. Stream directions in a gridded SDM are represented by grid cells with integer values that correspond to different flow directions (Figure 1).

The SIDE algorithm attributes FLs to each side of a stream channel based on geometric calculations. Once the orientations of all FLs are determined, other upslope landscape attributes that are linked to the stream network via FLs can be accordingly assigned to left or right stream sides.

The first step for calculating FL orientations is to determine the corresponding FL and streamflow directions  $\vec{f}_k$  and  $\vec{s}_{k,0}$  for every grid cell of the DEM that drains into one or several downslope SDM grid cells. Additionally, all stream vectors  $\vec{s}_{k,i}$  of the upstream SDM grid cells that are directly connected to  $\vec{s}_{k,0}$  are located. The second step

is to determine the orientation of the FLs relative to the streamflow direction (Figure 2).

For this the cross products  $\vec{c}_{k,i}$  of all pairs of each FL direction  $\vec{f}_k$  with different streamflow directions  $\vec{s}_{k,i}$  are calculated (1).

$$\vec{c}_{k,i} = \vec{f}_k \times \vec{s}_{k,i} \quad (1)$$

Since  $\vec{f}_k$  and  $\vec{s}_{k,i}$  are horizontal vectors with z-components equal to zero, the resulting cross products  $\vec{c}_i$  are perpendicular to the map plane and only their z-components  $Z_{k,i}$  (2) are different from zero, except when  $\vec{f}_k$  and  $\vec{s}_{k,i}$  are parallel.

$$Z_{k,i} = \vec{e}_z \cdot \vec{c}_{k,i} \quad (2)$$

The sign of  $Z_{k,i}$  indicates the orientation of corresponding FL relative to the streamflow direction. If left and right are defined in direction of the stream vector  $\vec{s}_0$ , i.e. looking in downstream direction of the stream, then a negative  $Z_{k,i}$  indicates that the corresponding FL is oriented right relative to the streamflow. Similarly, a positive  $Z_{k,i}$  value indicates that the corresponding FL is oriented left. If all  $Z_{k,i}$  values of all cross products have the same sign then the orientation of the FL can be directly inferred from the common sign of the  $Z_{k,i}$  values.

Occasionally FL orientations (and the corresponding stream sides) cannot be resolved directly and additional steps must be taken. These special cases occur at locations where the z-components of the cross products have opposite signs, are equal to zero or where the FLs point to channel heads.

The first exception occurs when two stream directions  $\vec{s}_{k,0}$ , and  $\vec{s}_{k,i}$  form a sharp bend with an inner angle equal to or less than  $90^\circ$  (Figure 2). In this case the z-components of  $\vec{c}_{k,0}$  and  $\vec{c}_{k,i}$  have opposite signs or one z-component equals zero. If the FL was located on the inner side of the sharp bend then both z-components would necessarily have the same sign and the orientation of the FL relative to the stream could be calculated as described previously. However, in this case the FL is located on the outer side of the bend and the z-components of  $\vec{c}_{k,0}$  and  $\vec{c}_{k,i}$  have different signs. The solution to this problem is to find the position of  $\vec{s}_{k,i}$  relative to  $\vec{s}_{k,0}$  by calculating the cross product  $\vec{c}_{k,0,i}$  of the two stream vectors (3).

$$\vec{c}_{k,0,i} = \vec{s}_{k,i} \times \vec{s}_{k,0} \quad (3)$$

If the z-component of  $\vec{c}_{k,0,i}$  is negative then  $\vec{s}_{k,i}$  lies on the right side relative to  $\vec{s}_{k,0}$ . The inner side of the sharp bend is therefore oriented right relative to  $\vec{s}_{k,0}$ . However, the FL is located on the outer side of the sharp bend. Hence, the FL has to be oriented left to the stream while the opposite is true in case of a positive z-component of  $\vec{c}_{k,0,i}$ . More generally, the side of the RZ is indicated by the sign of  $Z_{k,i}$ , which is calculated by multiplying the z-components of  $\vec{c}_{k,0,i}$  by minus one (4).

$$Z_{k,i} = -\vec{e}_z \cdot \vec{c}_{k,0,i} \quad (4)$$

Stream junctions represent another special case because the assessment of FL orientations requires comparing two or more upstream streamflow directions with the streamflow direction directly downstream of the junction. For computations, the junctions

are first subdivided into a number of stream bends and treated individually. The subdivided stream bends correspond to all possible combinations of the downstream stream vector  $\vec{s}_{k,0}$  with one of the upstream stream vectors  $\vec{s}_{k,i}$ . The side of each FL pointing towards the junction can then be determined relative to each bend, i.e. relative to every combination of  $\vec{s}_{k,0}$  and  $\vec{s}_{k,i}$ , in the same way as described previously. In the end, the FL orientation (as well as the side of the corresponding RZ) relative to the stream junction corresponds to its orientation relative to all individual stream bends. If the FL is oriented left relative to certain streamflow directions and, simultaneously, right relative to others then the FL is actually located in the middle of two confluences joining at a stream junction.

Channel heads are a third special case because they represent singularities where the orientation of FLs is undetermined (NA in Fig. 3). As a practical solution to avoid missing values FLs pointing to channel heads are treated as if they were pointing exactly to the middle of two confluences and are attributed to both stream sides.

## ***2.2 Calculation of lateral contributing areas***

After the relative orientation of all FLs is determined for all cases (Figure 3), the values of upslope contributing areas  $A_c$  [m<sup>2</sup>] calculated from the flow accumulation algorithm are assigned to the respective sides. Note that  $A_c$ , as we use it in this paper only refers to the local contribution of area to a stream segment and does not include any area entering from upstream stream segments. Length-specific values of contributing area  $a_c$  [m<sup>2</sup>/m] were calculated by dividing  $A_c$ -values by the local stream segment lengths  $\Delta l$  [m] (grid size in cardinal or diagonal direction). The result is two maps representing the

specific contributing areas entering the stream from left,  $a_{c,L}$ , and right,  $a_{c,R}$  (Figure 4). In most cases the assignment of the entering area to one of the sides is straight-forward (cases ‘left’ and ‘right’, Figure 3). In special cases where a FL points to a channel head or is located between two confluents to a junction (Figure 3, ‘MIDDLE’ case) the area is apportioned equally between the two sides. While it may be argued that the first grid cells of a stream, i.e., the channel heads, do not have a left or right side, counting half of the area to  $a_{c,L}$  respectively  $a_{c,R}$ , is a pragmatic solution to avoid missing values. The total local contributing area entering the stream at a certain location,  $a_c$  [ $\text{m}^2/\text{m}$ ] can easily be calculated as the sum of the contributions from the two sides (5).

$$a_c = a_{c,L} + a_{c,R} \quad (5)$$

The new algorithm has been implemented in the open source software SAGA GIS [Conrad, 2007; Böhner *et al.*, 2008]. Computationally the algorithm is similarly demanding as applying a flow routing algorithm only to the grid cells that are directly adjacent to the stream network. Since number of such riparian grid cells is usually small compared to the total amount of grid cells in a DEM, the additional computational load is small as well. For instance, applying the SIDE method in combination with the  $\text{MD}_\infty$  algorithm [Seibert and McGlynn, 2007] to a 570 x 832 sized DEM (with  $2.3 \cdot 10^6$  non-missing values) and the corresponding SDM (with  $1.5 \cdot 10^3$  non-missing values) took less than 2 seconds on a notebook with 2Gb virtual memory and 2.2Ghz Intel Pentium™ 2 Xeon processor.

### 3. Case study

To demonstrate the new algorithm and the value of separating the stream into its left and right sides, data from the Tenderfoot Creek Experimental Forest (TCEF) was used as example. TCEF is located in the Little Belt Mountains of the Lewis and Clark National Forest in Central Montana, USA. The research area consists of seven gauged catchments that form the headwaters of Tenderfoot Creek (22.8 km<sup>2</sup>), which drains into Smith River, a tributary of the Missouri River. Catchment headwater zones are typified by moderately sloping (avg. slope ~ 8°) extensive (up to 1200m long) hillslopes and variable width riparian zones. Approaching the main stem of Tenderfoot Creek the streams become more incised, hillslopes become shorter (< 500m) and steeper (average slope ~20°), and riparian areas narrow compared to the catchment headwaters. Stream sides and side-separated indices were calculated from a 10m DEM (Figure 5) using the new SIDE algorithm and the MD<sup>∞</sup> flow accumulation method [Seibert and McGlynn, 2007] to compute upslope area. The stream network and the stream direction map were derived from the DEM by applying the “Channel Network” module (Table 2) in SAGA GIS [Conrad, 2007; Böhner et al., 2008] using the DEM and a map of upslope area. A threshold area of 40 ha defined stream initiation. The derived channel heads and the stream network were further corroborated with results from field reconnaissance [Jencso et al., 2009].

To analyze the effect of the side-separated calculations, the specific lateral contributing areas, which were computed using the new algorithm, were compared by visual assessment of  $a_{c,R}$  and  $a_{c,L}$  maps and by plotting  $a_{c,R}$  against  $a_{c,L}$ . Furthermore, riparian buffer ratios [McGlynn and Seibert, 2003] with their associated catchment-wide

area-weighted distribution functions were computed to exemplify the use of the SIDE method to derive composite terrain indices. The  $R/H$  index was chosen over other composite terrain indices, such as the topographic wetness index [Beven and Kirkby, 1979], because all components ( $R$  and  $H$ ) are calculated based on flow fields and don't involve any local components (like e.g. local slope). The riparian buffer ratio  $R/H$  was here defined as the ratio between area of the lateral contributing riparian area,  $R$ , and the entire lateral contribution,  $H$ . The TCEF lateral riparian areas were mapped based on the field relationship described in Jencso et al. [2009]. Landscape analysis derived riparian area was delineated as all area less than two meters in elevation above the stream network. To compare the landscape analysis derived riparian widths to actual riparian widths at TCEF, Jencso et al. [2009] surveyed 90 riparian cross sections in Stringer Creek, Spring Park Creek, and Tenderfoot Creek. A regression relationship ( $r^2 = 0.97$ ) corroborated their terrain based riparian extent mapping [Jencso et al., 2009]. The total and side-separated lateral contributions,  $H$ , used in the  $R/H$  ratio correspond to the previously computed  $a_{c,L}$ ,  $a_{c,R}$  and  $a_c$  ( $a_c = a_{c,L} + a_{c,R}$ ) values. Total and side-separated riparian lateral contributions,  $R$ , were calculated by applying the SIDE method and the MD $\infty$  flow accumulation algorithm [Seibert and McGlynn, 2007] on the DEM excluding the parts outside the mapped riparian area.

Finally we report on results of hillslope connectivity measured using shallow groundwater recording in 24 transects and show how side-separated  $a_c$  values improved the correlations between this terrain index and water table connectivity across these 24 transects. Hydrologic connectivity between hillslope-riparian-stream zones (HRS) was inferred from the presence of saturation measured in well transects spanning the hillslope,

toeslope, and riparian positions. A HRS hydrologic connection was defined as a time interval during which stream flow occurred and both the riparian and adjacent hillslope well recorded water levels above bedrock. More detailed information about the experimental design and hydrological connectivity can be found in Jencso et al. [2009].

## 4. Results

Side-separated lateral contributions to the stream network were calculated for TCEF using the SIDE method (Figure 5). The contributions from the two sides generally varied considerably. Plotting  $a_{c,L}$  against  $a_{c,R}$  clearly demonstrated that contributions from two sides at different locations along the stream network were differed considerably (Figure 6) apart from the channel heads (Figure 6, label “1”). This also implies that total local contributing area  $a_c$  cannot be a proxy for side-separated local contributing areas. There are few patterns in the correlation plot which might need further explanation. The apparently well-correlated points in the upper right part of the figure (Figure 6, label “1”) correspond to channel heads. For these cells there is a perfect, but trivial, correlation because the total contributing area for these grid cells was partitioned equally according to the special case where FLs point to channel heads. The linear patterns (Figure 6, label “2”) are caused by stream cells receiving the minimal contributing area (a half cell) normalized by the stream length in either cardinal or diagonal direction. Such stream cells are typically found in locations where divergent slopes are adjacent to the stream. Here the lateral contribution can consist of just the stream cell itself, which means that only half of the  $100\text{m}^2$  grid cell is contributing from one side (streams are assumed to be in the center of the delineated stream cells).

In addition to lateral contributing areas, composite flow-related terrain indices that are calculated along streams are also potentially sensitive to the separation of lateral contributions. This was tested by the  $R/H$  index computed for TCEF. We calculated area-weighted distribution functions of the  $R/H$  index to compare our new method to the standard method. The results differed considerably for those values calculated from side-separated  $a_c$  values and those calculated from total  $a_c$  values (Figure 7a). Generally, the  $R/H$  indices calculated from total  $a_c$  values were larger than those obtained from side-separated  $a_{c,R}$  and  $a_{c,L}$  values. For instance, the  $R/H$  distribution derived from the side-separation algorithm indicates that 50% the catchment area enters the stream network along segments where the  $R/H$  index is less than 0.014. In contrast the  $R/H$  distribution derived from total  $a_c$  values overestimates this quantity by a factor of approximately 1.3, which is indicated by the ratios of the two distributions (Figure 7b). Overall, using total  $a_c$  values, the area-weighted  $R/H$  distribution can be up to 1.8 times or 80% higher than predicted when using side-separated  $a_c$  values (Figure 7b).

We further assessed the utility of the SIDE method for predicting local hydrologic observations from the Stringer catchment, a subcatchment of TCEF. When comparing  $a_c$  values to the time percentage for HRS water table connectivity the degree of correlation largely depended on whether total or side-separated  $a_c$  values were used (Figure 8). A poor relationship ( $r^2 = 0.42$ ) was observed when comparing total  $a_c$  for each transect cross-section against HRS water table connectivity (Figure 8a). When replacing total  $a_c$  with side-separated  $a_c$  values the correlation between specific lateral contributing area and HRS water table connectivity improved considerably ( $r^2 = 0.91$ , Figure 8b).

As an example more detailed results are presented for transect 5. The total  $A_c$  for the stream cell at this transect is about 48,000m<sup>2</sup> which corresponds to a total specific  $a_c$  of 4800m. However, the two stream sides contribute a disproportionate amount of area to the total value. The western (right) side is located at the base of a convergent hillslope (Figure 9). It has the largest side-separated  $a_c$  ( $a_{c,R} \cong 4600$  m) of all 24 TCEF transects under observation, a wide riparian zone (16.5 m) and  $\sim 20.5^\circ$  hillslopes. The eastern (left) side of transect 5 is located along a moderate ( $\sim 26^\circ$ ), divergent hillslope ( $a_{c,L} \cong 200$  m) with a 7.7 m wide riparian zone (Figure 9). On the western (right) side of transect 5 HRS water table connectivity was observed for the entire water year while on the eastern (left) side water table connectivity was transient during the same period and only occurred on 11 days with the largest snowmelt and rain events.

## 5. Discussion

In general, left and right lateral hillslope contributions at various stream locations differed substantially (Figure 6). This is plausible as values of  $a_{c,R}$  would only be strongly related to values of  $a_{c,L}$  in catchments with either highly symmetric or highly asymmetric local lateral inflows along the entire stream network. Such catchment structures are the exception and would be very unusual. Using total  $a_c$  instead of side-separated values can therefore give misleading results. We suggest that traditional GIS algorithms that are only capable of deriving total  $a_c$  are not appropriate for estimating variations in lateral contributions to the stream or for characterizing riparian zones.

The distribution of R/H indices varied systematically depending on whether total or side-separated  $A_c$  values were used. Using total  $A_c$  values caused substantial

overestimation and could lead to misconceptions when attempting to characterize riparian zone and their distributions and buffering potential. The previously described distinct patterns associated with channel heads and minimal contributing areas (clusters in Figure 6) are related to the resolution in the DEM cell size and the flow accumulation algorithm used. The same artifacts also emerge as distinct clusters in plots of area-weighted  $R/H$  distributions. Channel heads emerge as clusters when plotting the distributions (Figure 7a, label “1”) and when plotting the ratios of the distributions (Figure 7b, label “1”). TCEF channel heads are located in steep terrain with narrow riparian zones of only a few  $m^2$ . Since stream channels are initiated at high values of  $A_c$  while riparian zones are narrow and thus the corresponding  $R/H$  ratios are close to 0. Moreover,  $R/H$  values calculated using the side-separating algorithm are equal to those of the standard algorithm because the side-separating algorithm divides riparian and hillslope  $a_c$  values equally between left and right at channel heads.

Apart from artifacts, the ratios of the two distributions  $(R/H)_{sep} / (R/H)_{tot}$  also reveal that the distributions are skewed towards the higher values of  $R/H$ . At this end of the  $R/H$  spectrum the side-separating algorithm predicts higher  $R/H$  values than the standard algorithm. Many of the high  $R/H$  ratios are in fact related to riparian zones connected to little or no upslope parts of the catchment and emerge as clusters (Figure 7, label “2”). Using the standard algorithm, low hillslope  $a_c$  values from one side often are compensated by higher hillslope  $a_c$  values from the other side and, thus, high  $R/H$  ratios occur much less often. The lumping of hillslope and riparian  $a_c$  values affects the entire distribution of  $R/H$  values and leads to inaccurate characterization. The comparatively higher  $R/H$  values predicted by the side-separating algorithm are hence more realistic. We

further suppose, without having tested it in detail yet, that applying the SIDE method to derive other composite flow-related terrain indices along streams (e.g., the topographic wetness index [Kirkby, 1975]) would lead to similarly profound consequences compared to using a standard algorithm.

Lateral contributions of hillslope and riparian area on the opposite sides of the stream also varied considerably for all 24 transects with detailed groundwater observations. A closer look on individual transects such as transect 5 (Figure 9) indicates that differential convergence and divergence of catchment topography and hillslope lengths are among the most likely causes for the observed differences. These differences were also directly reflected by HRS water table dynamics. For all 24 transects, total  $a_c$  calculated with standard methods was not a suitable proxy for both streams sites and only weakly related to HRS water table connectivity whereas the opposite was found when using side-separated  $a_c$  values. The practical application of our SIDE algorithm hence enabled [Jencso *et al.*, 2009] to estimate the amount of the stream network connected to its uplands through time and to upscale these predictions to the entire catchment.

The proposed SIDE method is compatible with any existing flow accumulation algorithm and can, in its current implementation, be already combined with the D8 [O'Callaghan and Mark, 1984], MD8 [Quinn *et al.*, 1991],  $D^\infty$  [Tarboton, 1997] and  $MD^\infty$  [Seibert and McGlynn, 2007] algorithms. Flow accumulation algorithms not only allow computing the size of upslope contributing areas but can also be used for computing average values of upslope landscape attributes. For instance, the SIDE method would allow calculating the average forest coverage of upslope land portions for each stream cell on both stream sides. More generally, all calculations that fall into the broad

category of flow algebra [Tarboton and Baker, 2008] can be combined with the proposed SIDE method to provide more meaningful indices for stream segments and riparian zones.

The SIDE algorithm can be applied to streams in any type of environment and is only limited by the accuracy of the stream network position and by the chosen flow accumulation algorithm. In particular, topographically-derived flow fields can differ from actual flow fields as a result of heterogeneous soils, bedrock topography or temporally-varying flow directions [Hinton *et al.*, 1993; Devito *et al.*, 1996; Freer *et al.*, 2002]. There is, however, a potential to overcome at least some these limitations by the use of distributed hydrological models to derive flow fields. Such an approach has been demonstrated by Grabs *et al.* [2009], who used a distributed hydrological model to simulate flow fields in flat areas based on hydraulic gradients rather than on terrain slope..

## **6. Concluding Remarks**

We outline a new algorithm that is widely applicable and useful for interpreting, routing and assessing a wide variety of terrain analysis indices related to stream networks and hydrology. These include, but are not limited to, hillslope accumulated area contributing to streams, riparian buffering, wetness indices, lateral stream inflows of water and associated constituents, and any indices where orientation relative to the stream network is important. The new algorithm has been implemented as a module for the open source software SAGA GIS [Conrad, 2007; Böhner *et al.*, 2008] and can easily be used by others. The source code of the SIDE algorithm is included as supplementary material,

while a compiled SAGA-module along with usage instructions can be found at the main author's website (<http://thomasgrabs.com/side-algorithm>).

The new SIDE algorithm addresses an important shortcoming of standard hydrological landscape analysis where the possibility of calculating side-separated lateral contributions to the streams so far has been lacking. The side-separated calculations are crucial for a meaningful characterization of the riparian zone through terrain indices and provide a basis for an efficient up-scaling of riparian-controlled processes to the landscape scale.

## Acknowledgements

This project was partly funded by the Swedish Research Council (VR, grant no. 2005-4289).

## References

- Beven, K., and M. Kirkby (1979), A Physically Based, Variable Contributing Area Model of Basin Hydrology, *Hydrological Sciences Bulletin*, 24(1).
- Bishop, K. H., H. Grip, and A. O'Neill (1990), The origins of acid runoff in a hillslope during storm events, *Journal of Hydrology*, 116(1-4), 35-61.
- Böhner, J., T. Blaschke, and L. Montanarella (Eds.) (2008), *SAGA: System for an automated geographical analysis*, Institute of Geography, University of Hamburg, Hamburg.
- Burns, D. A., R. P. Hooper, J. J. McDonnell, J. E. Freer, C. Kendall, and K. Beven (1998), Base cation concentrations in subsurface flow from a forested hillslope: The role of flushing frequency, *Water Resources Research*, 34(12), 3535-3544.
- Cirno, C. P., and J. J. McDonnell (1997), Linking the hydrologic and biogeochemical controls of nitrogen transport in near-stream zones of temperate-forested catchments: a review, *Journal of Hydrology*, 199(1-2), 88-120.

- Conrad, O. (2007), SAGA - Entwurf, Funktionsumfang und Anwendung eines Systems für Automatisierte Geowissenschaftliche Analysen, Electronic doctoral dissertation thesis, 221 pp, University of Göttingen, Göttingen.
- Costa-Cabral, M. C., and S. J. Burges (1994), Digital elevation model networks (DEMON): A model of flow over hillslopes for computation of contributing and dispersal areas, *Water Resources Research*, 30(6), 1681-1692.
- Devito, K. J., A. R. Hill, and N. Roulet (1996), Groundwater-surface water interactions in headwater forested wetlands of the Canadian Shield, *Journal of Hydrology*, 181(1-4), 127-147.
- Freeman, T. G. (1991), Calculating catchment area with divergent flow based on a regular grid, *Computers & Geosciences*, 17(3), 413-422.
- Freer, J., J. J. McDonnell, K. J. Beven, N. E. Peters, D. A. Burns, R. P. Hooper, B. Aulenbach, and C. Kendall (2002), The role of bedrock topography on subsurface storm flow, *Water Resour. Res.*, 38(12), 1269.
- Grabs, T., J. Seibert, K. Bishop, and H. Laudon (2009), Modeling spatial patterns of saturated areas: A comparison of the topographic wetness index and a dynamic distributed model, *Journal of Hydrology*, 373(1-2), 15-23.
- Gregory, S. V., F. J. Swanson, W. A. McKee, and K. W. Cummins (1991), An Ecosystem Perspective of Riparian Zones, *BioScience*, 41(8), 540-551.
- Gruber, S., and S. Peckham (2009), Land-Surface Parameters and Objects in Hydrology, in *Geomorphometry: concepts, software, applications*, edited by T. Hengl and H. I. Reuter, pp. 293-308, Elsevier Science, Amsterdam.
- Hill, A. (1990), Ground water flow paths in relation to nitrogen chemistry in the near-stream zone, *Hydrobiologia*, 206(1), 39-52.
- Hill, A. R. (1996), Nitrate removal in stream riparian zones, *Journal of Environmental Quality*, 25(4), 743-755.
- Hinton, M. J., S. L. Schiff, and M. C. English (1993), Physical properties governing groundwater flow in a glacial till catchment, *Journal of Hydrology*, 142(1-4), 229-249.
- Hooper, R. P., B. T. Aulenbach, D. A. Burns, J. McDonnell, J. Freer, C. Kendall, and K. Beven (1998), Riparian control of stream-water chemistry: implications for hydrochemical basin models, *International Association of Hydrological Sciences, Publication*(248), 451-458.
- Jansson, R., H. Laudon, E. Johansson, and C. Augspurger (2007), The importance of groundwater discharge for plant species number in riparian zones, *Ecology*, 88(1), 131-139.

Jencso, K. G., B. L. McGlynn, M. N. Gooseff, S. M. Wondzell, K. E. Bencala, and L. A. Marshall (2009), Hydrologic connectivity between landscapes and streams: Transferring reach-and plot-scale understanding to the catchment scale, *Water Resources Research*, 45(4).

Jencso, K. G., B. L. McGlynn, M. N. Gooseff, K. E. Bencala, and S. M. Wondzell (2010), Hillslope hydrologic connectivity controls riparian groundwater turnover: Implications of catchment structure for riparian buffering and stream water sources (revised version submitted), *Water Resources Research*.

Kirkby, M. J. (1975), Hydrograph modelling strategies, in *Processes in physical and human geography: Bristol essays*, edited by R. Peel, et al., pp. 69-90, Heinemann, London, UK.

McClain, M. E., E. W. Boyer, C. L. Dent, S. E. Gergel, N. B. Grimm, P. M. Groffman, S. C. Hart, W. H. Judson, C. A. Johnston, E. Mayorga, W. H. McDowell, and G. Pinay (2003), Biogeochemical Hot Spots and Hot Moments at the Interface of Terrestrial and Aquatic Ecosystems, *Ecosystems*, 6(4), 301-312.

McGlynn, B. L., and J. J. McDonnell (2003), Quantifying the relative contributions of riparian and hillslope zones to catchment runoff, *Water Resour. Res.*, 39.

McGlynn, B. L., and J. Seibert (2003), Distributed assessment of contributing area and riparian buffering along stream networks, *Water Resources Research*, 39(4), 1082.

O'Callaghan, J. F., and D. M. Mark (1984), The extraction of drainage networks from digital elevation data, *Computer vision, graphics, and image processing*, 28(3), 323-344.

Quinn, P., K. Beven, P. Chevallier, and O. Planchon (1991), The prediction of hillslope flow paths for distributed hydrological modelling using digital terrain models, *Hydrological Processes*, 5(1), 59-79.

Seibert, J., and B. L. McGlynn (2007), A new triangular multiple flow direction algorithm for computing upslope areas from gridded digital elevation models, *Water Resources Research*, 43(4).

Tarboton, D. G. (1997), A new method for the determination of flow directions and upslope areas in grid digital elevation models, *Water Resources Research*, 33(2), 309-319.

Tarboton, D. G., and M. E. Baker (2008), Towards an Algebra for Terrain-Based Flow Analysis, in *Representing, Modeling and Visualizing the Natural Environment: Innovations in GIS*, edited by N. Mount, et al., p. 496, CRC Press, Florida, Boca Raton, Florida, USA.

Vidon, P., and A. R. Hill (2005), Denitrification and patterns of electron donors and acceptors in eight riparian zones with contrasting hydrogeology, *Biogeochemistry*, 71(2), 259-283.

Vidon, P., and A. P. Smith (2007), Upland Controls on the Hydrological Functioning of Riparian Zones in Glacial Till Valleys of the Midwest, *Journal of the American Water Resources Association*, 43(6), 1524-1539.

## Tables

**Table 1:** Overview of symbols and abbreviations.

| Symbol      | Description   | Units             |
|-------------|---|-------------------|
| $A_c$       | Lateral contributing area                           | [m <sup>2</sup> ] |
| $a_c$       | Specific lateral contributing area                  | [m]               |
| $a_{c,L}$   | Left specific lateral contributing area             | [m]               |
| $a_{c,R}$   | Right specific lateral contributing area            | [m]               |
| $\vec{c}$   | Cross product                                       | [m <sup>2</sup> ] |
| $\Delta l$  | Grid size in cardinal or diagonal direction         | [m]               |
| $\vec{e}_z$ | Unit vector in z-direction (vertical)               | [-]               |
| $i$         | Index of (upstream) tributaries to a stream segment | [-]               |
| $k$         | Index of riparian (flow line) vectors               | [-]               |
| $NA$        | Missing value                                       | [NA]              |
| $\vec{f}$   | Flow line direction (vector)                        | [m]               |
| $H$         | Hillslope area                                      | [m <sup>2</sup> ] |
| $R$         | Riparian area                                       | [m <sup>2</sup> ] |
| $R/H$       | Riparian-hillslope ratio                            | [-]               |
| $\vec{s}$   | Streamflow direction (vector)                       | [m]               |
| $Z$         | Z-component of cross-products                       | [m <sup>2</sup> ] |

| Abbreviation | Description  |
|--------------|--|
| D8           | Single flow direction algorithm                              |
| D $\infty$   | Single flow direction algorithm based on triangular facets   |
| DEM          | Digital elevation model                                      |
| FL           | Flow Line  |
| GIS          | Geographical information system                              |
| HRS          | Hillslope-riparian-stream                                    |
| MD8          | Multiple flow direction algorithm                            |
| MD $\infty$  | Multiple flow direction algorithm based on triangular facets |
| SDM          | Stream direction map   |
| SIDE         | Stream index division equations                              |
| TCEF         | Tenderfoot Creek Experimental Forest                         |

**Table 2:** List of parameters used in the SAGA GIS “Channel Network” module.

| Parameter                   | Value  |
|-----------------------------|--------|
| Minimum Segment Length      | 10     |
| Tracing: Maximum Divergence | 5      |
| Initiation Threshold        | 40'000 |

## Figures

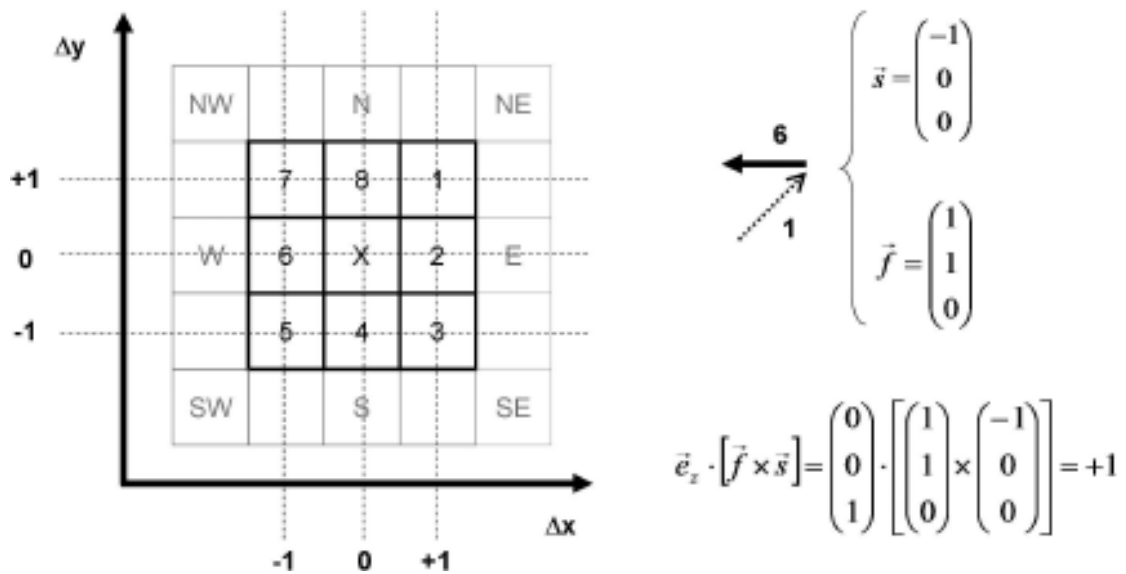


Figure 1: Directions relative to the center grid cell X are coded from 1 to 8 clockwise from northeast (NE) to north (N). The corresponding vector notation is illustrated for a flow line vector  $f$  in direction 1 (dotted arrow) and for a streamflow vector  $s$  in direction 6 (plain arrow). Calculating the cross product  $f \times s$  reveals a positive  $z$ -component and therefore the flow line vector  $f$  is located on the left relative to the stream vector  $s$ .

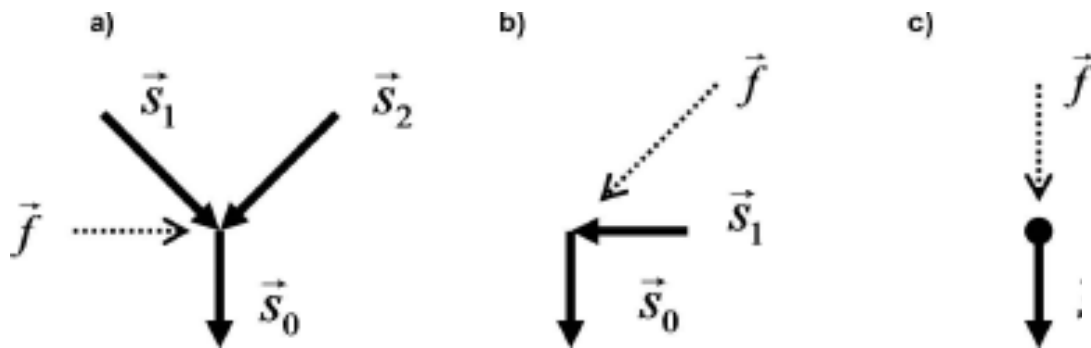


Figure 2: Different configurations of flow lines  $f$  (dotted arrows) and stream vectors  $s, i \geq 0$  (plain arrows). The left paragraph depicts a flow line vector  $f$  pointing to a stream junction. In this case, the flow line is located on the right stream side because it is on the right side relative to all stream vectors  $s_i$ . A sharp stream bend is shown in the middle graph.  $f$  is on the left side relative to  $s_0$  and on the right side relative to  $s_1$  and therefore on the outer side of the bend. Since the cross product  $s_1 \times s_2$  has a positive  $z$ -component the inner bend must be located on the left stream side and  $f$  hence on the right stream side. The graph on the right illustrates a channel head. In this case the orientation of the flow line relative to  $s_0$  is not definable.

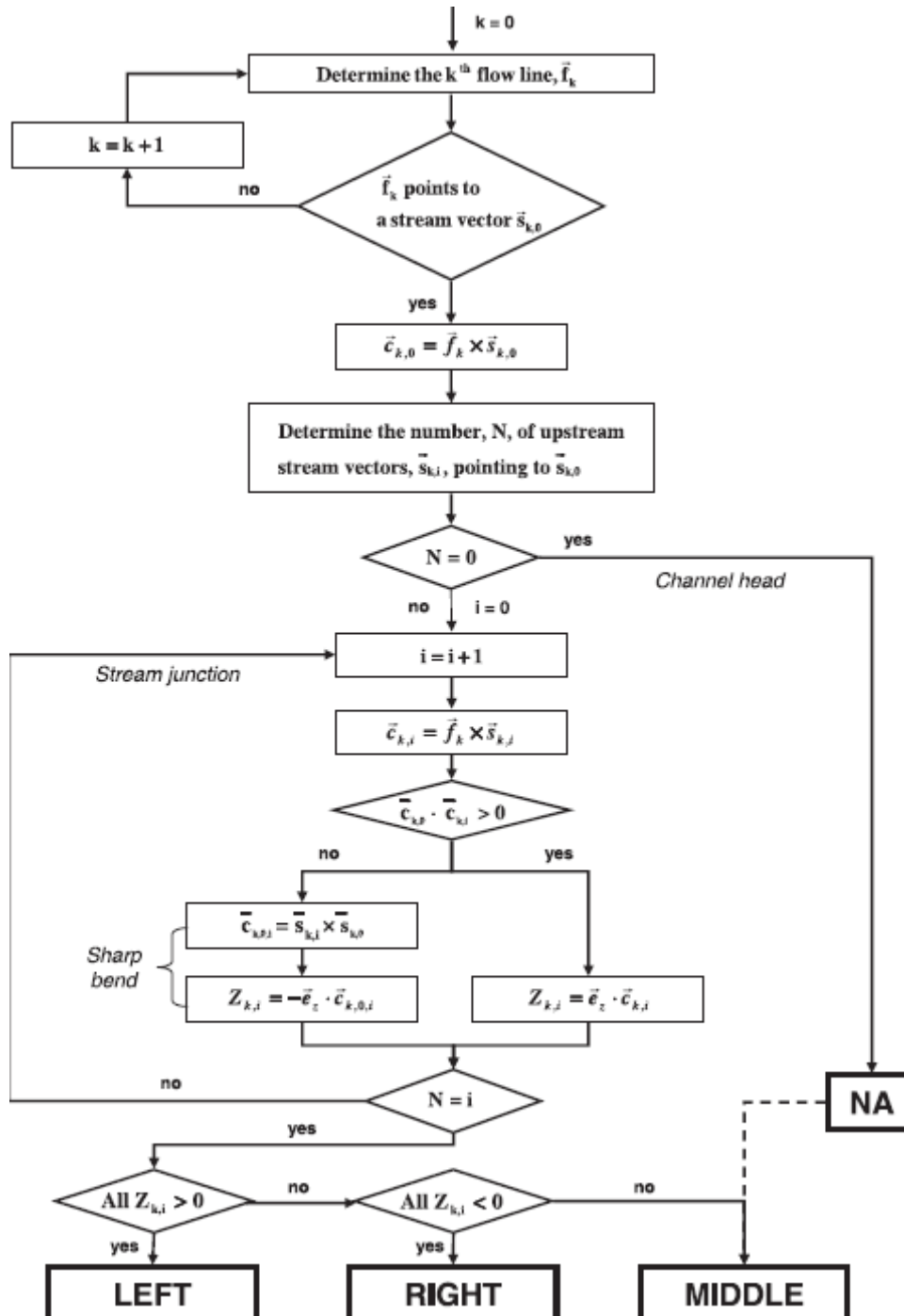


Figure 3: Flowchart illustrating the determination of a hillslope position. Symbols and abbreviations are defined in Table 1.

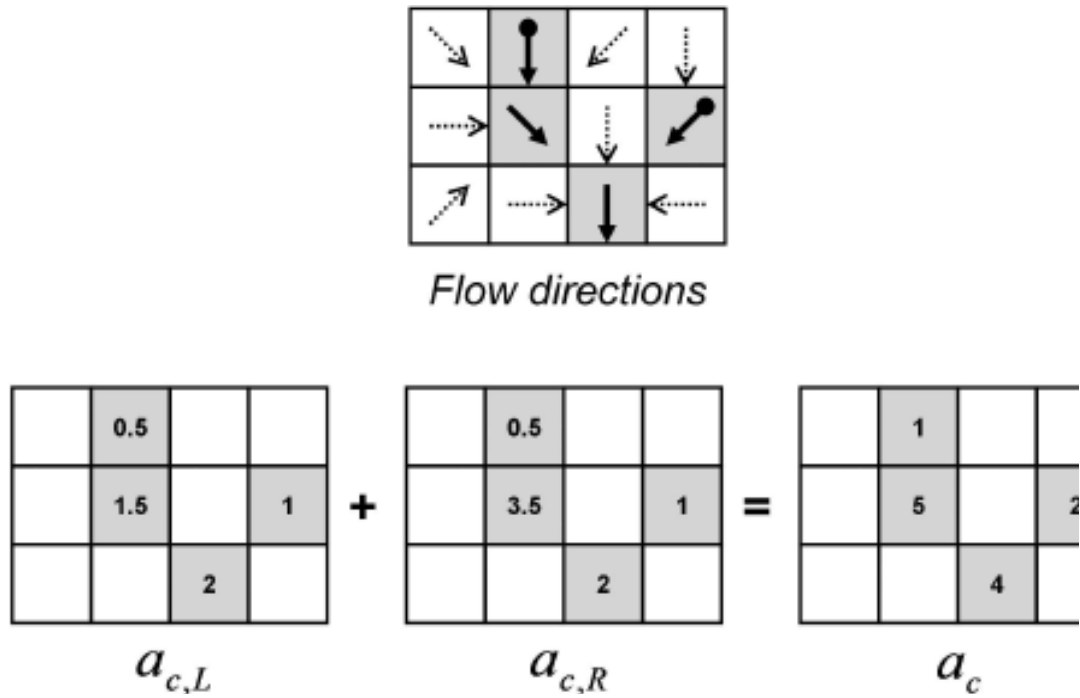


Figure 4: Illustrations of a flow direction map and maps showing values of specific lateral contributing area  $a_c$ . The flow direction map shows hillslope and stream flow directions. The three lower maps feature  $a_c$  entering the stream from left,  $a_{c,L}$  and  $a_c$  entering the stream from the right,  $a_{c,R}$  as well as the total  $a_c$ , which equals the sum of  $a_{c,L}$  and  $a_{c,R}$ . For simplicity, the  $a_c$  values presented in the illustration are equal to the number of contributing grid cells.

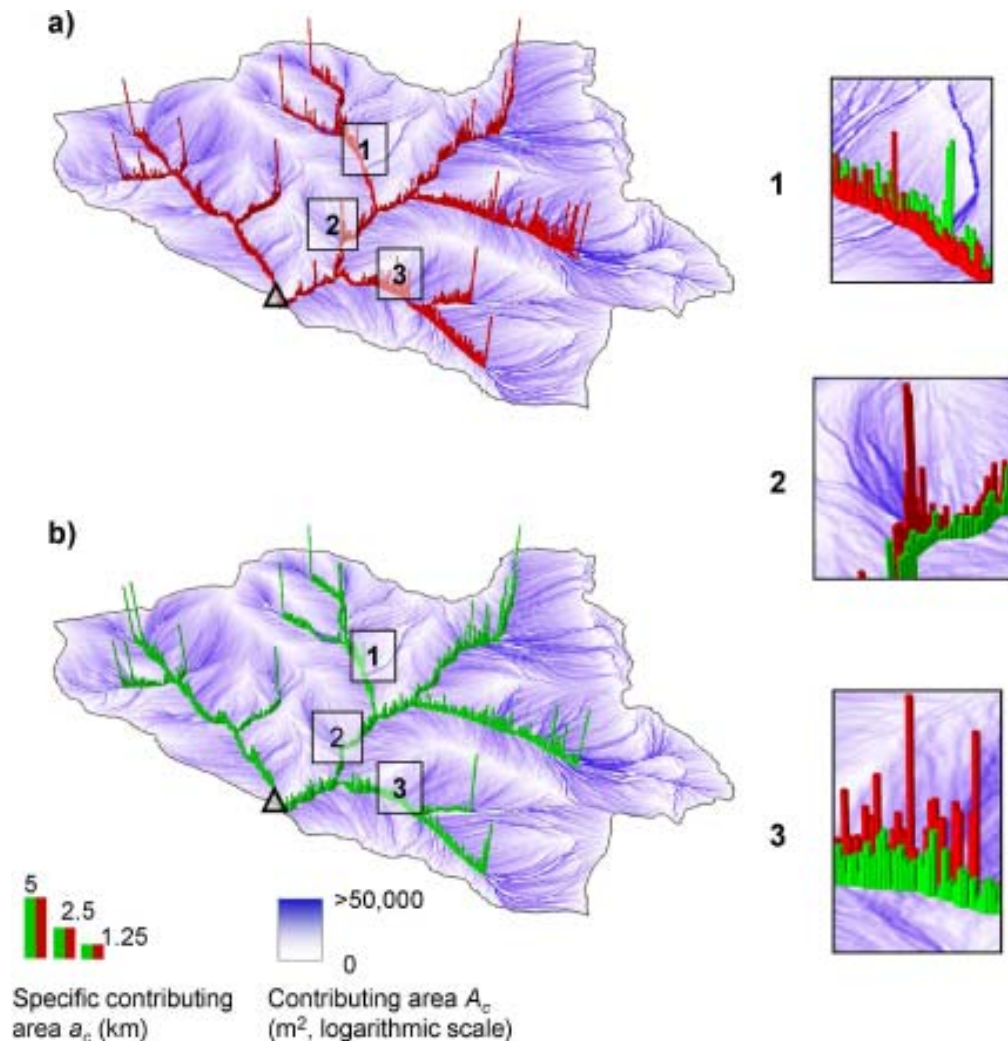


Figure 5: Spatial representation of contributing area  $A_c$  (grey-shaded flow lines) and side-separated specific contributing area values  $a_c$  (dark-grey and light-grey bars).

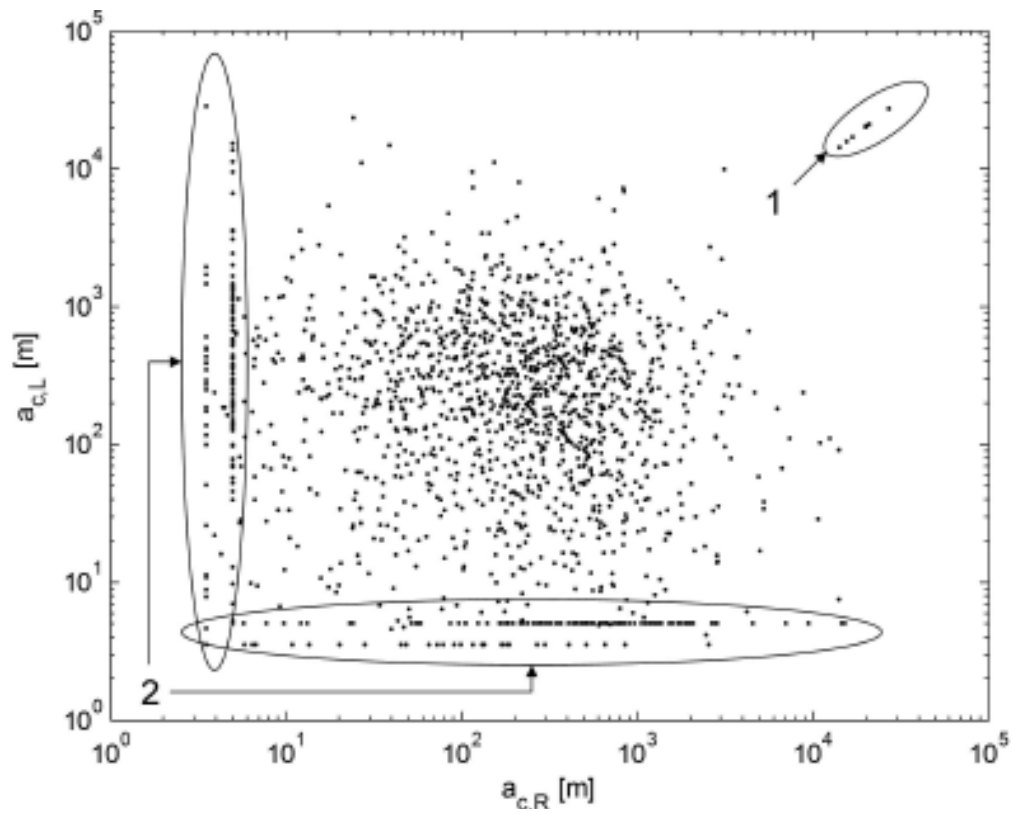


Figure 6: Scatter plot of right specific lateral contributing areas ( $a_{c,R}$ ) versus their counterpart on the left stream side ( $a_{c,L}$ ) along the stream network of the 23km<sup>2</sup> TCEF catchment. The labels 1 and 2 refer to explanations in the text.

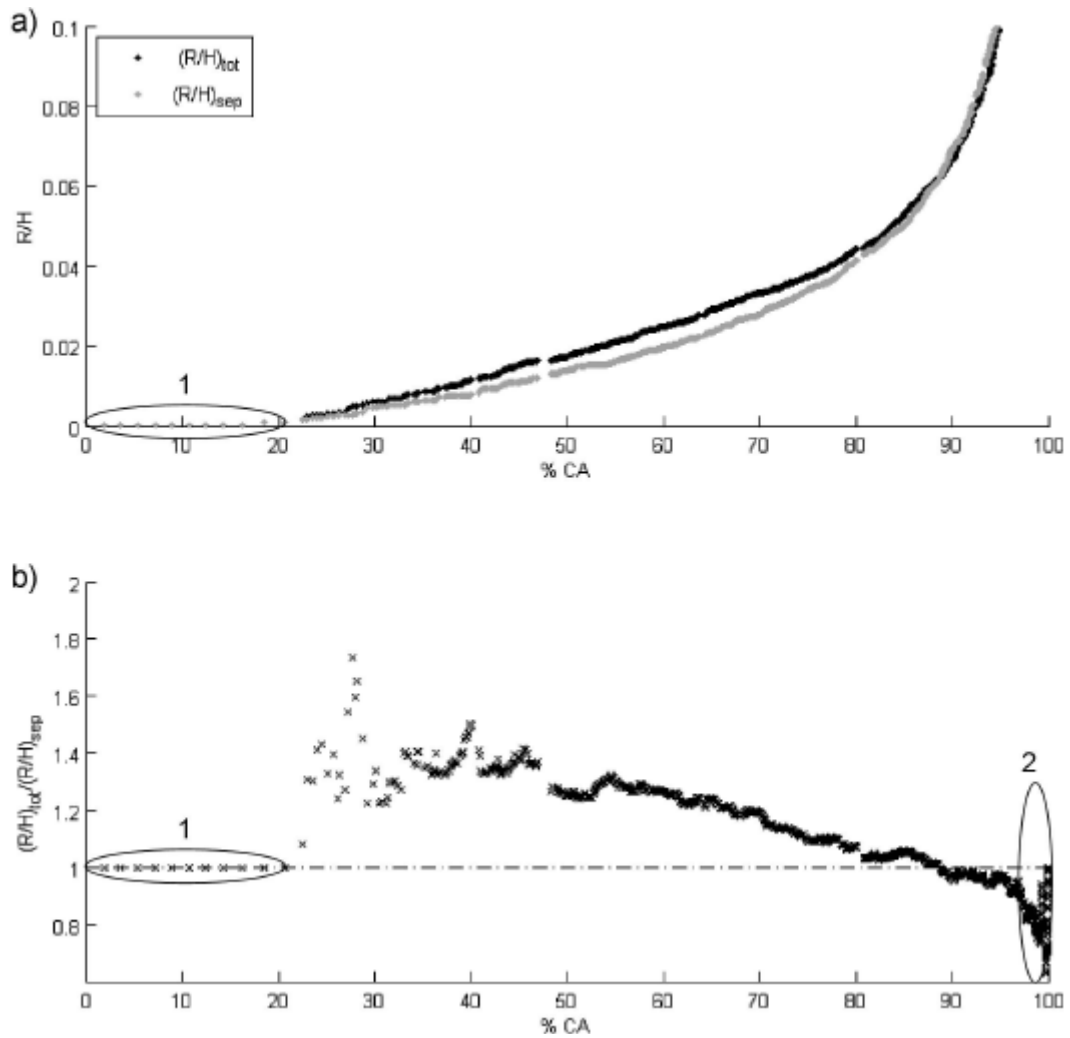


Figure 7: Comparison of riparian-hillslope ratios ( $R/H$ ) calculated based on total and side-separated values. a) Cumulative area-weighted distributions of riparian to hillslope ratios ( $R/H)_{sep}$ , and ( $R/H)_{tot}$ . b) the ratios of the above distribution functions. The labels 1 and 2 refer to explanations in the text.

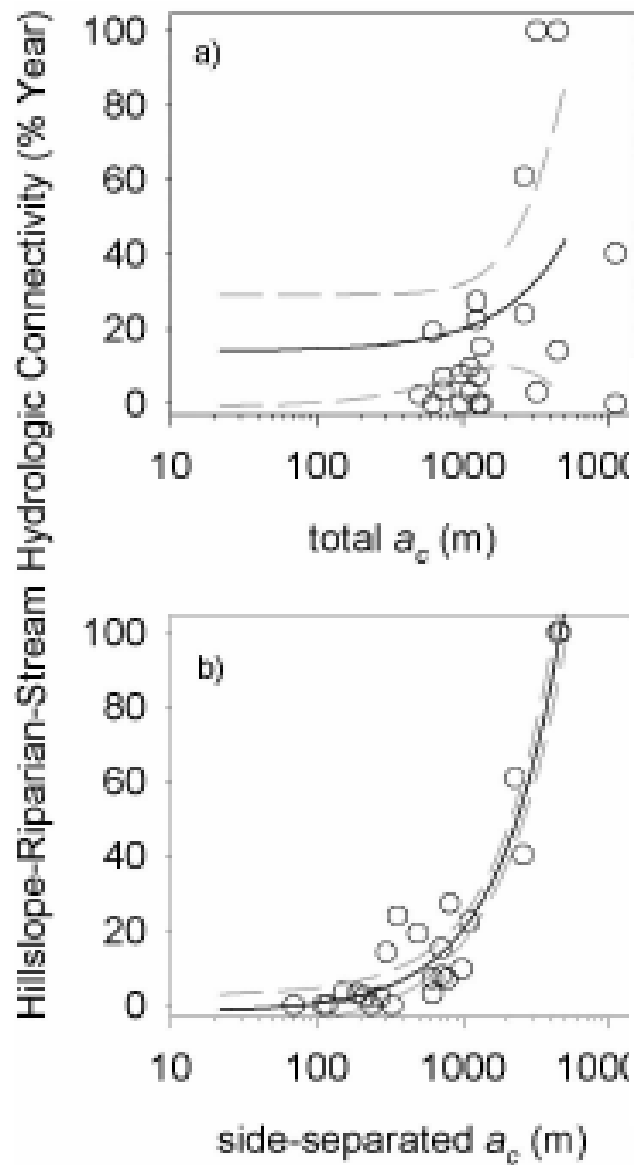


Figure 8: Hillslope  $a_c$  regressed against the percentage of the water year that a hillslope-riparian-stream water table connection existed for well transects. a) Total  $a_c$  from both sides of a transect cross section and b)  $a_c$  separated into left and right sides of the stream. A connection was defined as occasions when there was stream flow and water levels were recorded in both the riparian and hillslope wells (modified from Jencso et al. [2009]).

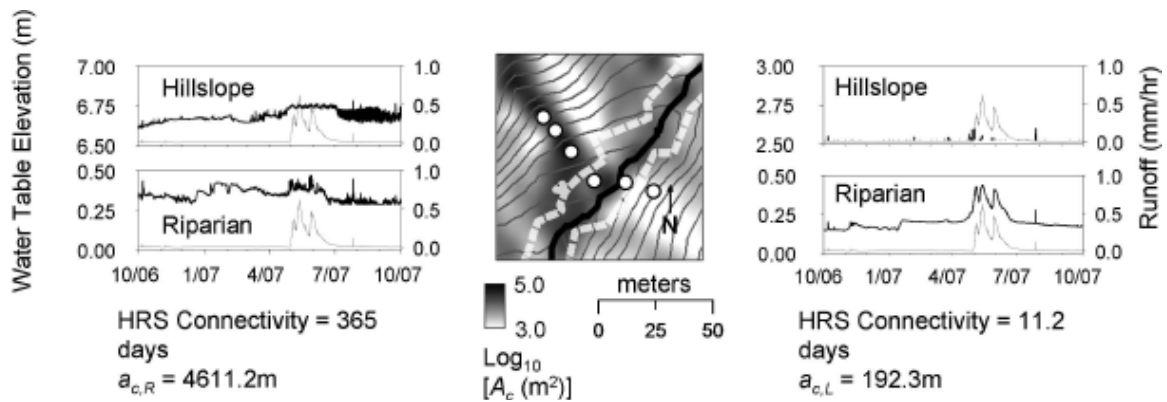


Figure 9: Stringer Transect 5 East and West hillslope and riparian water table (black lines, elevation is relative to the local datum) and runoff (grey lines) dynamics. Specific area for each side of the transect and the total time of HRS connectivity (days) during the 2007 water year is listed below each time series. The map in the middle depicts the transects contributing area  $A_c$  (dark to light shading), riparian zone extents (white dashed lines), well locations (white circles) and stream position (black line).

## DISSERTATION SUMMARY

Summary

A plethora of hydrologic investigations have been conducted to improve our understanding of the hydrologic mechanisms that can affect catchment water quantity and quality. The numbers of documented processes are numerous and can be highly heterogeneous in time and space. This has resulted in the development of detailed and complex characterizations of potential runoff generation and solute mobilization mechanisms, but minimal transferability of general principles across catchment scales or divides. In this dissertation we developed and analyzed the concept of hydrologic connectivity between landscape source areas as a “mechanism to whittle down unnecessary details and transfer dominant process understanding from the hillslope to catchment scales” [Sivapalan, 2003]. The preceding chapters synthesized landscape structure controls on catchment hydrology and solute response. A hydrologic connectivity based conceptual model and assessment framework was presented, and iteratively built upon, according to information gained through successive chapters (Figure 1). This provided a better understanding of how catchment structure influenced HRS connectivity, riparian buffering of solute/nutrient dynamics, and catchment scale runoff and solute contributions.

In chapter two I developed a metric of hillslope-riparian-stream water table connectivity as an integrative measure of runoff source area contributions through time. I tested this metric across 24 hillslope-riparian-stream landscape assemblages for an entire

year. On the basis of high frequency, long duration observations coupled within a landscape analysis framework I found that the topographically driven lateral redistribution of water (as represented by UAA) controls upland-stream connectivity and transient connectivity drives runoff generation through time. This emerging space time behavior represented the relationship between landscape structure/topology and runoff dynamics.

Landscape analysis of catchment structure provided a context for scaling source area dynamics to those observed at the catchment outlet and for exploring the spatially explicit links between source area connectivity and runoff generation. The magnitude of runoff generation at the TCEF was driven by variability in hillslope UAA size distributions and the frequency of their lateral connections along the stream network (Figure 1a). During baseflow periods, the majority of the stream network was hydrologically disconnected from the uplands except those adjacent to the largest hillslopes. As snowmelt proceeded HRS connectivity was initiated across progressively smaller hillslope UAA sizes and runoff increased with each subsequent connection. These observed relationships suggested that landscape structure (topography and topology) is a first order control on runoff response characteristics. The relationship between stream network connectivity and runoff also suggested that bi-directional prediction of runoff generation and source area dynamics may be possible through analysis of catchment structure and landscape topology.

Chapter 3 described how the intersection of hillslope hydrologic connectivity with riparian zones can alter the spatial sources of water and solutes detected in streamflow. I

tested the relationship between the duration of HRS connectivity duration and the rate and degree of riparian shallow groundwater turnover along four HRS transects and across 7 of the TCEF catchments during snowmelt. The degree of riparian water turnover (riparian buffering) was a function of hydrologic connectivity and the size of the riparian zone relative to the adjacent hillslope. Extrapolation of this relationship within a landscape analysis framework suggested that, while the sequencing of connectivity initiation across the stream network determines runoff magnitude through time (chapter 2), it is the intersection of connectivity dynamics with riparian area extents that controls riparian buffering and the source waters measured at the catchment outlet (figure 1b). Independently determined source water separations corroborated landscape analysis estimates of each stream networks turnover dynamics. Catchments with a higher frequency of large riparian buffering values exhibited slower turnover and therefore greater riparian runoff contributions (and vice versa). Each catchments riparian buffering potential decreased through time according to antecedent wetness conditions and connectivity frequency and duration to riparian zones within the stream network. This dynamic is the flushing or turnover of riparian zone water. Additionally, analysis of landscape scale riparian water turnover dynamics suggested that climate variability (wet vs. dry years) could introduce a quantifiable shift in stream network connectivity and the differential mobilization of water and solutes from riparian-hillslope assemblages.

Chapter 4 built upon the information presented in chapters 2 and 3 by examining the implications of landscape structure and HRS connectivity for DOC export. Stream DOC dynamics during snowmelt have been the focus of much research, and numerous

DOC mobilization and delivery mechanisms have been proposed. However, landscape structure controls on DOC export from riparian and hillslope landscape source areas had previously been unclear. Comparison of connectivity and DOC dynamics at three transects with large differences in landscape setting and HRS connectivity demonstrated the range of riparian and upland DOC export that can occur according to differences in landscape structure and organization. The mobilization and delivery mechanisms of DOC to the stream were dependent upon the degree of hydrologic connectivity across the hillslope-riparian-stream continuum, and the distribution and size of DOC source areas. DOC export from 7 catchments ranged from 6.3 to 12.4 kg ha<sup>-1</sup> with the greatest DOC export occurred from catchments with both high hydrologic connectivity (large UAA) and large DOC source areas. Further, the relative extent of DOC rich riparian and wetland zones strongly influenced catchment DOC export. Those catchments with larger proportions of riparian to upland area had the highest cumulative DOC export. The research presented in this chapter suggests that the intersection of hydrologic connectivity and DOC source areas drives catchment scale DOC export. Put another way, greatest export of DOC occurred where mobilization met accumulation.

Chapter 5 provided insight into the complex ways in which catchment characteristics such as topography, vegetation, and geology affect hydrological connectivity, water redistribution-storage, and resultant runoff dynamics. This chapter extended the findings of chapter 2 by comparing stream network connectivity and runoff dynamics across 11 adjacent, but structurally diverse catchments in the TCEF. Again, the magnitude of runoff observed at the catchment outlet was strongly related to the timing

and frequency of stream network connectivity. This further supported the premise that runoff generation was driven by the transient connections that occur across different UAA sizes. However, the slope of the relationship between stream network connectivity and runoff magnitude suggested the importance of factors that can reduce or slow the lateral redistribution of water through connected landscape positions leading to differences in water yield per unit connectivity (Figure 1a). These included distributions of the ratio of flow path lengths and gradients, catchment vegetation, and the intersection of more permeable geologic layers with wetter landscape positions. The relative influence of these predictors changed through time according to wetness states. Upslope accumulated area mediated HRS hydrologic connectivity was the dominate control of runoff dynamics. Following upslope accumulated area, topography mediated distributions of flowpath length and gradient ratios were most influential for water redistribution and connectivity dynamics during wetter catchment periods. Vegetation and geology become more influential during drier baseflow periods. These relationships highlighted the intersection of topographically controlled shallow flow systems with vegetative and geologic controls, providing a more comprehensive picture of the hierarchical controls on runoff generation across space and time in catchments of differing structure.

Chapter 6 described and tested a new terrain analysis algorithm (SIDE). This algorithm addressed an important shortcoming of standard landscape analysis techniques which do not distinguish between areal contributions from separate sides of the stream network. The side separated calculations were crucial for accurate characterization of

hydrologic connectivity and potential riparian buffering within the TCEF. Comparison of the SIDE and existing landscape analysis methods suggested that a significant overestimate of lateral inputs to riparian zones and riparian buffering occur using total hillslope and riparian lateral area contributions (not separated). This would lead to misconceptions when attempting to characterize riparian zone distributions and buffering potential. The SIDE algorithm provided a basis for more realistic up-scaling of HRS connectivity and riparian controlled processes in the TCEF.

Hydrological science has continually searched for new insight into watershed response based on landscape properties. The chapters summarized above sought internal catchment metrics that linked hydrologic process observations to the landscape and watershed scale response. This approach discretized the catchment into its component landscape elements and analyzed their topographic and topologic attributes as surrogates for their lateral hydrologic connectedness, as determined through detailed physical and tracer based field observations. This approach provided insight into where runoff and solute mobilization occurred within the landscape, the relative timing and magnitude of landscape element connectivity along the stream network, and how the integration of distributed landscape hydrologic connectivity and riparian buffering controls the magnitude of runoff and solute export across catchments of differing scale and structure.

#### Implications and Recommendations for Future Research

Based upon the knowledge gained from my dissertation, I offer the following recommendations for future catchment hydrology research:

1. Few tools exist to aid prioritization of riparian management by assessing the relative importance of riparian zones across the landscape and their potential to influence upland runoff and associated water quality constituents [Allan et al., 2008]. In this dissertation I presented a hydrological context and volumetric buffering quantification that provides an estimate of each riparian zones volumetric buffering potential relative to the upland delivery of runoff. I focused on the physical hydrology and tracer behavior across riparian zones. However, this context is also critical for understanding potential biogeochemical transformations because it demonstrates the first order landscape controls on riparian water turnover rates and provides tools to quantify these processes. For example, water delivery from hillslopes can influence the supply of nitrate, carbon, and oxygenated water to riparian zones. Each of these water quality parameters could strongly influence riparian zone redox states and therefore microbial denitrification potential. Future studies that examine the relationships between volumetric turnover and biogeochemical transformations that occur within riparian zones and how these interactions are distributed in time and space along stream networks are a requisite for adequate characterization of stream water quality. Additionally, a better understanding of how connectivity and turnover dynamics shift with climate forcing (wet vs. dry years) is also needed (Figure 2; [Jencso et al. 2008]).
2. In catchment hydrology, riparian and hillslope zones are often considered the prominent landscape positions for setting stream water biogeochemistry.

However, Bencala [1993] emphasized that “the stream is not a pipe.” Hydrologic exchange between streams and hyporheic zones can enhance biogeochemical reactions through contact with chemically reactive mineral coatings and microbial colonies and can therefore exert substantial influence on downstream water quality [Harvey and Wagener, 2000; Mulholland et al., 1997]. A limited amount of work has focused on a better understanding of the variable gains and losses of water once it enters the stream network [Covino and McGlynn, 2007; Payn et al., 2009; Covino et al., 2010]. Catchment scale integration of hydrologic connectivity and turnover dynamics from individual hillslope and riparian assemblages coupled with quantification of reach scale hydrologic gains and losses is needed to fully understand how these combined processes influence solute fate/transport and the evolution of stream biogeochemical signatures in a downstream direction. This may be partially achieved through landscape analysis of upland and valley structure and the organization of hillslope and riparian area along the stream network.

3. Chapter 5 indicated that the intersection of topographically controlled HRS connectivity with geologic and vegetative characteristics is important for describing runoff generation across catchments of differing structure and land cover. These factors may also explain some variance in the UAA-connectivity relationship described in chapter 2 [George Hazen et al., 2010] and could be highly influential on the upslope water balance and thresholds of connectivity initiation and cessation observed across different UAA positions. Future work

that aims to physically quantify the influence of these and other factors on distributed HRS connectivity dynamics within catchments is crucial to deconvoluting their relative influence for runoff dynamics observed at the catchment outlet.

4. In addition to hillslope and riparian area accumulation patterns, the SIDE algorithm presented in chapter 6 would be broadly applicable for assessing a variety of terrain analysis indices related to stream networks and their hydrology. Flow accumulation algorithms can also be used to compute average values of upslope landscape attributes. For example, the SIDE method could be implemented to calculate forest cover of upslope land portions for each stream cell on both sides. Additionally, the utility of the SIDE method for predictions of connectivity and buffering metrics in the TCEF suggests that other flow related terrain indices (e.g. the topographic wetness index; [Beven and Kirkby, 1979]) and models that incorporate them (TOPMODEL; [Beven et al., 1984]) might benefit from its implementation for more accurate descriptions of runoff generation.
5. Mathematical models based on simple conceptualizations and that represent internal system response characteristics are required for better prediction of catchment water quality and quantity. Traditionally, complexity resulting from the addition of many parameters within rainfall runoff models has lead to increased uncertainty, decreased predictive power, and limited flexibility when attempting to model catchment hydrology and biogeochemistry in catchments

with limited *a priori* information. The conceptualizations of HRS connectivity and riparian buffering developed in this dissertation represent simple empirically based metrics for predicting runoff and solute response. When incorporated within a modeling framework, these conceptualizations may prove to be useful tools for prediction of runoff and solute response across catchments of differing structure and for accurate representation of internal landscape source area response dynamics [Smith et al., 2009].

References Cited

- Allan, C. J., P. Vidon, and R. Lowrance (2008), Frontiers in riparian zone research in the 21st century, *Hydrological Processes*, 22(16), 3221-3222. 10.1002/hyp.7086
- Bencala, K.E. (1993), A perspective on stream-catchment connections. *Journal of North American Benthological Society*, 12 (1): 44-47
- Beven, K. J., M. J. Kirkby, N. Schoffield, and A. Tagg (1984), Testing a Physically-based Flood Forecasting Model (TOPMODEL) for Three UK Catchments, *Journal of Hydrology*, 69; 119-143
- Beven, K. J. and M. J. Kirkby (1979), A physically based variable contributing area model of basin hydrology *Hydrological Sci. Bull.*, 24(1),43-69.
- Covino, T.P., B.L. McGlynn, and M.A. Baker (2010), Separating physical and biological nutrient retention and quantifying uptake kinetics from ambient to saturation in successive mountain stream reaches. *Journal of Geophysical Research - Biogeosciences*. VOL. 115, G04010, doi:10.1029/2009JG001263, 2010.
- George Hazen, A.R., R.E. Emanuel; K.G. Jencso, and B.L. McGlynn. (2010). Vegetation influences on hillslope-stream connectivity in a forested northern Rocky Mountain watershed. *Eos Trans. AGU, Fall Meet. Suppl.*, Abstract H53B-1011.
- Jencso, K.G., B. McGlynn, M.N. Gooseff, R. Payn and S. Wondzell. (2008) Landscape structure as a 1st order control on whole catchment hydrologic and solute response characteristics across contrasting climate conditions. *Eos Trans. AGU, Fall Meet. Suppl.*, Abstract H31E-0927.
- Mulholland, P.J., E.R. Marzolf, J.R. Webster, D.R. Hart, and S.P. Hendricks (1997), Evidence that hyporheic zones increase heterotrophic metabolism and phosphorus uptake in forest streams. *Limnology and Oceanography*, 42:443-451.
- Sivapalan, M. (2003), Process complexity at hillslope scale, process simplicity at the watershed scale: is there a connection?. *Hydrological Processes*, 17(5), 1037-1041. 10.1002/hyp.5109
- Smith, T.J, K.G. Jencso, L.A. Marshall, and B.L. McGlynn (2009) A Stream Network Based Semi-Distributed Model for Prediction of Hydrologic Connectivity and Runoff Generation. *Eos Trans. AGU, Fall Meet. Suppl.*, Abstract H33B-0868

Payn, R.A., M.N. Gooseff, B.L. McGlynn, S.M. Wondzell, K.E. Bencala. 2009. Longitudinal distribution of channel water balance through summer discharge recession in a Rocky Mountain headwater stream, Montana, USA. *Water Resources Research*. doi:10.1029/2008WR007644.

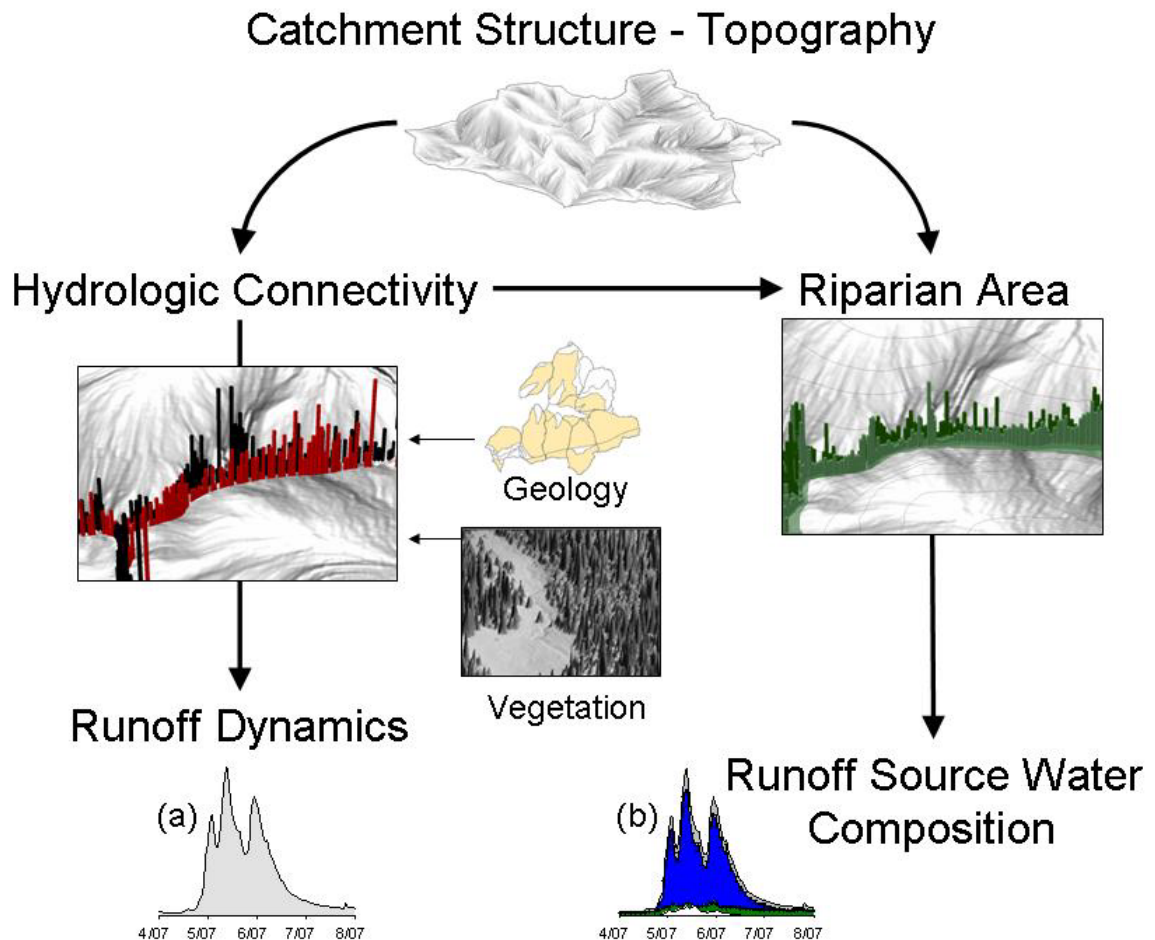
Figures

Figure 1: Conceptual model of runoff generation and solute mobilization for the TCEF catchment. (a) The topographically driven lateral redistribution of water determines the frequency and duration of hydrologic connectivity across the stream network. The extent of stream network connectedness and its intersection with catchment geology and vegetation determine the magnitude of runoff observed at the catchment outlet. (b) The intersection of hydrologic connectivity frequency and duration with riparian area extents determines the degree of riparian buffering/turnover and the spatial sources of water and solutes observed at the catchment outlet.

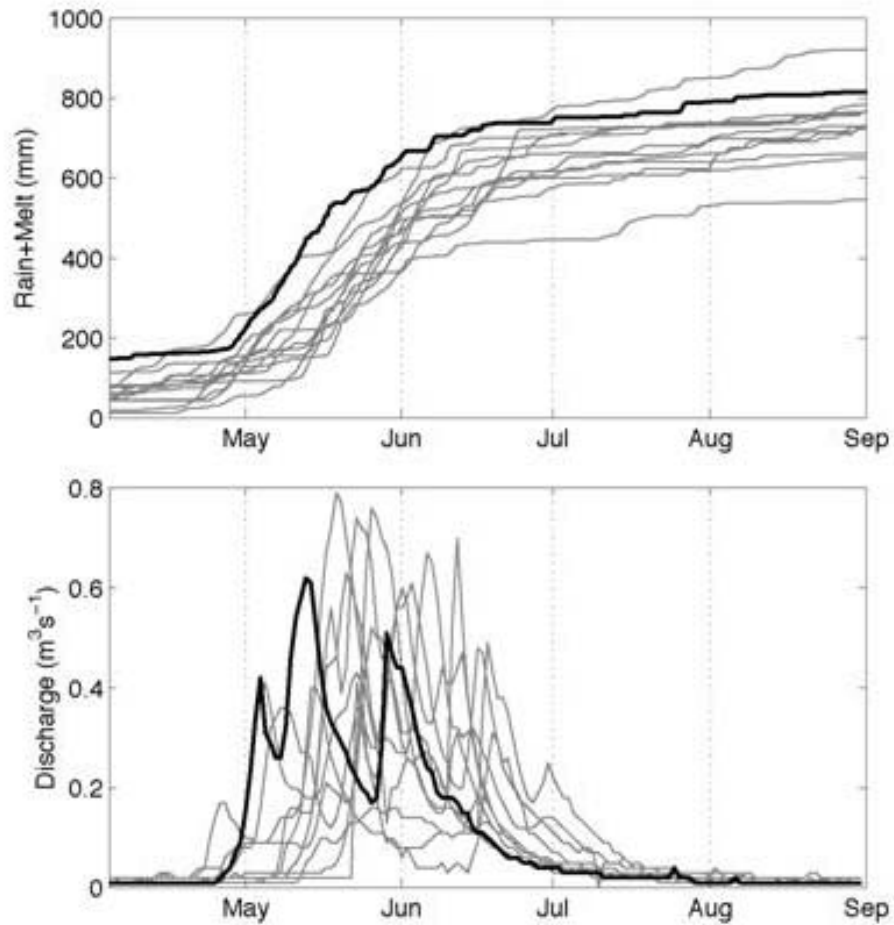


Figure 2: 1999-2008 Stringer Creek discharge and cumulative melt + rain time series (top). The 2007 water year is highlighted in black. Changes in HRS connectivity duration, as a function of precipitation variability and wetness state, could alter the degree of turnover within HRS sequences along the stream network. This may significantly alter the amount, timing, and riparian buffering of water and solutes exiting a catchment as a function of the intersection of climatic variability and catchment structure.